An Analytical Method for Predicting Delamination Onset and Growth induced by Matrix Cracks under Quasi-Static loading.

Master of Science Thesis

Javier Romarís Villanueva

Delft University of Technology

TU Delft

An Analytical Method for Predicting Delamination Onset and Growth induced by Matrix Cracks under Quasi-Static loading.

Master of Science Thesis

by

Javier Romarís Villanueva

to obtain the degree of Master of Science
at the Delft University of Technology,
to be defended publicly on Monday August 31st, 2023 at 9:30 AM.

Thesis committee:	Prof. Dr. C. Kassapoglou,	TU Delft, supervisor
	Dr. R. C. Alderliesten,	TU Delft
	Dr. S. G. P. Castro,	TU Delft

An electronic version of this thesis is available at
http://repository.tudelft.nl/URLENDHERE.

TU Delft

Essentially, all models are wrong, but some models are useful.

George E.P. Box

Abstract

An analytical model for the onset and growth of delaminations induced by matrix cracks under static loading is proposed. The model introduces four distinct configurations of delaminations originating from crack tips, which are applicable to cross-ply and general symmetrical laminates subjected to tension or tension + shear.

The delamination onset method employs Kassapoglou & Socci's analytical crack propagation model to describe matrix cracks within the laminate. This leads to closed-form expressions for the Strain Energy Release Rate associated with both crack propagation and the initiation of delaminations at crack tips. Both expressions are used to predict the delamination onset load and crack spacing. Predictions show excellent agreement with test results for cross-plies under tension.

Regarding the delamination growth model, it assumes a constant distance between cracks during growth (crack saturation). Experimentally-obtained Mode II interlaminar fracture toughness equation and closed-form expressions for Strain Energy Release Rate for delamination growth are employed for predictions. The model overpredicts the initial delamination length but exhibits satisfactory agreement with test results for the delamination growth in cross-ply laminates under tension.

Combining all 3 models allows for a comprehensive prediction of crack propagation, delamination onset and delamination growth for general symmetrical laminates. This comprehensive approach enables the visualization of all relevant information in a single figure, providing a concise and informative representation of the damage processes. Moreover, the analytical model facilitates the construction of design curves to investigate delamination onset in detail.

List of Figures

Contents

1 Introduction

Composite materials have provided significant improvements in the performance and efficiency of aerospace structures in the last decades. Composite materials by definition are made up of two or more materials with different properties, such as carbon fibers and epoxy resin, that are combined to create a material with superior strength, stiffness and durability compared to traditional materials such as aluminum. Composite materials used in the Aerospace sector are generally made of Uni-Directional laminae (UD plies) that are stacked following different orientations to obtain specific properties in those directions, this allows higher optimization compared with the metal alloys in terms of weight and performance. Composites are used in a wide range of aerospace applications, from primary structural components such as wings and fuselages to secondary structures such as engine nacelles. In addition to reducing weight, composites also offer other benefits such as improved resistance to fatigue, corrosion, or design flexibility among others. As a result of these benefits, the use of composite materials is expected to continue to grow in the aerospace sector, even expanding to other fields.

However, the use of composite materials also has disadvantages, one of which is their failure behaviour. Composite materials are formed by two microscopically different materials (fibers and matrix) and present different and complex failure modes. Some intrinsic to each component, those that occur at the interfaces of both and more complex ones that appear as a result of intricate combinations and interactions between the materials. The most common failure modes, among others, are: the failure of the matrix with the consequent creation of matrix cracks, the failure of the fibers (uncommon since they are very strong) and the delaminations that occur on the interfaces of the laminate. These mechanisms depend on the stacking sequence of the laminate (symmetric/non-symmetric , balanced/non-balanced ...etc), the loads applied (in-plane or flexural), the geometry of the structure and the manufacturing imperfections. Many of the behaviors of composite materials are not yet fully understood. Failure modes for example are not yet perfectly characterized and there is still much room for improvement in the models and theories.

Among all the possible failure cases, the most common damages in an aerospace structure are the creation of matrix cracks in the polymer matrix and the formation of delamination between plies [1]. Matrix cracks can occur at very low loads, well within the design ultimate loads of the structure [2, 3]. This type of damage usually do not cause the complete collapse of the structure but reduce the transverse properties of the ply and consequently, the stiffness and Poisson's ratio of the whole laminate [4–6]; it is important then to assess the damage to keep track of the properties reduction. Matrix cracks multiply and usually induce the delamination

onset to relieve the local stress concentration at the crack tips [7]. Its further growth then leads to the final failure [7, 8]. This specific failure mechanism is prevalent in Aerospace structures which emphasizes the importance of gaining a profound understanding of this phenomenon and the physics behind it.

The most commonly employed methods for studying these types of damages independently include a Shear Lag Analysis [9], Variational methods [10] and micromechanics models [11]. In recent years, numerical techniques like Cohesive Zone Models (CZM) in FEM analysis have also been developed [12]. Very few analytical or experimental studies have been conducted specifically on the delamination onset induced by matrix cracks. O'Brien [13] developed a simple analytical model to study the delamination onset and growth under quasi-static and fatigue loading. He was a pioneer proposing the use of the Strain Energy Release Rate (SERR) to effectively predict the behaviour of the delamination initiation in cross-ply laminates. Later on, others like Takeda & Ogihara [7] expanded upon a shear-lag approach to also study delaminations triggered by transverse cracks and they employed the mode II interlaminar fracture toughness obtained from ENF tests to predict the progression of these delaminations. Consequently, they made the assumption that the growth of a delamination in a $0^{o}/90^{o}$ interface exhibits pure mode II behavior. However, there is still a lack of precise models capable of accurately predicting the interactions between delaminations and matrix cracks in a general situation.

The objective of this thesis is to obtain an analytical method to predict the delamination onset induced by matrix crack and its growth in a symmetrical laminate subjected to quasi-static in-plane loads. This will follow a previous work by C. Kassapoglou & C.A. Socci. In their paper "*Prediction of matrix crack initiation and evolution and their effect on the stiffness of laminates with off-axis plies under in-plane loading*" [3], they obtained closed form expression to predict the cracks formation and propagation under in-plane loads. These very accurate equations will be used to derived analytical SERR expressions to predict the delamination onset which is induced by the cracks. The model will be later validated using adequate test data from the literature.

2

Literature Review

The Literature Review focuses on two main topics: matrix crack initiation and propagation models and delamination onset and growth models. The techniques proposed in the literature can be divided in analytical models, FEM analysis methods and experimental or empirical approaches. Usually analytical methods to predict matrix cracks are based on the continuum mechanics [14–16], a Shear Lag Analysis [17, 18] or a Variational approach [10, 19, 20] while the delamination prediction usually involves the calculation of an Energy Release Rate (ERR) [13, 21, 22]. Even though a variety of numerical and semi-analytical models have also been proposed [23–27], this review will be mainly centered around analytical and experimental studies. This emphasis is driven by the intention to propose an analytical method in this thesis.

When it comes to predicting damage in composite laminates, it is worth considering why developing an analytical method is preferable to other techniques that may occasionally yield more accurate results. Analytical methods, based on mathematical equations and theoretical frameworks, provide distinct advantages in this context:

- Speed & efficiency: analytical methods often provide closed-form solutions or equations that can be solved relatively quickly, allowing for rapid analysis and decision-making. In the aerospace industry where efficiency is crucial and time-consuming processes like numerical methods or costly approaches like testing are not preferred, the development of an analytical method becomes particularly important.
- Insight into underlying mechanisms/Interpretability: analytical methods provide a deeper understanding of the underlying mechanisms and relationships governing a system. This understanding can offer valuable insights and facilitate generalizations beyond specific empirical data points and also facilitates the interpretation of how variables and parameters interact with each other.
- Extrapolation & generalization: in the aerospace sector, where the optimization and complexity of designs result in unique characteristics for each composite laminate, the ability to predict beyond the range of observed data holds greater significance than having a perfect understanding of specific behaviors. Analytical models, relying on theoretical principles, offer valuable insights into the behavior of systems under various conditions and future scenarios. This becomes particularly advantageous in situations where empirical data is lacking or when you need to predict different processes but fall under the same physical principles. For instance, in design processes where precision may be less crucial and the focus is on studying delamination behavior across a large number of laminates, an analytical method proves to be more useful.

- Parameter sensitivity analysis: analytical models allow for systematic sensitivity analysis of the impact of different parameters on the model's output. By manipulating the mathematical equations, it is possible to determine the sensitivity of the model to changes in input parameters, aiding in understanding the relative importance of different factors and guiding decision-making. This is again very useful for the industry in the validation and certification processes because you have a deep understanding on the strengths and weakness of the model.

Despite their numerous advantages, analytical methods usually face challenges when dealing with materials exhibiting complex behavior. These methods usually rely on simplistic assumptions and equations and if the material in question demonstrates intricate behavior, the model will likely fail to accurately capture its complexities in general scenarios due to the huge amount of variables to take into consideration. In that sense, the unpredictability of inherent material defects and the interactions between all the damage models are a huge obstacle in the modelling process [7, 10, 11]. These defects and interactions can significantly alter the behavior of matrix cracks and delaminations, as highlighted by Wang et al. [22]. Additionally, analytical methods often suffer from limited scope and applicability. In some cases, these methods narrow down their focus to specific situations in order to be accurate. For instance, Takeda & Ogihara [7] proposed a method that offers highly accurate predictions but only for a very specific combination of laminate and load conditions. Nevertheless, by employing appropriate assumptions, possessing a strong understanding of the underlying physics and employing sufficiently complex equations, analytical models can still provide predictions for highly complex scenarios.

Another interesting discussion is related with the challenges associated with experimental studies aimed at measuring crack distances and delamination lengths in composite laminates, which can impact the validation of predictive methods. Matrix cracks are very small and their detection and accurate measurement are not straightforward. Delaminations are also difficult to detect as they can occur between layers or at the edges, often being mistaken for fiber breakages, crack clusters or pre-existing defects [28, 29]. Sometimes stacking sequences like cross-plies are commonly used to make measurement feasible and more accurate, where the ply of interest or interface is distinct from the others to minimize false readings. However, this approach may overlook complex geometries and placing measurement devices in small areas can result in incomplete data if the damage has global behaviour [30].

While visual inspection and digital image correlation (DIC) techniques can measure surface damage, they may not account for internal delaminations and cracks within the laminate. Optical microscopy and scanning electron microscopy offer high accuracy but are challenging to implement for continuous damage monitoring [28]. Non-destructive testing (NDT) techniques such as ultrasonic testing, acoustic emission (AE) techniques, and X-ray computed tomography (CT) are generally considered more effective [31]. It is important to note that the choice of technique depends on specific research objectives, material properties and available resources. Researchers often combine multiple methods to address the challenges associated with crack distance and delamination length measurements in composite laminates [31]. When evaluating the validation of a method, caution must be exercised with test data and associated errors, particularly in the onset of cracks and delaminations, as these processes can be spontaneous and exhibit some level of randomness [32]. A correct assessment of the errors and the measurements and its limitations should be taken into consideration in the analysis of the predictions.

2.1. Matrix cracks prediction

Matrix cracks (often called transverse cracks when they appear in 90º plies [33]) emerge due to various factors such as manufacturing defects, static and fatigue loading or impact on the composite laminate [34]. These cracks typically manifest in regions where the material exhibits lower transverse properties, usually the matrix. The matrix, often composed of a polymer resin, tends to possess lower stiffness and higher susceptibility to cracking compared to the reinforced fibers [33]. Figure 2.1a illustrates this phenomenon. Besides compromising the overall properties of the laminate, the presence of matrix cracks can lead to additional types of damage such as localized delaminations [5, 7], depicted in Figure 2.1b.

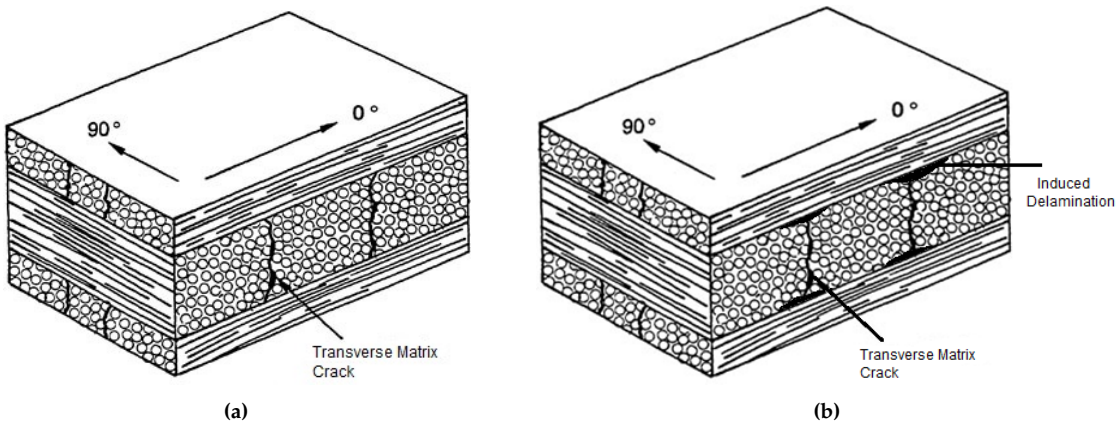

Figure 2.1: (a) Matrix cracks in the 90º plies of a cross ply. (b) Delaminations induced by the matrix cracks in the 0º/90º interfaces. Obtained from [35]

All models used to predict crack initiation and growth in composites take into account material properties and incorporate specific criteria for crack initiation and propagation. These criteria often consider stress or strain levels in the matrix material, drawing upon fracture mechanics principles or failure theories. Some models also consider load transfer between fibers and the matrix, accounting for stress redistribution caused by the presence of cracks [3, 10]. However, explicit modeling of the fiber/matrix interphase or fiber sizing is typically not necessary in most models, even though these components do impact the overall properties of the composite. The complexity of modeling the gradual transition of properties between the fiber and matrix, along with the relatively smaller effect of the interphase compared to load transfer, contribute to this decision [36, 37]. In general, failure is more likely to occur at free surfaces where fibers intersect, such as holes, edges, defects or cracks, rather than in the middle of the fiber within the matrix interface [36]. However, it's important to note that if there are issues with the manufacturing process or the fiber/matrix interface, the fiber/matrix interphase and sizing can become relevant factors in crack formation and propagation [37]. Assuming proper manufacturing and sizing processes, the loads required to cause debonding failure at the fiber/matrix interface are significantly lower than in other regions [36]. This serves as an illustration of the significance of making sound assumptions grounded in observations, prior research and fundamental understanding. The application of sizing is aimed at enhancing adhesion, thereby improving the interfacial shear strength and, notably, preventing fiber-matrix debonding.

The first challenge for many authors was the estimation of the laminate stiffness and how the cracks influence the elastic properties of the material. Reifsnider & Highsmith [17] and Laws et al. [2] used a Shear Lag Analysis to model the axial stiffness of composite ply and

relate it to the average distance between cracks. Ogin et al. [38] also obtained relations between the crack density and the mechanical properties degradation under fatigue loading. However, these approaches have limitations, as they mainly consider uniaxial tension and fail to account for the complexity of ply response and crack formation under more general in-plane loads. Additionally, they overlook the influence of adjacent plies on the cracked ply, which may result in inaccuracies and underestimations of loads.

Kashtalyan & Soutis [18] applied a two-dimensional shear lag methodology in order to compute the stresses occurring between cracks within a representative portion of the laminate. In a more recent study, Chen & Yan [39] utilized a shear lag model incorporating a cohesive fiber-matrix interface. They derived equations in a closed form to determine the maximum force required for fiber pull-out and evaluated the distribution of stress during the process of interface debonding.

Hashin [10] introduced the variational approach as a mean to provide an approximate stress analysis for cross-ply laminates that experience matrix cracking within the 90° plies. Subsequently, Hashin [19] conducted further research and discovered that cracks in certain plies have a significant impact on the Poisson's ratio but only a minimal influence on longitudinal stiffness. Larijani & Farrokhabadi [20] made additional advancements by developing a complex model based on the variational approach. This model was capable of predicting the effect of cracks on stiffness and even preemptively identifying the initiation of delaminations at specific crack distances. Hajikazemi & Sadr [40] also obtained expression for arbitrary lay-ups and later on, Nairn [41] expanded the concept to study the outer ply cracking in cross-ply laminates.

Talreja [14, 15] incorporated continuum damage mechanics and micromechanics to create a model that effectively predicted off-axis cracked plies. Similar approaches were adopted by Van Paepegem & Degrieck [42], who focused on crack formation under pure shear. At the same time, Varna et al. [16] obtained precise models to predict the crack density on cross-ply laminates. Although this model demonstrated accuracy, it required empirical data to fit certain parameters. Talreja & Singh [43] later on proposed a method to predict the crack initiation and evolution in off-axis plies. Their approach integrated FEM analysis with empirically-derived parameters to accurately anticipate the deterioration of properties resulting from matrix cracks.

In a more recent study, Socci & Kassapoglou [3] developed closed-form expressions to calculate the stresses between cracks, taking into account the elastic effects resulting from the nonlinear behavior of the shear stress-strain response. They integrated these expressions with an energy-based method to forecast the occurrence of new crack formations. Additionally, they derived closed-form equations to predict the reduction in stiffness of a ply under different in-plane loads. The model considered factors such as ply thickness, stacking sequence and load redistribution effects, making it applicable to a wide range of laminates. Notably, the derived expressions exhibited excellent correlation with experimental data gathered from various literature sources.

2.2. Delamination onset & growth

Delaminations in composite laminates can manifest in various forms. Two commonly observed types are edge delaminations and delaminations induced by cracks in the polymer matrix. Edge delaminations occur due to the highly concentrated stress fields present at the free edges of the laminate. Similarly, matrix cracks act as stress concentrators , creating localized areas of weakened bonding between the plies, leading to localized delaminations [13, 44](see Fig.

2.2 for a schematic representation). This is particularly significant because, as previously mentioned, matrix cracks appear well within the design ultimate loads [3]. In real-life scenarios, these delamination types can interact with each other and other forms of damage, resulting in complex damage patterns throughout the laminates. The specific nature and extent of delaminations depend on factors such as laminate design, material properties, loading conditions, and inherent manufacturing defects [10].

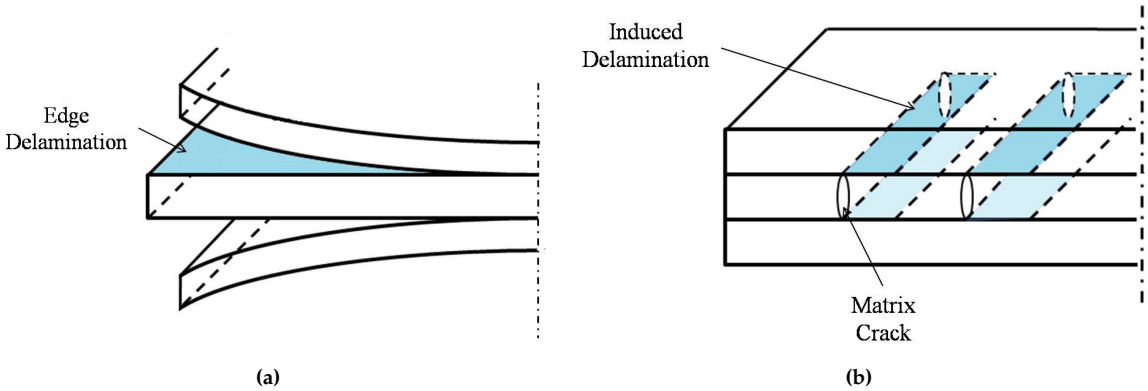

Figure 2.2: (a) Free edge delamination. (b) Delamination induced by matrix cracks.

The authors initially directed their research towards exploring free edge delaminations, which originate at the edges of composite laminates and propagate throughout the thickness. Subsequently, the authors shifted their focus to investigating delaminations induced by matrix cracking which present greater complexities due to local interactions in the material. Rodini & Eisenmann [8] were among the very first to study in detail delaminations although they didn't take into account the influence of matrix cracks. They performed extensive experimental tests in graphite/epoxy laminates, mainly cross-plies, to study the variables influencing the phenomena.

Wang et al. [22] then studied 2 types of delamination: 1D delamination (free edge delamination for example) and 2D delamination (contoured delamination). They used finite-element method to obtained Strain Energy Release expressions for both cases and they compared with experimental data obtained from their previous studies [45]. In a specific case, they focused on the analysis of a delamination occurring at the intersection of transverse cracks and the free edge of the laminate. Their study was one of the earliest to acknowledge the complexities associated with the interactions between these two types of damages. In the majority of tests, it was observed that matrix cracks in the 90^{o} plies induced localized delaminations. These delaminations then underwent growth and led to the formation of a contoured delamination front. Conversely, in other tests from the same study, free-edge delaminations appeared first, leading to the formation of matrix cracks that later induced local delamination onset. The researchers emphasized that the onset of delamination and subsequent interactions were highly sensitive to manufacturing defects and other local imperfections. These findings align with the results of other experimental studies conducted by Brewer & Lagace [46], Wang [47] and Crossman et al. [48]. Due to the various challenges encountered, the development of a satisfactory analytical model was complicated.

Independently, O'Brien [13] studied the edge delamination onset and growth on symmetric laminates under quasi-static and fatigue loads. He was a pioneer proposing the use of the Strain Energy Release Rate (SERR) and he derived simple analytical expressions to predict the initiation and growth of edge delaminations. Initially, O'Brien determined the stiffness of the

pristine laminate using Classical Laminate Theory (CLT) (Fig. 2.3.a). He then employed a rule of mixture analysis, assuming a fully delaminated laminate (Fig. 2.3.b). By assuming complete delamination in one or more interfaces and applying the rule of mixture assumption that the resulting sublaminates (Fig. 2.3.b) experience the same axial strain but different transverse strains, he calculated the corresponding degraded properties. Subsequently, he obtained an equation for a partially delaminated laminate by employing again the rule of mixture, assuming equal-sized delaminated strips at both edges of the laminate (Fig. 2.3.c). This led to a closed-form equation for stiffness loss, which enabled the derivation of an SERR expression. He then obtained a critical SERR value from a $[\pm 30/\pm 30/90/\bar{90}]_s$ laminate and successfully utilized this value to predict the onset of edge delamination in $[+45_n/-45_n/0_n/90_n]_s$ (n = 1,2,3) laminates. Subsequently, he studied the delamination growth. He employed a delamination resistance curve (R-curve) to predict the growth behavior and established a correlation between his SERR equation and delamination growth rates using a power law relationship. This allowed him to investigate the behavior of laminates under fatigue loads. Although O'Brien's study did not explicitly consider matrix cracks, he acknowledged the significance of stiffness changes resulting from secondary mechanisms such as matrix cracking in the 90º plies.

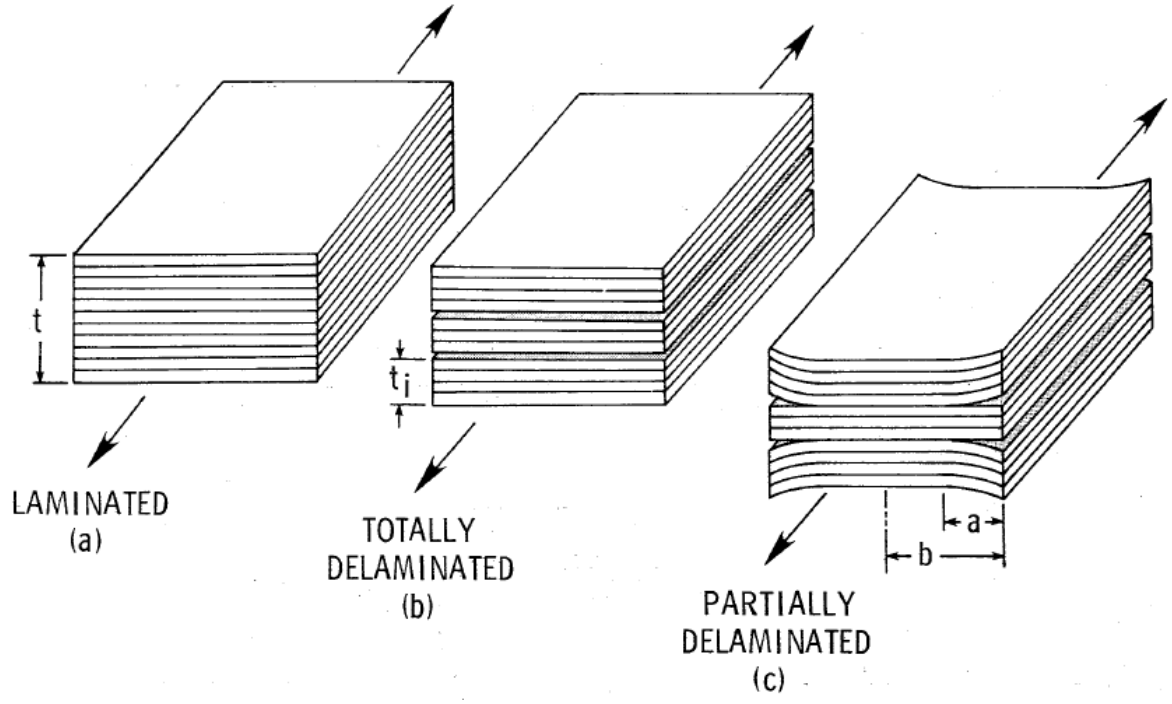

Figure 2.3: Rule of mixture analysis of stiffness loss. Obtained from [13]

Nairn & Hu [21] used a Variational approach to study the delaminations initiating from matrix crack tips taking into consideration complex three-dimensional effects on the shape of the delamination front as shown in Figure 2.4. They obtained SERR expression to predict the critical crack spacing at the delamination onset in $[0/90_n]_s$, $[0_2/90_n]_s$ and $[\pm 45/90_n]_s$ laminates. The critical crack spacing is defined as the distance between the crack at which the local delaminations first appear in the tips. Similar approaches were proposed by Lem & Lui [49] in which they derived expressions to compare the energy dissipation of both delaminations and cracks.

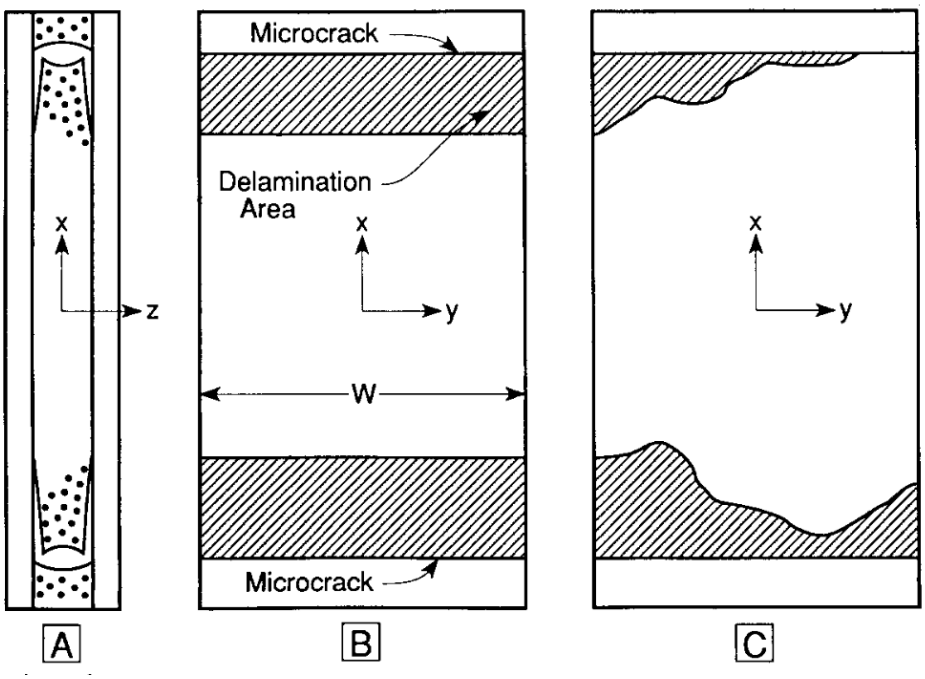

Figure 2.4: (A) An edge view of a representative element of damage having microcracks and delaminations. (B) A side view of the through-the-width delaminations. The shaded areas indicate areas of delaminations. (C) A side view of arbitrarily shaped delamination fronts. Obtained from [21].

Salpekar & O'Brien [50] investigated local delaminations induced by matrix cracks in $[\pm\theta/90_4]_s$ laminates using 3D finite element analysis. They proposed three configurations for local delaminations and placed particular emphasis on a triangular-shaped delamination emanating from a matrix crack (see Fig.2.5). Using Virtual Crack Closure Techniques (VCCTs), the authors obtained SERRs expressions corresponding to modes I,II & III. Then they study the SERRs values along the delamination front and obtained predictions for its shape and growth.

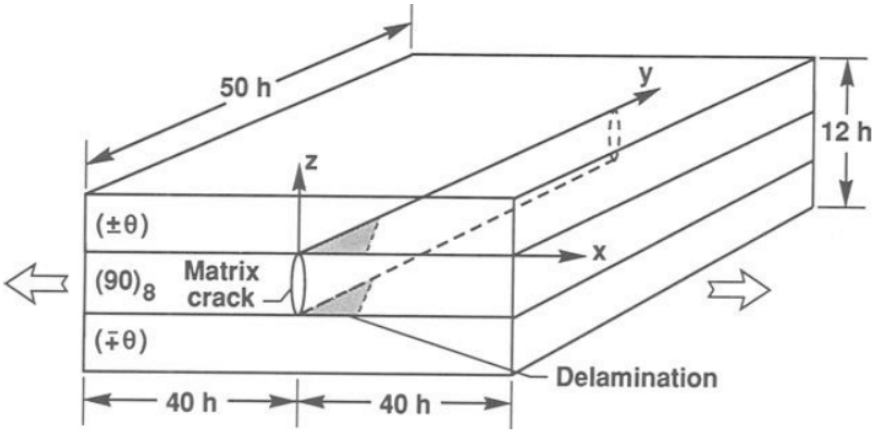

Figure 2.5: Schematic of an inclined delamination growing from a transverse crack. Obtained from [50].

Takeda & Ogihara [7] extended a shear-lag stress analysis to cross-ply laminates containing delamination at the matrix crack tips. Then, they compared the predictions for the delamination onset load and crack spacing with experimental data obtained from CFRP (T800H/3631) laminates. Strain Energy Release Rate (SERR) expressions were derived as a function of the

material properties, crack distance, delamination length and applied strain. In addition, they proposed to use the experimentally obtained mode II interlaminar fracture toughness (G_{IIc}) in combination with the SERR equations to predict the total delamination length with respect to the applied strain as shown in Figure 2.6. The model is very restricted to $[0/90_n/0]$ laminates under uniaxial tension due to the complexity of obtaining stress field equations for more intricate laminates. It is worth noting that the shear lag analysis employed in the model provides approximate solutions, which are not reliable for accurately calculating local stress fields near the crack tips. Additionally, the applied boundary conditions are not valid for increasingly small crack spacings. Furthermore, the Energy Release Rate (ERR) associated with a delamination, as calculated by these approaches lacks information about mode mixity. This is a critical parameter for accurately predicting the initiation and growth of delaminations in more general cases. Despite these drawbacks, the model exhibited excellent correlation in predicting the onset of delamination and transverse crack density when compared to experimental data. The correlation in predicting the growth of delamination for $[0/90_4/0]$, $[0/90_8/0]$ and $[0/90_{12}/0]$ laminates was also deemed satisfactory.

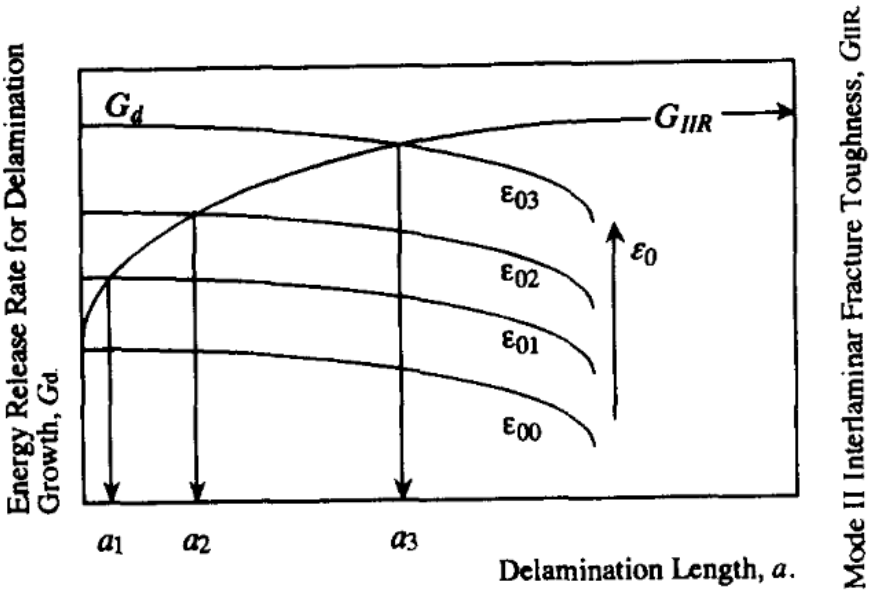

Figure 2.6: Schematic illustration of the delamination growth prediction proposed by Takeda & Ogihara. Obtained from [7].

More recently, Carraro et al. [44] proposed a method to predict the delamination onset induced by matrix cracks in cross-ply laminates under static loads. They used all the previous experimental evidences and studies to present closed form expressions for the mode I,II & III stress fields around the matrix crack tips as a function of the so-called Generalized Stress Intensity Factors (GSIFs). Then, a fracture criterion was proposed for assessing the onset of delamination, based on a critical value of the mode I GSIF. The researchers conducted several quasi-static tests on GFRP laminates with configurations of $[0/90_2]_s$ and $[0_2/90_4]_s$ to validate their predictions of crack density and delamination onset. In their findings, they observed irregularities in the delamination onset at the $0^o/90^o$ interfaces. It was noted that in some cases, delamination did not initiate in both symmetric interfaces or occurred with jumps between interfaces through the 90^o ply block (see Figure 2.7).

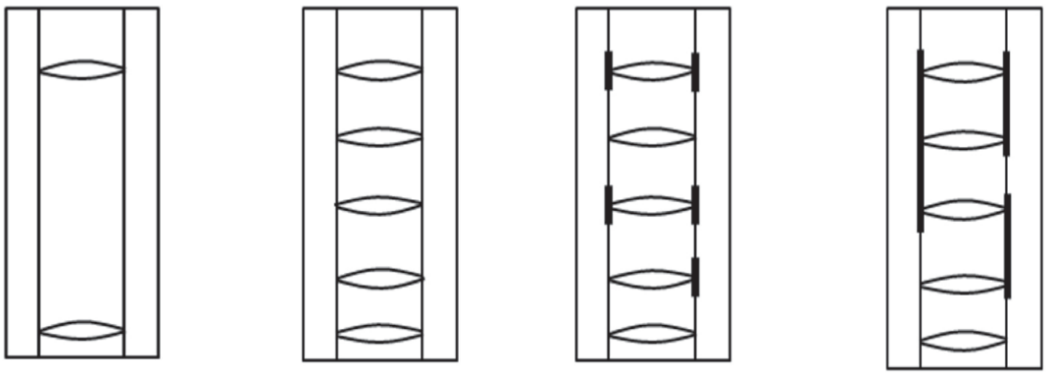

Figure 2.7: Schematic of the damage evolution in a cross-ply under quasi-static load. Obtained from [44].

This behaviour is in accordance with previously published studies in which similar pattern were reported. For example, Schellekens & Borst [51] reported similar jumps in $[0_n/\pm 35_n/90_n]_s$ CFRP laminates subjected to uniaxial tensile loading as shown in Fig. 2.8. Others like Lammerant & Verpoest [52] and Pakdel et al. [53] also reported similar behaviour in laminates under impact and fatigue loading respectively. All these experimental evidences emphasize the complex interactions among cracks, delaminations, interfaces, manufacturing imperfections, fiber breakages and applied load asymmetries [29]. Consequently, proposing an analytical method that accurately correlates with test data becomes challenging.

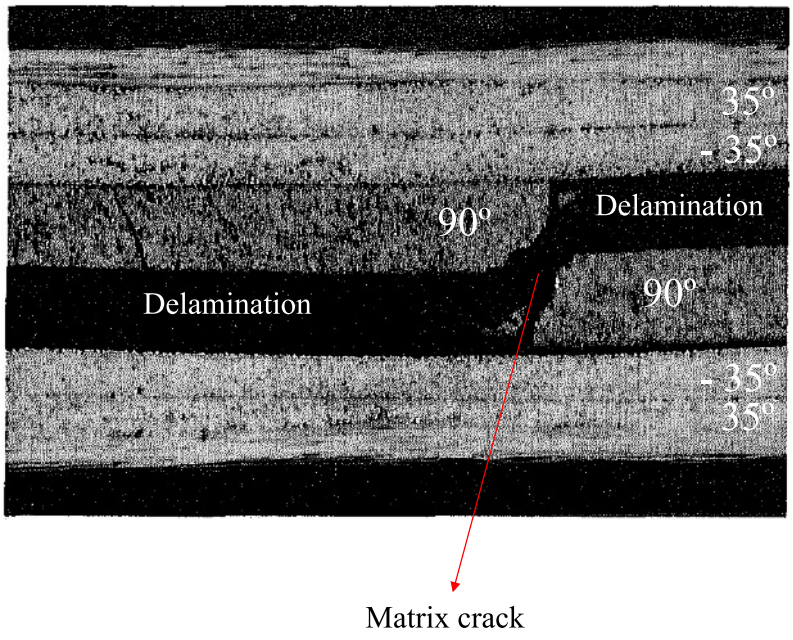

Figure 2.8: Jumping of the delamination between the -35/90 interfaces using the 90º ply matrix crack. Obtained from [51].

Through an analysis of the relevant literature, it becomes evident that analytical models for predicting the delaminations induced by matrix cracks in a symmetric laminate under generic in-plane loading conditions are lacking. Although numerous detailed methods have been derived for specific scenarios with the help of empirical fits or numerical methods, a comprehensive and universally applicable analytical model is yet to be developed.

2.3. Research Question(s)

The main research question that can be derived from the Literature Review is formulated as follows: **To what extent can an analytical model predict the delamination onset induced by matrix cracks and their subsequent growth in a symmetric composite laminate subjected to quasi-static in-plane loads?**

Current approaches for predicting damage in composite laminates typically rely heavily on FEM analysis or experimental testing to ensure accuracy. However, the integration of an analytical model would significantly enhance efficiency, adaptability and speed compared to other methods. While the accuracy might not be on par, an analytical model that offers quick results without the need for extensive computational resources, applicable to a generic laminate under various loading conditions would prove immensely valuable, particularly in the design phase. Also, other sub-questions can be formulated to break-down and further explore the main research question:

- **To what degree can the model accurately predict the spacing of cracks in a critical plies under a specific quasi-static applied load?**
- **How feasible is it to predict the load at which delamination onset will occur in a cross-ply laminate?**
  - And in a general symmetric laminate?
  - What are the key factors and variables that significantly influence the accuracy?
- **How can the delamination length in a cross-ply laminate be effectively correlated with the quasi-static applied load?**
  - And in a general symmetric laminate?
  - What is the level of correlation between the experimental test data and the delamination growth prediction?

3

Methodology

The approach followed in this study is outlined in this section, providing an overview of the general methodology. The fundamental principle of the entire model is based on the Strain Energy Release Rate (SERR) concept, which aims to investigate the most effective methods by which a material, in this case a composite laminate, can dissipate energy through an increase in its damaged area [54]. This concept holds significant importance in fracture mechanics because the energy that must be supplied to a crack tip or a delamination to grow must be balanced with the formation of new surfaces [55]. Previous studies [7, 13, 33] have demonstrated the effectiveness of the SERR concept in predicting delamination initiation and growth as well as crack propagation.

Within the framework of this study, three specific processes will be examined using the SERR concept. Then, analytical expressions will be derived for symmetric laminates and cross plies subjected to in-plane loading. These processes include: the formation of new cracks, the creation of a delamination in a crack tip and the growth of a existing delamination. By obtaining these expressions, it will be possible to determine, for a given load and laminate, which process will dissipate more energy (yielding a higher associated SERR) and thus is more likely to occur [55]. To put it simply, the objective is to identify the most optimal means of dissipating the energy introduced into the laminate due to the applied load. By doing so, it would be possible to predict when and how the different processes occur. Although other energy-dissipating processes such as fiber pullout and fiber breakage are not considered in this study, they may be relevant in other load cases involving for example impact [56, 57].

Figure 3.1 displays the three aforementioned processes, which are characteristic behaviors of a composite laminate subjected to in-plane loading. These processes occur sequentially as follows:

1. Matrix cracks initiate at relatively low loads, well below the ultimate design loads [2]. Subsequent loading leads to the formation of new cracks, assumed to appear at the midpoint between two existing cracks (refer to Chapter 4)
2. At a certain point, delamination onset occurs in the crack tips at a specific crack spacing (D_{onset}). This is a commonly observed phenomenon reported by various authors [7, 21, 44, 58].
3. Assuming the crack spacing remains constant (discussed in Chapters 5 and 6), the delaminations induced by matrix cracks continue to grow until complete failure of the interface.

The Strain Energy Release Rates corresponding to these processes are denoted as G^{cr}, G^{cr+del}_{onset} and G^{cr+del} respectively. The superscript "cr" represents the state in which only cracks are present, while "cr + del" indicates the coexistence of both cracks and delaminations within the laminate. The forthcoming chapters will propose and discuss closed-form expressions for these variables.

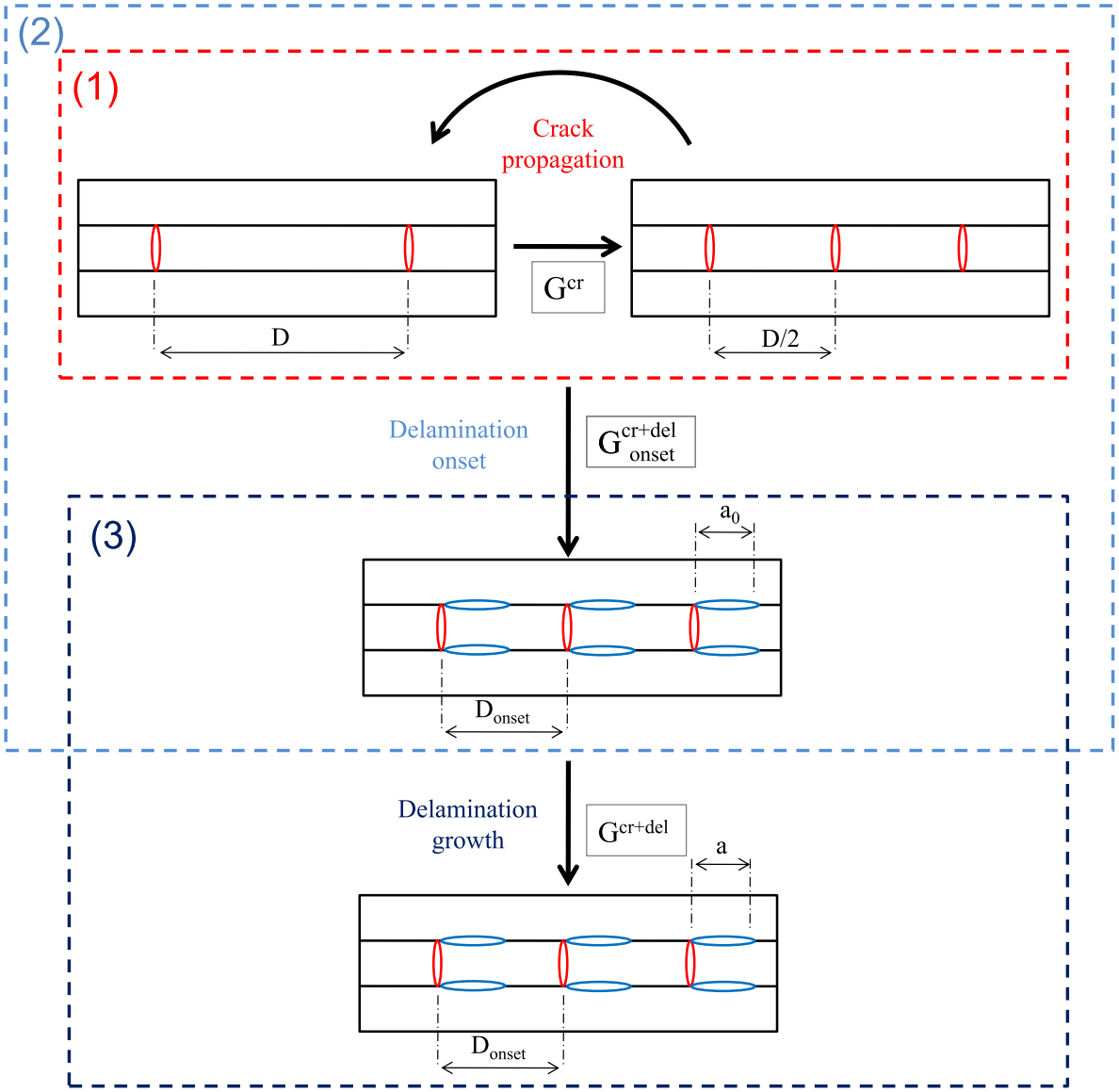

Figure 3.1: Typical damage process of a cross-ply under in-plane loading.

Figure 3.1 illustrates that delaminations initiate at the crack tip and symmetrically grow in the same direction. However, for a more complete analysis, four different variations of delamination geometry are proposed, as shown in Figure 3.2. All four cases consist of repeating unit cells throughout the entire length (L) of the laminate.

The aim is to develop equations for the Strain Energy Release Rate (SERR) in each of these

variations. Among these, the highest value will be chosen, a priori, to ensure a conservative approach although this will be discussed more in depth in later sections.

- Case I represents a delamination that advances in one direction from the crack tip.
- Case II corresponds to a delamination propagating in both directions from the crack tip.
- Case III involves two pairs of delaminations going in different directions.
- Case IV is a special case inspired by experimentally observed patterns where a delamination jumps to another interface through a crack (see Fig. 2.8). This is also observed in laminate after impact damage, where the delamination grow away from the impact point jumping through interfaces [52, 59, 60].

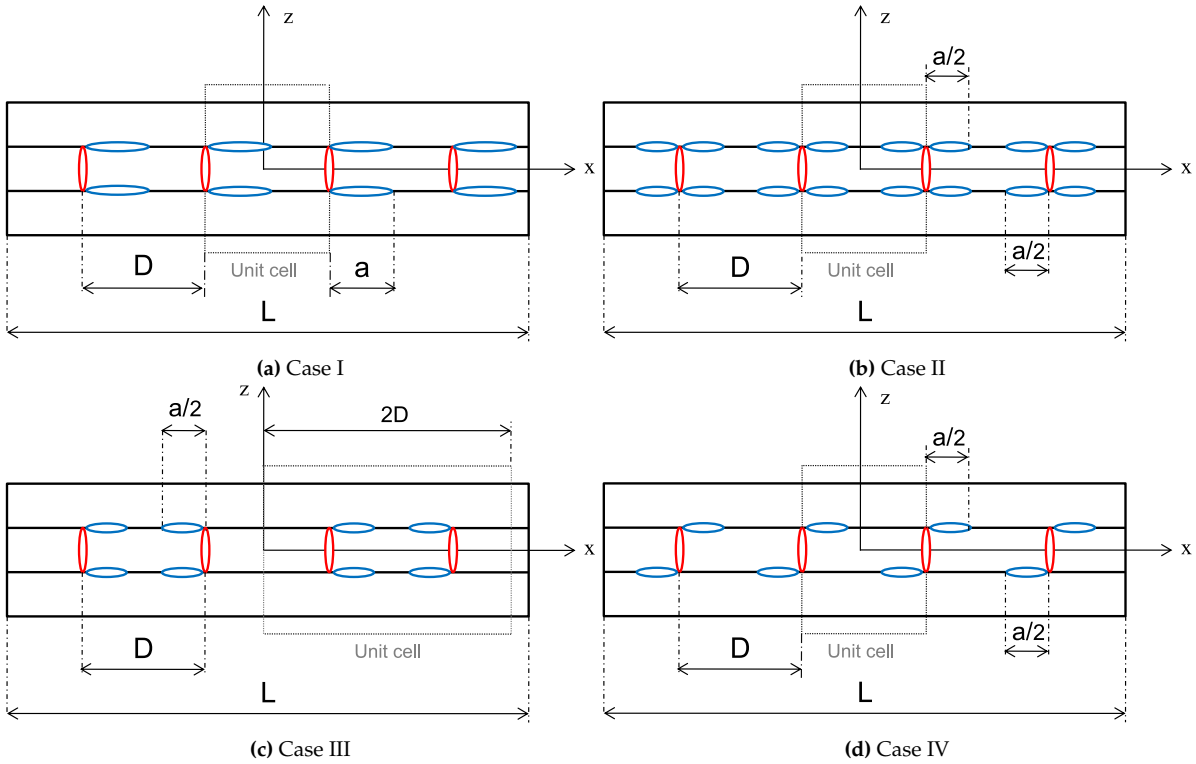

(a) Case I **(b)** Case II

(c) Case III **(d)** Case IV

Figure 3.2: Possible configurations of delaminations nucleating from the crack tips.

Once the SERR (Stress Energy Release Rate) expressions are derived with respect to the crack spacing D for the crack propagation and delamination onset, a comparison can be made to distinguish two distinct regions, as illustrated in Figure 3.3. The first region corresponds to cases where $G^{cr} > G^{cr+del}_{onset}$, while the second region represents situations where $G^{cr} < G^{cr+del}_{onset}$.

For larger values of D, it is more optimal for the laminate to dissipate energy by generating additional cracks, resulting in G^{cr} being greater than G^{cr+del}_{onset}. However, as the distance between cracks decreases upon loading, there comes a point where it becomes more advantageous to dissipate energy through delaminations ($G^{cr} < G^{cr+del}_{onset}$). This critical point, depicted in Figure 3.3, is considered as the onset of delamination. The crack spacing D_{onset} at which the delamination start can be related with the load that generates that amount of cracks and therefore the delamination onset load can be obtained, as it will be discussed in Section 5.

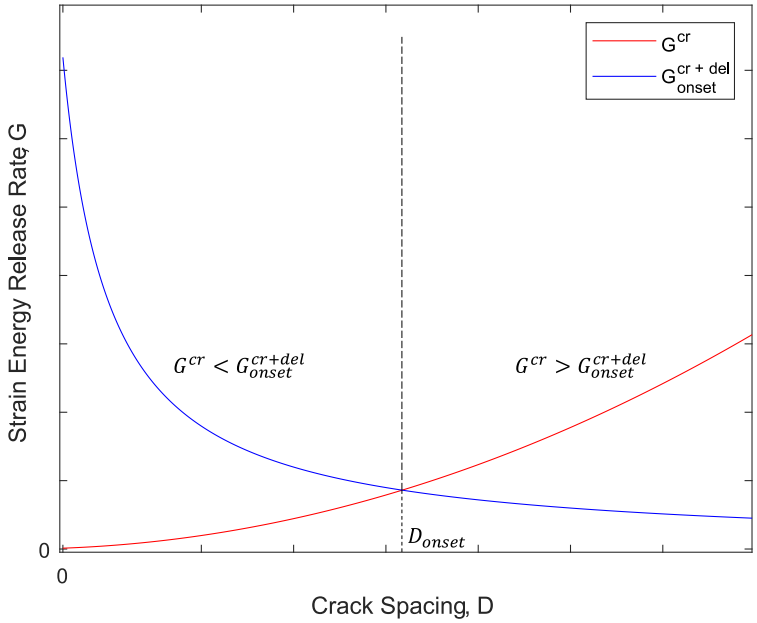

Figure 3.3: Schematic representation of the SERR expressions that model the crack propagation and the delamination onset.

Following the initiation of delaminations at the crack tips, the growth of delaminations can be predicted using the corresponding Stress Energy Release Rate (G^{cr+del}) expression that is derived in following chapters and the mode II interlaminar fracture toughness (G_{IIR}), as proposed by Takeda and Ogihara [7]. The SERR expression will be influenced by the applied load, crack spacing, delamination length and material properties. However, in Section 5 & 6, it will be assumed that the crack spacing remains constant after the onset of delaminations due to crack saturation. A schematic representation of the delamination length prediction concept is illustrated in Figure 3.4.

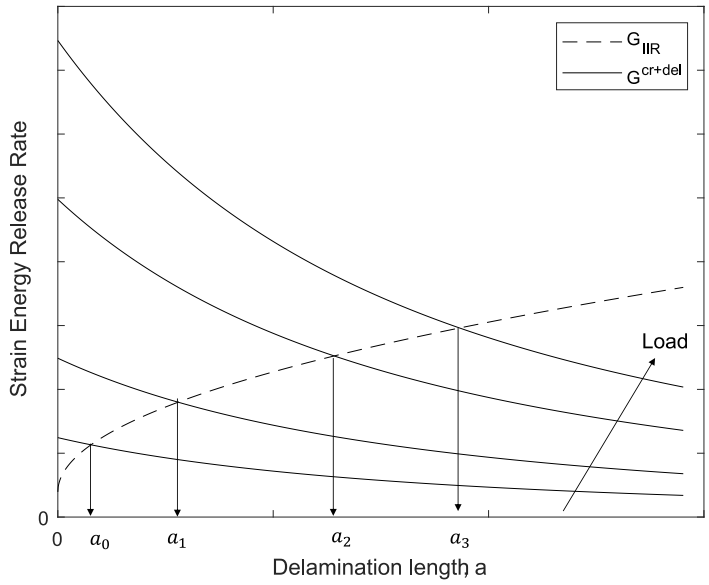

Figure 3.4: Schematic representation of delamination growth prediction.

The energy release rate for delamination growth (G^{cr+del}) is a decreasing function of the delamination length a but it increases with the applied load. The mode II interlaminar fracture toughness is considered as the critical value that initiates growth at each load level. Therefore, the intersection of G^{cr+del} and G_{IIR} corresponds to the delamination length at each specific load case which allows the prediction of the delamination growth. A comprehensive explanation of the entire model will be provided in Section 6. A schematic of both the delamination onset method and the delamination growth method that will be presented in this thesis are presented next:

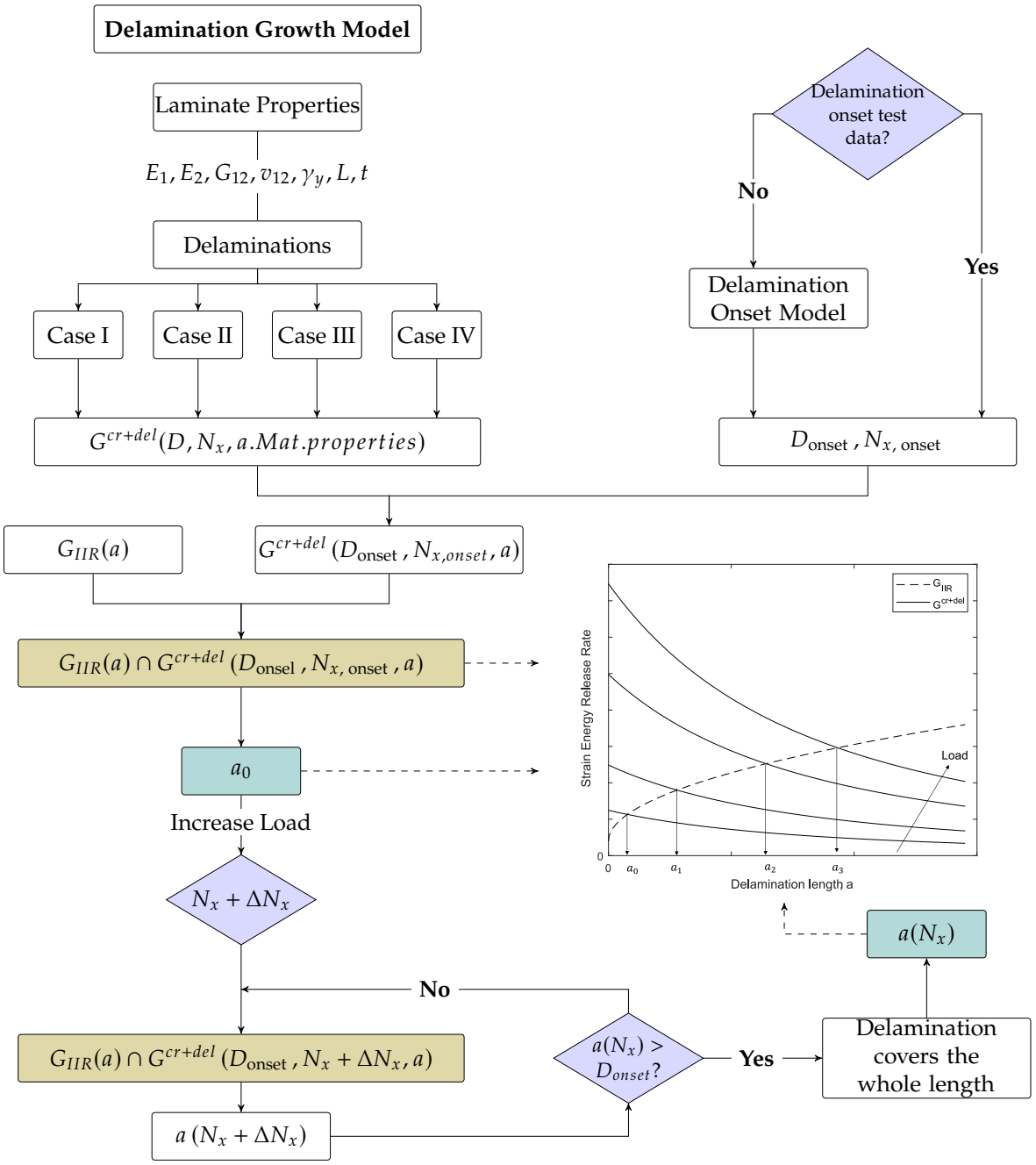

Figure 3.5: Delamination Growth Model

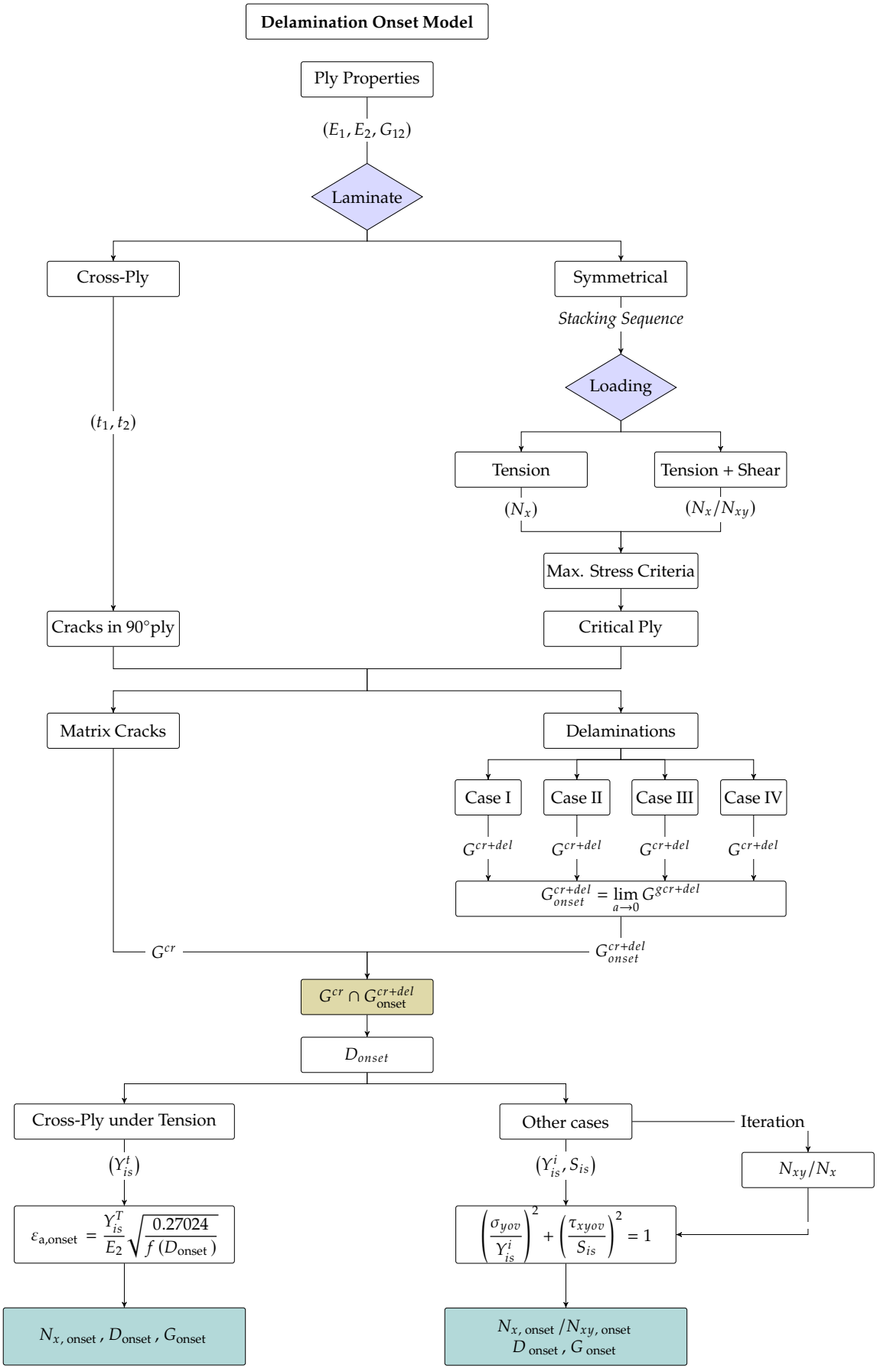

Figure 3.6: Delamination Onset Model

4

Matrix Crack Model

This section presents and validates the model utilized for predicting the initiation and propagation of matrix cracks. The model's accuracy is verified using crack spacing data obtained from relevant literature sources although it has already been extensively validated for stiffness degradation. A Strain Energy Release expression is also derived and additionally, an investigation of the influential variables and a sensitivity analysis of the parameters are conducted to gain further insights into the process.

The analytical model, developed by C. Kassapolou & C. A. Socci [3], serves as a fundamental basis for the proposed method to study induced delaminations, as will be discussed in Chapters 5 and 6. The selection of this model is based on three key principles:

- Efficiency & Interpretability: the chosen method should possess an analytical nature, allowing for an analytical delamination model. Parameters and physical concepts should be easily comprehensible and easy to study.
- No layups restriction: the model should be applicable to a wide range of cases, aiming to yield similar results for the proposed model in this study.
- Accuracy: extensive validation has been conducted to establish the model's accuracy. An erroneous representation of the cracks would likely lead to inaccurate delamination predictions.

4.1. Summary of Socci & Kassapoglou's [3] model for stiffness degradation due to matrix cracks.

Socci & Kassapoglou [3] introduced an analytical approach for investigating the deterioration of properties in a unidirectional (UD) ply caused by the presence of matrix cracks. They derived closed-form expressions for the stresses within a cracked ply subjected to in-plane loading, incorporating the elastic effects resulting from a non-linear shear stress-strain relationship. Furthermore, they obtained analytical expressions for the elastic constants. To predict the crack propagation, they proposed an energy criterion that will be explained in 4.2.

In a laminate under pure tension, it is assumed that the cracks are confined within the ply of interest and span the entire width of the laminate. The axial stiffness between the cracks remains constant and equivalent to the pristine properties while only the transverse properties are affected. It is assumed that a matrix crack appears when the transverse in-situ strength (Y_{is}^T) is

attained within a ply. Consequently, there is no occurrence of inelastic behavior prior to cracking. Additionally, the laminate is assumed to have considerable length in the longitudinal direction, thereby eliminating any dependence of stresses on the x-axis. Closed-form expressions for the stresses between the cracks σ_y, σ_z and τ_{xy}, where z is the out-of-plane direction, are derived with respect to the distance between them D, material properties and the thickness of the cracked ply t_c. For a detailed derivation of the complete stress expressions, please refer to the source cited [3].

The transverse Young's modulus ($E_{2,red}$) of the cracked ply within a laminate can be determined by dividing the average stress at $D/2$ by the applied strain. By substituting in the equations derived in [3] and adjusting the notation for consistency with this study, the reduced transverse Young's modulus of a ply caused by the existence of cracks normalized with the pristine Young's modulus can be expressed as follows:

$$\frac{E_{2,red}}{E_2} = 1 + \frac{8}{\pi^2}\sum\frac{1}{n^2}\frac{2e^{\frac{\varphi_n D}{2}} - 2e^{\frac{-\varphi_n D}{2}} + \varphi_n D\left(e^{\frac{\varphi_n D}{2}} + e^{\frac{-\varphi_n D}{2}}\right)}{e^{-\varphi_n D} - e^{\varphi_n D} - 2\varphi_n D} \tag{4.1}$$

with n odd, D being the crack spacing, E_2 the pristine transverse Young's modulus of the ply, $\varphi_n = n\pi/t_c$ and t_C the thickness of the cracked ply. The $E_{2,red}$ value obtained in eq. 4.1 is now used to calculated the minor Poisson's ratio of the cracked ply:

$$\nu_{21,red} = \frac{E_{2,red}}{E_1}\nu_{12} \tag{4.2}$$

When shear is present, it is again assumed that the matrix cracks remain confined within the ply of interest and similarly, there is no dependence on the longitudinal direction. However, unlike in transverse tension, where the stress-strain curve is linear, the shear stress-strain response is considered to be nonlinear [3]. The distribution of τ_{xy} exhibits significant non-linearity for small values of D and remains constant throughout the thickness for larger values of D (refer to [3]). Consequently, under sufficiently high loads, permanent shear strains occur and the calculation of this permanent shear strains becomes crucial in accurately determining the new shear modulus [61, 62]. It is worth noting that due to the nonlinear behavior of the shear stress-strain curve, the magnitude of strain required to induce the formation of a new crack is greater than in the case of transverse strain. The elastic shear modulus in a cracked ply can now be calculated by using the average elastic shear stress (τ_{xyav}) immediately before cracking. For a detailed description of the step-by-step process, please refer to Appendix B for clarity. The final expression is provided as follows:

$$\frac{G_{12,red}}{G_{12}} = \frac{1 - 8B_n}{1 - \dfrac{8B_n\left(1 - \dfrac{\gamma_y}{\gamma_a}\right)\left[(1-8B_n)\left(1 - \dfrac{\gamma_y}{\gamma_a}\right) + \dfrac{\gamma_y}{\gamma_a}\right]}{1 - 8B_n + \dfrac{\gamma_y}{\gamma_a}}} \tag{4.3}$$

where:

$$B_n = \sum \frac{e^{k_n \frac{D}{2}} + e^{k_n D} e^{-k_n \frac{D}{2}}}{\left(1 + e^{k_n D}\right)(n\pi)^2} \tag{4.4}$$

with n odd, D is the distance between cracks, G_{12} the pristine shear modulus of the ply, $k_n = n\pi/t_c$, t_c the thickness of the cracked ply, γ_y the yield shear strain and γ_a the local applied shear strain in a ply. As it can be seen, the reduced modulus is not a constant and it depends on the local applied shear γ_a due to the non linear behaviour. The local shear applied to a ply γ_a oriented in the θ direction can be linked to the applied strains in the laminate through the Classical Laminate Theory (CLT):

$$\gamma_a(\theta) = -2sin\theta cos\theta \varepsilon_x + 2cos\theta sin\theta \varepsilon_y + \left(cos^2\theta - sin^2\theta\right)\gamma_{xy} \tag{4.5}$$

4.2. Summary of Socci & Kassapoglou's [3] model for crack propagation.

Socci & Kassapoglou [3] proposed a method to predict the propagation of cracks based on the stress fields between two existent cracks before and after the formation of a new cracks (see $\sigma_{yav,before}$, $\sigma_{yav,after}$, $\tau_{xyav,before}$, $\tau_{xyav,after}$ in [3]). By relating these stresses with the in situ strengths of the ply (Y_{is}^T, S_{is}), they were able to predict the crack spacing D on a layer induced by a local applied transverse or shear strain (ε_a, γ_a).

They observed that for large D, the stresses between cracks only depart from the value that a pristine ply would have near the matrix cracks [3]. This means that there is a region of constant stresses where the new crack is going to appear at location of local defects. If, however, the crack spacing is short enough, the region of maximum stress degenerates to a point, the mid point between two cracks. In this case, the crack spacing becomes uniform and every crack will appear at a distance $D/2$ in the middle of two previous cracks. In the subsequent sections of the report, detailed explanations of Socci & Kassapoglou's model are provided specifically for two cases: when the ply is subjected to transverse tension and when it experiences combined loading, transverse tension and shear.

4.2.1. Ply under transverse tension

In cases where D is relatively large, a simple maximum stress criteria is sufficient to estimate the crack spacing. This estimation is made by considering the condition when the transverse stress at the midpoint between two existing cracks, denoted as $\sigma_y(y = D/2)$, equals the in-situ strength Y_{is}^t. This approach is discussed in detail in Kassapoglou & Socci's work [3].

However, when the crack spacing D is small, an alternative energy-based method was proposed. This method suggests that the appearance of a new crack can be determined by analyzing the difference between the average energy density immediately after crack formation and the energy density just prior to crack initiation. A critical value of this energy density difference is considered. Further explanation and details of this energy-based method can be found published in [3]. The average energy density normalized with $K = \varepsilon_a E_2$, as defined by Socci & Kassapoglou [3] will be adopted, although some notation changes are made to maintain consistency:

$$\frac{\Delta\sigma^2}{K^2} = f(D) = \frac{64}{\pi^4}\left[\left(\sum\frac{T_n}{C_n}\right)^2 - F_n^2\right] + \frac{16}{\pi^2}\left[\sum\frac{T_n}{C_n} - F_n\right]. \tag{4.6}$$

with:

$$\begin{aligned} T_n = \frac{1}{n^2}\Bigg[&\frac{1}{2}e^{\frac{5}{4}\varphi_n D}\left(1+\frac{3}{4}\varphi_n D+\frac{1}{8}\varphi_n^2 D^2\right) - e^{\frac{-1}{4}\varphi_n D}\left(1+\frac{1}{4}\varphi_n D-\frac{1}{4}\varphi_n^2 D^2\right)+\\ &\frac{1}{2}e^{\frac{3}{4}\varphi_n D}\left(1+\frac{5}{4}\varphi_n D+\frac{3}{8}\varphi_n^2 D^2\right) - e^{\frac{1}{4}\varphi_n D}\left(1-\frac{1}{4}\varphi_n D-\frac{1}{4}\varphi_n^2 D^2\right)\\ &+\frac{1}{2}e^{\frac{-5}{4}\varphi_n D}\left(1-\frac{3}{4}\varphi_n D+\frac{1}{8}\varphi_n^2 D^2\right) + \frac{1}{2}e^{\frac{-3}{4}\varphi_n D}\left(1-\frac{5}{4}\varphi_n D+\frac{3}{8}\varphi_n^2 D^2\right)\Bigg] \end{aligned} \tag{4.7}$$

$$C_n = \left[\frac{1}{2}e^{\frac{1}{2}\varphi_n D}\left(1+\frac{1}{2}\varphi_n D\right) - \frac{1}{2}e^{-\frac{1}{2}\varphi_n D}\left(1-\frac{1}{2}\varphi_n D\right)\right]\left(e^{-\varphi_n D} - e^{\varphi_n D} - 2\varphi_n D\right) \tag{4.8}$$

$$F_n = \frac{1}{n^2}\frac{2e^{\frac{1}{4}\varphi_n D} - 2e^{-\frac{1}{4}\varphi_n D} + \frac{1}{2}\varphi_n D\left(e^{\frac{1}{4}\varphi_n D} + e^{-\frac{1}{4}\varphi_n D}\right)}{e^{-\frac{1}{2}\varphi_n D} - e^{\frac{1}{2}\varphi_n D} - \varphi_n D} \tag{4.9}$$

with n odd, D being the crack spacing, t_c the thickness of the cracked ply under study and $\varphi_n D = \frac{n\pi}{t_c}$.

The determination of the crack spacing parameter D for a specific applied strain ε_a can now be achieved using the normalized average energy density $\Delta\sigma^2/K^2$. This is accomplished by relating it to the normalized crack spacing $\pi D/t_c$. The step-by-step process is illustrated in Figure 4.1. It is important to note that the master curve of $\Delta\sigma^2/K^2$ remains constant across different materials and its fundamental shape remains unaffected by varying applied transverse strains.

Cracking initiates when the applied strain ε_a induces a transverse stress equal to Y_{is}^t, corresponding to a maximum value of $(\Delta\sigma^2/K^2)max = 0.27024$ at $\pi D/t_c = 9.3167$. As the applied load is increased, the curve shifts upwards, while the maximum value still occurs at the same position. Consequently, when cracking commences, the critical value of $\Delta\sigma^2/K^2$ associated with a ply transverse stress of $Y^t is$ can be determined by evaluating the maximum of the $\Delta\sigma^2/K^2$ curve when the applied strain induces a transverse stress equivalent to Y_{is}^t [3].

$$\Delta\sigma_{crit} = 0.27024(E_2\varepsilon_{crit})^2 = 0.27024(Y_{is}^t)^2 \tag{4.10}$$

When the applied strain exceeds the critical value ($\varepsilon_a > \varepsilon_{crit}$), assuming the Young's modulus remains constant as described in [3], the quantity $\Delta\sigma_{crit}$ is still applicable. In this case, for a given applied strain ε_a, the master curve $f(\pi D/t_c) = \Delta\sigma^2/K^2$ (depicted by the blue curve in Figure 4.1) is multiplied by $(\varepsilon_a/\varepsilon_{crit})^2$, resulting in the red curve $g(\pi D/t_c)$ (see Figure 4.1). The ordinate corresponding to the intersection of $g(\pi D/t_c)$ with the horizontal line $\Delta\sigma^2/K^2 = 0.27024$ provides the new crack spacing D induced by the transverse applied strain ε_a.

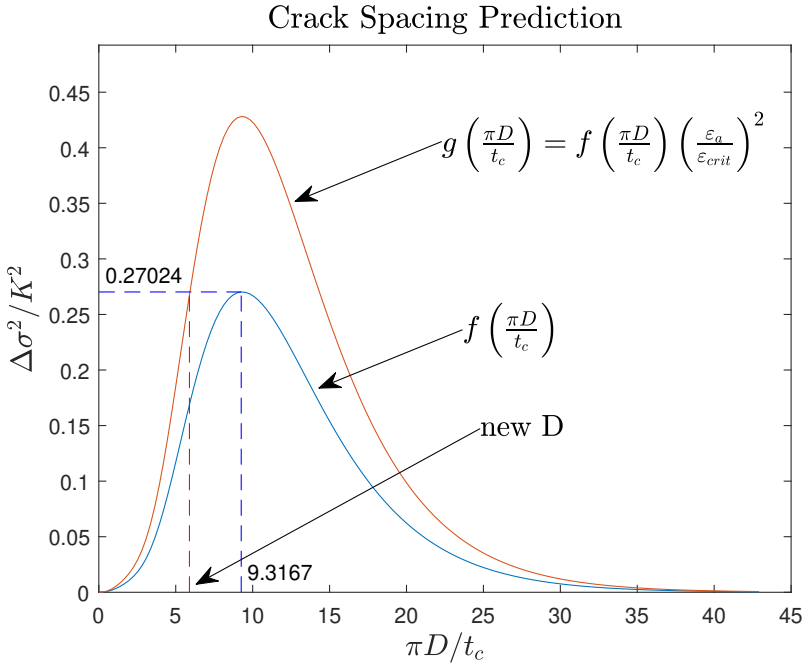

Figure 4.1: Normalized average density ($\Delta\sigma^2/K^2$) vs normalized crack spacing ($\pi D/t_c$).

It is important to note that Figure 4.1 becomes relevant only when the transverse applied strain in the examined ply surpasses the critical strain value $\varepsilon_{crit} = Y_{is}^t/E_2$, which varies depending on the material properties. If the applied strain is lower than ε_{crit}, the crack spacing is very large and non-uniform, making the concept of a constant crack distance unreliable. Despite the limited accuracy in describing the cracks under such conditions, the value of D remains sufficiently large to neglect any significant degradation in the properties of the ply. It should be noted that for comparisons with crack spacing measured from test, twice the value from Fig. 4.1 should be used because, for a given strain, D corresponds to the moment new cracks will be created and it is unlikely test measurements capture exactly that moment [3].

4.2.2. Ply under transverse tension and shear

The previously discussed concept is applied in a similar manner when considering a ply under shear. Similar to the transverse strain case, we analyze the difference between the shear stress before and after cracking, denoted as $\Delta\tau^2/2G_{12}$, in relation to D/t_c. It is important to note that, unlike the constant E_2 in transverse tension, G_{12} is not a constant value, as explained earlier. Once again, we determine $\left(\Delta\tau^2/2G_{12}\right) crit$ by identifying the maximum point on the curve where the applied shear strain γ_a leads to a shear stress equal to the in-situ shear strength Sis. For a detailed explanation and derivation of the equations, refer to [3]. By employing the Classical Laminate Theory (CLT), it is straightforward to calculate the local applied shear strain γ_a and transverse strain ε_a experienced by a ply oriented at an angle θ with respect to the applied strains in the laminate (ε_x, ε_y and γ_{xy}):

$$\varepsilon_a(\theta) = sin^2\theta\varepsilon_x + cos^2\theta\varepsilon_y - 2sin\theta cos\theta\gamma_{xy} \tag{4.11}$$

$$\gamma_a(\theta) = -2sin\theta cos\theta\varepsilon_x + 2cos\theta sin\theta\varepsilon_y + \left(cos^2\theta - sin^2\theta\right)\gamma_{xy} \tag{4.12}$$

When considering a ply subjected to a combination of shear and transverse strain, it is possible to combine the models used for pure tension and pure shear. In this case, a new crack will form when the combined effect of the difference between the transverse and shear stress fields, before and after the crack, exceeds a critical value [3]. Mathematically, this can be expressed as:

$$\frac{\Delta\sigma^2}{2E_2} + \frac{\Delta\tau^2}{2G_{12}} = \Delta U_{davcrit} \tag{4.13}$$

Here, $\Delta U_{davcrit}$ represents the critical value for a given load ratio ε_a/γ_a. This critical value is determined by considering the scenario where, for a large value of D, the stresses throughout the ply thickness are approximately uniform [3]. Under such conditions, a failure criterion of Hashin-type would predict local failure, which can be expressed as:

$$\frac{\sigma_{yav}^2}{(Y_{is}^t)^2} + \frac{\tau_{xyav}^2}{(S_{is})^2} = 1 \tag{4.14}$$

For a comprehensive and detailed explanation of the process and the stress field depicted in equation 5.31, please refer to the work by Kassapoglou & Socci [3].

4.3. Strain Energy Release Rate

This section aims to derive an expression for the Strain Energy Release Rate (SERR) related to the propagation of matrix cracks. In this particular case, the SERR expression describes the energy dissipated during the formation of new cracks due to the increase in the cracked surface [63]. It will be named using the superscript "cr" to refer to "cracks". G^{cr} is therefore defined as follows:

$$G^{cr} = -\frac{\partial U}{\partial A_{cr}} \tag{4.15}$$

where U is the potential strain energy available in the laminate which depends on the applied load and A_{cr} is the total area of the cracks. In a general case, the potential strain energy for a composite laminate under tension and shear loading is defined as;

$$U = \iiint \frac{1}{2}\left(E_x^{cr}\,\varepsilon_x^2 + g_{xy}^{cr}\,\gamma_{xy}^2\right) dV = \frac{1}{2}\left(E_x^{cr}\,\varepsilon_x^2 + g_{xy}^{cr}\,\gamma_{xy}^2\right) Lwh \tag{4.16}$$

where $V = Lwh$ is the volume of the laminate, ε_x is the applied tensile strain to the laminate, γ_{xy} is the applied shear strain, E_x^{cr} is the longitudinal modulus of the laminate with cracks and g_{xy}^{cr} is the shear modulus of the laminate with cracks (no capital G used to avoid confusion with the SERR expressions).

A maximum stress criterion is used to obtain the first ply failure of the laminate. The critical ply or plies are assumed to contain cracks that extend throughout the entire width of the laminate, as shown in Figure 4.2. The contribution of cracks in other plies to the SERR expression is considered negligible compared to the first ply failure cracks where the growth of the cracked area is way faster. Additionally, assuming cracks in every ply would introduce more crack spacing independent variables, making the analytical calculations overly complex. t_c is defined as the thickness of the cracked ply while h, w, and L correspond to the overall thickness, width, and length of the laminate respectively. Additionally, D denotes the distance

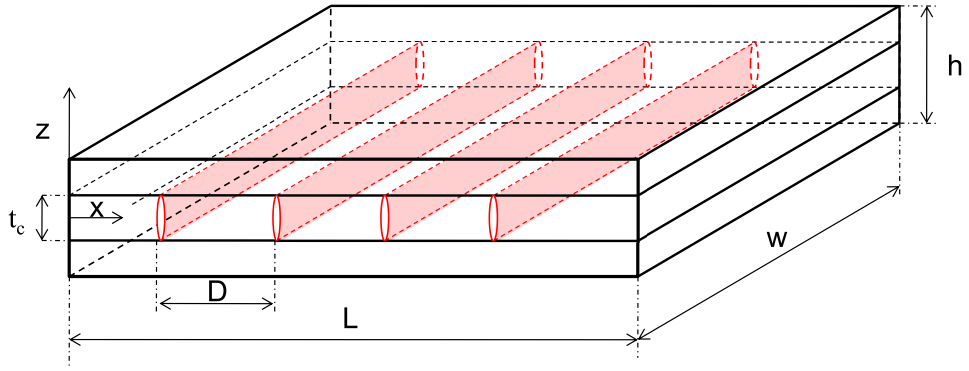

Figure 4.2: Diagram of a laminate with matrix crack in a ply.

between cracks. With these definitions in place, the total cracked area can be expressed as follows:

$$A_{cr} = t_c w \left(\frac{L}{D}\right) \tag{4.17}$$

Substituting eq. 4.17 & 4.16 in eq. 4.15 and considering that t_c, h, w and L are constants in the integration, the SERR expression for the cracked laminate under tension and shear loads is:

$$G^{cr} = \frac{1}{2}\left(\frac{h}{t_c}\right)\left[\frac{\partial E_x^{cr}}{\partial(1/D)}\,\varepsilon_x^2 \quad + \quad \frac{\partial g_{xy}^{cr}}{\partial(1/D)}\,\gamma_{xy}^2\right] \tag{4.18}$$

4.3.1. General Symmetric Laminate

In order to determine the expression for crack propagation-related SERR (G^{cr}), it is necessary to obtain first the engineering constants of the laminate [64]. Using the well-known Classical Laminate Theory (CLT), it becomes feasible to derive the elastic properties of a symmetrical laminate by first obtaining the stiffness matrix of a single lamina (Q_{ij}) based on its ply properties and then constructing the ABD matrix. The equations required to compute the ABD matrix are summarized in Appendix C. Recalling now that for a symmetric laminate $B_{ij} = 0$, the axial and shear engineering constants of the laminate can be defined as:

$$E_x = \frac{1}{h}\left\{A_{11} + A_{12}\left(\frac{A_{26}A_{16} - A_{12}A_{66}}{A_{22}A_{66} - A_{26}^2}\right) + A_{16}\left(-\frac{A_{16}}{A_{66}} + \frac{A_{26}A_{12}A_{66} - A_{26}^2A_{16}}{A_{22}A_{66}^2 - A_{26}^2A_{66}}\right)\right\} \tag{4.19}$$

$$g_{xy} = \frac{1}{h}\left\{A_{66} - \frac{A_{26}^2}{A_{22}} + \frac{2A_{12}A_{16}A_{26}A_{22} - A_{12}^2A_{26}^2 - A_{16}^2A_{22}^2}{A_{11}A_{22}^2 - A_{12}^2A_{22}}\right\} \tag{4.20}$$

The expressions defined in Appendix C do not take into account the degradation of the properties of a ply due to the presence of matrix cracks. Consequently, equations 4.1, 4.2 & 4.3 are substituted in eq. C.8 to obtain the reduced stiffnesses of the plies (Q_{ij}):

$$
\begin{aligned}
Q_{11} &= \frac{E_1}{1 - \nu_{12}\nu_{21,red}} \\
Q_{22} &= \frac{E_{2,red}}{1 - \nu_{12}\nu_{21,red}} \\
Q_{12} &= \frac{\nu_{12}E_{2,red}}{1 - \nu_{12}\nu_{21,red}} \\
Q_{66} &= G_{12,red}
\end{aligned}
\tag{4.21}
$$

By substituting equations 4.21 into the definition of the A matrix and applying the appropriate calculations, the laminate elastic properties (or engineering constants) E_x^{cr} and g_{xy}^{cr} can be derived as functions of the material properties and the crack distance D.

To obtain the associated Strain Energy Release Rate G^{cr}, as defined in equation 4.18, it is now required to differentiate E_x^{cr} and g_{xy}^{cr} with respect to $1/D$. Since E_x^{cr} and g_{xy}^{cr} rely on the terms of the A matrix (see Appendix C), the differentiation of these terms follows the subsequent process:

$$
\frac{\partial A_{ij}}{\partial(1/D)} = \sum_{k=1}^{n} \frac{\partial \left[\bar{Q}_{ij}\right]_k}{\partial(1/D)} (h_k - h_{k-1}) = \underbrace{\frac{\partial \left[\bar{Q}_{ij}\right]_c}{\partial(1/D)} (h_c - h_{c-1})}_{f(D)} + \underbrace{\sum_{\substack{k=1 \\ k \neq c}}^{n} \frac{\partial \left[\bar{Q}_{ij}\right]_k}{\partial(1/D)} (h_k - h_{k-1})}_{\neq f(D)}
\tag{4.22}
$$

By assuming that cracks are only present in the critical ply obtained by FPF method, only the $[Q_{ij}]$ corresponding to the cracked ply has a dependence on D (in case of more than one critical ply, the sumation of the cracked $[Q_{ij}]$). Subsequently, as shown in eq. 4.22, the differential of the A matrix term is going to be the differential of the Q matrix of the cracked ply. The differential of the rest of the Q's is 0. Subscript "c" indicates the cracked ply (or plies) as shown schematically in Fig. 4.3.

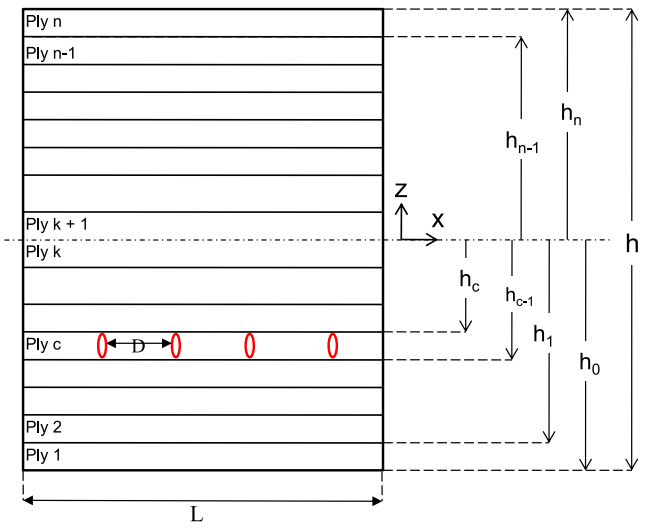

Figure 4.3: Arbitrary laminate with a cracked ply.

Differentiating $\left[\bar{Q}_{ij}\right]_c$ and denoting the operator $\partial\Omega/\partial(1/D)$ as Ω' to obtain simpler equations:

$$\begin{aligned}
\frac{\partial\left[\bar{Q}_{11}\right]_c}{\partial(1/D)} &= \left[\bar{Q}_{11}\right]'_c = \left[U'_1 + U_2 cos(2\theta) + U'_3 cos(4\theta)\right]_c \\
\frac{\partial\left[\bar{Q}_{22}\right]_c}{\partial(1/D)} &= \left[\bar{Q}_{22}\right]'_c = \left[U'_1 - U_2 cos(2\theta) + U'_3 cos(4\theta)\right]_c \\
\frac{\partial\left[\bar{Q}_{12}\right]_c}{\partial(1/D)} &= \left[\bar{Q}_{12}\right]'_c = \left[U'_4 - U'_3 cos(4\theta)\right]_c \\
\frac{\partial\left[\bar{Q}_{66}\right]_c}{\partial(1/D)} &= \left[\bar{Q}_{66}\right]'_c = \left[U'_5 - U'_3 cos(4\theta)\right]_c \\
\frac{\partial\left[\bar{Q}_{16}\right]_c}{\partial(1/D)} &= \left[\bar{Q}_{16}\right]'_c = \left[\tfrac{1}{2}U'_2 sin(2\theta) + U'_3 sin(4\theta)\right]_c \\
\frac{\partial\left[\bar{Q}_{26}\right]_c}{\partial(1/D)} &= \left[\bar{Q}_{26}\right]'_c = \left[\tfrac{1}{2}U'_2 sin(2\theta) - U'_3 sin(4\theta)\right]_c
\end{aligned} \tag{4.23}$$

where c is a ply of orientation θ w.r.t the global axis of the laminate and U_i is defined as:

$$\begin{aligned}
U'_1 &= \tfrac{3}{8}\left(Q'_{11} + Q'_{22}\right) + \tfrac{1}{4}Q'_{12} + \tfrac{1}{2}Q'_{66} \\
U'_2 &= \tfrac{1}{2}\left(Q'_{11} - Q'_{22}\right) \\
U'_3 &= \tfrac{1}{8}\left(Q'_{11} + Q'_{22}\right) - \tfrac{1}{4}Q'_{12} - \tfrac{1}{2}Q'_{66} \\
U'_4 &= \tfrac{1}{8}\left(Q'_{11} + Q'_{22}\right) + \tfrac{3}{4}Q'_{12} - \tfrac{1}{2}Q'_{66} \\
U'_5 &= \tfrac{1}{8}\left(Q'_{11} + Q'_{22}\right) - \tfrac{1}{4}Q'_{12} + \tfrac{1}{2}Q'_{66}
\end{aligned} \tag{4.24}$$

Differentiating now equation 4.21 and rearranging the terms:

$$\begin{aligned}
Q'_{11} &= \frac{\nu_{12}^2 E'_{2,red}}{\left(1 - \nu_{12}\nu_{21}\dfrac{E_{2,red}}{E_2}\right)^2} \\
Q'_{22} &= \frac{E'_{2,red}}{1 - \nu_{12}\nu_{21}\dfrac{E_{2,red}}{E_2}}\left[1 + \nu_{12}^2 \frac{\dfrac{E_{2,red}}{E_1}}{1 - \nu_{12}\nu_{21}\dfrac{E_{2,red}}{E_2}}\right]
\end{aligned} \tag{4.25}$$

$$Q'_{12} = \frac{\nu_{12} E'_{2,red}}{1 - \nu_{12}\nu_{21}\dfrac{E_{2,red}}{E_2}} \left[1 + \nu_{12}^2 \frac{\dfrac{E_{2,red}}{E_1}}{1 - \nu_{12}\nu_{21}\dfrac{E_{2,red}}{E_2}} \right] \tag{4.26}$$

$$Q'_{66} = G'_{12,red}$$

The last step consists of differentiating the expressions 4.1, 4.2 & 4.3 proposed by Socci & Kassapoglou [3] for the degraded properties:

$$\frac{\partial E_{2,red}}{\partial(1/D)} = -\frac{4D^2 E_2}{t_c^2} A_n \tag{4.27}$$

$$\frac{\partial G_{12,red}}{\partial(1/D)} = \frac{-8B'_n}{1 - \dfrac{8B_n\left(1 - \dfrac{\gamma_y}{\gamma_a}\right)\left[(1-8B_n)\left(1 - \dfrac{\gamma_y}{\gamma_a}\right) + \dfrac{\gamma_y}{\gamma_a}\right]}{1 - 8B_n + \dfrac{\gamma_y}{\gamma_a}}}$$

$$+ \frac{64\,(1-B_n)\,B_n\left(1 - \dfrac{\gamma_y}{\gamma_a}\right)\left[(1-8B_n)\left(1 - \dfrac{\gamma_y}{\gamma_a}\right) + \dfrac{\gamma_y}{\gamma_a}\right] B'_n}{\left[1 - \dfrac{8B_n\left(1 - \dfrac{\gamma_y}{\gamma_a}\right)\left[(1-8B_n)\left(1 - \dfrac{\gamma_y}{\gamma_a}\right) + \dfrac{\gamma_y}{\gamma_a}\right]}{1 - 8B_n + \dfrac{\gamma_y}{\gamma_a}}\right]^2 \left(1 - 8B_n + \dfrac{\gamma_y}{\gamma_a}\right)^2} \tag{4.28}$$

with:

$$A_n = \sum \frac{e^{\frac{\varphi_n D}{2}}\left(e^{\varphi_n D} - 1\right)\left[\frac{1}{D}\left(e^{2\varphi_n D} - 1\right) - 2\varphi_n e^{\varphi_n D}\right]}{\left[2\varphi_n e^{\varphi_n D} + \frac{1}{D}\left(e^{2\varphi_n D} - 1\right)\right]^2} \tag{4.29}$$

$$B_n = \sum \frac{e^{0.5k_n D} + e^{k_n D} e^{-0.5k_n D}}{\left(1 + e^{k_n D}\right)(n\pi)^2} \tag{4.30}$$

$$B'_n = \sum \frac{k_n e^{0.5k_n D\left(e^{k_n D} - 1\right)}}{\left(1 + e^{k_n D}\right)^2 (n\pi)^2} D^2 \tag{4.31}$$

where $\varphi_n = k_n = n\pi/t_c$, D is the crack spacing, t_c is the thickness of the cracked ply, γ_a is the applied shear in the cracked ply, γ_Y is the yield shear strain of the ply and E_1, E_2, G_{12} and

ν_{12} the pristine properties of the ply.

Finally, by substituting equations 4.19-4.31 into equation 4.18, the Strain Energy Release Rate for crack propagation in a general symmetric laminate can be obtained. The resulting equation is expressed in terms of the A matrix and its derivatives (A'_{ij}).

$$
\begin{aligned}
G^{cr} = -\frac{1}{2}\varepsilon_x^2 \Bigg\{ & A'_{11} + A'_{12}\left(\frac{A_{26}A_{16}-A_{12}A_{66}}{A_{22}A_{66}-A_{26}^2}\right) + A_{12}\left(\frac{A'_{26}A_{16}+A_{26}A'_{16}-A'_{12}A_{66}-A_{12}A'_{66}}{A_{22}A_{66}-A_{26}^2}\right) \\
& -A_{12}\left[\frac{\left(A_{26}A_{16}-A_{12}A_{66}\right)\left(A'_{22}A_{66}+A_{22}A'_{66}-2A_{26}A'_{26}\right)}{\left(A_{22}A_{66}-A_{26}^2\right)^2}\right] + A'_{16}\left(-\frac{A_{16}}{A_{66}} + \frac{A_{26}A_{12}A_{66}-A_{26}^2A_{16}}{A_{22}A_{66}^2-A_{26}^2A_{66}}\right) \\
& +A_{16}\left[-\frac{A'_{16}}{A_{66}} + \frac{A_{16}A'_{66}}{A_{66}^2} + \frac{A'_{26}A_{12}A_{66}+A_{26}A'_{12}A_{66}+A_{26}A_{12}A'_{66}-2A_{26}A'_{26}A_{16}-A_{26}^2A'_{16}}{A_{22}A_{66}^2-A_{26}^2A_{66}}\right] \\
& -A_{16}\left[\frac{\left(A_{26}A_{12}A_{66}-A_{26}^2A_{16}\right)\left(A'_{22}A_{66}^2+2A_{22}A_{66}A'_{66}-2A_{26}A'_{26}A_{66}-A_{26}^2A'_{66}\right)}{\left(A_{22}A_{66}^2-A_{26}^2A_{66}\right)^2}\right]\Bigg\} \\
& -\frac{1}{2}\gamma_{xy}^2 \Bigg\{ A'_{66} - \frac{2A_{26}A'_{26}}{A_{22}} + \frac{A_{26}^2A'_{22}}{A_{22}^2} + \frac{2\left(A'_{12}A_{16}A_{26}A_{22}+A_{12}A'_{16}A_{26}A_{22}+A_{12}A_{16}A'_{26}A_{22}+A_{12}A_{16}A_{26}A'_{22}\right)}{A_{11}A_{22}^2-A_{12}^2A_{22}} \\
& -\frac{2\left(A_{12}A'_{12}A_{26}^2+A_{12}^2A_{26}A'_{26}+A_{16}A'_{16}A_{22}+A_{16}^2A_{22}A'_{22}\right)}{A_{11}A_{22}^2-A_{12}^2A_{22}} \\
& -\frac{\left(2A_{12}A_{16}A_{26}A_{22}-A_{12}^2A_{26}^2-A_{16}^2A_{22}^2\right)\left(A'_{11}A_{22}^2+2A_{11}A_{22}A'_{22}-A_{12}A'_{12}A_{22}-A_{12}^2A'_{22}\right)}{\left(A_{11}A_{22}^2+A_{12}^2A_{22}\right)^2}\Bigg\}
\end{aligned}
\tag{4.32}
$$

4.3.2. Cross-ply

A cross-ply laminate is a special case of the formulation presented before. In a cross-ply laminate, the composition consists of plies oriented at 0º and 90º, resulting in a balanced structure. Figure 4.4 provides a schematic representation where t_c represents the thickness of the 90º plies, t_1 represents half the thickness of the 0º plies, L denotes the length and D indicates the distance between cracks. In the case of a cross-ply laminate subjected to uniaxial tension or tension combined with shear, the 90º plies are always the critical layer where matrix cracks will first appear. Note that in this scenario, t_c can refer to a thick 90º ply or a 90º plies block but esentially will exhibit identical behavior.

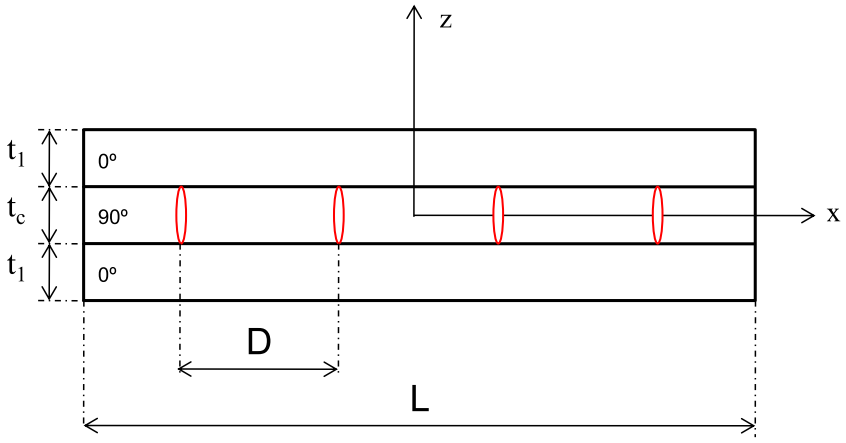

Figure 4.4: Cross-ply laminate with cracks in the 90º ply.

Recalling that for symmetric and balanced laminates $B_{ij} = 0$ and $A_{16} = A_{26} = 0$ respectively, the longitudinal and shear modulus of the laminate can be defined as:

$$E_x = \frac{1}{2t_1 + t_c}\left[A_{11} - \frac{A_{12}^2}{A_{22}}\right] \tag{4.33}$$

$$g_{xy} = \frac{A_{66}}{2t_1 + t_c} \tag{4.34}$$

By substituting the terms of the A matrix, considering the degradation of properties in the 90º ply using equation 4.21 and assuming the pristine properties for the 0º ply, we can calculate the axial and shear moduli of the cracked laminate:

$$E_x^{cr} = \frac{1}{2t_1 + t_c}\left[\frac{2E_1}{1 - \nu_{12}\nu_{21}}t_1 + \frac{2E_{2red}}{1 - \nu_{12}\nu_{21red}}t_c + \frac{\left(\frac{2\nu_{12}E_2}{1 - \nu_{12}\nu_{21}}t_1 + \frac{\nu_{12}E_{2red}}{1 - \nu_{12}\nu_{21red}}t_c\right)^2}{\frac{2E_2}{1 - \nu_{12}\nu_{21}}t_1 + \frac{E_1}{1 - \nu_{12}\nu_{21red}}t_c}\right] \tag{4.35}$$

$$g_{xy}^{cr} = \frac{1}{2t_1 + t_c}\left[2t_1 G_{12} + t_c G_{12,red}\right] \tag{4.36}$$

Differentiating eq. 4.35 & 4.36, introducing the result in equation 4.18 and rearranging the terms, the Strain Energy Release Rate expression G^{cr} for a cross-ply under shear and tension is obtained:

$$G^{cr} = \frac{2E_2\nu_D}{1 - \nu_{12}\nu_{21}}\varepsilon_x^2\left(\frac{D}{t_c}\right)^2 A_n\left[1 + \frac{\nu_D\nu_{12}^2}{1 - \nu_{12}\nu_{21}}\frac{E_{2,red}}{E_2}\frac{E_2}{E_1}\right.$$

$$-2\nu_{12}^2\left(\frac{2\frac{t_1}{t_c}+\nu_D\frac{E_{2,red}}{E_2}}{2\frac{t_1}{t_c}+\nu_D\frac{E_1}{E_2}}\right)\left(1+\frac{\nu_D\nu_{12}^2}{1-\nu_{12}\nu_{21}}\frac{E_{2,red}}{E_2}\frac{E_2}{E_1}\right)+\frac{\nu_D\nu_{12}^4}{1-\nu_{12}\nu_{21}}\left(\frac{2\frac{t_1}{t_c}+\nu_D\frac{E_{2,red}}{E_2}}{2\frac{t_1}{t_c}+\nu_D\frac{E_1}{E_2}}\right)^2\Bigg]$$

$$+\gamma_{xy}G_{12}\left\{\frac{-8B_n'}{1-\frac{8B_n\left(1-\frac{\gamma_y}{\gamma_a}\right)\left[(1-8B_n)\left(1-\frac{\gamma_y}{\gamma_a}\right)+\frac{\gamma_y}{\gamma_a}\right]}{1-8B_n+\frac{\gamma_y}{\gamma_a}}}\right.$$

$$\left.+\frac{64\,(1-B_n)\,B_n\left(1-\frac{\gamma_y}{\gamma_a}\right)\left[(1-8B_n)\left(1-\frac{\gamma_y}{\gamma_a}\right)+\frac{\gamma_y}{\gamma_a}\right]B_n'}{\left[1-\frac{8B_n\left(1-\frac{\gamma_y}{\gamma_a}\right)\left[(1-8B_n)\left(1-\frac{\gamma_y}{\gamma_a}\right)+\frac{\gamma_y}{\gamma_a}\right]}{1-8B_n+\frac{\gamma_y}{\gamma_a}}\right]^2\left(1-8B_n+\frac{\gamma_y}{\gamma_a}\right)^2}\right\} \tag{4.37}$$

E_1, E_2, G_{12} are the pristine properties of the laminate, t_1 and t_c the thicknesses of the 0º and 90º plies respectively, γ_a is the applied shear on the cracked ply, γ_y the yield shear strain, ε_x & γ_{xy} the longitudinal and shear strain applied to the laminate and ν_D is defined as:

$$\nu_D = \frac{1-\nu_{12}\nu_{21}}{1-\nu_{12}\nu_{21red}} = \frac{1-\nu_{12}\nu_{21}}{1-\nu_{12}\nu_{21}\frac{E_{2red}}{E_2}} \tag{4.38}$$

4.4. Parameters study

This section provides an analysis of the Strain Energy Release Rate (SERR) expressions derived for both symmetrical laminates and cross-plies with a focus on examining how various parameters influence the resulting curves. Figure 4.5 illustrates the fundamental shape of G^{cr} using a cross-ply under tension as an example. Note that the graph should be read from right to left for increasing loading. A pristine laminate will have $D \to \infty$ and increasing loads will generate more cracks, hence the crack distance D will decrease.

For large values of D, it is observed that G^{cr} remains constant until D reaches a critical value of $D = 2.966t_c$. This behavior is attributed to the crack initiation process explained in

Section 4.2, where cracks start forming at $r = \pi D/t_c = 9.3167$ (refer to Figure 4.1). Prior to this point, when D is larger, cracks are scattered and randomly distributed and the material properties remain unaffected. Consequently, as there is no increase in the cracked area and the properties remain constant, the value of G^{cr} remains constant and equal to $G^{cr}(D = 2.966t_c)$ (refer to equation 4.3.2).

Beyond the critical point mentioned, for smaller values of D, G^{cr} exhibits an increasing trend until it reaches a maximum after which, it starts to decline as the distance between cracks decreases. This behavior signifies that the laminate is capable of dissipating a significant amount of energy when the crack spacing is relatively large (but smaller than $D = 2.966t_c$). However, as the distance between cracks decreases, the efficiency of energy dissipation diminishes. Hence, there exists a tendency for the formation of cracks to decrease with a decrease in their spacing.

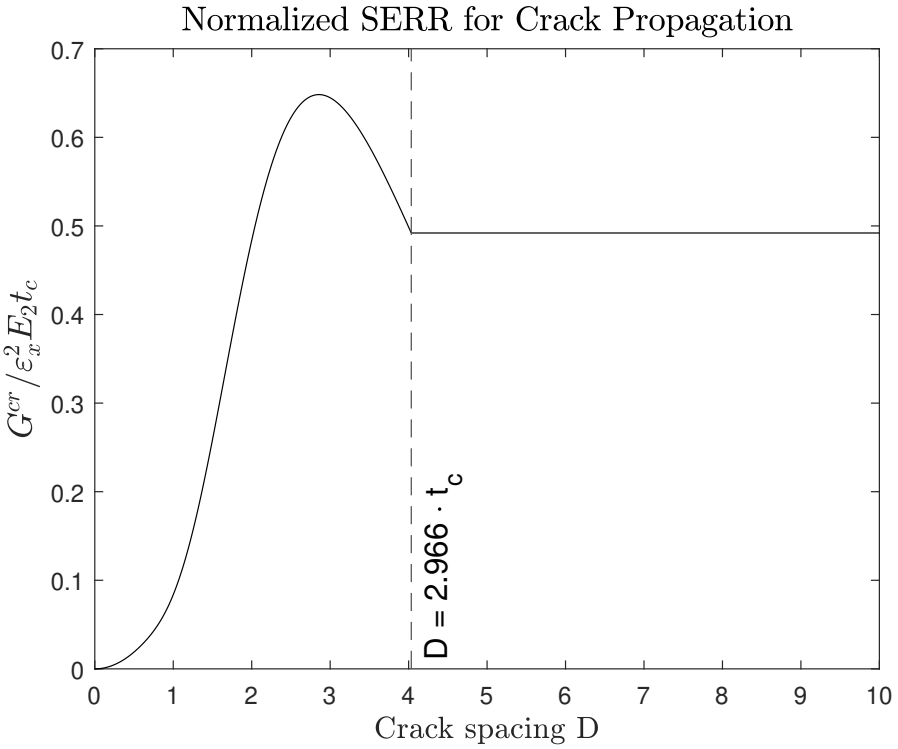

Figure 4.5: UT-E500/Epikote RIMR235 $[0/90_2]_s$ laminate under tension.

Figure 4.6 shows different cross-plies under tension and illustrates the effect of increasing the number of 90º plies, which effectively results in an increase in t_c. The behavior of the 90º ply block resembles that of a thick ply, meaning that the curve's behavior remains consistent whether the thickness of the 90º ply is increased or more 90º plies are added. As shown in Fig. 4.6, increasing the number of 90º plies increases the G^{cr} values and also shifts the curves towards the right. The width of the curve's maximum region also expands, suggesting a greater likelihood of crack occurrence across a wider range of D. Furthermore, the critical point where cracks initiate, $D = 2.966t_c$, also shifts to the right, indicating that cracks are more likely to form earlier in cross-plies with thicker 90º plies. In general, the curves indicate that it is more likely for cracks to initiate and propagate in cross-plies with thicker 90º blocks. This is in accordance with the numerical findings of Wang [65] and experimental campaign conducted by Crossman et al. [66].

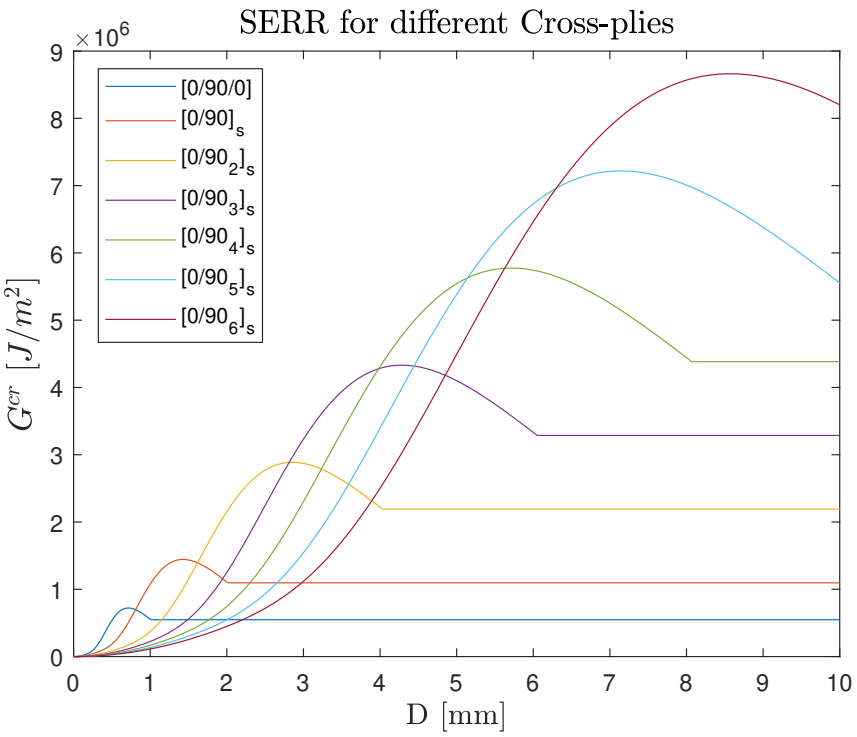

Figure 4.6: Influence of t_c in UT-E500/Epikote RIMR2 cross-plies under a tension of $\varepsilon_x = 0.5$.

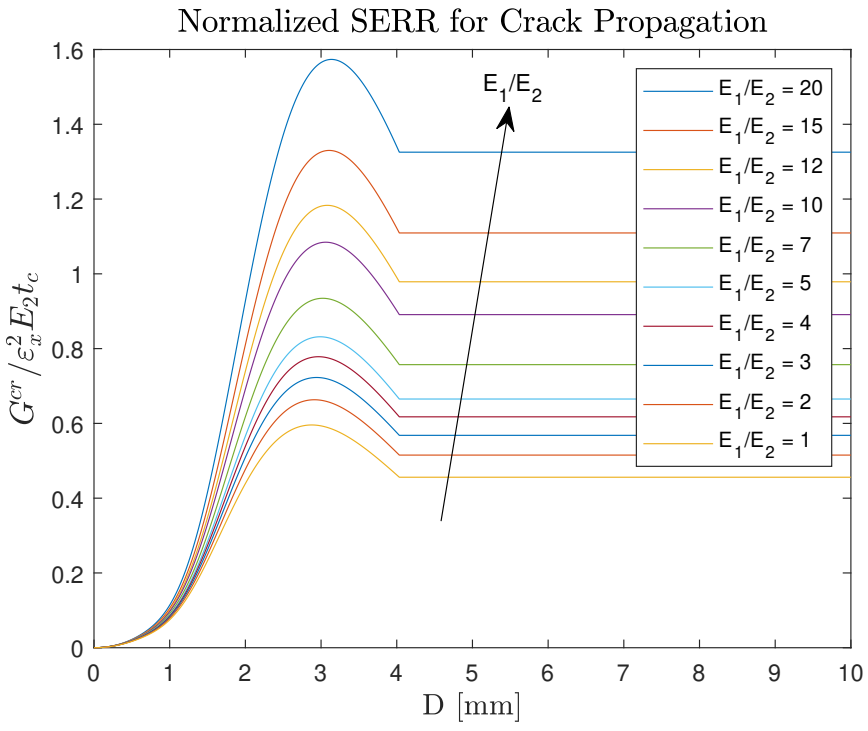

Figure 4.7: Influence of E_1/E_2 in a UT-E500/Epikote RIMR2 $[0/90_2]_s$ laminate under tension.

The properties of the plies also have an influence on G^{cr}, as evident from the equation derived for a cross-ply (see eq. 4.3.2). Figure 4.7 illustrates a $[0/90_2]_s$ laminate under tension

with varying ratios of the ply Young's moduli E_1/E_2. G^{cr} is normalized using the applied tensile strain in the laminate ε_x, the transverse Young's modulus E_2 and the 90º ply thickness t_c. It is observed that higher E_1/E_2 ratios result in greater values of the normalized SERR. The critical 90º ply (or plies) in a cross-ply under tension are subjected to local transverse strain hence it is more likely to experience crack initiation and propagation if their transverse properties are lower (i.e., higher E_1/E_2 ratio), thereby leading to a higher SERR. Additionally, it is interesting to note that crack initiation occurs at the same crack spacing D because, as explained earlier, this value in a cross-ply depends solely on the 90º ply thickness.

The relative ratio between the thicknesses of the 90º and 0º plies also has an impact on the curve, although to a lesser extent. This effect is demonstrated in Figure 4.8, where various ratios of t_1/t_c are employed while keeping t_c constant. It is observed that as the t_1/t_c ratio increases, G^{cr} decreases. This behavior can be attributed to the fact that the 0º plies are not prone to cracking. Therefore, increasing the thickness of these plies does not significantly alter the likelihood of crack initiation or propagation. Since G^{cr} is based on the study of cracks and their influence on the 90º plies, the impact of varying the t_1/t_c ratio on G^{cr} is less pronounced.

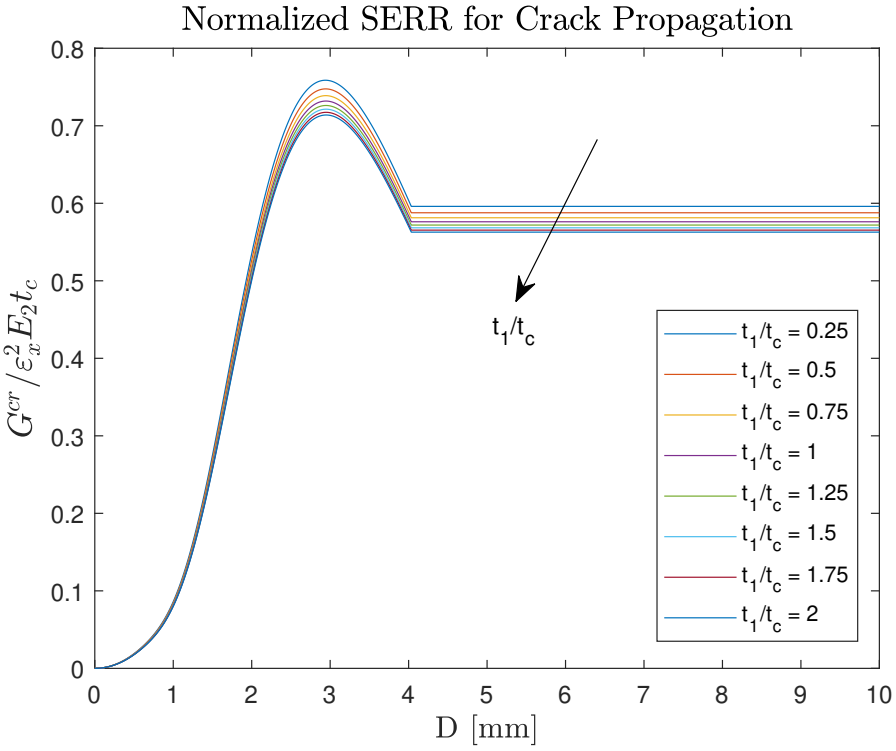

Figure 4.8: Influence of t_1/t_c in a UT-E500/Epikote RIMR2 $[0/90_2]_s$ laminate under tension.

The Strain Energy Release Rate (SERR) can be computed for symmetrical laminates even when the critical ply is not perpendicular to the longitudinal axis. In such cases, the ply experiences a combination of local shear and transverse tension, with the proportions varying based on the loading conditions (tension or tension + shear) and the angle of the ply. Figure 4.9 illustrates the relationship between the Strain Energy Release Rate and the crack spacing D for $[0/\theta_2]_s$ laminates subjected to $\epsilon_x = 0.05$. It can be observed that laminates with angles ranging from $\theta = 90$ to $\theta = 60$ exhibit behavior similar to that of a cross-ply configuration although with smaller values. This is because these laminates experience comparatively lower levels of transverse strain, which is the primary driver for crack initiation. Due to the nonlinear

nature of shear strain-stress response, a higher shear strain is required to initiate a new crack compared to transverse strain [3]. Consequently, laminates where the critical ply experiences more local shear are less prone to matrix propagation, resulting in lower values of G^{cr} for lower θ angles, as depicted in Fig. 4.9.

The $[0/10_2]_s$ configuration represents an extreme case where both transverse strain and shear strain are very low, leading to an extremely low G^{cr} when compared to other cases. As a result, this laminate is highly unlikely to develop cracks under tension. This observation aligns with the general understanding that $[0/10_2]_s$ closely resembles a pure unidirectional block, which exhibits high resistance to cracking under pure tension. Furthermore, it is worth noting that the shape of the SERR changes for small D values, particularly for lower angles. This phenomenon arises from the highly nonlinear nature of shear stress under such conditions [3].

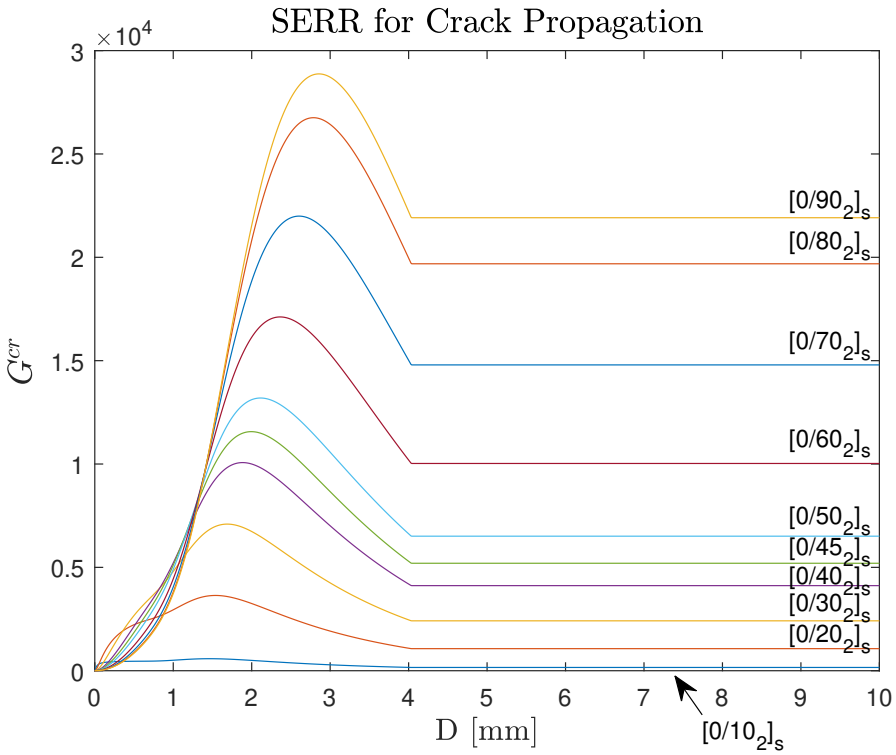

Figure 4.9: G^{cr} for UT-E500/Epikote RIMR2 $[0/\theta_2]_s$ laminate under tension.

In general, establishing direct relationships for symmetrical laminates is challenging due to the complexity of interactions among the terms in the equation. By examining equation 4.32, it becomes evident that all terms of the A matrix and its derivatives are involved, including the expressions and derivatives of the reduced ply properties (refer to equations 4.27 - 4.31). The focus of the study in this section was primarily on laminates under tension (ε_X). This approach aimed to achieve more straightforward relationships between the parameters (for instance, the second term of equations 4.32 & 4.3.2 are null under pure tension). Additionally, the validation of the models throughout this thesis revolves around utilizing tensile tests obtained from relevant literature. Obtaining accurate crack distances or delamination lengths in relation to loads is not straightforward. Hence, most experimental tests involve simple tensile tests that gather information for a specific ply.

The ideas presented in this section about the SERR for crack propagation (G^{cr}) can be summarized as follows:

- G^{cr} significantly increases with an increase in t_c (critical ply thickness).
- Increasing t_c (critical ply thickness) shifts the graph towards longer crack spacings.
- G^{cr} increases with an increase in the ratio E_1/E_2.
- G^{cr} mildly reduces with an increase in t_1.
- G^{cr} increases when there is a greater relative angle difference on a $[0/\theta_2]$ laminate.
- The critical point at which G^{cr} initiates is solely dependent on t_c.
- $G^{cr} = f(E_1, E_2, \nu_{12}, t_c, t_1, D, \varepsilon_x)$ for a cross-ply under tension.
- $G^{cr} = f(E_1, E_2, G_{12}, \nu_{12}, t_c, t_1, D, \varepsilon_x, \gamma_{xy}, \gamma_a)$ for a symmetrical laminate under tension and shear.

4.5. Validation

The validation process will now assess the model proposed by Socci and Kassapoglou [3] in section 4.2. The primary objective of this study is to accurately predict the initiation and growth of delamination resulting from matrix cracks. Therefore, it is crucial to establish the accuracy of the model in predicting cracks because any inaccuracies could affect the reliability of delamination onset predictions based on this model. The transverse in-situ strength Y_{is}^{t} is a critical parameter in the model because it defines how the cracks are going to behave in the material. This value is not always found in the papers and sometimes has to be estimated (see Appendix A). Thickness effects are accounted for by changing the in-situ transverse strengths as necessary and the relative angle between adyacent plies is also taken into account [67]. It is worth mentioning that the model has already undergone extensive validation for laminate property degradation [3]. However, in this case, it will be compared with experimental data on the crack spacing D and/or crack density $1/D$.

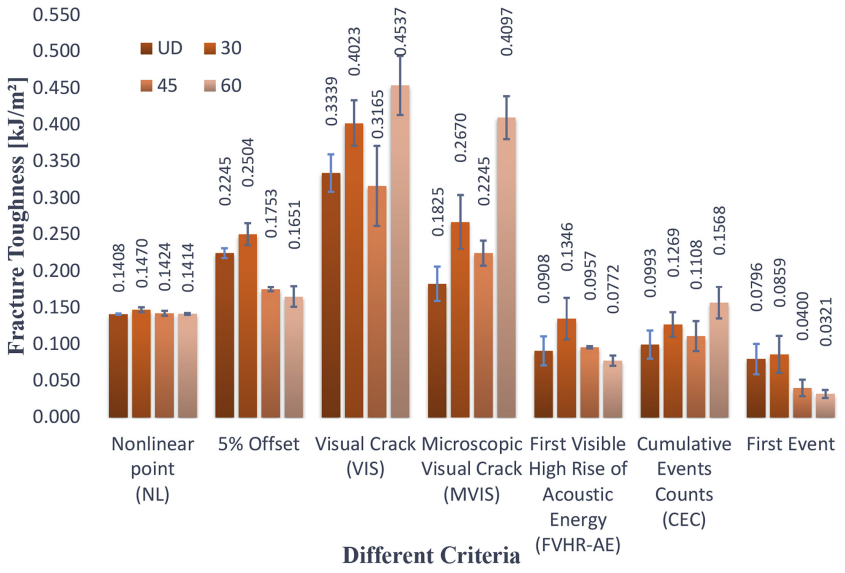

Figure 4.10: Fracture toughness obtained with different techniques. Obtained from [68].

It is important to acknowledge that obtaining crack spacing data is not a straightforward task. The distances involved are very small, requiring precise measurement methods. Each technique employed for measurement presents its own challenges and inherent inaccuracies.

Proper utilization of these techniques relies on a comprehensive understanding of the laminate under testing and the equipment being used. For instance, Figure 4.10 illustrates different techniques employed to measure fracture toughness, which essentially involves measuring a crack. Ideally all techniques should yield identical results. However, considering for example the measurements of a UD ply (depicted in darker red), the values obtained from these methods span a considerable range, from 0.076 KJ/m^2 to 0.3339 KJ/m^2 which presents a significant disparity. This measurement pertains to the initial crack identified within the laminate. Consider the implications of consistently tracking and measuring cracks during the propagation. Consequently, caution must be exercised when comparing a model with experimental data, taking into account the differences arising from the techniques employed and the inherent error and complexity associated with the measurement.

4.5.1. Carraro et al. [44]

Carraro et al. [44] conducted experiments on two cross-ply configurations of glass fiber UT-E500/Epikote RIMR235. They measured the crack density as a function of the applied tensile load. The obtained results, along with the model described in section 4.2, are presented below. The material properties used in the analysis are provided in Appendix A.

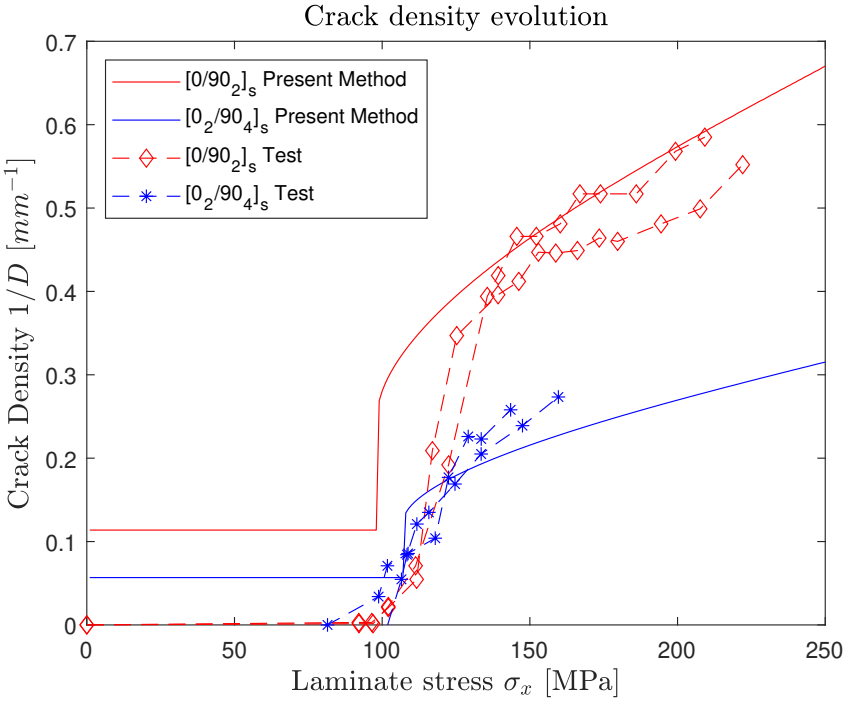

Figure 4.11: Crack propagation of a cross-ply under uniaxial tension.

Figure 4.11 illustrates the model's prediction of the crack density, which demonstrates good agreement, particularly after crack initiation. In the case of the $[0/90_2]s$ configuration, the model slightly overestimates the crack density, while for the $[0_2/90_4]s$ configuration, it underpredicts the crack density at higher loads. It is evident that the model does not perfectly capture the accurate initiation of cracks. The abrupt jumps in crack density around 100 MPa correspond to the critical strain at which the stress between cracks equals the in-situ strength $Y^t is$ (as explained in section 4.2). The accuracy of initiation predictions heavily relies on the value of $Y^t is$, which was not provided by the author. Hence, a value from a similar material was used (refer to Appendix A), potentially explaining the less accurate prediction. Typically,

Y_{is}^t is determined through experimental tests, although approximations can be made using the ply strength Y^t. A commonly used approximation, assuming the ply is sufficiently thick, is $Y_{is}^t = 1.12\sqrt{2}Y^t$ [67].

To address this issue, a Maximum Stress First Ply Failure (FPF) criterion is proposed to determine the load at which cracks initiate, followed by assuming linear multiplication until reaching the critical crack density obtained from Socci & Kassapoglou's model. By employing this approach, a new prediction is obtained, as demonstrated in Figure 4.12. The linear prediction starts from the FPF load at $1/D = 0$ and progresses towards the critical crack density, which occurs when the transverse stress between cracks equals Y_{is}^t. It is important to note that Socci & Kassapoglou [3] did not assume that cracks initially appear at this specific point. Instead, they assumed that cracks begin with uniform spacing at that point, while prior to that, cracks nucleate randomly. This assumption worked well in their study for predicting the degradation of laminate properties because before reaching the critical point, the crack spacing is sufficiently large to preserve the material properties. Hence, a more precise approximation was not required. However, in our case, the focus is specifically on the cracks. Therefore, by combining the FPF criterion with Socci & Kassapoglou's model, the combined method performs very well, as depicted in Figure 4.12.

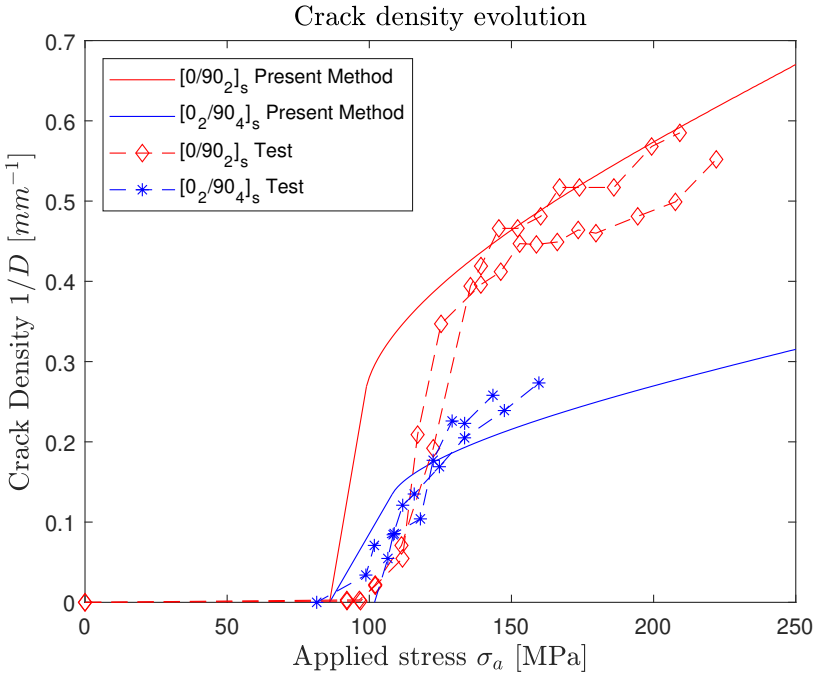

Figure 4.12: Crack propagation of a cross-ply under uniaxial tension combining a FPF with the proposed model.

Representing the data in terms of crack spacing D instead of crack density $1/D$ provides valuable insights, as it allows for a broader range of lower D values to be observed. In Figure 4.13, the relationship between crack spacing and stress is depicted, revealing a phenomenon commonly reported in the literature known as crack saturation [21, 69, 70]. When the load is continuously increased, a point is reached where no further cracks initiate, resulting in a relatively constant number of cracks. This saturation effect is evident for $\sigma_x > 150MPa$ and is observed under both quasi-static loading and fatigue conditions [69, 70]. This crack saturation usually occurs after the first delamination is detected which supported by the reported findings of Carraro et al. [44]. This concept of crack saturation will be utilized later in assumptions regarding delamination growth.

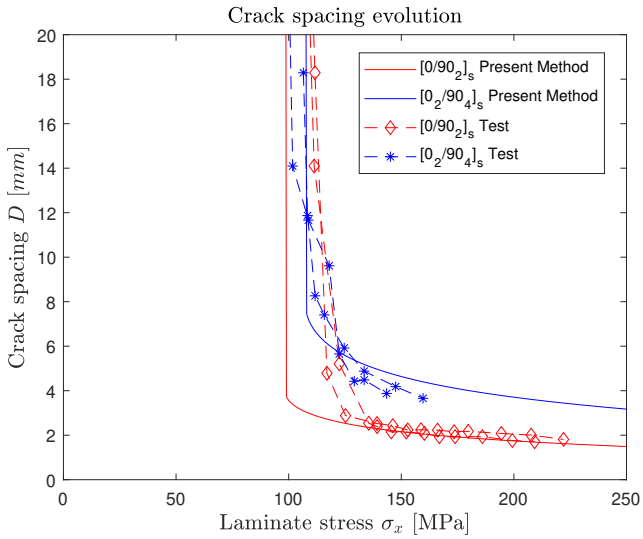

Figure 4.13: Crack propagation of a cross-ply under uniaxial tension combining a FPF criteria with the proposed model.

4.5.2. Chou et al. [71] & Crossman et al. [66]

The experiments conducted by Crossman et al. [66] and by Chou et al. [71] (both papers based on the same US military report) focused on investigating the occurrence of matrix cracks and delaminations in AS/3501-6 $[\pm 25/90_n]_s$ graphite-epoxy laminates subjected to both quasi-static and fatigue loading conditions. The study involved applying uniaxial tension to the laminates and evaluating the crack density within the 90º ply block. Their data, along with our proposed model, are presented in Figure 4.14. The graph incorporates already the assumption that the initial cracks initiate at the load determined by the Max. Stress FPF criterion and progress linearly until reaching the critical value defined by Socci & Kassapoglou's model.

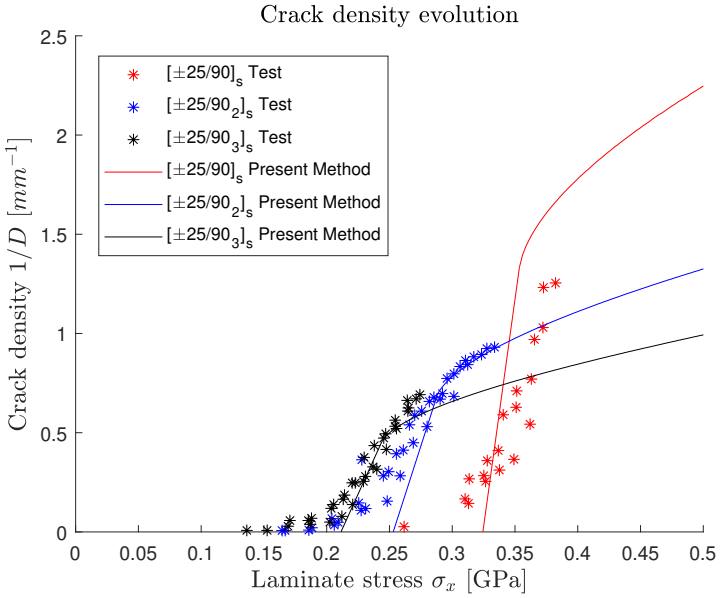

Figure 4.14: Crack density evolution for $[\pm 25/90_n]_s$ laminates under uniaxial loading.

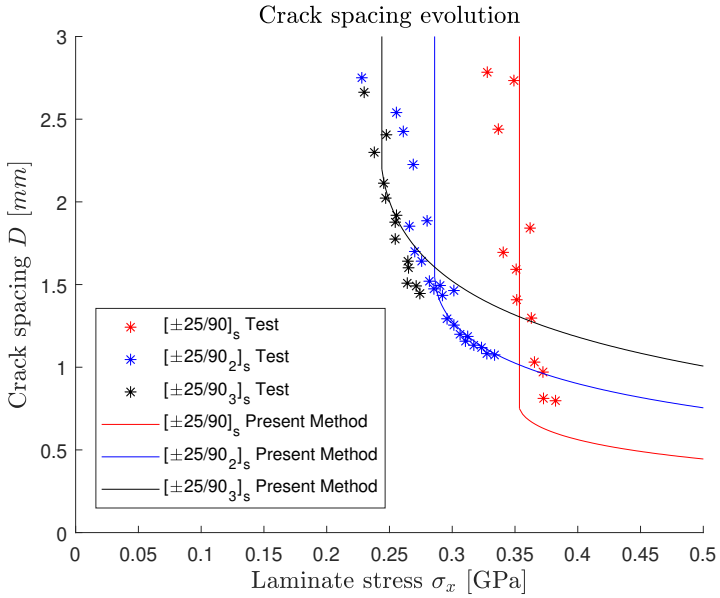

Figure 4.15: Crack spacing evolution for $[\pm 25/90_n]_s$ laminates under uniaxial loading.

The correlation between the test results and the model is reasonably good; however, it is worth noting that the critical point where the model becomes effective is near the last measured data points. Additionally, most of the data points fall within the assumed linear portion, particularly for the [±25/90] configuration where almost all points lie within this range. The authors of the study reported that the $[\pm 25/90_3]$ and $[\pm 25/90_2]$ laminates initially experienced matrix cracks, followed by observed edge delaminations. However, in the case of the [±25/90] layup, edge delaminations in the midplane were observed first. This observation was attributed to complex interactions between different crack modes and clusters of manufacturing defects [22, 71].

Examining the data in relation to the crack spacing D in Figure 4.15, it is evident that the cracks tend to continue multiplying. Unlike Figure 4.13, it does not appear to be a saturation of cracks in this case. This suggests that the cracks could still propagate, which could explain why all the data points are concentrated within the linear region of the predictive model.

4.5.3. Nairn et al. [41, 72]

Nairn et al. conducted an extensive experimental study for different cross-ply configurations using different materials: Hercules AS4/3501-6, DuPont Avimid K-Polymer/IM6 and Fiberite 977-2/T300-1800. Some of the results with the corresponding model prediction as shown below in order to validate the precision of crack prediction.

Figures 4.16 & 4.17 depict laminates with a $[0_2/90_n]_s$ configuration, showing relatively accurate predictions. At lower loads, the model tends to overestimate the density of cracks, while for higher loads, the predictions become less conservative. By transforming the crack density to crack spacing, it is observed that both the test data and predictions converge to a constant value, indicating crack saturation occurring at approximately 2.1 mm. Generally, information related with smaller crack spacings (higher crack densities) is more significant. Therefore, plotting the crack spacing (D) against the load provides more insights into the trends because a smaller crack density range can contain all the test points. Let us consider two ranges of crack density: [0 - 0.3] mm^{-1} and [0.3 - 0.6] mm^{-1}, which initially appear equally

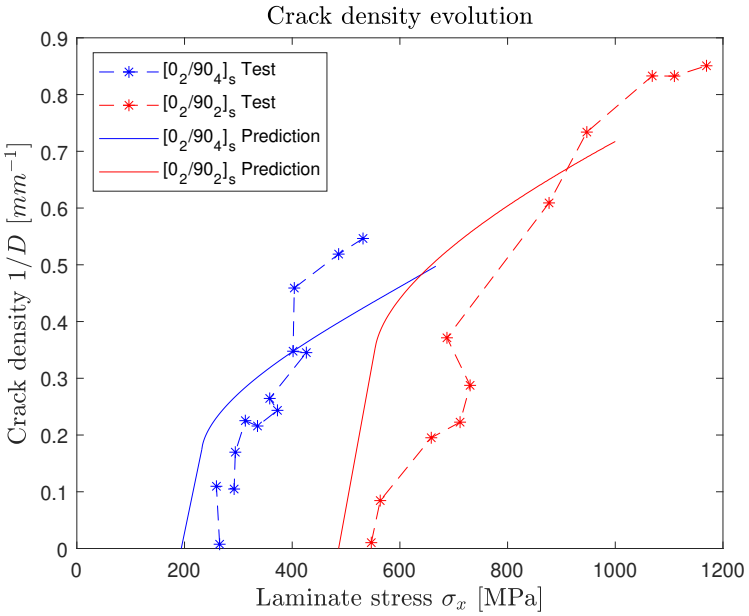

Figure 4.16: Crack density evolution for $[0_2/90_n]_s$ laminates under uniaxial loading.

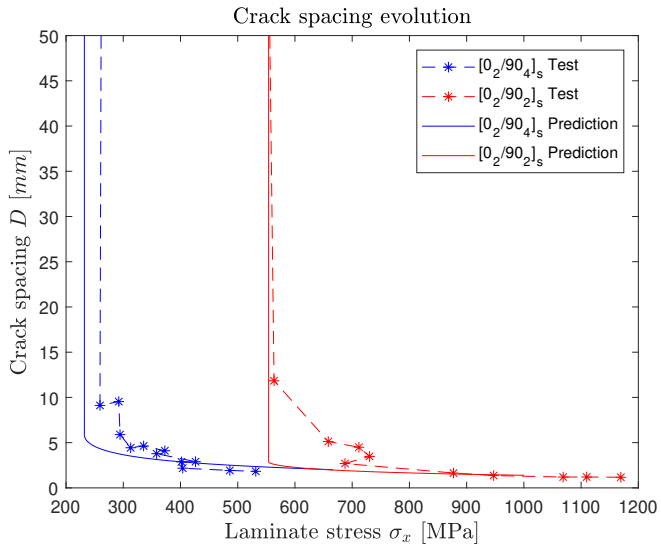

Figure 4.17: Crack spacing evolution for $[0_2/90_n]_s$ laminates under uniaxial loading.

important in Figure 4.16. When transformed into crack spacing (D), these ranges correspond to [3.33 - ∞] and [1.66 - 3.33] mm, respectively. The range [1.66 - 3.33] is of greater interest as it covers the laminate when it has a higher degree of degradation, whereas the other range represents a state closer to a pristine laminate. This disparity explains why the crack saturation is easily distinguishable in Figure 4.17 compared to Figure 4.16.

Figures 4.18 and 4.19 exhibit similar cross-ply configurations as previously discussed, but this time utilizing DuPont Avimid K-Polymer/IM6 UD plies. Once more, it's important to remind that the crucial transverse in-situ strength has been estimated by utilizing data from a comparable material (refer to Appendix A). Once again, there is a strong correlation, especially for lower loads. However, for higher crack densities, the model tends to underestimate the

occurrence of cracks. It is important to note that even though the predictions appear inaccurate within the crack density range of [0.7 - 1], this range actually corresponds to a crack spacing range of [1 - 1.43] mm. Therefore, considering such small distances, the model demonstrates remarkable precision. In a similar fashion to the other cross-ply cases, Figure 4.19 demonstrates that the crack spacing stabilizes at a value of approximately 1. It is noteworthy that for thicker 90º ply blocks, the saturation of crack spacing occurs at longer crack spacings (lower crack densities) for lower loads. This observation may suggest the formation of delamination that obstructs crack propagation occurs before for thicker 90º ply cross-plies [70].

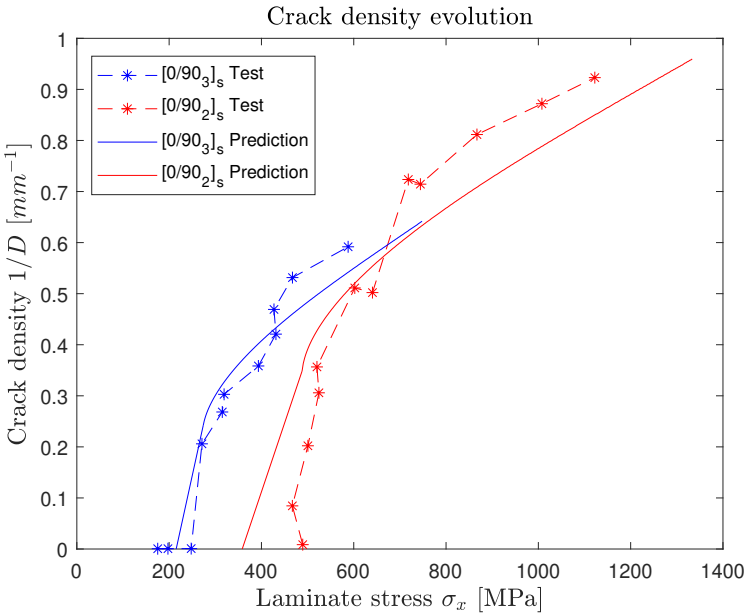

Figure 4.18: Crack density evolution for $[0/90_n]_s$ laminates under uniaxial loading.

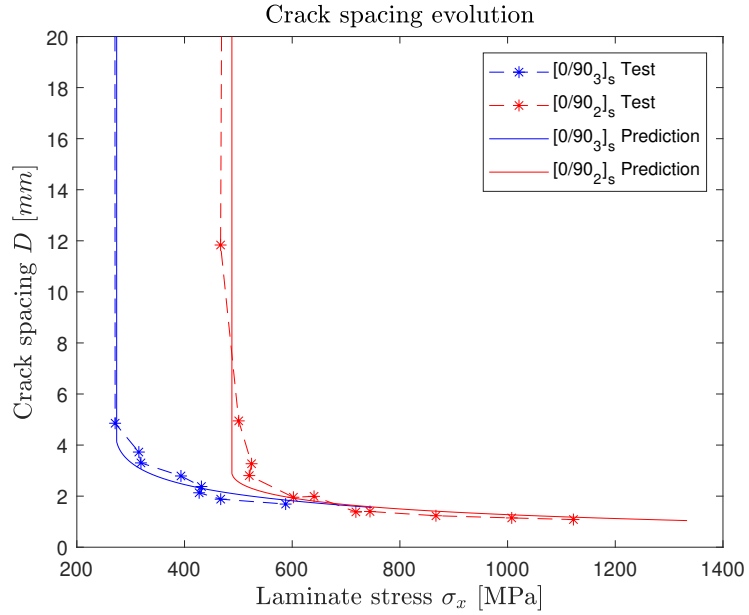

Figure 4.19: Crack spacing evolution for $[0/90_n]_s$ laminates under uniaxial loading.

Nairn et al. conducted additional tests on cross-ply laminates where the outer plies were

set at a 90º orientation, while varying the thickness of the embedded 0º plies. Test results for Hercules AS4/3501-6 plies are shown in Figures 4.20 and 4.21. One notable observation is the inaccuracies in the linear portion of the prediction, particularly for the $[90/0_2]s$ and $[90/0_4]s$ configurations. The maximum stress criteria used to determine the FPF load fail to accurately predict the initiation of cracks in the outer 90º plies. Surprisingly, cracks start at the same applied stress for the $[90/0_n]s$ configuration, which is somewhat peculiar considering that it would mean that the 90º have the same local transverse strain. In this case, the estimation of the in-situ strength for the outer ply is determined using the equation $Y_{is}^t(outer\ ply) = 1.79\sqrt{G_{ic}/\pi t \Delta_{22}}$, where $\Delta_{22} = 2(1/E_2 - \nu_{21}^2/E_1)$, t represents the thickness and G_{ic} is the microcrack fracture toughness mentioned in [41].

The critical point occurring after the linear portion occurs at the same crack density/spacing for all tested laminates. This is because that point corresponds to $D = 2.966t_c$, as explained in section 4.2. Since the critical 90º ply where the cracks are generated has the same thickness in all laminates, the critical D point remains consistent. As depicted in Fig. 4.20, the model's shape accurately follows the trends of all laminates after the critical point. Additionally, Fig. 4.21 demonstrates the stabilization of crack spacing D, suggesting saturation of cracks. Thicker laminates exhibit longer crack spacing to which they tend. For the same stress, the crack spacing in the 90º ply will be higher for thicker laminates due to the lower local transverse strain, resulting in fewer cracks being generated. Fig. 4.21 also clearly illustrates the overprediction of crack initiation for the $[90/0_2]_s$ and $[90/0_4]_s$ configurations. This overprediction is problematic since it does not provide a conservative estimate. However, one could argue that accurate predictions for lower D values are preferable as high crack spacing may have minimal impact on laminate properties.

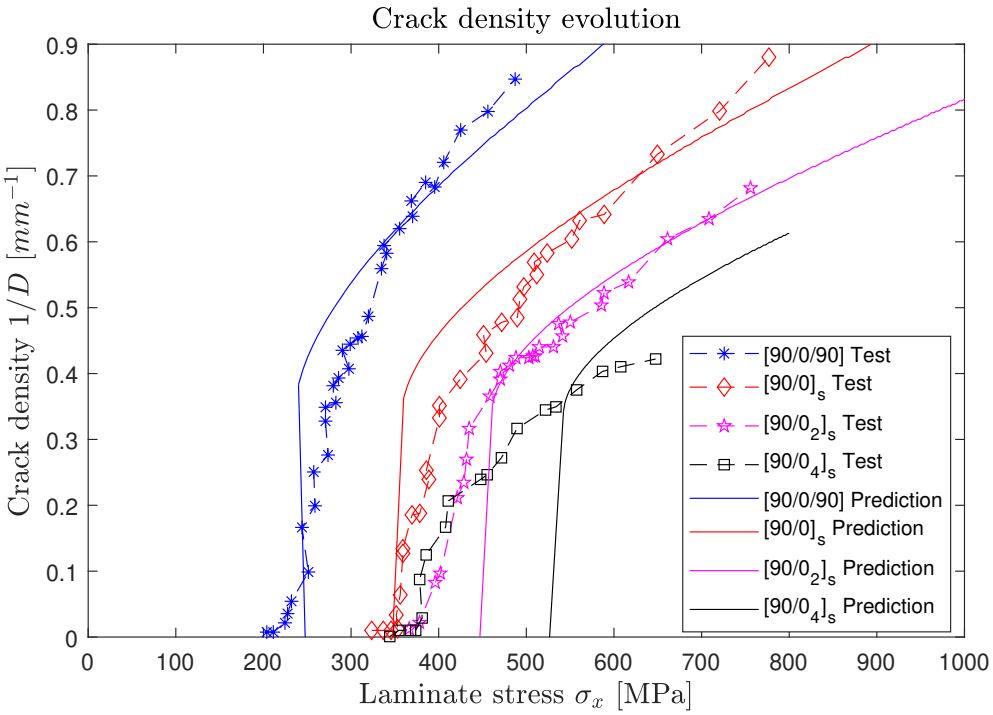

Figure 4.20: Crack density evolution for $[90/0_n]_s$ laminates under uniaxial loading.

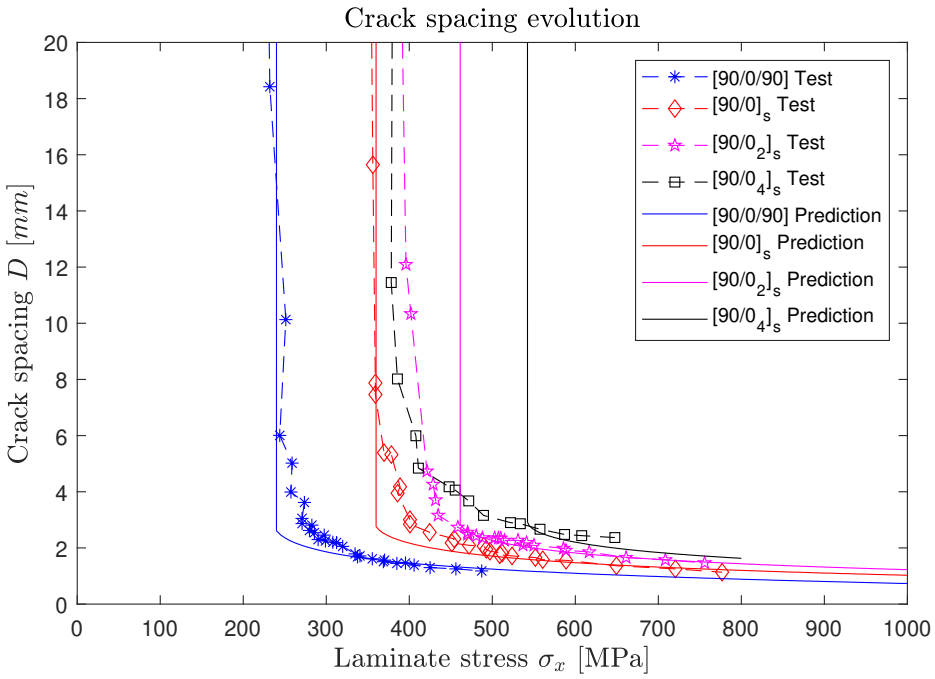

Figure 4.21: Crack density evolution for $[90/0_n]_s$ laminates under uniaxial loading.

5

Delamination Onset Model

This section introduces a model for predicting the onset of delamination in a general symmetric laminate. Firstly, the configurations of delamination arising from the tips of matrix cracks (refer to Fig. 3.2) and their associated Strain Energy Release Rate G^{cr+del} will be calculated. Subsequently, based on the Strain Energy Release Rate associated with crack propagation G^{cr} obtained in Section 4, a model will be proposed to predict the load and crack spacing at which delamination initiates.

5.1. Model principles & considerations

The proposed model in this section investigates the scenario where a laminate already contains matrix cracks and delaminations emanating from the crack tips. Figure 5.1 provides a general schematic overview of the problem, illustrating matrix cracks in red and delaminations in blue. The matrix cracks span the entire width of the laminate and are uniformly spaced with a distance denoted as D, which can be approximated using the model presented in Section 4. The delaminations, with a length of a, also cover the entire width of the laminate. Since the laminate is symmetric, there are always two critical interfaces around the critical ply, resulting in the consideration of two symmetrical delaminations. Figure 5.1 represents one of the proposed configurations, while Section 5.2.1 will introduce a total of four configurations to comprehensively study the problem.

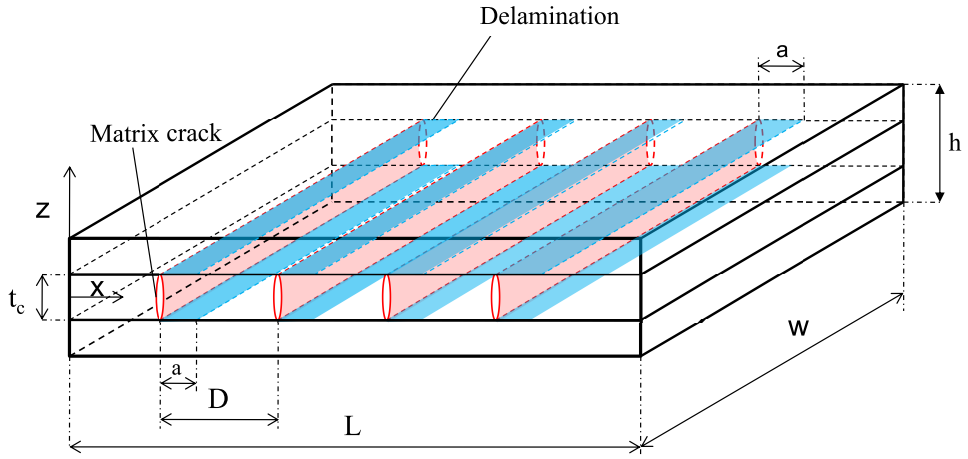

Figure 5.1: Schematic of a laminate with delaminations initiating from matrix crack tips.

In practical situations, it is unrealistic to expect perfectly uniform delaminations to occur in

every crack within the laminate. This aspect, in theory, makes the model conservative as it assumes a higher level of damage. In reality, delaminations typically initiate and propagate within one critical interface before transitioning to the other interface through transverse cracks, as observed in studies by Carraro et al. [44] and Schellekens et al. [51]. This characteristic also affects the validation process, as experimental tests usually measure the total delaminated area without considering the specific positions or intervals of delaminations.

However, since our approach employs an energy-based method, the results are primarily influenced by the total delaminated area rather than the specific distribution. Therefore, the influence of this occurrence on the results should be minimal. On a real case, the delamination front would not exhibit perfect uniformity and defects within the laminate can trigger faster initiation or growth, as well as more complex interactions between various modes. The critical interfaces where delaminations are expected to occur first are the $0/90$ interfaces in the case of a cross-ply laminate. For a general laminate, it will be assumed that delaminations initiate around the critical ply (defined as the one in which matrix cracks appear first) identified through a First Ply Failure (FPF) analysis. It is important to note that the location of delamination onset depends on the loading conditions. The model is specifically developed for laminates subjected to pure tension or tension combined with shear, although all validation will be conducted using literature data from tensile tests.

5.2. Laminate with cracks + delaminations

The forthcoming sections will introduce the different configurations of the delaminations emanating from cracks already mentioned in previous sections. These configurations will involve the calculation of laminate stiffness for each case, as well as the derivation of the corresponding Strain Energy Release Rates (SERR). Specifically, we will examine the SERR for delamination growth, referred to as G^{cr+del} and the SERR for the onset of delaminations, denoted as G^{cr+del}_{onset}, which is calculated based on the G^{cr+del}.

5.2.1. Damage configuration

Four different configurations or cases of delaminations originating from matrix cracks are introduced now. In each configuration, the delamination length a is defined such that when $a = D$, a single delamination covers the entire space between two cracks. In order to study the laminate stiffness in Section 5.2.2, a unit cell is defined for each configuration. This unit cell represents the minimum repetitive unit into which the laminate can be divided. It encompasses the entire thickness of the laminate and its length varies depending on the specific case being studied.

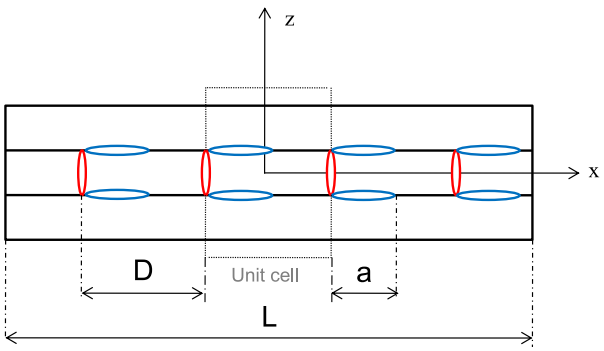

Figure 5.2: Case I: Schematic of a delamination initiating from a matrix crack.

The initial case, depicted in Figure 5.2, demonstrates delaminations that initiate and

propagate in the same direction along the longitudinal axis of the laminate. This configuration represents the simplest form. Figure 5.3 illustrates a more complex scenario where two delaminations emanate from each matrix crack tip, propagating in both directions within both the critical interface plies. This configuration has been observed in experimental tests and has been previously utilized to model such type of delaminations [7].

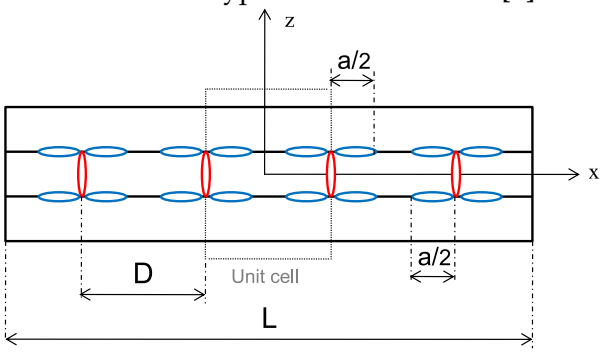

Figure 5.3: Case II: Schematic of a delamination initiating from a matrix crack.

Figure 5.4 presents the third configuration proposed, which involves two distinct delaminations propagating in opposite directions between two cracks, followed by two cracks without any delamination growth in between. While this configuration may appear unrealistic, it can be utilized as a limit case to explore extreme scenarios.

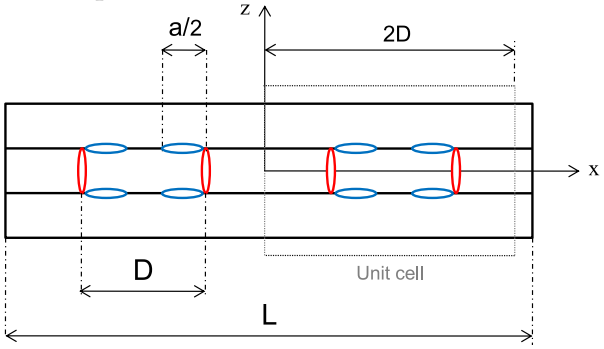

Figure 5.4: Case III: Schematic of a delamination initiating from a matrix crack.

Lastly, case IV is depicted in Figure 5.5. In this configuration, two delaminations propagate in opposite directions from the same crack but within different interfaces. This particular configuration is inspired by experimentally observed cases where cracks serve as pathways for delaminations to transition between interfaces [44, 52, 59]. Similar pattern can be observed in laminates under impact where the delaminations jump from interface to interface moving away from the vertical axis of impact.

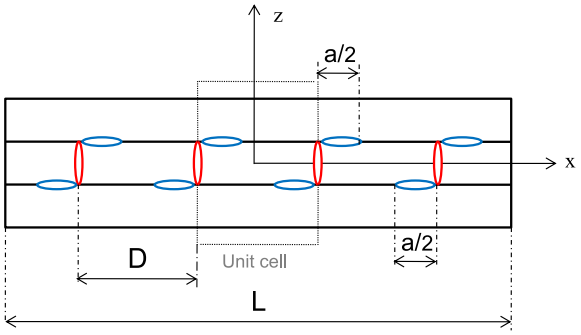

Figure 5.5: Case IV: Schematic of a delamination initiating from a matrix crack.

5.2.2. Laminate Stiffness

The longitudinal and shear laminate stiffness is now being calculated with respect to the distance between cracks D, the delamination length a and the material properties. This stiffness will then be used to obtain the Strain Energy Release Rate expressions. To calculate the stiffnesses for the different configurations shown in Fig. 5.2 - 5.5, it is necessary to calculate the equivalent modulus of the unit cells to then repeat it as many times as cracks are. To calculate the equivalent modulus of the unit cell, the laminate is divided in sections delimited by the presence or absence of delaminations.

Case I

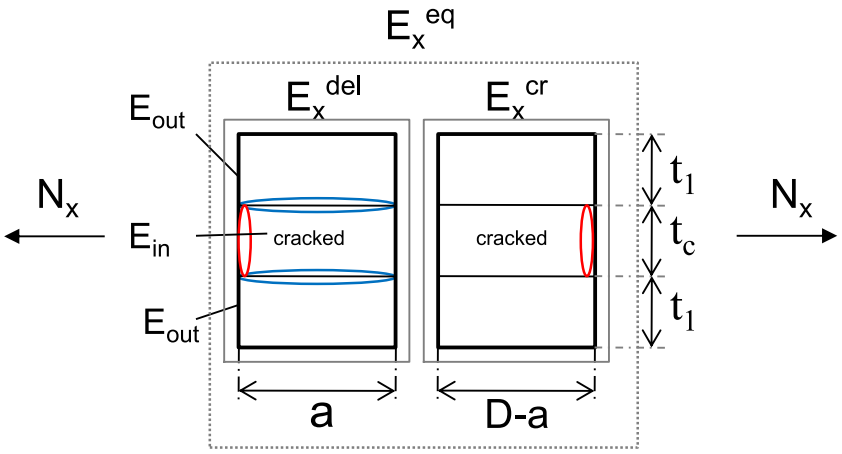

Figure 5.6: Schematic of the calculation of the longitudinal laminate stiffness.

The presence of delaminations causes the unit cell to be divided into two sections. Within the section containing the delamination, the longitudinal stiffness is denoted as E_x^{del}. This delamination further divides the section into three sub-laminates that act independently. To determine E_x^{del}, it is necessary to first obtain E_{in} and E_{out} using the Classical Laminate Theory (CLT), taking into account that the properties of the critical ply are reduced (as indicated by equation 4.21). In the case of a cross-ply laminate, this expressions are as follows:

$$E_{in} = \frac{1}{1 - \nu_{12}\nu_{21red}} \left[E_{2red} - \nu_{12}^2 \frac{E_{2red}^2}{E_1} \right] \tag{5.1}$$

$$E_{out} = \frac{1}{1 - \nu_{12}\nu_{21}} \left[E_1 - \nu_{12}^2 E_2 \right] \tag{5.2}$$

By considering that the three sub-laminates have identical strains, the longitudinal stiffness E_x^{del} can be determined using a compatibility equation:

$$(2t_1 + t_c)E_x^{del} = 2t_1 E_{out} + t_c E_{in} \rightarrow E_x^{del} = \frac{2t_1 E_{out} + t_c E_{in}}{2t_1 + t_c} \tag{5.3}$$

The stiffness E_x^{cr} represents the overall stiffness of the laminate with cracks occurring in the critical plies, which was previously calculated in equations 4.19 & 4.35. To compute the equivalent axial stiffness E_x^{eq} of the entire unit cell, the two sections are considered as springs connected in series. These sections are subjected to identical axial forces, resulting in the total deflection of the unit cell being the summation of the deflections of the two sections:

$$\overbrace{D}^{\text{length unit cell}} \cdot \frac{N_x}{E_x^{eq}} = \underbrace{a}_{\text{length delaminated section}} \cdot \frac{N_x}{E_x^{del}} + \overbrace{(D-a)}^{\text{length undelaminated section}} \cdot \frac{N_x}{E_x^{cr}} \tag{5.4}$$

Solving for E_x^{eq}:

$$E_x^{eq} = \frac{D E_x^{del} E_x^{cr}}{a E_x^{cr} + (D-a) E_x^{del}} \tag{5.5}$$

Finally , the repeating unit of stiffness E_x^{eq} is replicated a number of times equal to the quantity of matrix cracks present, specifically (L/D) times assumming again that the cells are string in series. L represents the length of the laminate and D represents the distance between cracks. Consequently, the longitudinal stiffness of the laminate with both cracks and delaminations, denoted as E_x^{cr+del}, can be determined as follows:

$$L\frac{N_x}{E_x^{cr+del}} = D\frac{N_x}{E_x^{eq}} + D\frac{N_x}{E_x^{eq}} \ldots = \left(\frac{L}{D}\right) D\frac{N_x}{E_x^{eq}} \rightarrow E_x^{cr+del} = E_x^{eq} \tag{5.6}$$

In order to calculate the shear laminate modulus for the aforementioned scenario, a similar procedure is employed, maintaining the same assumptions regarding shear loads and strains. The resulting expression is similar to the one shown before:

$$g_{xy}^{cr+del} = \frac{D g_{xy}^{del} g_{xy}^{cr}}{a g_{xy}^{cr} + (D-a) g_{xy}^{del}} \tag{5.7}$$

Case II

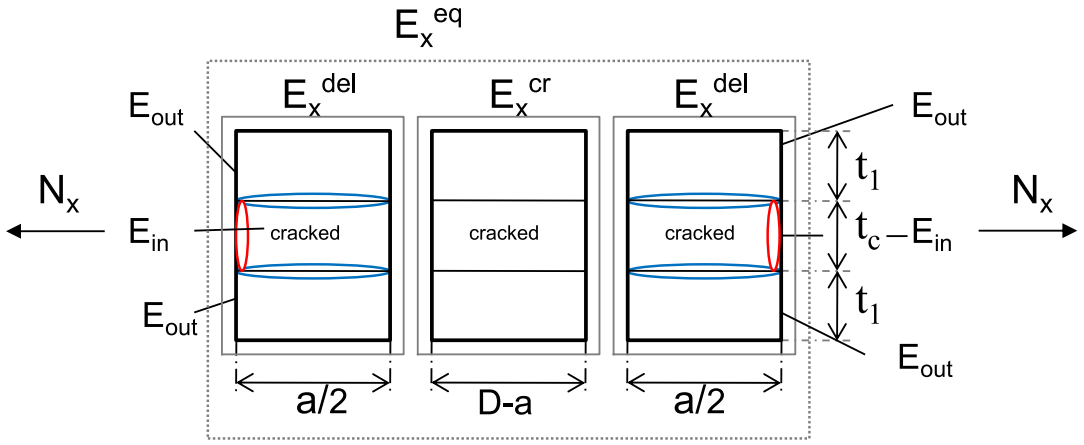

Figure 5.7: Schematic of the calculation of the longitudinal laminate stiffness.

In this configuration, the presence of delaminations divides the unit cell into three sections. The expressions for E_x^{del}, E_{in}, E_{out} and E_x^{cr} remain the same as in the previous case. Similarly, E_x^{eq} is obtained using a similar approach as in case I, treating the three sections as springs in series. This yields the following expression:

$$\overbrace{D}^{\text{length unit cell}} \cdot \frac{N_x}{E_x^{eq}} = \underbrace{2 \cdot \frac{a}{2}}_{\text{length delaminated section}} \cdot \frac{N_x}{E_x^{del}} + \overbrace{(D-a)}^{\text{length undelaminated section}} \cdot \frac{N_x}{E_x^{cr}} \tag{5.8}$$

The longitudinal stiffness for this configuration is obtained again solving for E_x^{eq} and assuming (L/D) cells, which gives the same result as before:

$$E_x^{cr+del} = \frac{D E_x^{del} E_x^{cr}}{a E_x^{cr} + (D-a) E_x^{del}} \tag{5.9}$$

In an analogous way, the shear laminate stiffness is obtained:

$$g_{xy}^{cr+del} = \frac{D g_{xy}^{del} g_{xy}^{cr}}{a g_{xy}^{cr} + (D-a) g_{xd}^{del}} \tag{5.10}$$

Case III

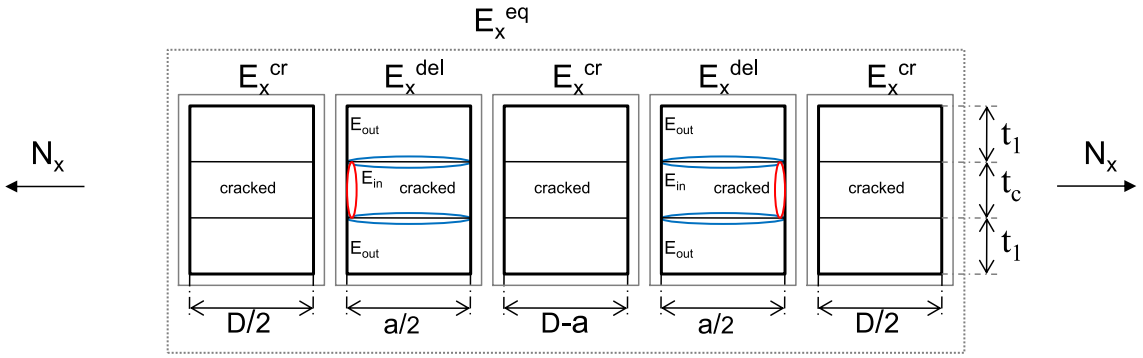

Figure 5.8: Schematic of the calculation of the longitudinal laminate stiffness.

The unit cell in this case has a length of $2D$ due to the particular configuration of the delaminations. This represents the minimum repeating unit size. As illustrated in Fig. 5.8, the cell is divided into 5 sections, two of which contain delaminations of length a. The calculations for E_x^{del}, E_{in}, E_{out} and E_x^{cr} have already been performed for the other cases. Once again, to determine the equivalent stiffness of the repeating cell, E_x^{eq}, it is assumed that the sections behave like springs in series due to the identical axial forces acting upon them. Consequently, the total deflection of the unit cell is obtained by summing the individual deflections:

$$\overbrace{D}^{\text{length unit cell}} \cdot \frac{N_x}{E_x^{eq}} = \underbrace{2 \cdot \frac{a}{2}}_{\text{length delaminated section}} \cdot \frac{N_x}{E_x^{del}} + \overbrace{\left[2 \cdot \frac{D}{2} + (D-a)\right]}^{\text{length undelaminated section}} \cdot \frac{N_x}{E_x^{cr}} \tag{5.11}$$

which lead to :

$$E_x^{eq} = \frac{2D E_x^{del} E_x^{cr}}{(2D-a) E_x^{cr} + a E_x^{del}} \tag{5.12}$$

The stiffness of the entire laminate is ultimately obtained, assuming the cells are string in series, by repeating E_x^{eq} a total of (L/2D) times, corresponding to the number of unit cells present. Hence, the axial stiffness of the laminate with both cracks and delaminations, denoted as E_x^{cr+del} for this specific configuration, is derived from equation 5.12 as follows:

$$E_x^{cr+del} = \frac{2DE_x^{del}E_x^{cr}}{aE_x^{cr} + (2D-a)E_x^{del}} \tag{5.13}$$

Once again, the shear modulus is similarly calculated:

$$g_{xy}^{cr+del} = \frac{2Dg_{xy}^{del}g_{xy}^{cr}}{ag_{xy}^{cr} + (2D-a)g_{xy}^{del}} \tag{5.14}$$

Case IV

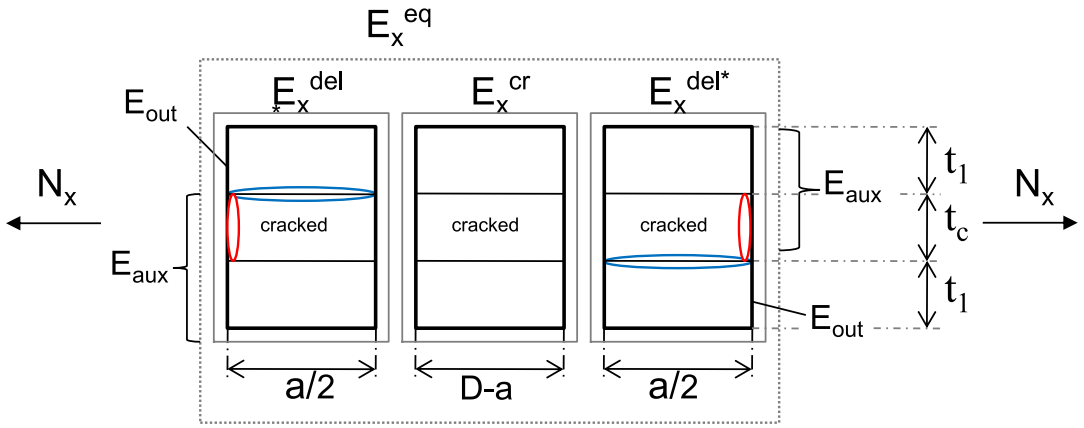

Figure 5.9: Schematic of the calculation of the longitudinal laminate stiffness.

In the final configuration, the unit cell is once again divided into three sections, with two of them containing the delamination. In this case, E_x^{del*} needs to be calculated using E_{out} & E_{aux} obtained through the Classical Laminate Theory (CLT) for a laminate composed of the cracked ply and half of the laminate. Assuming laminate symmetry, the values in both sections are the same for the longitudinal modulus calculation. Given that the two sub-laminates experience identical strains, E_x^{del*} can be determined again by employing a compatibility equation.

$$(2t_1 + t_c)E_x^{del*} = t_1E_{out} + (t_1 + t_c)E_{aux} \rightarrow E_x^{del*} = \frac{t_1E_{out} + (t_1 + t_c)E_{aux}}{2t_1 + t_c} \tag{5.15}$$

Following the same reasoning as for the previous cases, the three sections are subjected to equal axial forces, causing them to function as springs in series. Once E_x^{eq} is determined, the axial stiffness of the entire laminate, denoted as E_x^{cr+del}, is obtained by assuming the cells are string in series, (L/D) is the number of unit cells present within the length L:

$$\overbrace{D}^{\text{length unit cell}} \cdot \frac{N_x}{E_x^{eq}} = \underbrace{2 \cdot \frac{a}{2}}_{\text{length delaminated section}} \cdot \frac{N_x}{E_x^{del*}} + \overbrace{(D-a)}^{\text{length undelaminated section}} \cdot \frac{N_x}{E_x^{cr}} \tag{5.16}$$

$$E_x^{cr+del} = \frac{D E_x^{del*} E_x^{cr}}{a E_x^{cr} + (D-a) E_x^{del*}} \tag{5.17}$$

also:

$$g_{xy}^{cr+del} = \frac{D g_{xy}^{del*} g_{xy}^{cr}}{a g_{xy}^{cr} + (D-a) g_{xy}^{del*}} \tag{5.18}$$

It is worth noting that for the same material and stacking sequence, it is only necessary to calculate E_x^{cr}, E_x^{del}, E_x^{del*}, g_{xy}^{cr}, g_{xy}^{del} and g_{xy}^{del*} once, as these values remain consistent across all cases. When considering a cross-ply laminate, obtaining these stiffness values using CLT is simpler compared to a general symmetrical laminate. The derivations presented here assume the presence of a single critical ply or ply block in the laminate symmetry axis with two surrounding delaminations. However, if the FPF criteria identifies multiple critical plies or an outer critical ply, the same procedure for constructing the laminate stiffnesses can be applied by dividing the sections into additional sub-laminates and applying the same assumptions.

5.2.3. Strain Energy Release Rate

The Strain Energy Release Rate in this case, will describe the energy dissipated as the delamination area increases. It is assumed that the crack spacing D is constant and only the delaminations of length a are increasing the damaged area. This assumption is based in experimental observations that suggest that typically, once delaminations occur from a crack tip, the laminate reaches a state of crack saturation, where the crack density remains stable [21, 69, 70]. The subscript "cr + del" will refer to this case, where delaminations growing from cracks tips are present. Therefore, G^{cr+del} is defined as:

$$G^{cr+del} = -\frac{\partial U}{\partial A_{del}} \tag{5.19}$$

The potential strain energy (U) available for delamination growth is defined in relation to the applied strain on the laminate ε_x and γ_{xy}, the laminate stiffnesses E_x^{cr+del} and g_{xy}^{cr+del} and the volume of the laminate $V = Lwh$:

$$U = \iiint \frac{1}{2}\left(E_x^{cr+del}\,\varepsilon_x^2 + g_{xy}^{cr+del}\,\gamma_{xy}^2\right) dV = \frac{1}{2}\left(E_x^{cr+del}\,\varepsilon_x^2 + g_{xy}^{cr+del}\,\gamma_{xy}^2\right) Lwh \tag{5.20}$$

The delaminated area A_{del} varies depending on the configurations suggested earlier and its definition differs accordingly:

$$\begin{aligned} I: &\quad A_{del} = 2aw \\ II: &\quad A_{del} = 2\left(2\frac{a}{2}\right)w = 2aw \\ III: &\quad A_{del} = 2aw \\ IV: &\quad A_{del} = 2\frac{a}{2}w = aw \end{aligned} \tag{5.21}$$

G^{cr+del} can now be derived combining eq. 5.19, 5.20 & 5.21 assuming that the crack distance D is constant, as well as the laminate dimensions h, L and w. Depending on the configuration of the delaminations, four expressions are obtained:

$$\begin{aligned}
I: \quad G^{cr+del} &= -\frac{1}{4}hD\left(\frac{\partial E_x^{cr+del}}{\partial a}\varepsilon_x^2 + \frac{\partial g_{xy}^{cr+del}}{\partial a}\gamma_{xy}^2\right)\\
II: \quad G^{cr+del} &= -\frac{1}{4}hD\left(\frac{\partial E_x^{cr+del}}{\partial a}\varepsilon_x^2 + \frac{\partial g_{xy}^{cr+del}}{\partial a}\gamma_{xy}^2\right)\\
III: \quad G^{cr+del} &= -\frac{1}{2}hD\left(\frac{\partial E_x^{cr+del}}{\partial a}\varepsilon_x^2 + \frac{\partial g_{xy}^{cr+del}}{\partial a}\gamma_{xy}^2\right)\\
IV: \quad G^{cr+del} &= -\frac{1}{2}hD\left(\frac{\partial E_x^{cr+del}}{\partial a}\varepsilon_x^2 + \frac{\partial g_{xy}^{cr+del}}{\partial a}\gamma_{xy}^2\right)
\end{aligned} \tag{5.22}$$

It should be noted that the stiffness values derived in section 5.2.2, namely E_x^{cr+del} and g_{xy}^{cr+del}, are independent of the delamination length a, which simplifies the derivation process. By differentiating the expressions for these stiffness values obtained in section 5.2.2 with respect to a, we can derive the expressions for the Strain Energy Release Rate (SERR) in a laminate with cracks and delaminations growing from the crack tips:

$$\begin{aligned}
I: \quad G^{cr+del} &= \frac{1}{4}h\left(\frac{L}{D}\right)\left\{\frac{E_x^{cr}\left(\frac{E_x^{cr}}{E_x^{del}}-1\right)}{\left[1-\frac{a}{D}+\frac{a}{D}\frac{E_x^{cr}}{E_x^{del}}\right]^2}\varepsilon_x^2 + \frac{g_{xy}^{cr}\left(\frac{g_{xy}^{cr}}{g_{xy}^{del}}-1\right)}{\left[1-\frac{a}{D}+\frac{a}{D}\frac{g_{xy}^{cr}}{g_{xy}^{del}}\right]^2}\gamma_{xy}^2\right\}\\
II: \quad G^{cr+del} &= \frac{1}{4}h\left(\frac{L}{D}\right)\left\{\frac{E_x^{cr}\left(\frac{E_x^{cr}}{E_x^{del}}-1\right)}{\left[1-\frac{a}{D}+\frac{a}{D}\frac{E_x^{cr}}{E_x^{del}}\right]^2}\varepsilon_x^2 + \frac{g_{xy}^{cr}\left(\frac{g_{xy}^{cr}}{g_{xy}^{del}}-1\right)}{\left[1-\frac{a}{D}+\frac{a}{D}\frac{g_{xy}^{cr}}{g_{xy}^{del}}\right]^2}\gamma_{xy}^2\right\}\\
III: \quad G^{cr+del} &= \frac{1}{2}h\left(\frac{L}{D}\right)\left\{\frac{E_x^{cr}\left(\frac{E_x^{cr}}{E_x^{del}}-1\right)}{\left[2-\frac{a}{D}+\frac{a}{D}\frac{E_x^{cr}}{E_x^{del}}\right]^2}\varepsilon_x^2 + \frac{g_{xy}^{cr}\left(\frac{g_{xy}^{cr}}{g_{xy}^{del}}-1\right)}{\left[2-\frac{a}{D}+\frac{a}{D}\frac{g_{xy}^{cr}}{g_{xy}^{del}}\right]^2}\gamma_{xy}^2\right\}\\
IV: \quad G^{cr+del} &= \frac{1}{2}h\left(\frac{L}{D}\right)\left\{\frac{E_x^{cr}\left(\frac{E_x^{cr}}{E_x^{del*}}-1\right)}{\left[1-\frac{a}{D}+\frac{a}{D}\frac{E_x^{cr}}{E_x^{del*}}\right]^2}\varepsilon_x^2 + \frac{g_{xy}^{cr}\left(\frac{g_{xy}^{cr}}{g_{xy}^{del*}}-1\right)}{\left[1-\frac{a}{D}+\frac{a}{D}\frac{g_{xy}^{cr}}{g_{xy}^{del*}}\right]^2}\gamma_{xy}^2\right\}
\end{aligned} \tag{5.23}$$

These expressions depend on various parameters, including the crack spacing D, delamination length a, applied strains on the laminate (ε_x and γ_{xy}), laminate thickness h, laminate length L and the longitudinal and shear stiffnesses defined in the previous section. It is worth noting that Case I and Case II have identical expressions, suggesting that these delamination configurations behave energetically in the same manner. Case III denominator is bigger than case I & II and Case IV is difficult to evaluate a priori in relation to the other expressions because it depends on the parameters E_x^{del*} and g_{xy}^{del*}, which do not appear in the other expressions.

These expressions analyze the growth of delaminations under the assumption that they already exist. However, for the proposed method, it is crucial to derive an expression that describes the onset of delaminations. To achieve this, it is necessary to study the equation in the limits of the delamination length a; namely, when the delamination is extremely large ($a \to \infty$) and at its onset, when it is infinitesimally small ($a \to 0$):

$$\lim_{a \to \infty} G^{cr+del} = 0 \tag{5.24}$$

$$\lim_{a \to 0} G^{cr+del} = G_{onset}^{cr+del} = \frac{1}{4} h \left(\frac{L}{D}\right) \left\{ E_x^{cr} \left(\frac{E_x^{cr}}{E_x^{del}} - 1\right) \varepsilon_x^2 + g_{xy}^{cr} \left(\frac{g_{xy}^{cr}}{g_{xy}^{del}} - 1\right) \gamma_{xy}^2 \right\} \tag{5.25}$$

As it can be seen, when the delamination becomes large to the extent that it covers the entire length of the laminate ($(a \to \infty) \sim (a = D)$), the Strain Energy Release Rate (SERR) approaches zero. This indicates that the laminate loses its ability to dissipate additional energy by increasing the delamination area. This makes sense because the delamination area already covers the entire interface between the plies. On the other hand, at the onset of delamination (as shown in equation 5.25), G^{cr+del} approaches a value that primarily depends on the matrix crack distance D, the applied strains on the laminate (ε_x, γ_{xy}) and the stiffnesses of the respective sections E_x^{cr}, E_x^{del}, g_{xy}^{cr}, and g_{xy}^{del}. This equation will be particularly useful in subsequent sections for proposing a criterion to predict the load at which delamination onset occurs, and thus it is denoted as G_{onset}^{cr+del}. It is worth noting that the equation based on Case I is used to derive equation 5.25, but the same procedure is employed to obtain the onset SERR in the other cases:

$$\begin{aligned}
I: \quad & G_{onset}^{cr+del} = \frac{1}{4} h \left(\frac{L}{D}\right) \left\{ E_x^{cr} \left(\frac{E_x^{cr}}{E_x^{del}} - 1\right) \varepsilon_x^2 + g_{xy}^{cr} \left(\frac{g_{xy}^{cr}}{g_{xy}^{del}} - 1\right) \gamma_{xy}^2 \right\} \\
II: \quad & G_{onset}^{cr+del} = \frac{1}{4} h \left(\frac{L}{D}\right) \left\{ E_x^{cr} \left(\frac{E_x^{cr}}{E_x^{del}} - 1\right) \varepsilon_x^2 + g_{xy}^{cr} \left(\frac{g_{xy}^{cr}}{g_{xy}^{del}} - 1\right) \gamma_{xy}^2 \right\} \\
III: \quad & G_{onset}^{cr+del} = \frac{1}{8} h \left(\frac{L}{D}\right) \left\{ E_x^{cr} \left(\frac{E_x^{cr}}{E_x^{del}} - 1\right) \varepsilon_x^2 + g_{xy}^{cr} \left(\frac{g_{xy}^{cr}}{g_{xy}^{del}} - 1\right) \gamma_{xy}^2 \right\} \\
IV: \quad & G_{onset}^{cr+del} = \frac{1}{2} h \left(\frac{L}{D}\right) \left\{ E_x^{cr} \left(\frac{E_x^{cr}}{E_x^{del*}} - 1\right) \varepsilon_x^2 + g_{xy}^{cr} \left(\frac{g_{xy}^{cr}}{g_{xy}^{del*}} - 1\right) \gamma_{xy}^2 \right\}
\end{aligned} \tag{5.26}$$

Cases I and II are identical, while Case III differs only in terms of the pre-multiplier. In the case of Case IV, distinctions are also present in the E_x^{del*} and g_{xy}^{del*} variables making it more challenging to directly compare with the other cases. Case III will hence give the lowest G_{onset}^{cr+del} value while the highest value would depend on how E_x^{del*} & g_{xy}^{del*} differ from E_x^{del} & g_{xy}^{del}.

5.3. Parameters study

In this section, the shape of the SERR expressions derived and the influence of the parameters will be briefly discussed before proposing the method to predict the delamination onset. Focus will be placed in the case of a laminate under pure tension due to the fact that the validation data are tensile test (hence $\gamma_{xy} = 0$) but the derivation proposed earlier is valid for a laminate under tension, shear or combined loading.

5.3.1. SERR for delamination onset (G_{onset}^{cr+del})

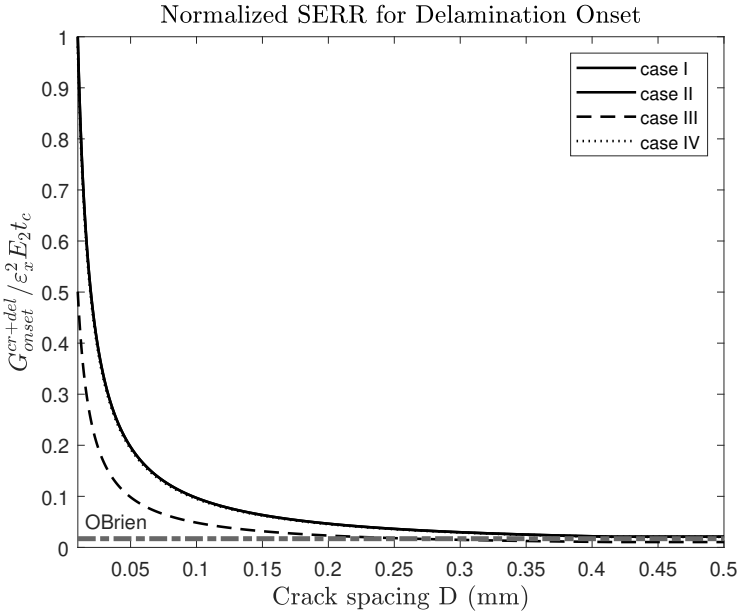

Figure 5.10: UT-E500/Epikote RIMR235 $[0/90_2]_s$laminate under tension.

Figure 5.10 illustrates the fundamental shapes of G_{onset}^{cr+del} for all the proposed cases (Case I and Case II being essentially equal). The derived expressions in equation 5.26 primarily depends on the crack distance D. All three expressions exhibit similar behavior. They decrease as D increases, indicating that a larger crack distance corresponds to a lower likelihood of delamination onset. Conversely, as D decreases, the Strain Energy Release Rate (SERR) increases rapidly, eventually reaching an infinite value at $D = 0$, indicating that the interface has already delaminated. Comparing these expressions with the SERR for crack propagation (see Fig. 4.5), it becomes evident that the trends are opposite. This suggests that at larger crack spacings, the appearance of new cracks is more probable, whereas for smaller crack spacings, the onset of delaminations is more likely to occur.

The expressions are also plotted alongside the well-known equation proposed by O'Brien [13] for the free-edge delamination onset in cross-ply laminates. This expression, defined in equation 5.27, does not consider matrix cracks and thus remains constant with respect to D. It assumes a free-edge delamination onset that covers the entire laminate. Similar to this study, O'Brien solved for $a = 0$ in his earlier derivation to obtain the onset, leading to the equation shown in eq. 5.27. In that equation, E_{LAM} represents the pristine axial stiffness of the laminate, h denotes the laminate thickness and E^* is the sum of the stiffnesses of the three sublaminates separated by the delaminations (equivalent to E_x^{del} in the present notation, with $D \to \infty$).

$$G_{OBrien} = \frac{1}{2}\varepsilon_x^2 h(E_{LAM} - E^*) \tag{5.27}$$

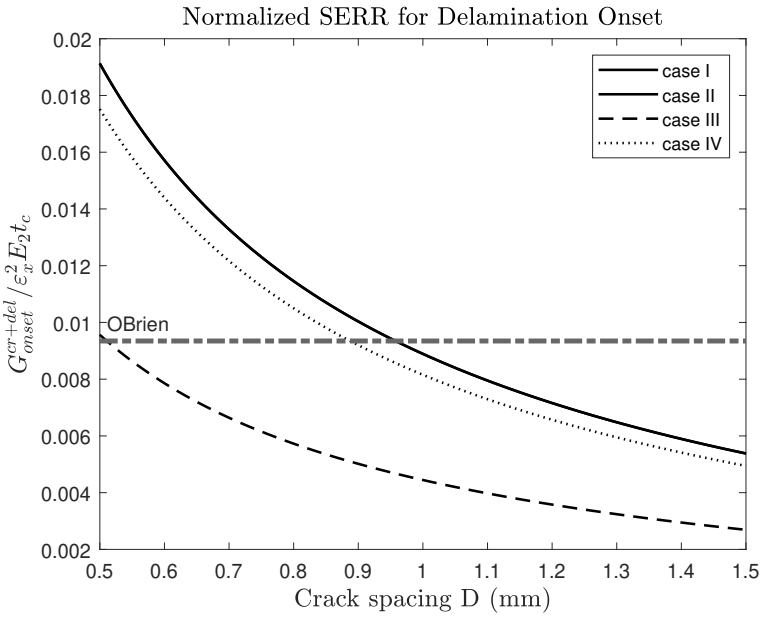

Figure 5.11: Magnified section of normalized SERR plot shown in Fig. 5.10.

Figure 5.11 displays a segment of the normalized SERR expressions for relatively large crack spacings D. It is evident that all the proposed G_{onset}^{cr+del} expressions are initially larger than the corresponding $G_{O'Brien}$ for short crack spacing values. However, at a certain point, $G_{O'Brien}$ surpasses them. For relatively large D values, the term (L/D) in equation 5.26 becomes very small, causing the entire equation to yield small values. This implies that when the laminate contains a significant number of cracks (relatively low D), the tendency is for delaminations to nucleate at the crack tips. Conversely, if the laminate has fewer cracks and is closer to its pristine properties (relatively large D), the tendency is for the nucleation of free-edge delaminations.

Applying the same line of reasoning, it appears that Case I and Case II are more likely scenarios because their SERR expressions give higher values for every D value. A larger SERR indicates a greater amount of dissipated energy, hence a higher likelihood of occurrence. Case IV follows closely behind them in terms of likelihood, suggesting that based on local imperfections it is possible to precede the other two cases thus leading to the behaviour observed some times in experiments where the delamination jumps to another interface [44, 51]. Case III consistently exhibits lower SERR values for all crack spacings D. This suggests that Case III is a configuration that is less likely to occur. With three different configurations and corresponding SERR expressions, it becomes possible to formulate delamination onset predictions that are more conservative or less conservative depending on which configuration is assumed. In a real case, it is probable that all these configurations, as well as more complex ones, may occur simultaneously. Therefore, it is reasonable to assume that the actual solution lies somewhere between the less conservative and more conservative predictions provided by these configurations.

Next, the principal parameters influencing the proposed expressions will be examined. Figure 5.12 demonstrates various cross-ply configurations subjected to tension, highlighting the impact of adding more 90º plies, which leads to an increase in t_c. The figure presents

G_{onset}^{cr+del} for case I (equivalent to case II), serving as a representative curve. Case III and case IV follow a similar pattern with the number of 90º plies, causing a proportional shift in the curve, as depicted in Figures 5.10 and 5.11. It can be observed that while increasing the number of 90º plies does increase the G_{onset}^{cr+del} values, the effect is not as substantial as in the corresponding SERR for crack propagation (refer to Figure 4.6). Consequently, it implies that the delamination onset behavior will not be excessively affected by this factor.

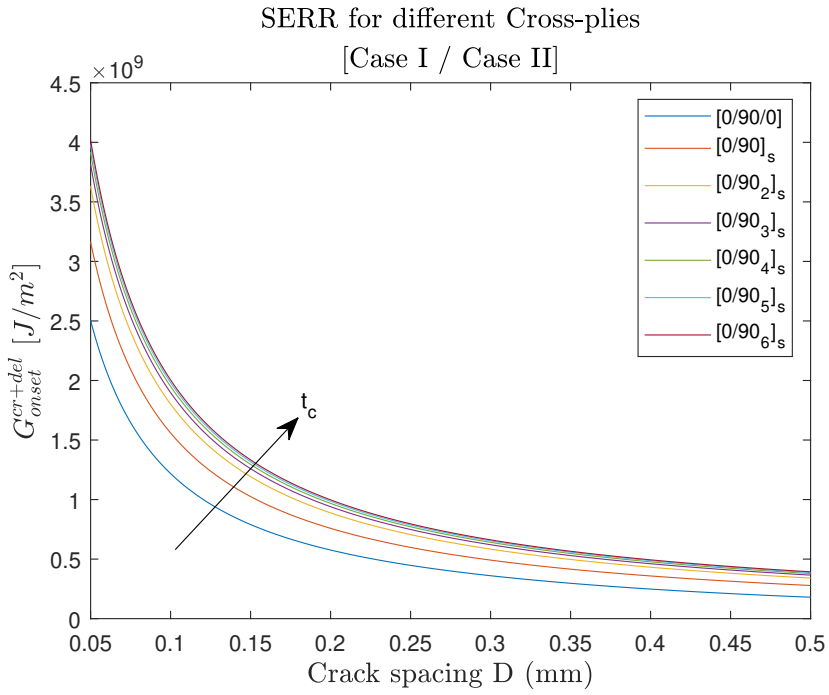

Figure 5.12: Influence of t_c in UT-E500/Epikote RIMR2 cross-plies under a tension of $\varepsilon_x = 0.5$

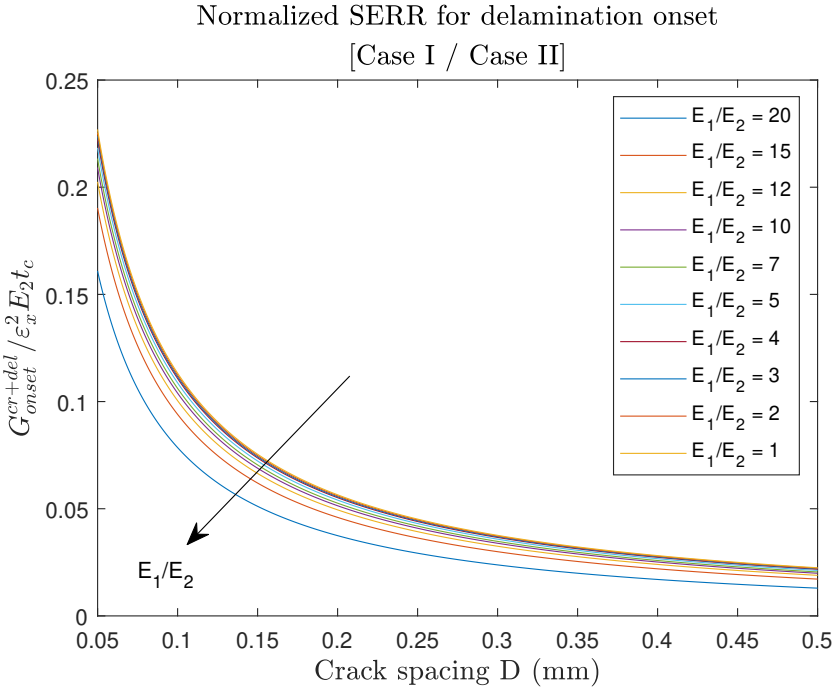

Figure 5.13: Influence of E_1/E_2 in a UT-E500/Epikote RIMR2 $[0/90_2]_s$ laminate under tension.

Figure 5.13 shows the influence of Young's modulus of the ply in SERR for delamination onset in a $[0/90_2]_s$ laminate under tension. G_{onset}^{cr+del} decreases for increasing E_1/E_2 which indicates that if the ply is stiffer in the longitudinal direction, the tendency to create a delamination decreases. This behaviour is the opposite that the SERR expression for the crack propagation (see Fig.4.7). Figure 5.14 shows the influence of the ratio between the critical ply thickness and the rest of the laminate thickness in the case of a $[0/90_2]_s$ under tension, maintaining t_c constant. The lower the t_1/t_c ratio, the lower the G_{onset}^{cr+del} which indicates that reducing the thickness of the plies surrounding the critical ply, makes more unlikely the delamination to appear in the interface between the critical ply and, in this case, the 0^o plies. It is interesting to note that this ratio influences the G_{onset}^{cr+del} curve the most, unlike G^{cr}, where the ratio of the thickness barely influences the behaviour for the crack propagation (see Figure 4.8).

Figure 5.13 illustrates the impact of the Young's modulus of the ply on the SERR for delamination onset in a $[0/90_2]s$ laminate subjected to tension. As E_1/E_2 increases, G_{onset}^{cr+del} decreases, indicating that a stiffer ply in the longitudinal direction reduces the likelihood of delamination occurring. This behavior is contrary to the SERR expression for crack propagation, as shown in Figure 4.7. Additionally, Figure 5.14 presents the influence of the ratio between the critical ply thickness and the overall laminate thickness in the case of a $[0/90_2]s$ laminate under tension, while maintaining t_c constant. A lower t_1/t_c ratio corresponds to a lower G_{onset}^{cr+del}, suggesting that reducing the thickness of the plies surrounding the critical ply makes delamination less likely to occur at the interface between the critical ply and, in this case, the 0^o plies. It is worth noting that this ratio has the most significant influence on the G_{onset}^{cr+del} curve, unlike G^{cr}, where the thickness ratio has minimal effect on crack propagation behavior (refer to Figure 4.8).

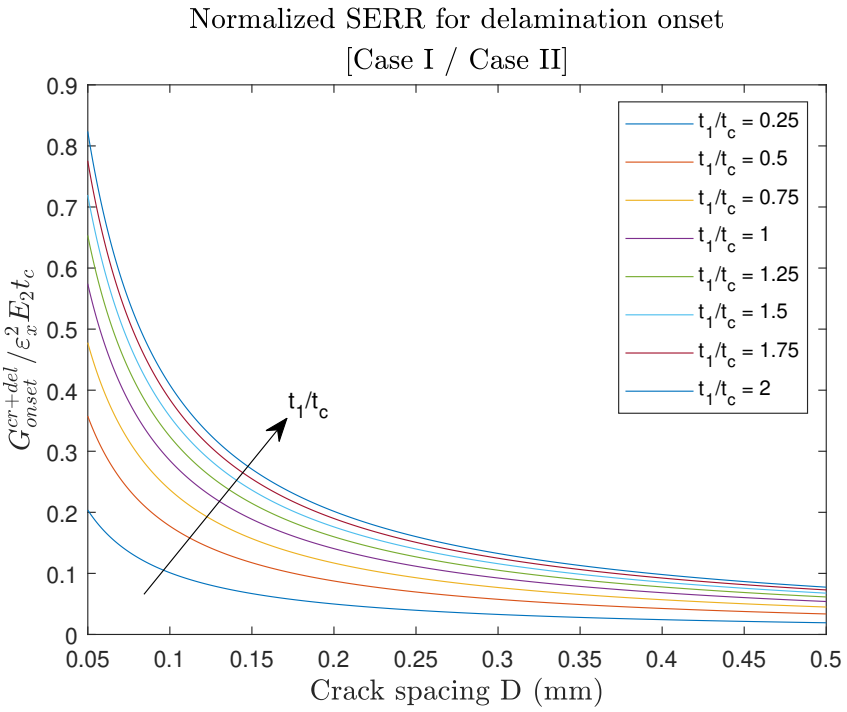

Figure 5.14: Influence of t_1/t_c in a UT-E500/Epikote RIMR2 $[0/90_2]_s$ laminate under tension.

Finally, the behavior of the SERR for the delamination onset is analyzed for different $[0/\theta_2]s$ laminates under pure tension, as depicted in Figure 5.15. The curves of G_{onset}^{cr+del} corresponding

to lower θ values are observed to be higher than those associated with θ values closer to 90º. This phenomenon arises from the strong dependence of the expressions on E_x^{cr} and E_x^{del} (as seen in equations 5.26), which represent the longitudinal stiffnesses of the cracked and delaminated sections. Therefore, θ values closer to 0º (the longitudinal direction) result in higher SERR values.

Interestingly, the SERR for the $[0/10_2]_s$ laminate is lower than that of the $[0/20_2]_s$, $[0/30_2]_s$ and $[0/40_2]_s$ laminates. This can possibly be attributed to the intricate interactions among the terms of the A matrix within the E_x^{cr} and E_x^{cr}/E_x^{del} expressions for that specific range of D. For even lower D values, the SERR corresponding to the $[0/10_2]_s$ laminate increases rapidly and surpasses the others. It should be noted that the definition of E_x^{cr} in equation 4.19 depends on the interactions among almost all the A terms of the ABD matrix when $\theta \neq 90$, and within these terms, equations 4.1, 4.2 and **??** establish complex relationships with the variable D. However, as explained in subsequent sections, the range of extremely low crack spacing depicted in Figure 5.15, where the curves start to approach infinity, is not relevant, and delamination onset will occur at higher D values.

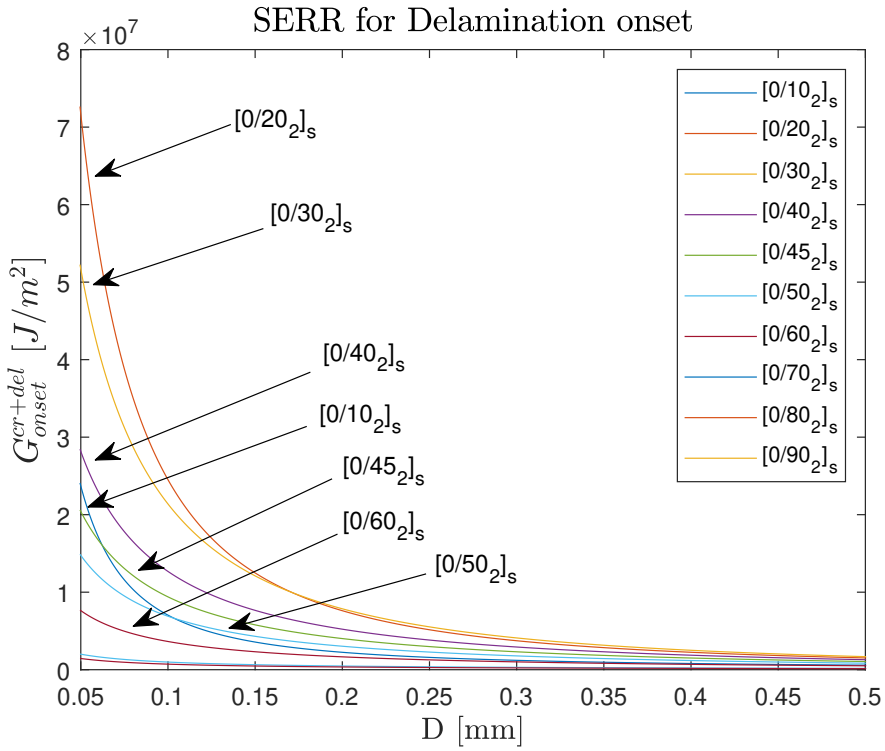

Figure 5.15: G^{cr} for UT-E500/Epikote RIMR2 $[0/\theta_2]_s$ laminate under tension.

The ideas presented in this section can be summarized as follows:

- The expressions for G_{onset}^{cr+del} in Case I and Case II are identical.
- G_{onset}^{cr+del} for case I (and II) is greater than G_{onset}^{cr+del} for case III and IV.
- G_{onset}^{cr+del} for all cases tend to a lower value than the SERR given by O'Brien for high D values.
- G_{onset}^{cr+del} for all cases tend to an infinite value for $D \rightarrow 0$.
- G_{onset}^{cr+del} increases with an increase in t_c (critical ply thickness).
- G_{onset}^{cr+del} decreases with an increase in the ratio E_1/E_2.

- G_{onset}^{cr+del} significantly increases with an increase t_1.
- G_{onset}^{cr+del} decreases when there is a greater relative angle difference on a $[0/\theta_2]_s$ laminate.
- $G_{onset}^{cr+del} = f(E_x^{cr}, E_x^{del}, h, L, D, \varepsilon_x, \gamma_{xy})$.

5.3.2. SERR for delamination growth (G^{cr+del})

In section 6, the Strain Energy Release Rate equation will be utilized to predict the growth of a pre-existing delamination. The expression, represented by equations 5.23, primarily relies on two factors: the spacing between cracks, denoted as D, and the length of the delamination, denoted as a. The stiffness of the laminate's cracked and delaminated sections also plays a role but it inherently depends on the aforementioned parameter D and the material properties. To illustrate this relationship, Figure 5.16 - 5.18 display the variation of G^{cr+del} with respect to a for different fixed crack spacings, considering all four cases.

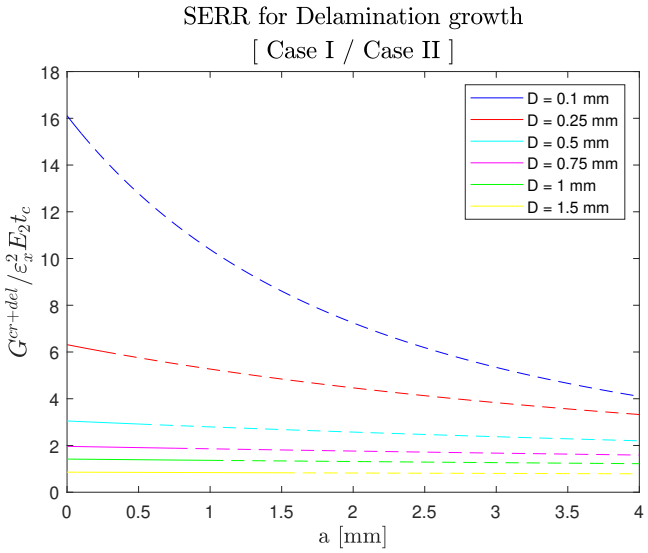

Figure 5.16: Case I & Case II normalized G^{cr+del} for UT-E500/Epikote RIMR2 $[0/90_2]_s$ laminate under tension.

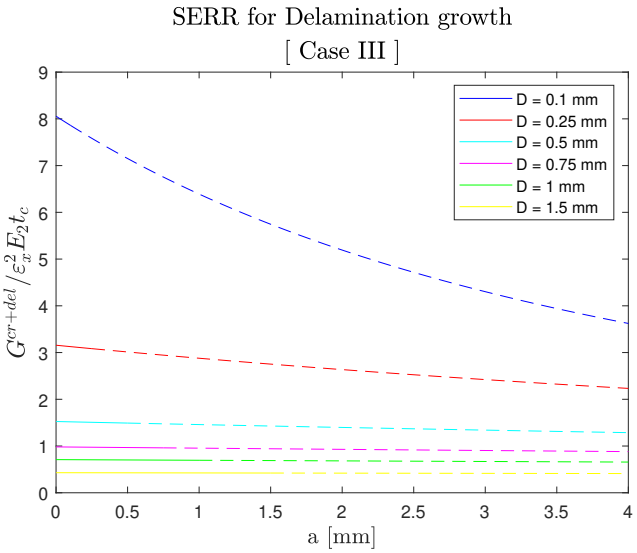

Figure 5.17: Case III normalized G^{cr+del} for UT-E500/Epikote RIMR2 $[0/90_2]_s$ laminate under tension.

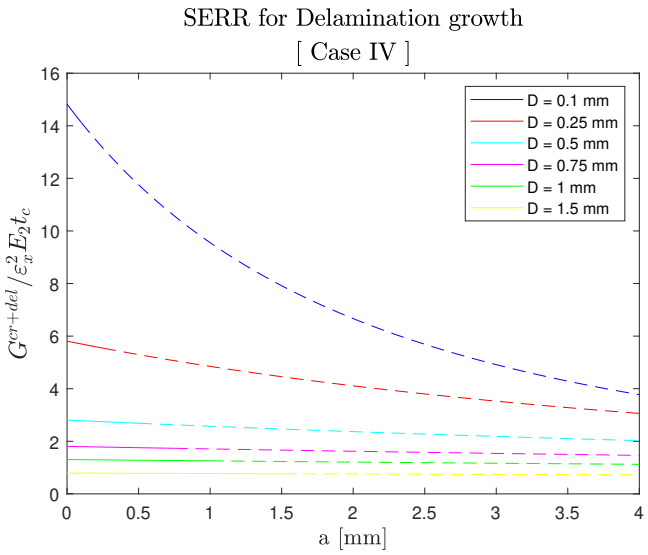

Figure 5.18: Case IV normalized G^{cr+del} for UT-E500/Epikote RIMR2 $[0/90_2]_s$ laminate under tension.

The depicted figures indicate a trend where the Strain Energy Release Rate (G^{cr+del}) decreases as the delamination length (a) increases; particularly in cases I, II and IV, compared to case III. This phenomenon can be attributed to the denominator of equations 5.23. As a increases, the denominator also increases because $E_x^{cr}/E_x^{del} > 1$, resulting in a reduction of the overall value of the function.

Furthermore, Figures 5.16 to 5.18 demonstrate that smaller values of the crack spacing (D) lead to higher overall values of G^{cr+del} for each delamination length, indicating an increased likelihood of delamination growth. This effect is primarily influenced by the L/D term in equations 5.23, while also depending on the ratio of a/D. This tendency holds true for all four cases. The figures presented cover a spectrum of a values ranging in the range [0 5] mm which is mathematically valid. However, from a physical perspective, it is unreasonable for a to exceed D. This is evident in Figures 5.6 to 5.9, where it can be observed that when $a = D$, the delamination spans the entire length of the laminate. In the graphs depicting G^{cr+del} for different fixed D values, the solid line corresponds to cases where $a < D$, while the dashed line represents situations where $a > D$.

5.4. Delamination Onset prediction

5.4.1. Cross-ply under tension

A method is proposed in order to predict the load at which delamination initiates in a cross-ply laminate subjected to tension. This prediction relies on two parameters: the Strain Energy Release Rate for crack propagation, denoted as G^{cr}, and the Strain Energy Release Rate for delamination onset, denoted as G_{onset}^{cr+del}. The key concept is that the Strain Energy Release Rate provides insight into the relative likelihood of different processes occurring. In this cases two processes can occur upon loading: the formation of a new crack or the initiation of a delamination in a crack tip. Both processes have their related SERR expression and they can be compared based on their common parameter D. Figure 5.19 illustrates the G^{cr} and G_{onset}^{cr+del} expressions.

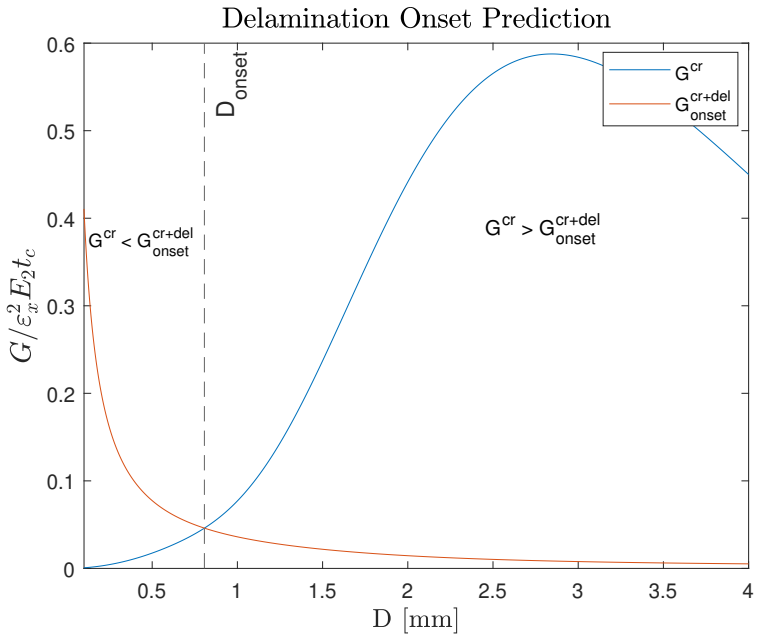

Figure 5.19: G^{cr} vs G^{cr+del}_{onset} of a laminate under tension.

Two distinct regions can be identified: the case where the creation of new cracks dissipate more energy than the creation of a delamination ($G^{cr} > G^{cr+del}_{onset}$) and the opposite ($G^{cr} > G^{cr+del}_{onset}$). The critical point, where G^{cr} is precisely equal to G^{cr+del}_{onset}, is determined by the intersection of both curves. This intersection represents a distance between cracks, denoted as D_{onset}, which is assumed to correspond to the onset of delamination. Essentially, G^{cr} serves as a critical Strain Energy Release Rate to predict the delamination onset as a function of D. It designates the point at which it is no longer advantageous for the laminate to dissipate energy by increasing the cracked area, but rather by expanding (or creating) a delaminated area.

It is important to note that this critical distance, D_{onset}, is dependent on the applied load to the laminate, as the SERR expressions also rely on the applied load. In the case of a cross-ply laminate subjected to pure tension, the SERR expressions defined in equation 4.3.2 and equation 5.26 can be normalized with the applied strain in the laminate ε_x, the transverse Young's modulus E_2 and the critical ply thickness t_c. This normalization allows for the straightforward calculation of D_{onset} by solving the following equation:

$$\frac{G^{cr}}{\varepsilon_x^2 E_2 t_c} = \frac{G^{cr+del}_{onset}}{\varepsilon_x^2 E_2 t_c} \tag{5.28}$$

To establish a relationship between the crack spacing at the onset of delamination D_{onset} and the applied load $N_{x,onset}$, we first need to connect the crack spacing with the local transverse strain that generates D_{onset}. Using equation 4.11 and the Classical Laminate Theory (CLT), the local transverse strain applied in the critical ply can be linked to the load. In this case, we employ Socci & Kassapoglou's model, as described in section 4.2, to calculate the local transverse strain in the ply that will result in the desired crack spacing D_{onset}. While the original approach by Socci & Kassapoglou assumes a known strain, in our case, the crack spacing is defined, and the load is the variable of interest. By following the equations presented in section 4.2.1, we can determine the applied local transverse strain in the 90º ply that corresponds to the

given spacing in a specific laminate. Subsequently, this strain can be easily linked to the tensile load required to induce delamination onset, denoted as $N_{x,onset}$:

$$\varepsilon_{a,onset} = \frac{Y_{is}^T}{E_2}\sqrt{\frac{0.27024}{f(D_{onset})}} = \varepsilon_{x,onset} = \frac{\sigma_{x,onset}}{E_x} = \frac{(N_{x,onset}/h)}{E_x} \tag{5.29}$$

where $f(D_{onset})$ is defined in eq. 4.6, Y_{is}^T is the transverse in-situ strength, E_2 is the transverse Young's modulus of the ply, $\sigma_{x,onset}$ is onset stress applied to the laminate, E_x is the longitudinal stiffness of the laminate calculated with CLT (assuming a spacing of cracks of D_{onset}), h is the laminate thickness and $N_{x,onset}$ is the onset load.

This method offers significant advantages as it does not rely on experimentally-obtained critical Strain Energy Release Rates (SERR), unlike other approaches such as the one proposed by O'Brien for free-edge delaminations [13]. Instead, it only requires the material properties and the transverse in-situ strength of the ply, denoted as Y_{is}^T. This makes the method more convenient and less dependent on specific experimental data. Furthermore, this method can also be applied to laminates in which the critical ply is subjected only to transverse tension, basically any general symmetrical laminate that contains 90º plies.

5.4.2. Symmetrical laminate under tension or tension + shear

When considering a general symmetrical laminate under pure tension or shear combined with tension, the procedure is fundamentally similar to the previous approach. However, in this case, the Strain Energy Release Rate (SERR) expressions cannot be normalized due to the presence of local shear loads in the critical ply. In a general laminate, the critical ply can have any orientation, resulting in the generation of local shear even under pure tension loading. To account for this, the SERR expression defined in equation 4.32 should be used, which includes the terms $G_{12,red}$ and $G'_{12,red}$ (refer to equations 4.3 and 4.28). These terms are dependent on the local applied shear, denoted as $\gamma_a = f(\varepsilon_x, \gamma_{xy})$. Consequently, an analytical normalization of the equation is not feasible.

To determine the onset load, an iterative process is required. It involves incrementally applying loads (N_x or N_x/N_{xy}) to the laminate and checking if the criteria proposed by Socci & Kassapoglou, as explained in section 4.2.2, is met for a ply subjected to combined shear and transverse tension. The onset load is obtained by imposing first the condition that, for a given load combination (N_x/N_{xy}), the following criterion is satisfied:

$$G^{cr}(N_x/N_{xy}, D) = G^{cr+del}_{onset}(N_x/N_{xy}, D) \tag{5.30}$$

By imposing this condition, a potential value for D_{onset} is obtained as a solution. However, it is essential to validate this value by evaluating it against the criteria outlined in section 4.2.2 that predicts the crack spacing in a ply for a combineD loading:

$$\frac{\sigma^2_{yav}(D_{onset})}{(Y^t_{is})^2} + \frac{\tau^2_{xyav}(D_{onset})}{(S_{is})^2} = 1 \tag{5.31}$$

If the criteria is met, the value of D_{onset} is determined. However, if the criteria is not satisfied, the load needs to be adjusted and the process is repeated until the correct value of D_{onset} is obtained. Once the value of D_{onset} is determined, the corresponding load at that point

will represent the onset load for delamination ($N_{x,onset}$ or $N_{x,onset}/N_{xy,onset}$). A flowchart in Figure 5.20 provides a simple visual representation of the iterative process.

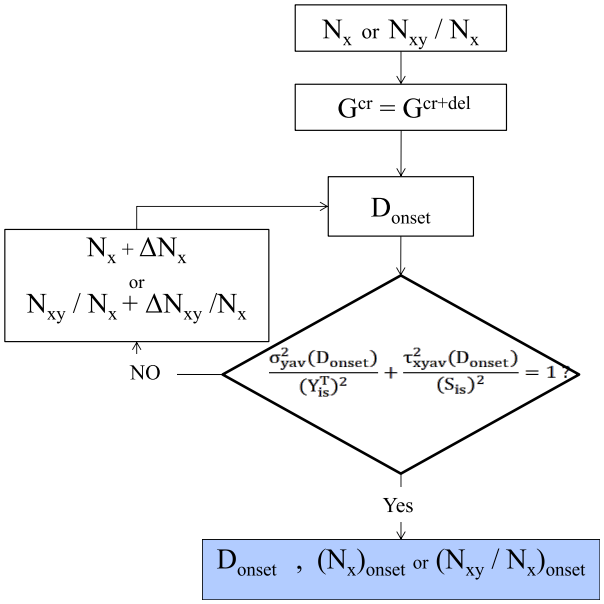

Figure 5.20: Flowchart of the iteration process to obtain the delamination onset load.

5.4.3. Influence of proposed delamination configurations

Both previously proposed methods use the Strain Energy Release Rate expression for delamination onset, denoted as G^{cr+del}_{onset}. However, as defined in section 5.26, there are three distinct equations that correspond to the four configurations of delaminations being considered. All three equations will be employed to determine a range of onset loads, as illustrated in Figure 5.21.

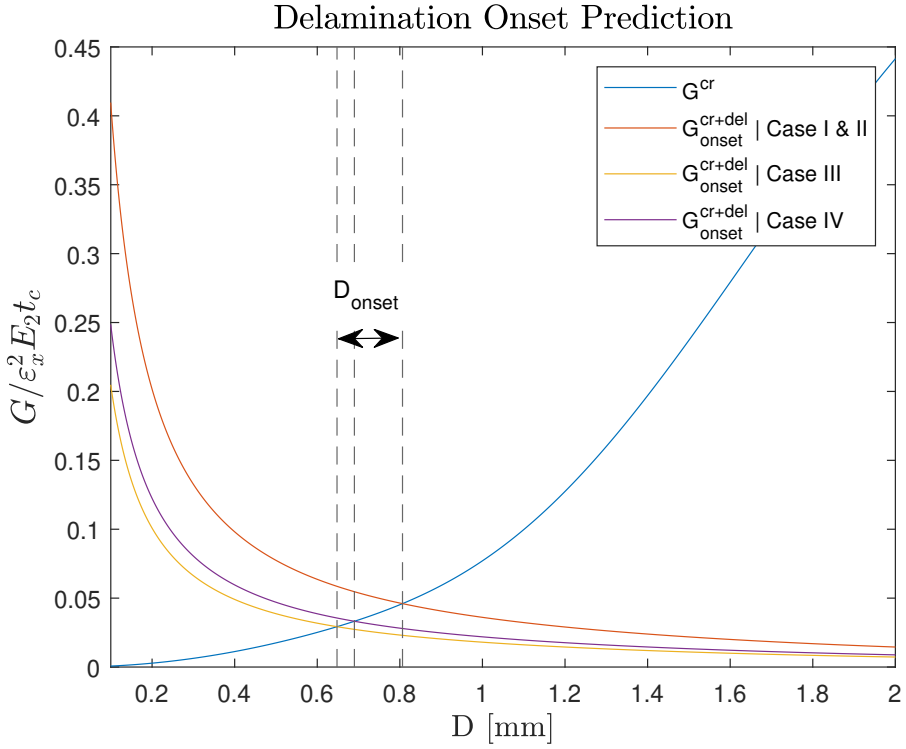

Figure 5.21: G^{cr} vs G^{cr+del}_{onset} for the four different delamination configurations.

As shown above, the intersection of the three different equations yields three distinct values of D_{onset}. Following the previously explained method, three different delamination onset loads can be obtained. Consequently, it becomes possible to establish a prediction range, with the upper and lower limits representing the most and least conservative D_{onset} values, respectively. Assuming the same laminate with consistent properties, including in-situ strengths, a smaller D_{onset} in a ply will require a higher load to achieve that spacing. Therefore, the smallest D_{onset} value will correspond to the highest delamination onset load. In this particular example, case I results in the highest D_{onset} value, which consequently corresponds to the lowest $N_{x,onset}$ value. Hence, case I is considered the most conservative one. Ideally, the real load at which delamination is initially detected should fall within this range and should be higher than the model's most conservative value.

It is worth noting that when the G^{cr} curve shifts towards the right, the intersections with the G^{cr+del}_{onset} expressions occur closer together. As a result, the range of D_{onset} (and consequently, the range of $N_{x,onset}$) becomes smaller. This shift can occur, for instance, if there is a thick 90º block present, as mentioned in Figure 4.6. The SERR expressions for delamination onset will also undergo changes. However, as discussed in section 5.3.1, most of the differences occur at very low crack spacings, whereas the intersections with G^{cr} are more likely to occur at higher D values.

5.5. Validation

A validation of the model to predict the delamination onset is presented in this section. Data from relevant literature sources is used.

5.5.1. Carraro et al. [44]

In their study, Carraro et al. [44] performed experiments on two cross-ply arrangements of glass fiber UT-E500/Epikote RIMR235. Their research focused on analyzing the development of cracks in the 90º ply block and determining the load at which initial delamination was observed. The reported delamination onset stress value came with an associated error but the specific number of tested specimens was not included. Figure 5.22 displays both their experimental findings and the outcomes predicted by our proposed method.

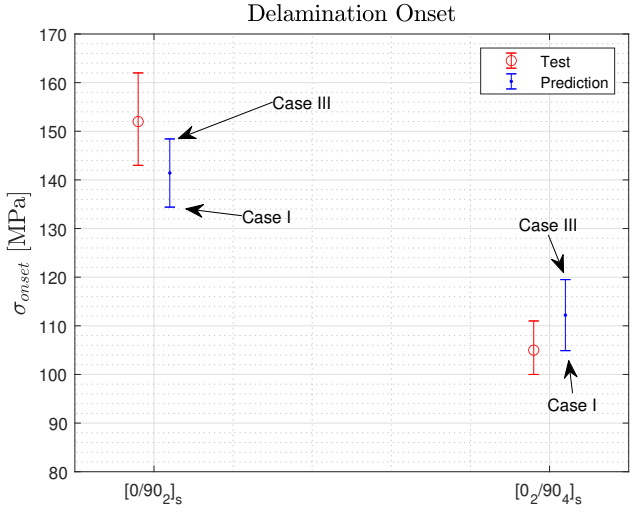

Figure 5.22: Delamination onset stress for a $[0/90_2]_s$ & $[0_2/90_4]_s$ laminate under uniaxial tension. Be aware that the test and predicted data were separated along the x-axis solely for the purpose of displaying the results more clearly.

The model exhibits small discrepancies in predicting the delamination onset stress for the $[0/90_2]_s$ and $[0_2/90_4]_s$ laminates, as depicted in Fig. 5.22. Specifically, it underpredicts the onset stress for $[0/90_2]_s$ and overpredicts it for $[0_2/90_4]_s$. Case I, as explained in section 5.4.3, gives the most conservative prediction being 134.4 MPa for $[0/90_2]_s$ and 104.9 MPa for $[0_2/90_4]_s$. Case III on the contrary constitutes the less conservative case giving an onset stress of 148.42 MPa and 119.5 MPa respectively. Overall, there is good correlation between the predictions and experimental results.

The observed trend in the model's behavior suggests that it may tend to be less conservative (overpredicts onset loads) for thicker 90º plies. This behavior is likely influenced by the parameter Y_{is}^T, representing the transverse in-situ strength, which plays a critical role in the prediction. In this study, the value of Y_{is}^T was approximated using the transverse strength of the ply, which is generally acceptable. However, for cases with very thick ply blocks (e.g., eight 90º plies), the block behaves more like a thick individual ply and thicker plies typically have less in-situ strength than thinner ones [67]. Therefore, if the same $Y_{[}^T is]$ is used for both the $[0/90_2]_s$ and $[0_2/90_4]_s$ laminates, the model might be assuming a higher strength in the latter, potentially explaining the overprediction.

The model assumes that all 90º plies have the same behavior since the transverse applied strain in them is identical which gives an identical crack distance in each ply for every load. Essentially, the model views the 90º ply block as a single, very thick ply around which delamination will initiate. To improve predictions, it is suggested to adapt the Y_{is}^T value based on the thickness of the 90º ply block or use experimental Y_{is}^T values when available. Additionally, Carraro et al. reported a damage evolution similar to that shown in Fig. 2.7, which essentially combines all four cases proposed in section 5.2.1. This means that the configurations proposed are relevant for a real scenario.

The calculation of the Strain Energy Release Rate (SERR) for delamination growth and onset relies on a rather restrictive assumption as it was mentioned during the derivation of the expression. It is assumed that once delamination begins at the crack tips, the propagation is halted by matrix cracks, leading to a state of crack saturation where the matrix crack spacing remain highly stable. This phenomenon, known as crack saturation, has been supported by experimental observations in the literature [21, 69, 70]. Carraro et al. conducted important work in which they monitored crack density and reported the delamination onset, providing valuable validation for this assumption.

Figure 5.23 illustrates the evolution of crack spacing (previously shown in the previous chapter) and the stress at which the first delamination is detected, both in the experimental test and our model. To avoid confusion, only the delamination onset stress predicted for Case III is plotted. For the $[0/90_2]_s$ laminate, after the delamination onset load, the crack spacing/density remains relatively stable. In the case of the $[0_2/90_4]_s$, this phenomenon is less clear, and crack propagation appears to continue at least within the range of [100 - 125] MPa. Nevertheless, the assumption that the crack spacing remains constant after the delamination onset, enabling the derivation of the SERR expression for both delamination growth and onset, seems reasonably accurate. Note that the predicted delamination onset for the $[0_2/90_4]_s$ laminate (continuos blue line) and the tested delamination onset (dashed blue line) in Figure 5.23 are almost superposed.

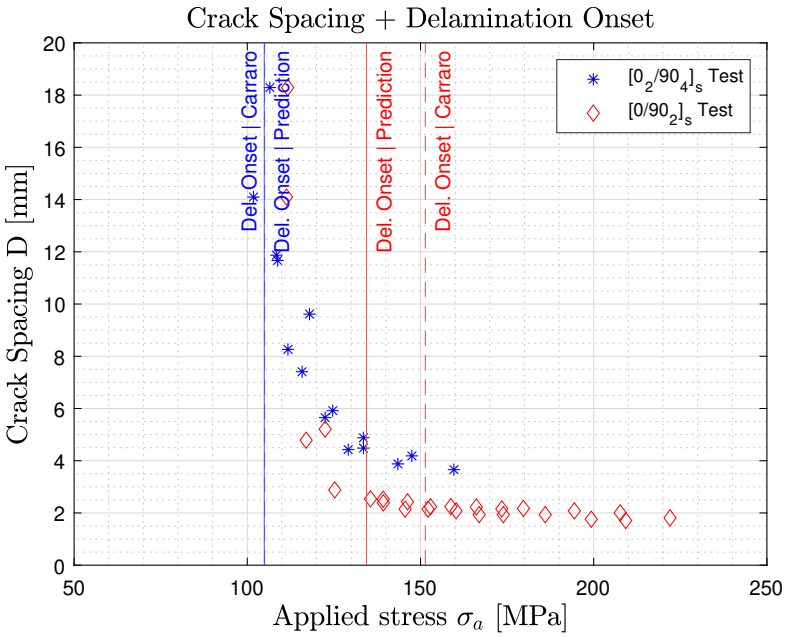

Figure 5.23: Crack spacing and delamination onset stress for a $[0/90_2]_s$ & $[0_2/90_4]_s$ laminate under uniaxial tension.

5.5.2. Chou et al. [71]

Chou et al. [71] conducted experiments to explore the presence of matrix cracks and delaminations in AS/3501-6 $[\pm 25/90_n]_s$ graphite-epoxy laminates under quasi-static and fatigue loading conditions. Their results, in which they do not reported an error interval, are plotted in Figure 5.24 with the predictions of the model. While not explicitly stated, the upper boundary of the prediction still corresponds to Case III and the lower boundary corresponds to Case I.

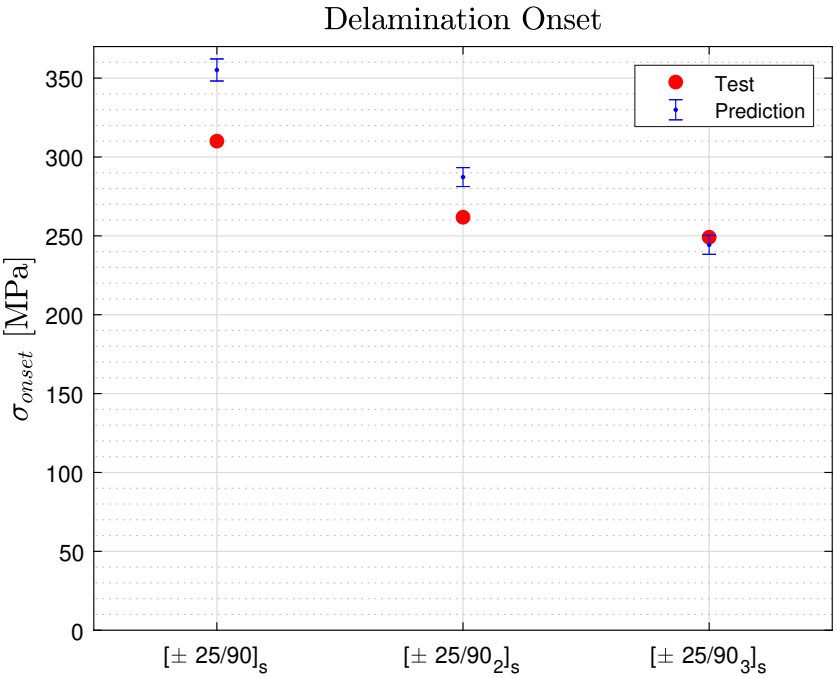

Figure 5.24: Delamination onset stress for $[\pm 25/90_n]_s$ laminates under uniaxial tension.

In this instance, the correlation between the test results and the model is not as strong, but the model successfully captures the trend where the delamination onset stress decreases with an increase in the number of 90º plies. Specifically, for the $[\pm 25/90]_s$ laminate, the model overpredicts by approximately 12%, while for the $[\pm 25/90_2]_s$ laminate, the overestimation is around 8.6%. However, for the thicker laminate, the prediction is notably accurate, with the test yielding 249.14 MPa and the model's prediction falling within the range of [240.84 - 246.30] MPa, resulting in an underestimation of the stress by approximately 3%. The in-situ transverse strength of a ply is influenced by the relative orientation of the adjacent ply as well [67]. Hence, in this scenario, the -25/90 interface may be exerting enough influence on the strength to result in poorer predictions. The approximation of Y_{is}^T has been solely based on the ply transverse strength, suggesting that a more precise value could potentially lead to further improvements in the predictions.

5.5.3. Takeda & Ogihara [7]

Ogihara & Takeda conducted a study on the initiation and growth of delaminations caused by matrix cracks in laminates with orientations $[0/90_4/0]$, $[0/90_8/0]$ and $[0/90_{12}/0]$ under quasi-static tension. Figure 5.25 illustrates the reported onset stress from their experiments along with the predictions made by our model. Additionally, our model predicts the delamination onset stress for laminates with orientations $[0/90_n/0]$ where n ranges from 1 to 14, which incorporate the tested cases. The blue curve represents a second-order fitting of the predicted values for n ranging from 1 to 14, aiming to capture the overall trend while including the three test values obtained from Takeda & Ogihara.

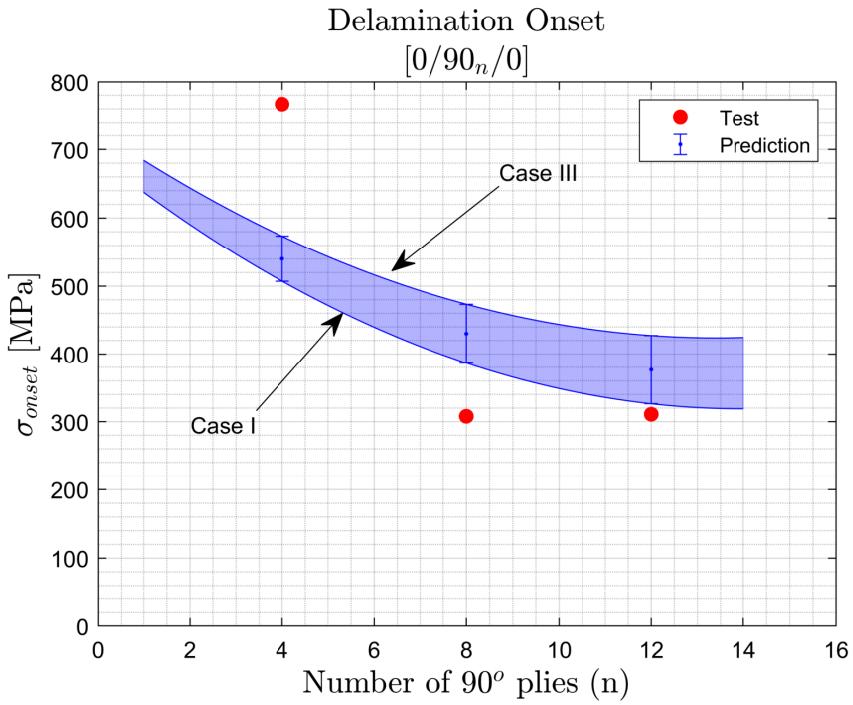

Figure 5.25: Delamination onset stress for $[0/90_n/0]_s$ laminates under uniaxial tension.

The model exhibits an underprediction for the onset of the $[0/90_4/0]$ laminate by approximately 33%, which, on one hand, is advantageous as it provides a conservative estimate. However, for improved accuracy, it should ideally be closer to the actual value. The other two reported values are overpredicted by approximately 24.5% and 4.9% respectively. Although

these results may initially appear somewhat imprecise, it is essential to consider the complexity of the physical process and the utilization of approximate transverse in-situ strength values, which contributes to the accuracy achieved.

One of the strengths of model could be seen in the prediction band for laminates with a number of 90º plies ranging from 1 to 14. Although the results may not be highly precise, they effectively capture the overall trend of the process. This feature proves immensely valuable in engineering applications where extreme precision may not be a strict requirement. For instance, during design phases involving numerous laminates, the model can rapidly offer a general understanding of their behavior and facilitate easy comparisons among them.

5.5.4. Brewer & Lagace [46]

Brewer & Lagace conducted a study on delamination initiation in graphite/epoxy laminates with 15º plies. They performed experimental tensile tests and also proposed a criteria for the process. The graphite/epoxy plies used in their experiments were Hercules AS1/3501-6 and the reported properties included the thickness of the plies (0.169 mm) and the length of the specimen (200 mm). Other properties of the material were obtained from existing papers with the same material.

Their main focus in the study was directed towards free edge delaminations for the family of $[\pm 15_n]s$ laminates. By employing our model and comparing its outcomes with their experimental data, valuable insights can be obtained regarding the applicability of our method. Since all plies are critical according to the Maximum Stress criteria, cracks are considered in all the plies. The delamination was assumed to occur at the interfaces between the 15/-15 plies due to the likelihood of experiencing the highest interlaminar normal and shear stresses. However, a limitation of our model is that it only considers two symmetrical delaminations, which is a common scenario. Nevertheless, as discussed in Section 5.2.2, the same assumptions and procedures can be employed to determine the stiffness of laminates with more than 2 delaminations. The stiffness is obtained from the schematics illustrated in Figure 5.26 for case I, and the same process is applied for the remaining cases and laminates. Subsequently, the procedure to determine G_{onset}^{cr+del} remains identical. The comparison between the test results and predictions is presented in Figure 5.27.

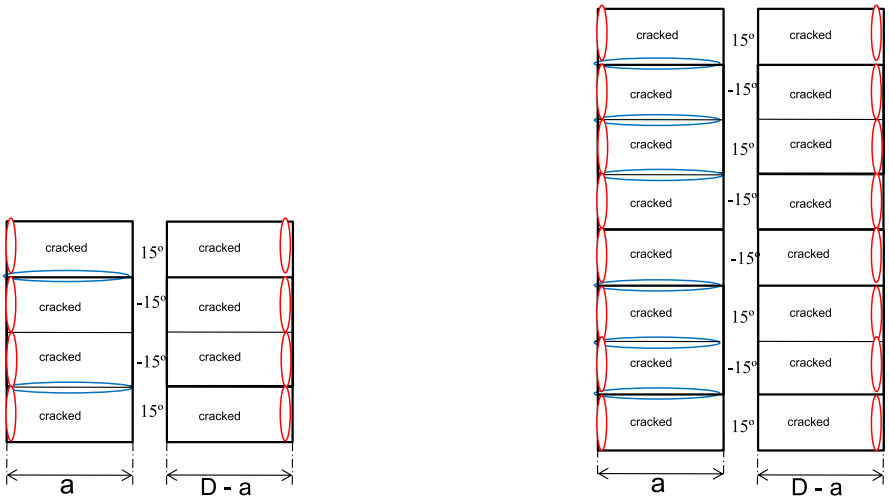

(a) $[\pm 15]_s$ **(b)** $[\pm 15_2]_s$.

Figure 5.26: Delamination and crack distribution for Case I.

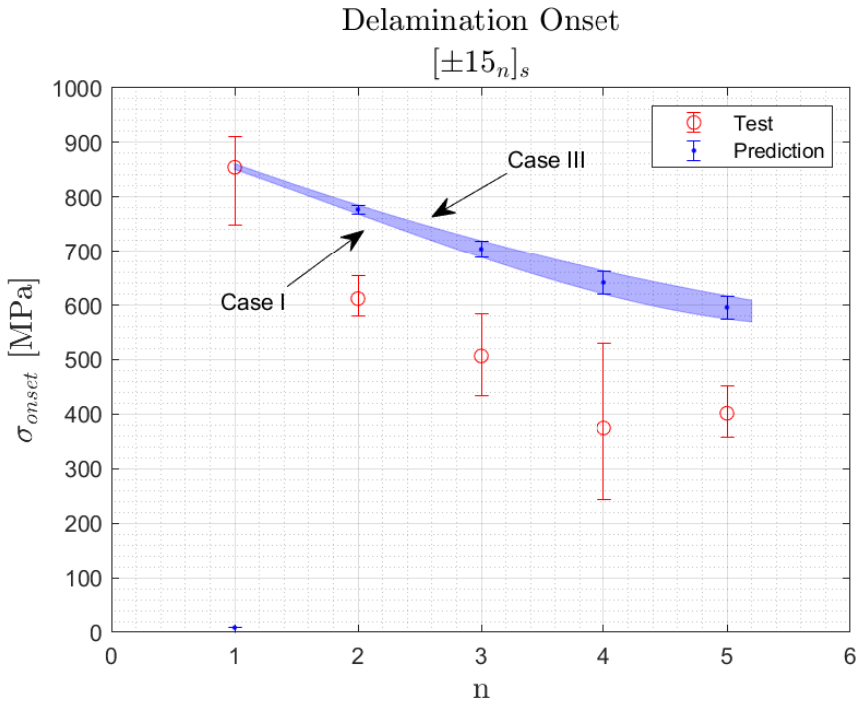

Figure 5.27: Delamination onset stress for $[\pm 15_n]_s$ laminates under uniaxial tension.

As evident from the results, the prediction is not highly accurate, with the delamination onset stress being approximately 40% higher on average, except in the case of n = 1. This outcome might seem reasonable, given that the measured stress corresponds to a free-edge delamination. However, the intriguing aspect is that, assuming our model is correct, the delamination induced by cracks will occur after the free-edge delamination. This is due to the $[\pm 15_n]_s$ laminate under tension being not prone to crack initiation, making delaminations starting at crack tips highly unlikely. The authors themselves support this fact, as they stated: "*The initiation stresses for the three laminate types are displayed in Figures 3 through 5 where the range of data is shown. In no cases did transverse cracks form before delamination initiation. Indeed, in many cases, delamination initiated without the formation of transverse cracks*" (Brewer & Lagace, [46]).

Despite this, the authors also confirmed that some specimens did exhibit delamination induced by matrix cracks, but these cases were not in the majority. The authors' statement reads: "*A number of specimens gave initiation stress data which fell outside the range of similar specimens. These fell into two categories. Some specimens exhibited initiations emanating from initial defects such as microvoids or preexisting transverse cracks. Other specimens exhibited massive delamination fracture. The cases of initiations emanating from existing defects clearly define a separate data set since the existing defect will change the stress field in its vicinity, thereby deviating from the straight free edge case being considered*" Brewer & Lagace, [46]). The high accuracy observed for n = 1 could potentially suggest that in this particular case, more cracks were formed, resulting in a behavior closer to what our method proposes. However, this is merely a speculation.

The absence of cracks could have been anticipated by analyzing the Strain Energy Release (SERR) for crack propagation, as obtained in this thesis. Figure 4.19 clearly indicates that the $[0/20_2]_s$ and $[0/10_2]s$ laminates, which can be extrapolated to a [±15] to some degree, exhibit extremely low G^{cr} values, signifying a very low likelihood of crack propagation. This finding explains why the delamination onset stress is overpredicted; the intersection with G^{cr+del}_{onset}

occurs at relatively low D values, which require relatively high loads to be produced. This suggests that our model might not be inaccurate; instead, another process, such as free-edge delamination as described by the authors, occurs before the delamination induced by cracks.

This comparison helps to understand the limitations of the model. The method presented in this thesis can theoretically be applied to any laminate, but an understanding of which processes are more prone to occur is also needed beforehand. As observed in previous validations, the method works remarkably well in cross-plies under tension or similar stack sequences, where delamination from a crack tip is more likely due to the higher occurrence of cracks. In those cases the method can predict the onset and that will most likely be the reason for the failure of the structure. However, in laminates where cracks are less likely, the assumption that cracks are present could be still valid but other processes will make the structure fail before our method can "kick-in". Nevertheless, as mentioned by the authors, delaminations induced by matrix cracks also occur in addition to free-edge delaminations, highlighting the complexity of these processes and the probable influence of localized defects.

In general, it is reasonable to deduce that the model exhibits a good correlation with reality. However, in specific cases like the one discussed here, where delaminations induced by cracks are less likely to occur, the model's usefulness is limited. While the model assumptions hold well for cross-plies and laminates with similar behaviours, its accuracy diminishes when applied to laminates that deviate from such behavior. This doesn't necessarily mean that the method cannot be used, but it indicates that other processes, like free-edge delaminations in this case, might occur before the development of delaminations induced by matrix cracks, which the model is designed to simulate.

5.5.5. Nairn & Hu [21]

The proposed method for modeling the delamination onset stress also provides predictions for the crack spacing at the onset (D_{onset}). This parameter represents the distance between cracks at which delaminations theoretically appear at their tips. It holds significant importance as it helps assess when a crack poses a real threat to the structure's integrity. Nairn & Liu introduced a variational method to study delamination onset induced by matrix cracks, and their research yielded various conclusions, including graphs that relate the cracks at the onset to different laminates. Specifically, their graph, shown in Figure 5.28, presents the critical crack density ($1/D_{onset}$ in our notation) for various thicknesses of $[0/90_n]_s$, $[0_2/90_n]_s$ and $[\pm 45/90_n]_s$ laminates. Using our model, the corresponding graph is presented in Figure 5.29.

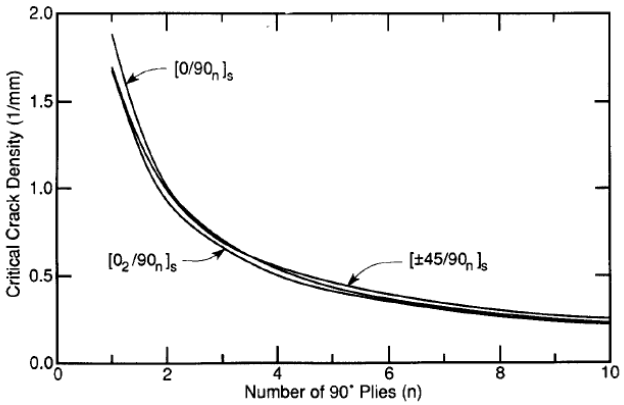

Figure 5.28: Critical crack densities ($1/D_{onset}$ in our notation) in the delamination onset. Obtained from [21].

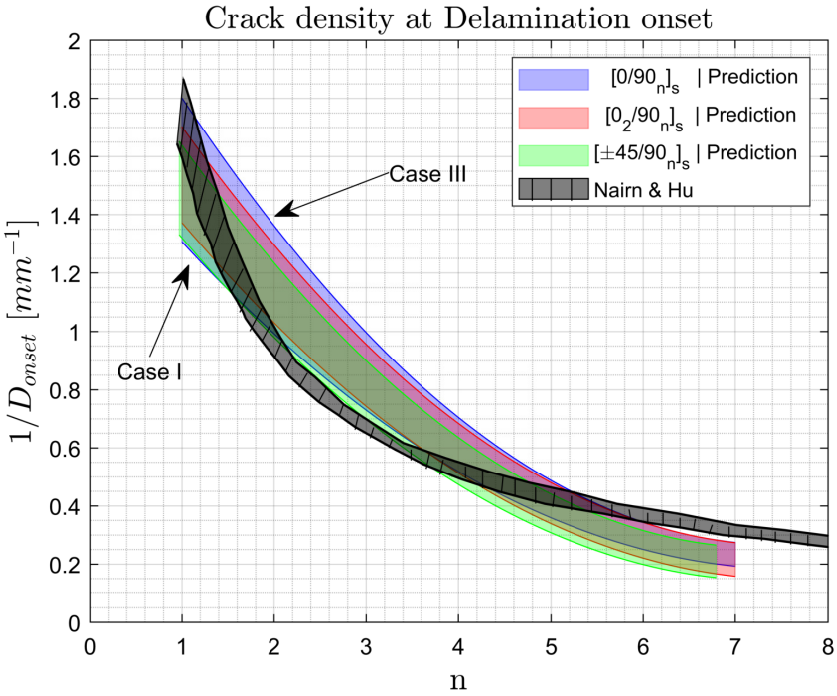

Figure 5.29: Crack density at the delamination onset for different laminates compared to Nairn & Liu's results. The hatched fill area contain all 3 curves from Fig. 5.28

While the trends observed in both Nairn and Liu's work and our present method are highly accurate, it is important to acknowledge that their model, like ours, is also a proposed model and there could be slight discrepancies between the predictions and experimental results. Both methods predict lower crack densities at the onset for thinner critical plies (90^o plies). However, our model slightly underpredicts the crack density for all n values. The band formed by the solution for case III and case I is wider in the $[0/90_n]_s$ laminate and narrows down for thicker laminates. Notably, all three families of laminates show similar values. This is because our model solely considers cracks in the 90^o plies and delamination in the $0^o/90^o$ interface, making the outer plies have minimal impact on the prediction, except for the calculation of laminate stiffnesses.

Thinner 90^o ply blocks require higher crack densities for the onset of delamination (resulting in lower crack spacing), which means a higher load is needed to generate that smaller spacing. Therefore, thinner 90^o plies exhibit better behavior against delamination initiation. This observation aligns with experimental cases, where thicker blocks of plies tend to generate higher interlaminar stresses, often leading to the appearance of delamination.

The plots generated by the model are valuable in determining how close the actual structure is to a potentially dangerous region. By inspecting the cracks in the laminate's 90^o plies and comparing the observed values to those predicted in Figure 5.29, one can assess the safety status. If the observed crack density is far from the values predicted in the graph, it can be assumed that the structure is not in imminent danger. On the other hand, if the observed crack density is approaching the predicted values, some concern should be warranted. These plots serve as a helpful tool to monitor damage and make comparisons between different laminates. It is important to note that the model is applicable only to quasi-static loading situations.

5.6. Sensitivity study

In order to enhance the method's applicability, it is crucial to identify the most vital parameters that ensure the model functions correctly. In this section, the parameters of the material used by Carraro et al. [44] will be perturbed and the resulting behavior of delamination onset stress will be observed. Figure 5.30 illustrates the ratio of delamination onset stress w.r.t. the original value ($\sigma_{onset/\sigma^*_{onset}}$) for various perturbations of the parameters denoted as Δ. Notably, within the 0%-20% range, the deviation from the original value exhibits linearity, with the transverse in-situ strength Y^T_{is} being the most critical property. This outcome was as anticipated, considering Y^T_{is} significantly influences crack propagation and is present in eq. 5.29.

Regrettably, obtaining an accurate value for the transverse in-situ strength (Y^T_{is}) can prove challenging without conducting experimental tests. On the other hand, S_{is} and G_{12} do not impact the properties due to the cross-ply configuration being under pure tension, meaning there is no shear in any ply. This observation is apparent in the close-form expressions of G^{cr} and G^{cr+del} for a cross-ply (eq. 4.3.2 & 5.26), where G_{12} is absent when there is no shear ($\gamma_{xy} = 0$).

Additionally, E_1, E_2 and L also significantly influence the solution; fortunately, the available values for these properties are usually accurate and should not exceed a 10% error. Its worth noting that if the parameters are perturbed more than a 25%, a non-linear behaviour appears although it is fair to assume that all properties values will be known with an error of less than 25%.

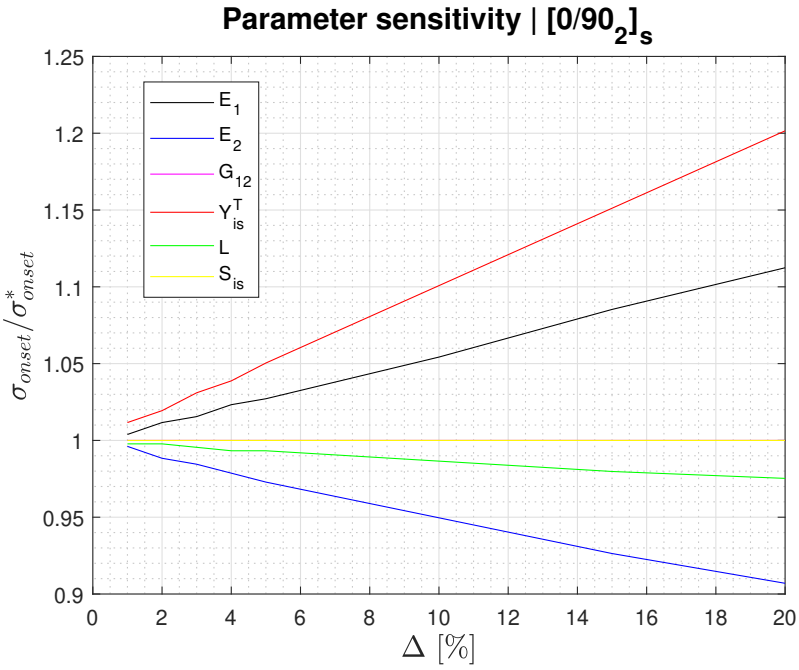

Figure 5.30: Delamination onset stress perturbing the parameters a certain percentage (Δ) normalized with the original solution.

The preceding analysis focused on the conservative solution, case III configuration. In Figure 5.31, 5.32 and 5.33, a comparison is presented between the behaviors of case III and case I when their parameters are perturbed. It is evident that both cases exhibit similar behavior, albeit with slight differences. Notably, the parameter L shows greater sensitivity in case III. This is attributed to the fact that the ratio L/D in eq. 5.26 is relatively larger than 1/8, in contrast to

the 1/4 ratio observed in case I.

Despite these differences, all parameters behave in a relatively similar manner, which aligns with expectations since only the expression for G_{onset}^{cr+del} changes "inside" the delamination onset prediction.

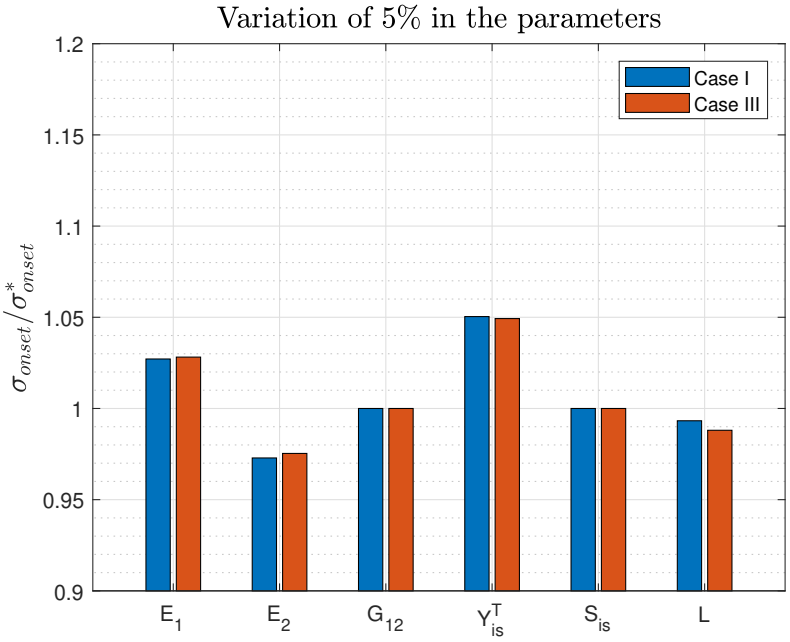

Figure 5.31: Case I & Case III solutions perturbing the parameters a 5%.

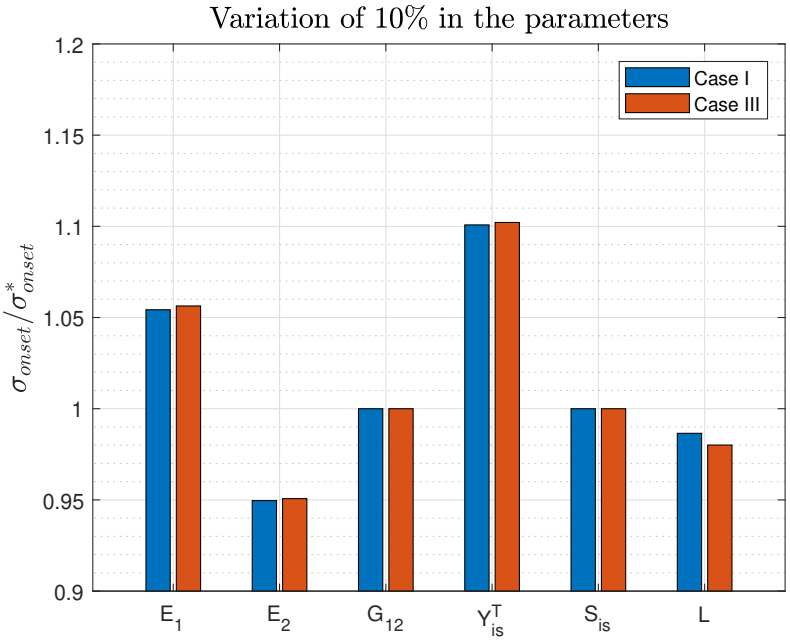

Figure 5.32: Case I & Case III solutions perturbing the parameters a 10%.

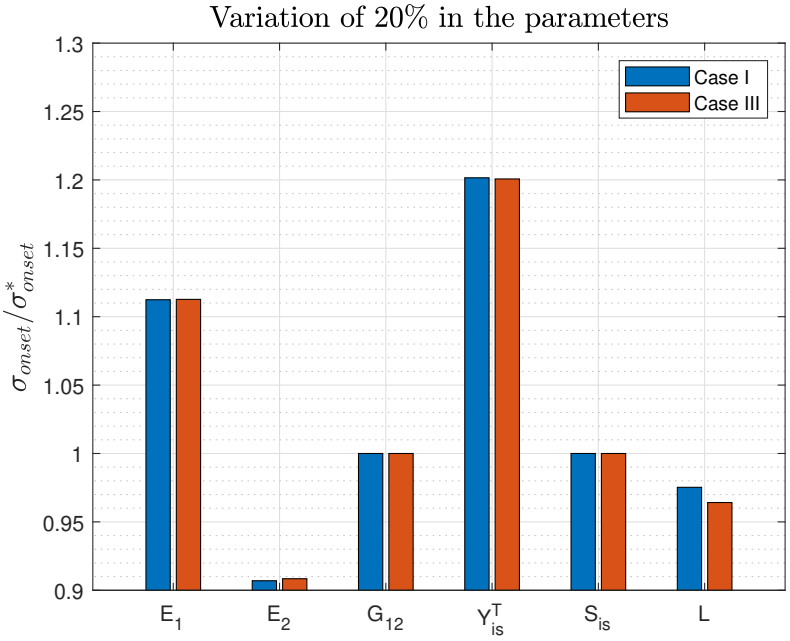

Figure 5.33: Case I & Case III solutions perturbing the parameters a 20%.

5.7. Design curves

The model introduced in this section also enables the creation of design curves that incorporate all the relevant parameters. These curves effectively represent and communicate the complete set of information and potential outcomes within a single set of plots. For instance, when considering a cross-ply under pure tension, the task of determining the delamination onset stress, denoted as $\sigma_{x,onset}$, involves certain variables outlined in detail in Section 5.4.1 which are presented below:

$$\sigma_{x,onset} = f\left(E_1, E_2, \nu_{12}, t_c, t_1, L, Y_{is}^T\right) \tag{5.32}$$

where E_1, E_2 and ν_{12} are the Young's moduli of the ply and the Poisson ratio, respectively. Additionally, t_c stands for the thickness of the 90º plies, t_1 corresponds to the thickness of half of the 0º plies (as shown in Fig.4.4), L denotes the laminate length and Y_{is}^T represents the in-situ strength. To simplify the problem and make it dimensionless, we can create new variables using E_2 and t_1, effectively reducing the problem to five variables:

$$\frac{\sigma_{x,onset}}{E_2} = f\left(\frac{E_1}{E_2}, \nu_{12}, \frac{t_c}{t_1}, \frac{L}{t_1}, \frac{Y_{is}^T}{E_2}\right) \tag{5.33}$$

It is important to note that a general $[0/90_n]_s$ cross-ply configuration can be used with any number of 90º plies. However, the key parameter influencing the problem is the ratio t_c/t_1, which represents the total thickness of the 90º plies (whether there is one or multiple plies) divided by the thickness of half of the 0º plies. By studying all the possible cases based on these dimensionless variables, we can generate curves that depict the solution for the chosen set of dimensionless parameters. Let's fix ν_{12} to be 0.3 and L/t_1 to be 200/0.15, which serves as a representative case of a unidirectional (UD) ply commonly used in the industry. With these parameters in place, we can now obtain the normalized delamination onset stress for various combinations of the ratios E_1/E_2, t_c/t_1 and Y_{is}^T/E_2. Figure 5.34 and 5.35 provide a

three-dimensional representation of the solutions, helping visualize the relationships between the variables and the resultant delamination onset stress.

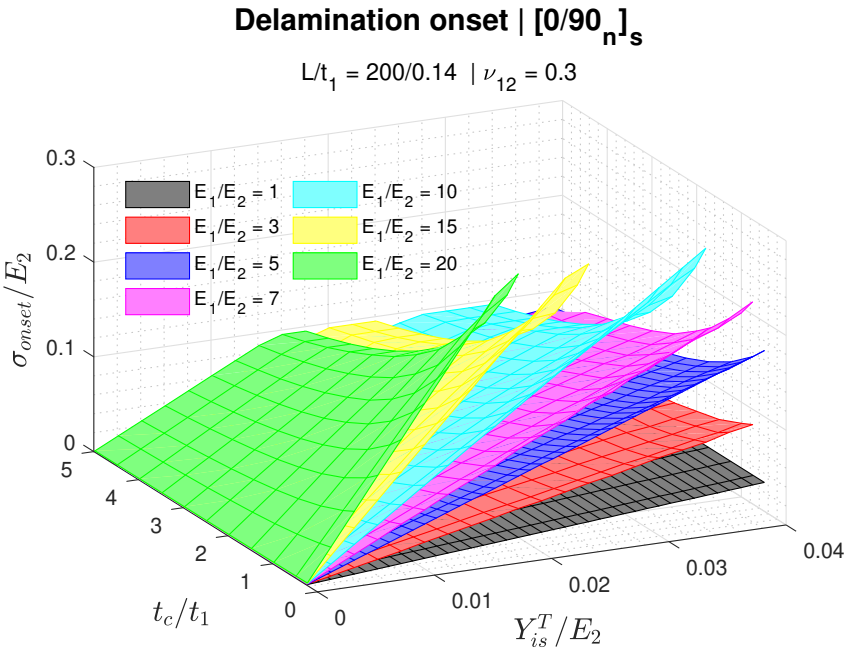

Figure 5.34: Normalized delamination onset stress as a function of E_1/E_2, t_c/t_1 and Y_{is}^T.

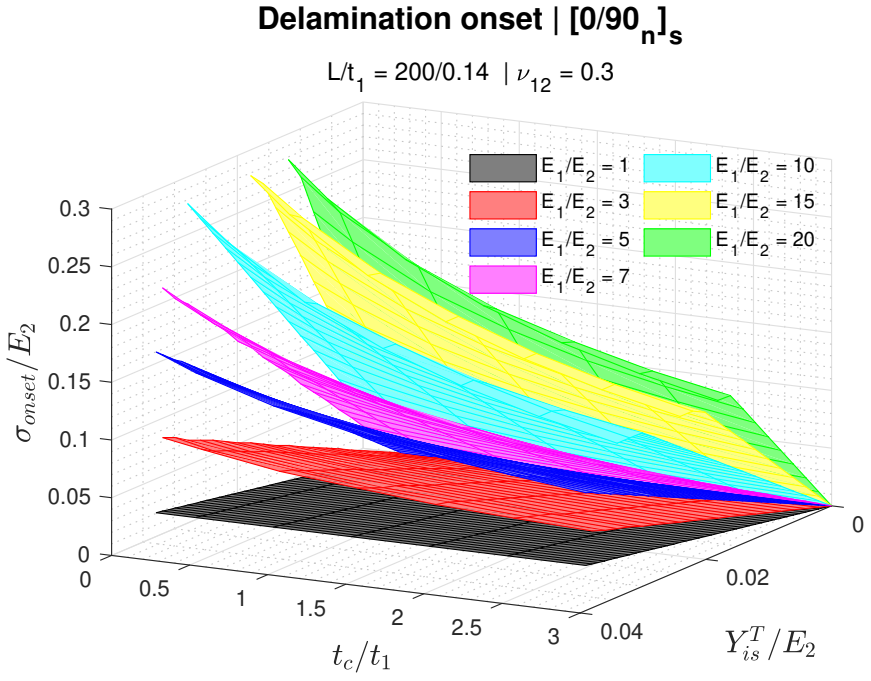

Figure 5.35: Normalized delamination onset stress as a function of E_1/E_2, t_c/t_1 and Y_{is}^T.

The previous graphs offer valuable insights into the overall trends of the delamination onset process. However, they may not be practical for directly extracting specific values required for other calculations or design procedures. To address this, isolines are constructed,

containing the $\sigma_{x,onset}/E_2$ values (representing the height in the 3D plot). Subsequently, distinct design curves corresponding to various E_1/E_2 ratios are introduced in Figures 5.36 - 5.42. These design curves provide a more detailed representation of the relationship between the parameters, making it easier to determine specific values needed for different design scenarios or engineering calculations. Note that the colorbar introduced is redundant with the numbered label in each isoline, curves could have been represented in a plain color.

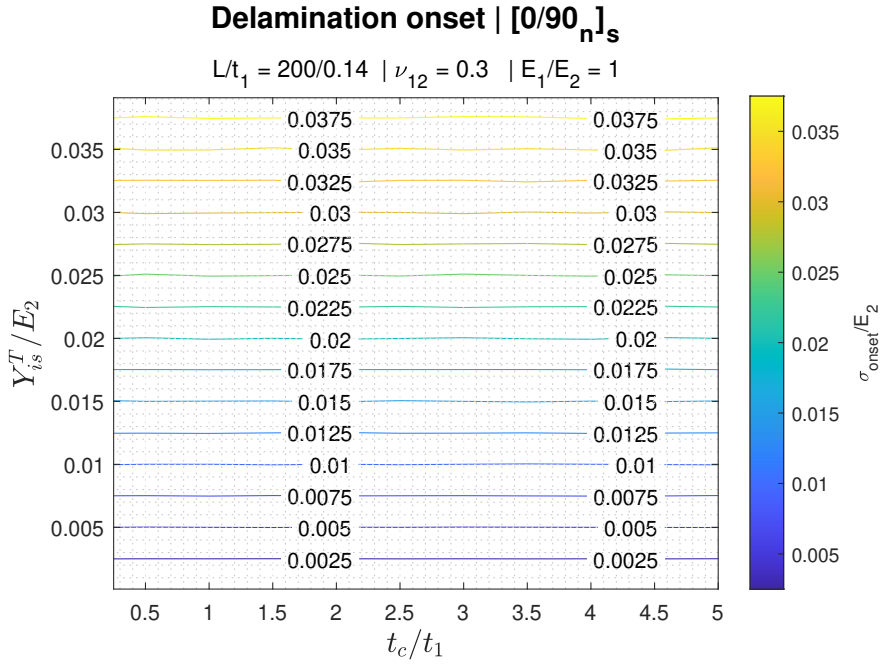

Figure 5.36: Normalized delamination onset stress as a function of t_c/t_1 and Y_{is}^T for $E_1/E_2 = 1$.

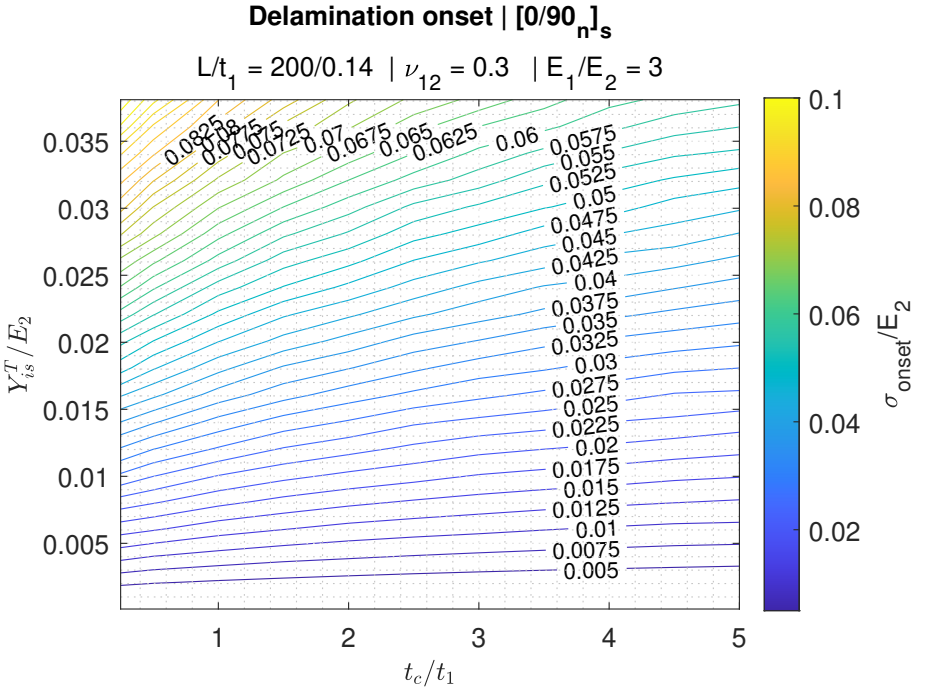

Figure 5.37: Normalized delamination onset stress as a function of t_c/t_1 and Y_{is}^T for $E_1/E_2 = 3$.

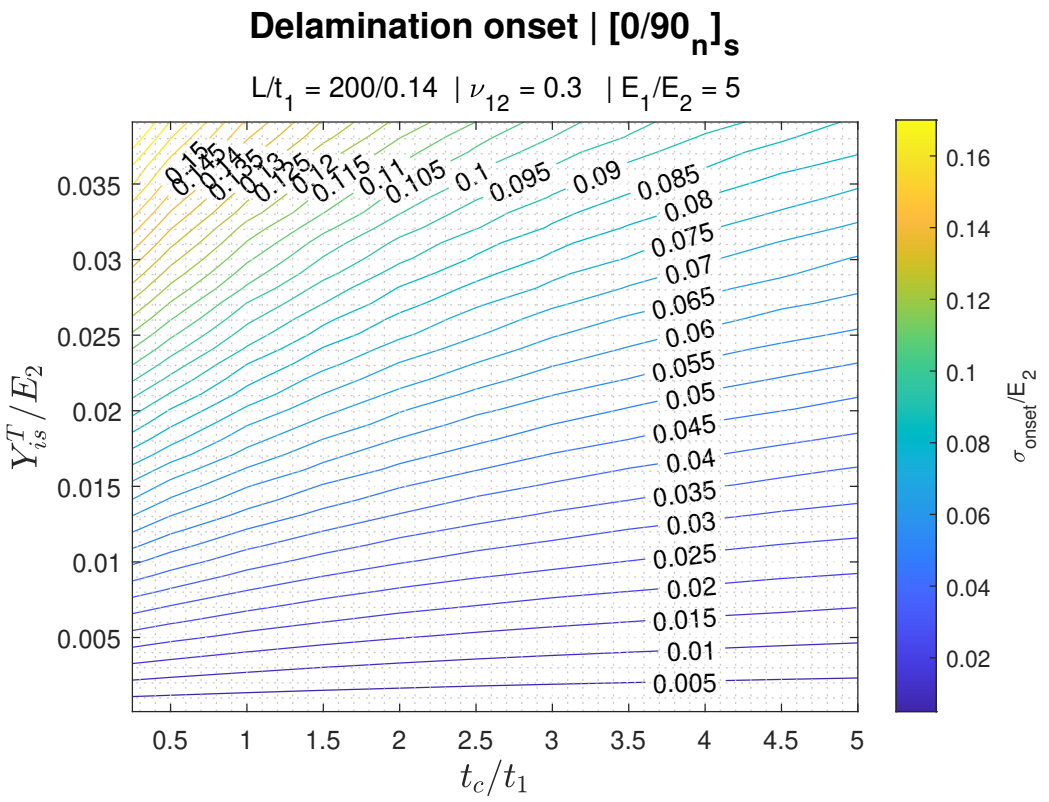

Figure 5.38: Normalized delamination onset stress as a function of t_c/t_1 and Y_{is}^T for $E_1/E_2 = 5$.

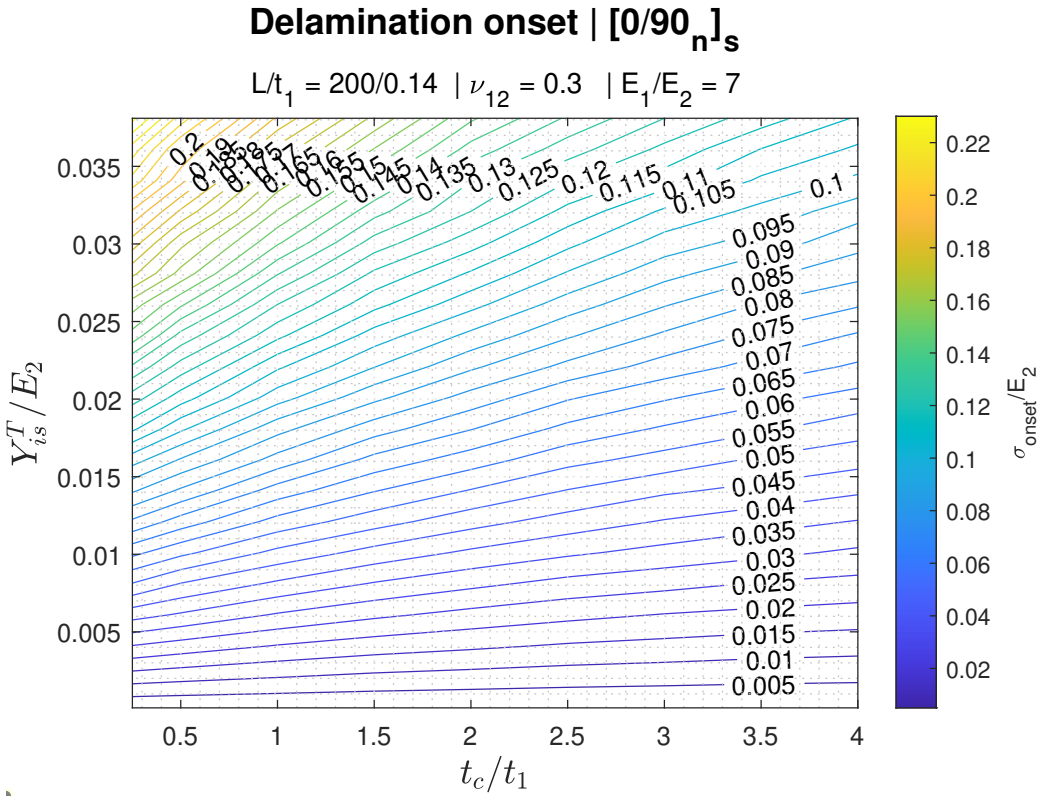

Figure 5.39: Normalized delamination onset stress as a function of t_c/t_1 and Y_{is}^T for $E_1/E_2 = 7$.

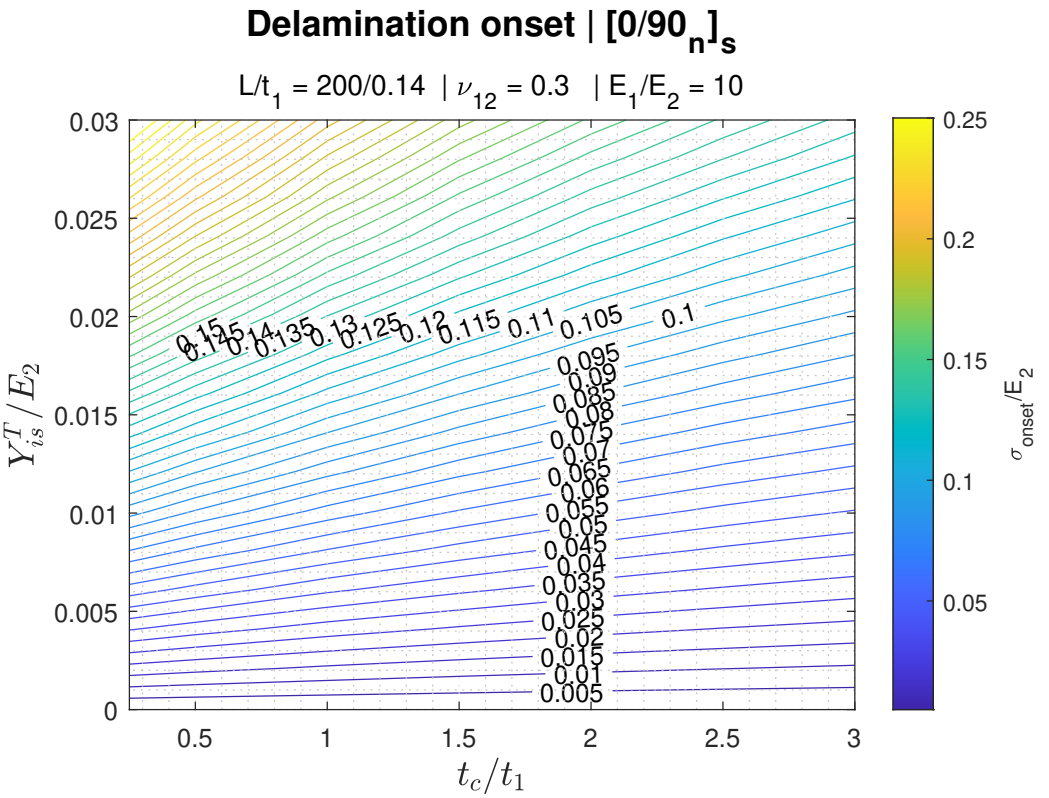

Figure 5.40: Normalized delamination onset stress as a function of t_c/t_1 and Y_{is}^T for $E_1/E_2 = 10$.

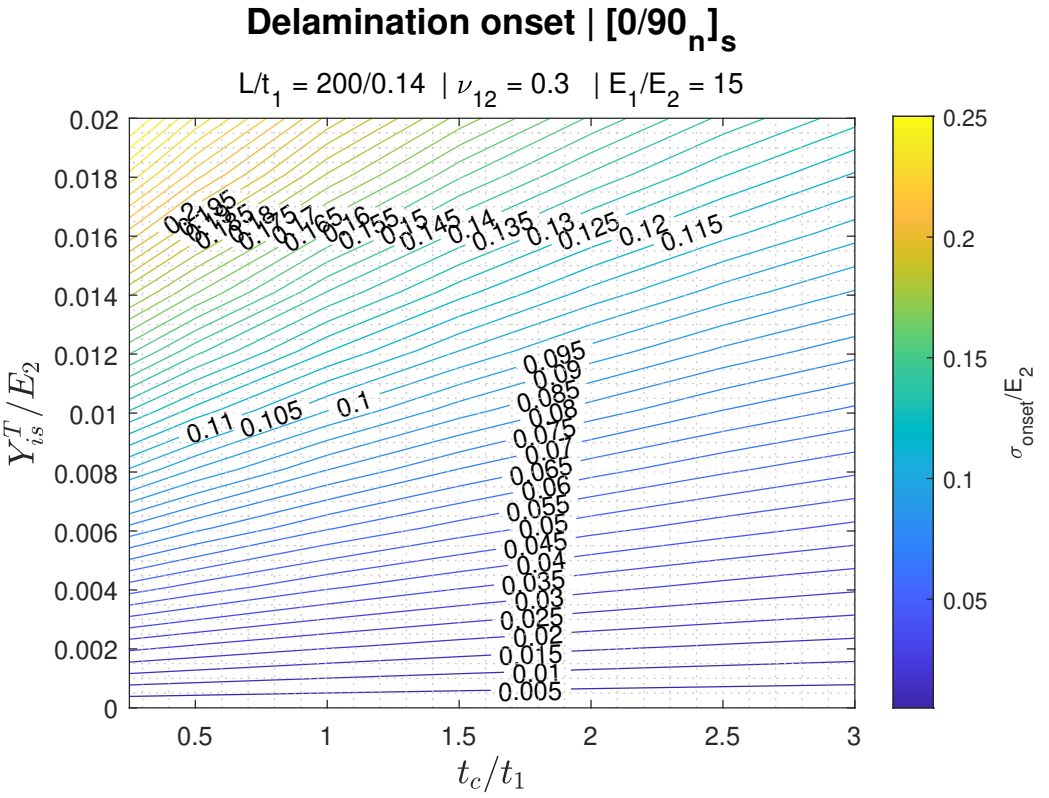

Figure 5.41: Normalized delamination onset stress as a function of t_c/t_1 and Y_{is}^T for $E_1/E_2 = 15$.

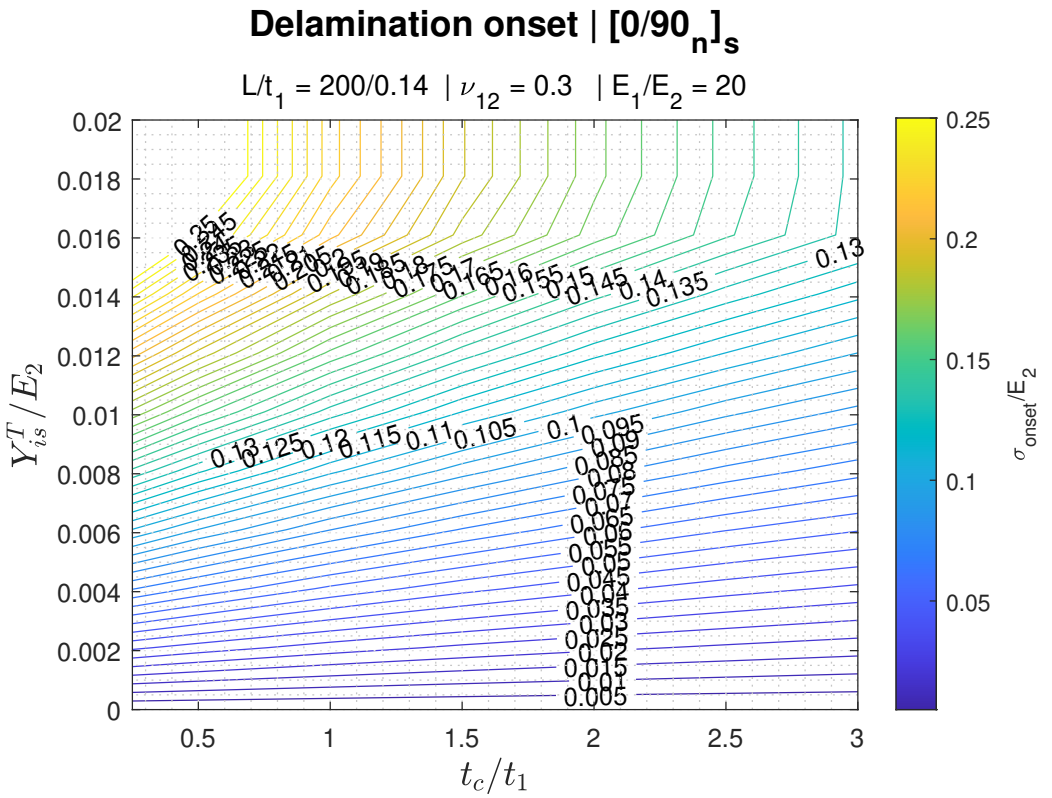

Figure 5.42: Normalized delamination onset stress as a function of t_c/t_1 and Y_{is}^T for $E_1/E_2 = 20$.

Similar curves can be derived for other fixed L/t_1 or ν_{12} values, for symmetrical laminates or for combined loading just following the method presented in Sections 4 & 5. However, it's important to acknowledge that, for example, in the case of a general symmetrical laminate under tension, additional variables come into play, such as G_{12}, γ_Y and S_{is}. Fixing these additional parameters will be necessary, increasing the complexity of the analysis.

In summary, the approach presented allows for the creation of design curves tailored to various specific situations, enabling a comprehensive exploration of how different laminate configurations affect the onset of delaminations induced by matrix cracks.

5.8. Generalization

If the material properties of a symmetrical laminate, such as the transverse in-situ strength Y_{is}^T, shear in-situ strength S_{is} and yield shear strain γ_Y (when not cross-ply), are known, the model can be used to obtain the delamination onset in a wide variety of cases. Next, the delamination onset stress is obtained for different symmetrical laminates with different ply thicknesses.

Figure 5.43 illustrates the behavior of various laminates concerning delamination onset stress. Among these laminates, the one with the most favorable behavior, i.e. highest load needed for the onset of delaminations induced by matrix cracks, is the $[0/30]_s$ configuration, which exhibits the highest onset stress. This superiority can be attributed to its similarity to a unidirectional (UD) block, as the difference in stiffness between the 0º and 30º plies is relatively small. Following this, the $[0/45]_s$ laminate experiences localized shear in its 45º ply, making it less resistant to delamination. Subsequently, the $[0/90]_s$ laminate suffers the most since it has the greatest difference between plies being the 90º ply very weak under tension.

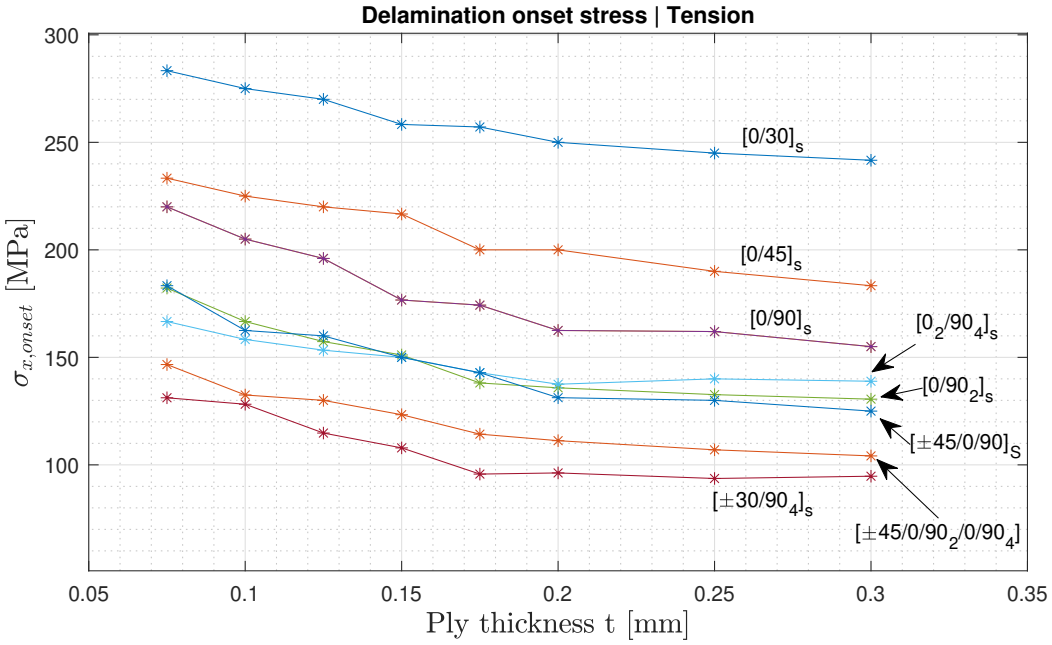

Figure 5.43: Delamination Onset stress for different laminates under tension with respect to the ply thickness.

The inferior performance of laminates with a 90º ply orientation can be explained by the ease with which matrix cracks propagate within such plies. This is supported by the SERR expression for crack propagation G^{cr} (refer to Figure 4.9), which shows significantly higher values for $[0/90]_s$ laminates. On the other hand, the SERR expression for delamination onset G^{cr+del} indicates that laminates exhibiting behavior similar to cross-ply will experience delamination after others, such as the $[0/30]_s$ laminate (refer to Figure 5.15). The intersection of both SERR expressions, defining the onset, occurs earlier in laminates with 90º plies.

Moreover, among the laminates with critical 90º plies, those with thicker ply blocks are more prone to earlier delamination. The relationships between the critical ply and the assumed pristine plies, specifically the ratio t_c/t_1, along with the laminate stiffnesses, significantly influence the delamination onset (see Figures 4.8, 5.12 and 5.14).

The model also enables the prediction of delamination onset for combined loading scenarios, involving tension and shear in the laminate. Figure 5.44 illustrates a $[0/90]_s$ laminate subjected to tension along with a fixed ratio of that load applied as shear to the laminate. Upon observation, it is evident that the case of pure tension and tension + 10% shear show nearly identical behavior. This similarity arises because the local shear in a ply, as explained in section 4.1, does not have as significant an influence as transverse strain. Thus, the introduction of a small amount of shear does not markedly affect the laminate's behavior under tension.

However, when the amount of shear increases proportionally to the tension, the delamination onset stress is significantly reduced. This reduction occurs mainly because tension and shear are being applied at similar magnitudes or even greater. If the ratio of the shear applied to the laminate is not fixed and the shear and tension can be applied independently, the delamination onset will consist of an envelope of stresses of ratio $\sigma_{onset}/\sigma_{xy}$. These examples demonstrate how the model can be applied to different types of laminates and loading scenarios, enabling

the study of various parameters.

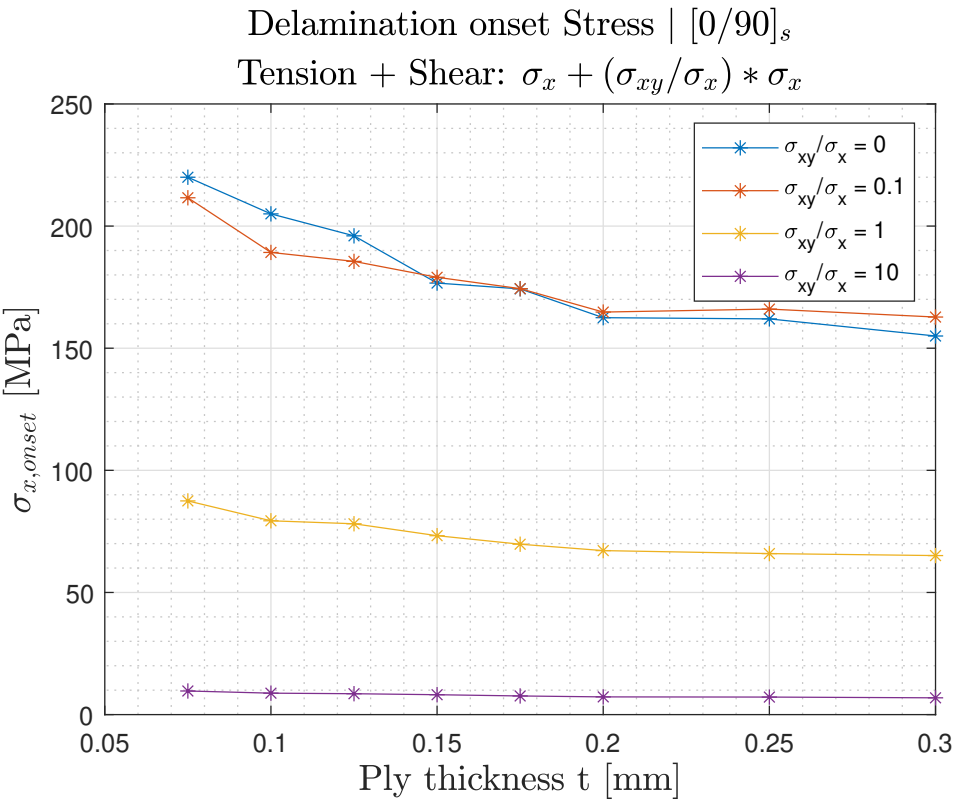

Figure 5.44: Cross.ply under tension and shear for different ply thicknesses.

6

Delamination Growth Model

This section introduces a model to predict the initial delamination length and its subsequent growth, utilizing the mode II Interlaminar fracture toughness (G_{IIR}). The assumption that only mode II is critical is discussed briefly in section 6.2.1 below. The model adopts a similar line of reasoning as the previous section,comparing different SERR expressions, but now incorporates the expression for delamination growth (G^{cr+del}) derived earlier, which had not been employed until now.

6.1. Model Principles & Considerations

After delamination initiates, the laminate will have cracks in the critical plies, with a spacing of D_{onset} between them as described in the previous section. Delaminations will swiftly emerge at the crack tips, each having an initial length denoted by a_0, as illustrated in Figure 6.1. While the figure depicts configuration I, the concept applies equally to cases II, III and IV.

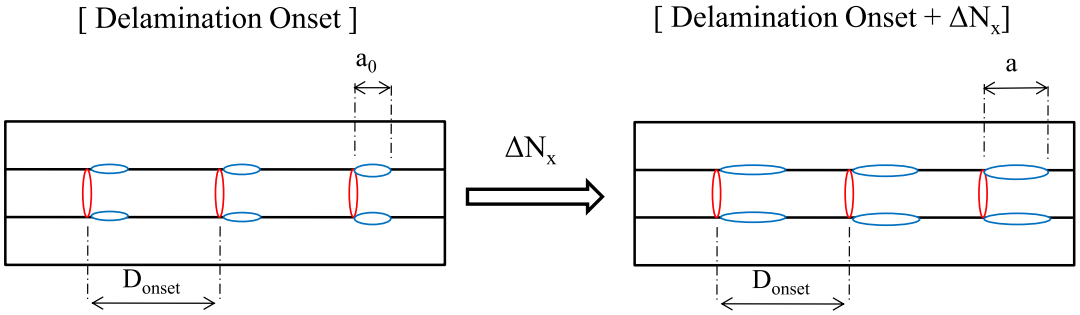

Figure 6.1: Schematic of the crack growth under uniaxial tension.

From this point onward, the distance between cracks will be assumed to remain constant and equal to the value obtained at the delamination onset (D_{onset}). This assumption is supported by experimental findings, indicating that at a certain stage, crack saturation occurs in the laminate, leading to a relatively stable crack spacing during delamination growth [21, 69, 70]. This assumption was already considered when calculating G^{cr+del}, which facilitated the differentiation $\partial U/\partial A_{del}$. If the crack spacing were not constant, the variable A_{del} would depend on the ratio a/D and the analytical differentiation would have been more complex or even impossible.

When $a = D$, a delamination will cover the entire length of the laminate (L) and the delamiantion growth will stop. In experimental studies, researchers typically measure the sum of the delamination lengths of the laminate or interface. In such cases, the value to be compared is $a(L/D_{onset})$, which represents the delamination length (a) multiplied by the number of spaces between cracks.

For now, the only required inputs are the material properties, the delamination onset load/stress and the distance between cracks at the onset (D_{onset}). These last two values can be obtained from the model proposed in Section 5. However, if these values are determined through alternative means, such as experimental studies, this method can still be utilized independently by employing those obtained values.

6.2. Delamination growth prediction

The approach presented in this section to study the delamination growth subsequent to the onset is derived from the method proposed by Takeda & Ogihara [7]. They introduced the concept that with a SERR expression to analyze delamination growth, it becomes possible to predict the delamination length for a given load using the experimentally obtained Mode II interlaminar fracture toughness (G_{IIR}). In this context, G_{IIR} acts as a critical value dependent on the delamination length a, which can be correlated with our SERR expression G^{cr+del}.

6.2.1. Mode II Interlaminar fracture toughness

The mode II interlaminar fracture toughness (G_{IIR}) characterizes a composite laminate's ability to resist delamination growth when the delaminated surfaces slide parallel to the plane of the layers. Typically, this parameter is determined through an End-Notched Flexure (ENF) test, where a unidirectional (UD) ply block of the material is tested with a film inserted in the mid-plane, acting as a pre-set delamination. During the test, load and delamination length are recorded and from these data, the mode II energy release rate for the ENF test can be calculated using the following expression:

$$G_{II} = \frac{9a^2P^2C}{2B\left(2L_s^3 + 3a^3\right)} \tag{6.1}$$

In this equation, a represents the delamination length, P is the applied load, C denotes the compliance (see [7] for reference), B is the width of the specimen, and L_s is half of the span length. To determine the fracture resistance G_{IIR} associated with this value, it is necessary to study the region of the Load-displacement curve after the onset of non-linearity [7]. By analyzing this region, the mode II interlaminar fracture toughness (G_{IIR}) as a function of the increase in delamination length $\Delta a = a_i - a_0$ can be obtained. Figure 6.2 illustrates the results obtained by Takeda & Ogihara for a CFRP Toray-T800H/3631 at various temperatures. Crack extension in their notation refer to the increase in the delamination length.

Mode II interlaminar fracture toughness is typically characterized by a constant value, as elaborated in the ASTM-D7905 standard [73]. This standard provides detailed instructions on conducting the ENF test, outlining the steps to derive relevant parameters such as G_{IIR}. To determine G_{IIR}, a specific load level from the load-displacement curve obtained in the ENF test is employed. This load value is not straightforward to obtain and the ASTM-D7905 standard employs a rather intricate calculation process, complemented by meticulous statistical analysis, to ensure the acquisition of a conservative yet representative G_{IIR} value. By employing this load value, accounting for the precrack distance and considering certain statistical factors (as mentioned in [73]), a standardized definition of G_{IIR} is established.

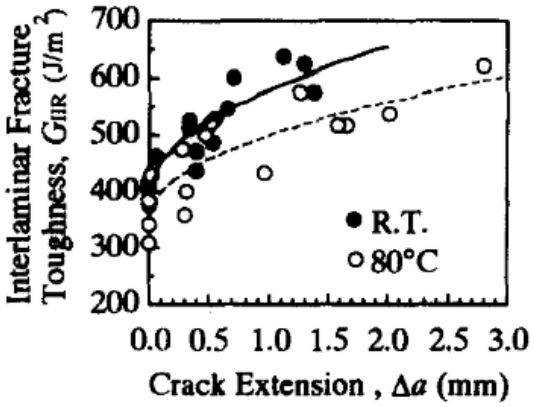

Figure 6.2: Mode II interlaminar fracture toughness G_{IIR} vs delamination extension Δa. Obtained from [7]

For most practical applications, a constant value suffices, particularly in engineering scenarios where the aim is to simplify material behavior characterization and comparison across different samples and experimental conditions, streamlining the approach for practical usage. Delamination length measurements are also prone to being influenced by factors like specimen geometry, loading rate and test conditions, rendering it intricate to directly compare outcomes from disparate studies. This is why the single value stipulated by the ASTM-D7905 standard [73] finds preference in the industry.

However, our model's primary goal is to predict delamination growth, encompassing even exceedingly low values. Consequently, it is more advantageous to employ a variable G_{IIR} value. Takeda & Ogihara also acknowledge this concern, highlighting that matrix cracks and the initiation of delamination occur within the range of extremely small delamination lengths, which vary rapidly. Therefore, utilizing a varying G_{IIR} would offer a more precise prediction of the behavior [7]. They slightly modify the procedure outlined in the ASTM-D7905 standard, deriving the mode II interlaminar fracture toughness as a function of delamination length in the subcritical region of delamination propagation, as manifested in the load-displacement curve obtained through a standard ENF test. This subcritical region, as depicted in Figure 6.3, is marked by the initiation of non-linear behavior in the curve.

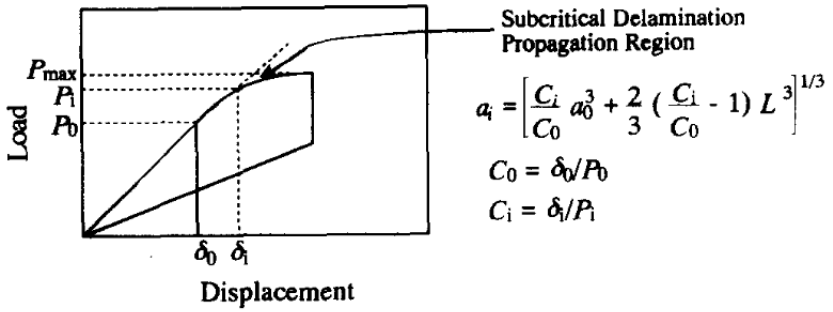

Figure 6.3: Typical Load-Displacement curve obtained by ENF tests. Obtained from [7]

The method that will be explained in this chapter could, in principle, be implemented with the conventional constant G_{IIR} value, represented by a horizontal line w.r.t Δa. However, guaranteeing the proximity of outcomes to those demonstrated in the subsequent pages remains uncertain. A priori, since using a constant G_{IIR} value is a simplification, using G_{IIR} as a function of Δa would yield more accurate results.

Takeda and Ogihara [7], following their proposed method, obtained G_{IIR} values as a function of the increase in delamination length $\Delta a = a_i - a_0$ and fitted the points using the following expression:

$$G_{IIR} = G_0 + k\sqrt{\Delta a} \tag{6.2}$$

where G_0 and k are constants. For the Toray-T800H/3631 composite at room temperature, the specific values are $G_0 = 394\ J/m^2$ and $k = 5850\ J/m^{3/2}$, as determined by the authors [7]. This curve, using these values, will be employed to predict and validate the method presented in this section. It's worth noting that any expression linking G_{IIR} with the delamination length a can be used as well.

It is essential to consider that the application of the mode II fracture toughness restricts the method's applicability. Mode II refers to situations where the delaminated surfaces slide parallel to the plane of the layers, as depicted in Figure 6.4. Consequently, this model is expected to be particularly accurate for a cross-ply configuration under pure tension, where delaminations occur in the 0º/90º interface, growing locally in parallel to the laminate's longitudinal axis. However, if local shear exists in the plies surrounding the delaminated area, it is highly probable that mode III effects are also present, making the predictions less accurate.

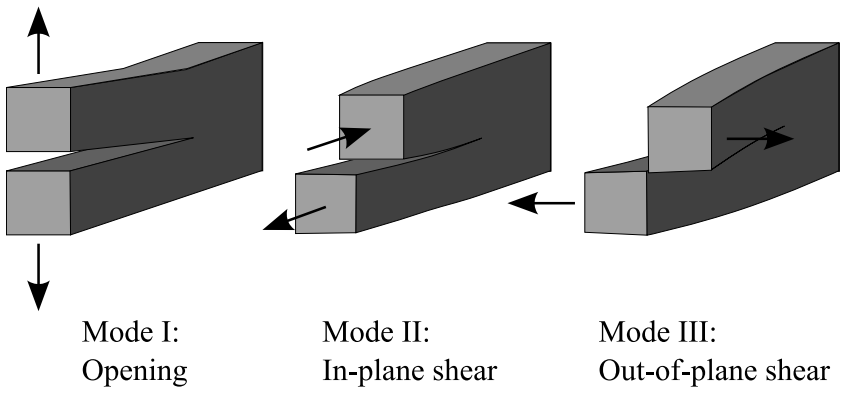

Figure 6.4: Fracture mechanics modes.

6.2.2. Initial delamination length

Now, the delamination onset load $N_{x,onset}$ and the crack spacing at onset D_{onset} obtained in the previous section can be used to predict the initial delamination length a_0 based on the mode II interlaminar fracture toughness G_{IIR}. Assuming that the load just before the delamination creation and immediately after the creation is the same (thus, the onset is instantaneous), the load for a_0 is known and equal to $N_{x,onset}$. Additionally, the distance between cracks at that moment is also known as D_{onset}, allowing the particularization of the SERR expression for delamination growth for that specific moment as $G^{cr+del}(N_{x,onset}, D_{onset}, a_0)$.

Next, by assuming that the critical energy release rate for delamination growth is equal to the mode II interlaminar fracture toughness G_{IIR}, the delamination length can be determined for any given load, including at the onset. The expression for G_{IIR} assumes that a corresponds to the total delamination length, as explained by Takeda & Ogihara. However, in this case, the variable a represents the delamination length between two matrix cracks. Hence, it is necessary to divide the mode II interlaminar fracture toughness by the number of matrix spacings L/D_{onset}. Consequently, the initial delamination length a_0 can be found by solving

the following equation:

$$G^{cr+del}\left(N_{x,onset}, D_{onset}, a_0\right) = \left(\frac{D_{onset}}{L}\right) G_{IIR}\left(a_0\right) \tag{6.3}$$

Expanding the equation, we employ the G_{IIR} expression derived by Takeda & Ogihara (eq.6.2) and the SERR expression for delamination growth for case I (eq. 5.23). It is assumed that the laminate is under pure tension ($\gamma_{xy} = 0$) to exclude any shear-induced mode III delamination growth:

$$\frac{1}{4}h\left(\frac{L}{D_{onset}}\right)\left\{\frac{E_x^{cr}\left(\frac{E_x^{cr}}{E_x^{del}}-1\right)}{\left[1-\frac{a_0}{D_{onset}}+\frac{a_0}{D_{onset}}\frac{E_x^{cr}}{E_x^{del}}\right]^2}\varepsilon_{x,onset}^2\right\} = \left(\frac{D_{onset}}{L}\right)\left(G_0 + k\sqrt{a_0}\right) \tag{6.4}$$

The equation can be solved numerically for a_0, which represents the point of intersection between G_{IIR} and the specific G^{cr+del} corresponding to $N_{x,onset}$ and D_{onset}, as illustrated in Figure 6.5. This value of a_0, obtained from the intersection, corresponds to the initial delamination length. It is important to note that when comparing with experimental tests, where the total delaminated length is usually measured, the a_0 obtained from this method should be multiplied by L/D_{onset} to account for all the delaminations originating from the crack tips.

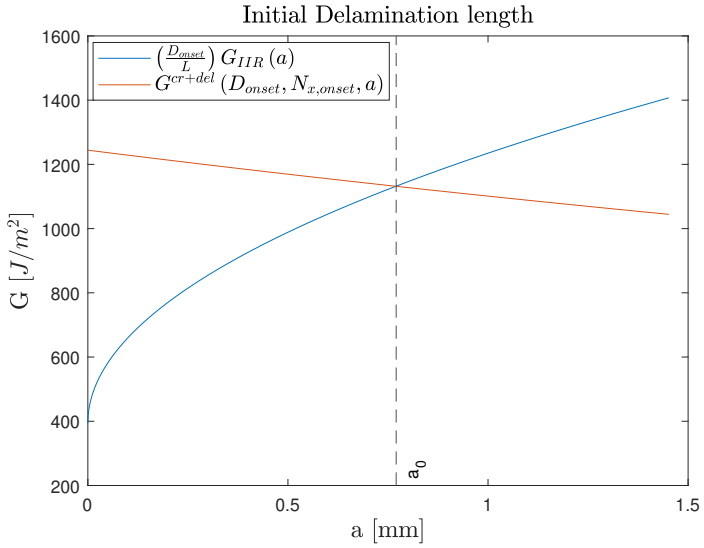

Figure 6.5: G^{cr+del} vs G_{IIR} for a $[0/90_2]_s$ laminate under tension

An attempt can also be made to solve Equation 6.4 analytically. To do this, the left term of the equation is expanded into a Taylor series as follows:

$$\frac{1}{4}h\left(\frac{L}{D_{onset}}\right)\left\{\frac{E_x^{cr}\left(\frac{E_x^{cr}}{E_x^{del}}-1\right)}{\left[1-\frac{a_0}{D_{onset}}+\frac{a_0}{D_{onset}}\frac{E_x^{cr}}{E_x^{del}}\right]^2}\varepsilon_{x,onset}^2\right\} \simeq \frac{1}{4}h\varepsilon_{x,onset}^2\left(\frac{L}{D_{onset}}\right)E_x^{cr}\Delta E\left\{1-2\frac{a_0}{D_{onset}}\Delta E\right.$$

$$+3\left(\frac{a_0}{D_{onset}}\Delta E\right)^2 - 4\left(\frac{a_0}{D_{onset}}\Delta E\right)^3 + 5\left(\frac{a_0}{D_{onset}}\Delta E\right)^4 - 6\left(\frac{a_0}{D_{onset}}\Delta E\right)^5 + O(a_0^6)\Bigg\} \quad (6.5)$$

where $\Delta E = (E_x^{cr}/E_x^{del} - 1)$. Taking now the first two terms of the expansion and substituting in eq.6.4, it is possible to obtain a close form expression for the initial delamination length a_0 which is:

$$a_0 = \frac{4A^2\frac{\Delta E}{D_{onset}} - 4A\frac{\Delta E}{D_{onset}}G_0 + k^2 + k\sqrt{8A^2\frac{\Delta E}{D_{onset}} - 8A\frac{\Delta E}{D_{onset}}G_0 + k^2}}{8A^2\left(\frac{\Delta E}{D_{onset}}\right)^2} \quad (6.6)$$

with:

$$A = \frac{1}{4}h\varepsilon_{x,onset}^2\left(\frac{L}{D_{onset}}\right)E_x^{cr}\Delta E \quad (6.7)$$

$$\Delta E = \frac{E_x^{cr}}{E_x^{del}} - 1 \quad (6.8)$$

In this expression, $\varepsilon_{x,onset}$ and D_{onset} represent the strain and crack spacing at the delamination onset respectively. G_0 and k are constants obtained from the mode II interlaminar toughness fit, L is the length of the laminate and E_x^{cr} and E_x^{del} are the longitudinal stiffness of the cracked and delaminated sections of the laminate. The accuracy of this approximation will be discussed in section 6.3.

It is important to note that this derivation and the graph shown in Figure 6.5 were obtained specifically for the case I configuration. A similar derivation can be carried out for the other delamination configurations, resulting in three different expressions for the initial delamination length. Just like the delamination onset, these three different expressions will provide three distinct initial delamination length values.

6.2.3. Delamination growth

The same procedure is employed to predict the growth of delaminations once the onset has occurred. As the laminate is further loaded ($N_x > N_{x_{onset}}$), a new Strain Energy Release Rate expression with respect to a is obtained, keeping the distance between cracks constant and equal to the value at the onset. Assuming that the critical energy release rate for delamination growth is equal to G_{IIR}, the delamination length can be determined as a function of the applied laminate load (or strain). By solving equation 6.9 with respect to a, the delamination length at any given load N_x can be obtained:

$$\underbrace{\frac{1}{4}h\left(\frac{L}{D_{onset}}\right)\left\{\frac{E_x^{cr}\left(\frac{E_x^{cr}}{E_x^{del}} - 1\right)}{\left[1 - \frac{a}{D_{onset}} + \frac{a}{D_{onset}}\frac{E_x^{cr}}{E_x^{del}}\right]^2}\varepsilon_x^2\right\}}_{G^{cr+del}} = \left(\frac{D_{onset}}{L}\right)\underbrace{\left(G_0 + k\sqrt{a}\right)}_{G_{IIR}} \quad (6.9)$$

Figure 6.6 graphically demonstrates the procedure for a $[0/90_2]s$ laminate. As the load increases, G^{cr+del} also increases, leading to intersections with G_{IIR} occurring at higher values of a. This process continues until $a = D_{onset}$, indicating that the delamination has extended the entire distance between two cracks, covering the entire length of the laminate. By using this methodology, the length of the delamination is determined for each load, resulting in a graph similar to Figure 6.7, where the delamination length a is plotted against the load N_x. It is important to note that ε_x and N_x can be related easily through the Classical Laminate Theory (CLT).

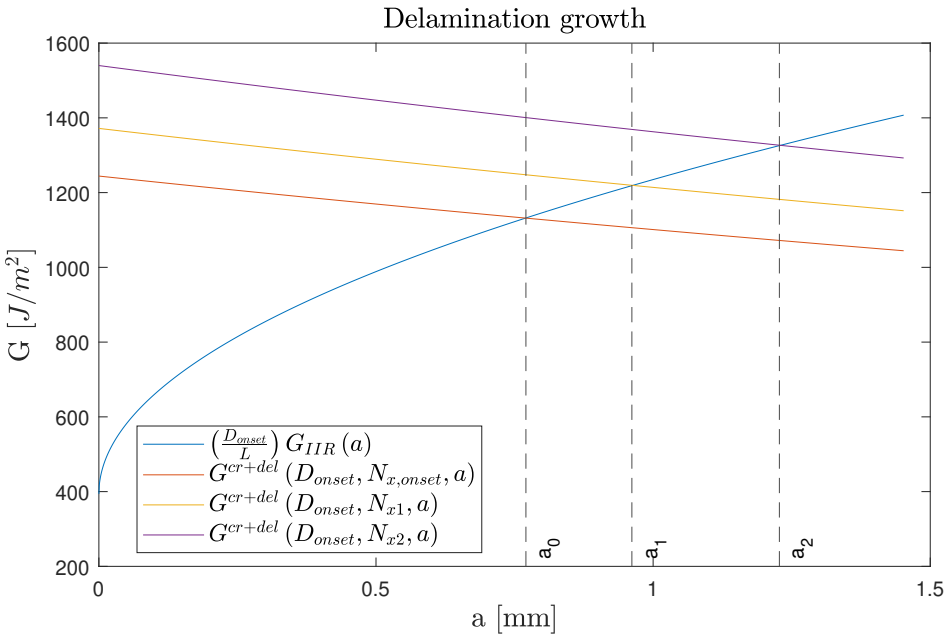

Figure 6.6: G^{cr+del} vs G_{IIR} for different loads in a $[0/90_2]_s$ laminate under tension.

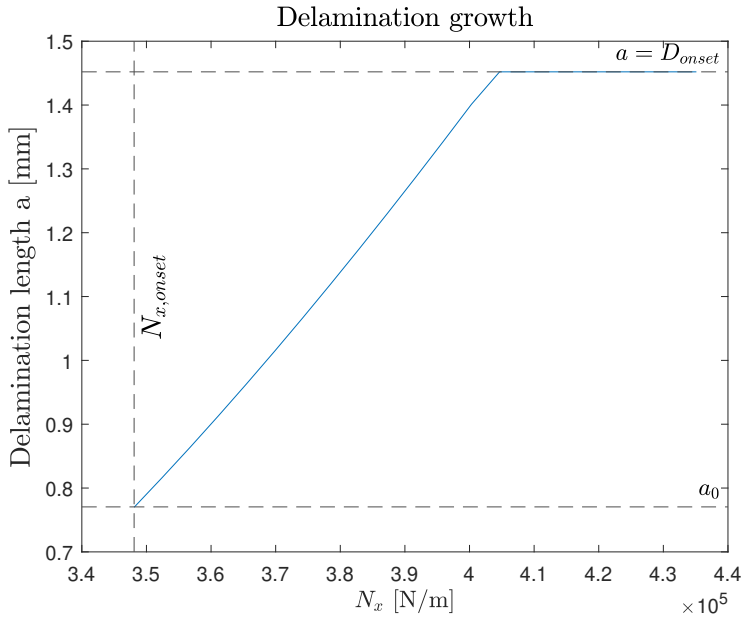

Figure 6.7: Delamination growth in a $[0/90_2]_s$ laminate under tension.

As it can be seen in Fig. 6.7, the delamination onset load obtained through the model presented in Section 5 marks the initiation of the delamination that will have a initial length of a_0. The delamination will grow upon loading until its length is equal to the distance between cracks (remember that this distance is assumed constant and equal to the value at the onset D_{onset}). Once this value is obtained, a delamination expands through the whole length of the laminate marking the total failure. Comparing the range of loads required for the whole growth of the delamination, it is observed that is significantly lower than for the crack propagation until the onset. This means that once the delamination is initiated, the growth is relatively fast compared with the whole cracking phase. Fig. 6.7 is not linear even though it is close. As it will be discussed later, the shape depends on the laminate under study.

Figure 6.6 & 6.7 are obtained using the case I G^{cr+del} & G^{cr+del}_{onset} equations but the same procedure can be followed for the rest of the cases. This will give 3 different predictions of the delamination growth. Following the same procedure used for the initial delamination onset, it is possible to approximate the expressions of the G^{cr+del} (for tensile loading) using Taylor's series. Expanding in series all expressions for the G^{cr+del} case I, II, III and IV in the same way as before and solving $G^{cr+del} = G_{IIR}$ taking the first two terms of the expansion, the delamination growth expressions for all four cases are derived:

$$
\begin{aligned}
I: \quad a(D_{onset}, \varepsilon_x) &= \frac{4A^2\frac{\Delta E}{D_{onset}} - 4A\frac{\Delta E}{D_{onset}}G_0 + k^2 + k\sqrt{8A^2\frac{\Delta E}{D_{onset}} - 8A\frac{\Delta E}{D_{onset}}G_0 + k^2}}{8A^2\left(\frac{\Delta E}{D_{onset}}\right)^2} \\
II: \quad a(D_{onset}, \varepsilon_x) &= \frac{4A^2\frac{\Delta E}{D_{onset}} - 4A\frac{\Delta E}{D_{onset}}G_0 + k^2 + k\sqrt{8A^2\frac{\Delta E}{D_{onset}} - 8A\frac{\Delta E}{D_{onset}}G_0 + k^2}}{8A^2\left(\frac{\Delta E}{D_{onset}}\right)^2} \\
III: \quad a(D_{onset}, \varepsilon_x) &= \frac{A^2\frac{\Delta E}{D_{onset}} - 2A\frac{\Delta E}{D_{onset}}G_0 + 2k^2 + 2k\sqrt{A^2\frac{\Delta E}{D_{onset}} - 2A\frac{\Delta E}{D_{onset}}G_0 + k^2}}{A^2\left(\frac{\Delta E}{D_{onset}}\right)^2} \\
IV: \quad a(D_{onset}, \varepsilon_x) &= \frac{8A^2\frac{\Delta E^*}{D_{onset}} - 4A\frac{\Delta E^*}{D_{onset}}G_0 + k^2 + k\sqrt{16A^2\frac{\Delta E^*}{D_{onset}} - 8A\frac{\Delta E^*}{D_{onset}}G_0 + k^2}}{8A^2\left(\frac{\Delta E^*}{D_{onset}}\right)^2}
\end{aligned}
\tag{6.10}
$$

with:

$$
A = \frac{1}{4}h\varepsilon_x^2\left(\frac{L}{D_{onset}}\right)^2 E_x^{cr}\Delta E \tag{6.11}
$$

$$\Delta E = \frac{E_x^{cr}}{E_x^{del}} - 1 \tag{6.12}$$

$$\Delta E^* = \frac{E_x^{cr}}{E_x^{del*}} - 1 \tag{6.13}$$

On the contrary to the delamination onset, it is not easy a priori to predict which case will give a lower or higher value for the initial delamination length a_0 or for the range of the loads in which the delamination grows. Case I for example will give a higher crack spacing at the onset (D_{onset}) as shown in Section 5.4.3 but will have a lower onset strain $\varepsilon_{x,onset}$. The different crack spacing will also give different values of the E_x^{cr} and E_x^{del} and because the D_{onset} is constant through the growth, the behaviour of the equations will differ due to the terms $\Delta E/D_{onset}$. The equations themselves are also different (see eqs.6.9) so in short, the most conservative case cannot be determined a priori. In any case, 3 predictions will be made (case I & II are defined by the same equations thus give the same results) so a range of values can be predicted in which, a priori, the real case will be contained in. This again due to the fact that most propably, the real case is a combination of all 4 cases proposed. As an example of a real case, Carraro et al. in Fig. 2.7 reported how a delamination will grow jumping though the 90º ply cracks, not initiating in all cracks and growing in different directions with no particular uniformity.

6.3. Validation

Getting experimental data on delaminations caused by matrix cracks, where the length or area of the delamination is measured, is a challenging task. As mentioned in Section 2, the majority of studies focus on measuring edge delamination or examining fatigue propagation. Consequently, only one study with pertinent data was found to validate the delamination growth model.

6.3.1. Taheda & Ogihara [7]

Ogihara & Takeda conducted a study on the initiation and propagation of delaminations resulting from matrix cracks in TS00H/3631 CFRP laminates. They explored laminates with orientations $[0/90_4/0]$, $[0/90_8/0]$ and $[0/90_{12}/0]$ under quasi-static tension. In Figure 6.8, their measured data is presented alongside our model predictions using case I expressions. It's important to note that the original published data was presented using what they referred to as "delamination ratio," which represents the sum of delamination lengths measured in the specimen divided by the specimen length. In our notation, this can be expressed as follows:

$$Delamination\ \ ratio = \left(\left(\frac{L}{D_{onset}}\right)a\right)/L = a/D_{onset} \tag{6.14}$$

In the absence of delamination, the ratio will be 0 and as soon as a full delamination covers the entire length of the laminate, the ratio will reach 1. The delamination onset strains, $\varepsilon_{x,onset}$, obtained from the model presented in Section 5, are indicated by vertical dotted lines. The initial delamination length is represented by horizontal dashed lines.

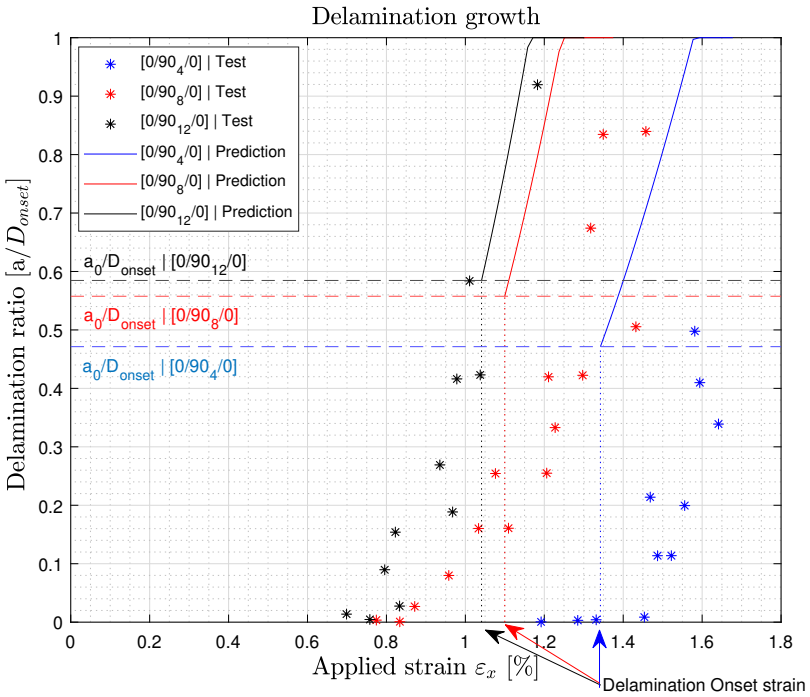

Figure 6.8: Delamination growth for the TS00H/3631 CFRP laminates under tension.

As depicted in Fig. 6.8, the model predicts that the initial delamination length for all three laminates falls within a a/D_{onset} range of 0.4 to 0.6. This implies that according to case I, the initial length would cover nearly 50% of the distance between cracks. However, the experimental data show very low initial values for delamination ratios, close to 0. The authors' comments shed light on this observation: "*[...] were then subjected to optical microscopic examination. The total delamination length was defined as the sum of the delamination lengths at the tips of transverse cracks in the specimens*" . Consequently, it is unclear whether the low ratio is a result of numerous small delaminations appearing at all crack tips or just a few relatively long delaminations forming in some cracks, which seems more likely. Both of this cases will give low delamination ratios.

Nevertheless, the general trend is decently predicted, as the delamination ratio increases almost linearly with an increase in the applied strain to the laminate. The model also successfully predicts that the $[0/90_4/0]$ laminate experiences delamination onset last, while both $[0/90_8/0]$ and $[0/90_{12}/0]$ are more prone to initiate delaminations first. In the experimental data, both the latter laminates initiate delaminations at nearly the same strain. Similarly, the prediction indicates that the $[0/90_4/0]$ laminate is the last one to have its entire length covered with a delamination. In all three cases, this occurs rapidly, within the range of [1%-1.2%] strain for the $[0/90_{12}/0]$, [1.1%-1.3%] for the $[0/90_8/0]$, and [1.35%-1.6%] for the $[0/90_4/0]$ laminate. However, in reality, the authors reported catastrophic failure of the laminates before the delamination ratio reached 1.

Due to the significant overestimation of the initial delamination ratio (and subsequently the delamination length) in the prediction, a solution is proposed to estimate the region from $a = 0$ (delamination ratio = 0) to the predicted initial delamination length a_0 (delamination ratio = a_0/D_{onset}) using a linear approximation. To determine the point at $a = 0$, the delamination onset SERR expression proposed by O'Brien [13] (see equation 5.27) will be employed. Although originally developed for an edge delamination onset, this well-known expression could be

useful in predicting delamination behavior for strains or loads smaller than our predicted onset.

By setting $G^{cr+del}(a = 0) = G_{O'Brien}$, a crack spacing and hence a strain can be obtained, establishing the initial point for the linear prediction. As demonstrated in Section 5.3.1, our G^{cr+del}_{onset} expressions yield higher values than $G_{O'Brien}$, indicating that the intersection of these expressions will give a load/strain significantly lower than our predicted delamination onset induced by matrix cracks.

For all the laminates, if the strain at which $G^{cr+del}(a = 0) = G_{O'Brien}$ is calculated, a linear approximation can be performed from that point to the originally predicted onsets. This linear approximation is represented by the dash-dotted lines in Figure 6.9. These three points yield slightly different values, although they are relatively close to each other, as evident from the graph. The predicted behavior in this region seems reasonably accurate for the $[0/90_8/0]$ and $[0/90_{12}/0]$ laminates but is less accurate for the $[0/90_4/0]$ laminate. An alternative approach to approximate this region could involve using a linear interpolation from the delamination onset to the delamination ratio equal to 0 using the predicted curves.

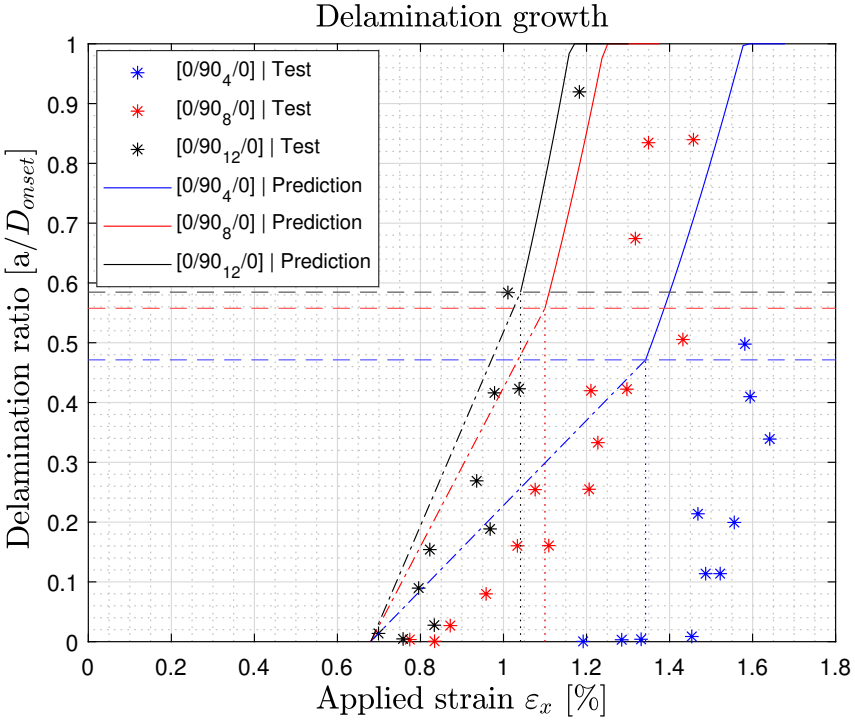

Figure 6.9: Delamination growth for the TS00H/3631 CFRP laminates under tension.

So far, only case I has been utilized in the predictions. However, by incorporating all cases (three different expressions), it becomes possible to establish a prediction band using the two extreme cases, which is a reasonable assumption to expect that most experimental points will fall within this range. Figure 6.10 illustrates the obtained prediction band. As discussed in section 6.2.3, each case has distinct equations with different onset loads and crack densities, making it challenging to anticipate the prediction behavior beforehand.

As shown in Figure 6.10, the initial delamination lengths and the range until complete delamination growth differ for each case and laminate. Ultimately, the prediction turns out to

be reasonably accurate, providing a range of prediction values, which is always superior to a simple prediction. Case I, as depicted in Figure 6.8, represents the most conservative scenario, being the one that occurs first and hence exhibits faster growth. Nonetheless, it is noteworthy that the initial delamination length does not necessarily have to be the longest, as evident in Figure 6.10.

In general, representing the predictions with bands provides a more accurate containment of all the experimentally obtained data. This approach offers a broader and more realistic range of possibilities, accommodating the complexities and variations in the laminates' behavior.

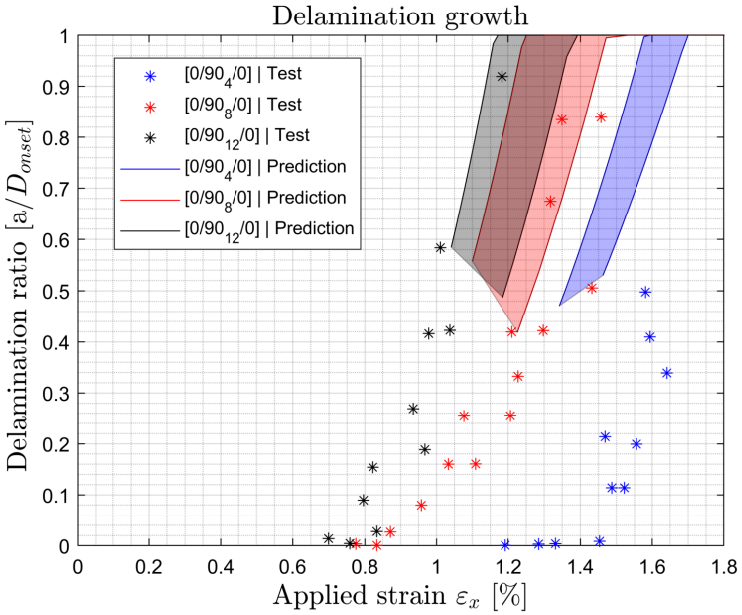

Figure 6.10: Delamination growth for the TS00H/3631 CFRP laminates under tension. Case I and Case III represented the extreme predictions of the band.

6.3.2. a_0 approximation

In sections 6.2.2 and 6.2.3, we approximated G^{cr+del} using a Taylor series, allowing us to obtain a closed-form for the solution of the equation for $G^{cr+del} = G_{IIR}$ instead of relying on numerical methods. While obtaining the numerical value (intersection of the two curves) is relatively straightforward, having a closed-form equation for the delamination length a is always preferable. In this section, we will briefly discuss the accuracy of this approximation.

Equations 6.6 & 6.10 are derived by considering the first two terms of the Taylor series expansion of the G^{cr+del} function. As G_{IIR} is dependent on $a^{1/2}$, the resulting equation to solve becomes a second-order polynomial, yielding the solutions for all four delamination configurations as presented in equations 6.10. To validate the accuracy of the obtained expressions, the material properties and laminates previously used will be employed. A comparison will be made between the initial delamination length value (for case I) obtained numerically, using the 2-term Taylor series and using the 3-term Taylor series. It is important to note that the numerical value is considered the most accurate a priori.

In Figure 6.11, we observe that the values obtained using only the first two terms of the Taylor expansion are very close together, indicating that this approximation is sufficiently

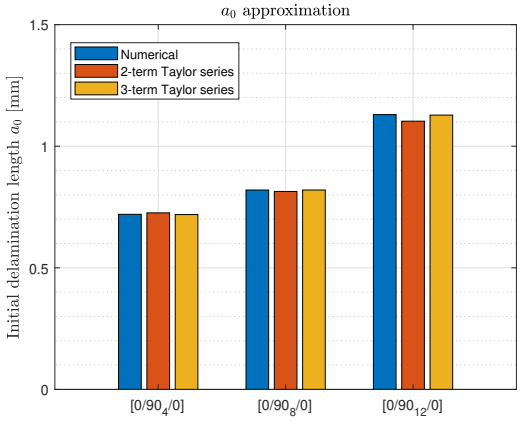

Figure 6.11: Comparison of the initial delamination length obtained by numerical methods and with the Taylor series approximation.

accurate. The error of the Taylor series solutions compared to the numerical value is depicted in Figure 6.12. It is evident that the 2-term Taylor series approximation, which gives rise to the equations presented in 6.10, exhibits less than 1.5% error when compared to the numerical approach. This result demonstrates that a 2-term series effectively represents G^{cr+del} for a cross-ply under pure tension, especially concerning the determination of the delamination length.

This outcome could have been anticipated from the behavior depicted in Figure 6.6, where G^{cr+del} is linear for small a values at the corresponding D_{onset} values (remembering that G^{cr+del} primarily depends on D and a). If we refer to Figures 5.16 - 5.18 in section 5.3.2, where these equations were initially derived, we notice that for very small D values, the function behaves non-linearly. Fortunately, the crack spacing at the onset, and hence throughout the delamination growth process, remains greater than 0.5 mm. For this particular material, D_{onset} equals 1.14, 1.78 and 2.3 for the $[0/90_4/0]$, $[0/90_8/0]$ and $[0/90_{12}/0]$ laminates respectively. This correlation could also have been expected when examining Figures 5.28 and 5.29 from section 5.5.5, which depict the crack spacing behavior at the onset for cross-ply laminates (although for a different material). Thus, as long as D_{onset} is not excessively small, the closed-form expressions for $a\,(D_{onset}, \varepsilon_x)$ shown in equation 6.10 remain accurate and valid.

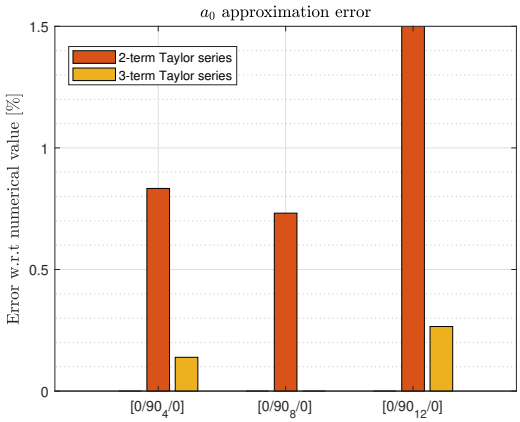

Figure 6.12: Error of the initial delamination length value obtained by the Taylor series approximation with respect to the numerical value.

7

Complete Damage Evolution

It is now possible to integrate the crack propagation model (described in section 4), the delamination onset model (explained in section 5) and the delamination growth model (outlined in section 6) into a unified plot. This consolidated representation offers a convenient and general overview of the composite laminate's behavior. Figure 7.1 illustrates the general shape of the graph for a typical cross-ply configuration subjected to tension, allowing for quick insights into the laminate's response.

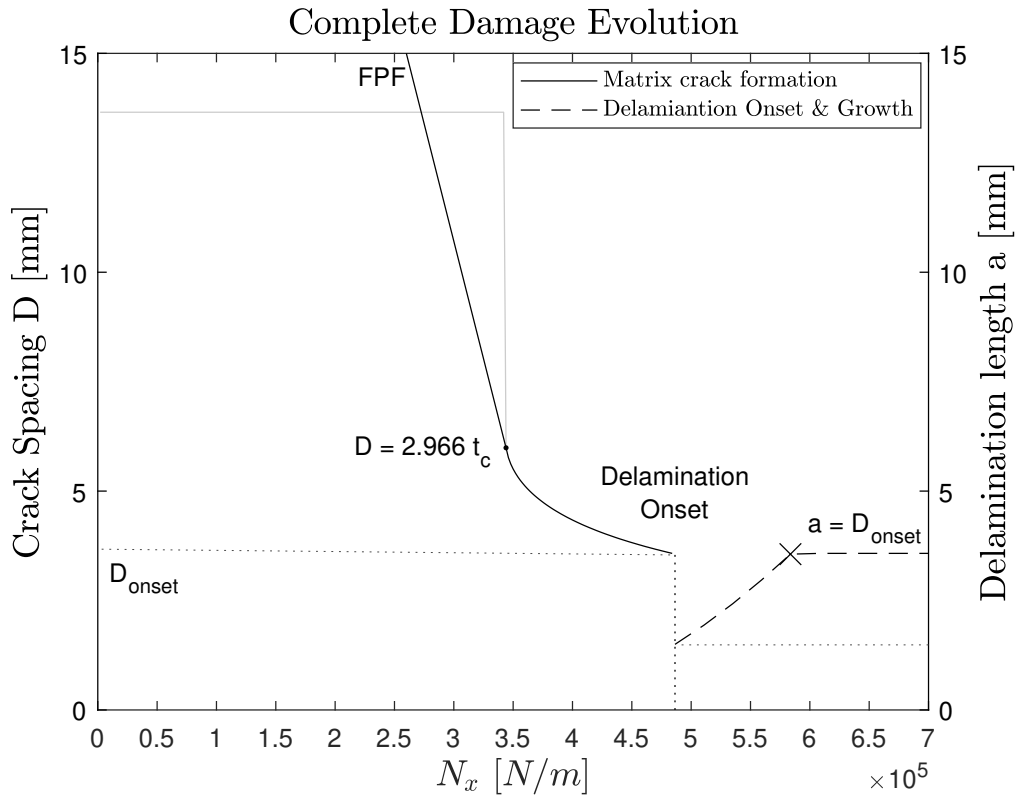

Figure 7.1: Schematic of the damage evolution of a cross-ply under tension.

Initially, the laminate experiences cracking in the critical ply or plies, but the crack spacing remains sufficiently wide that it does not significantly affect the material properties [3]. This phase extends from the unloaded condition until the cracks start propagating uniformly at

$D = 2.966t_c$, as defined by Kassapoglou and Socci's model (see section 4.2). Within this range, Socci & Kassapoglou's model is represented by the grey line, while the linear approximation derived from the FPF (First Ply Failure) load, discussed in section 4.5.1, is depicted in black. This early phase is generally considered less critical as the cracks are present but spaced far enough apart that the material properties remain largely unaffected [3]. For assessing the actual crack spacing D on the graph, the linear approximation to the FPF load is more practical as it closely aligns with reality, as validated in section 4.5.1. However, if not explicitly required, the original approximation can be utilized.

Beyond the point where $D = 2.966t_c$, the cracks propagate uniformly following Kassapoglou & Socci's model. This crack multiplication process continues until the delamination onset occurs at the tips of the cracks. At this stage, crack saturation is assumed, and the crack distance at onset D_{onset} remains constant during delamination growth (see section 5). The formed delaminations start with an initial delamination length a_0, which depends on the material properties and loading conditions. From this point onwards, the delaminations grow (as represented by the dashed line in Figure 7.1) until they cover the entire space between the cracks, resulting in $a = D_{onset}$.

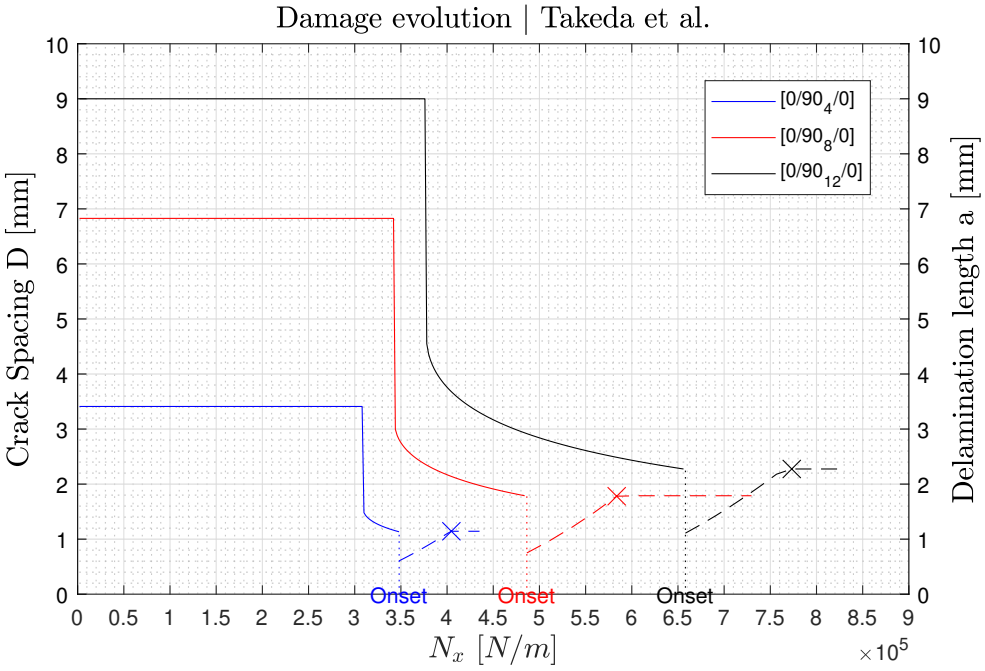

Figure 7.2: Damage evolution of $[0/90_4/0]$, $[0/90_8/0]$ and $[0/90_{12}/0]$ laminates under tension.

This representation is now applied to the laminates studied by Takeda & Ogihara [7], namely, the $[0/90_4/0]$, $[0/90_8/0]$ and $[0/90_{12}/0]$ laminates. In Figure 7.2, the delamination growth, as previously shown, is now illustrated along with the crack propagation. It is evident that the crack spacing at delamination onset increases with an increasing number of 90º plies, as does the initial delamination length to a lesser extent. Additionally, the crack spacing at which the cracks start behaving with uniform spacing also increases, which is logical since this point is proportional to the thickness of the critical ply or plies ($D = 2.966t_c$). The representation is plotted against the applied load, and Figure 7.3 depicts the exact same figure but for the applied stress.

With just a single glance, a comparison can be easily made among the three laminates and a ton of information can be obtained. The thicker the 90º ply block, the lower the stress required to reach delamination onset, and the higher the crack spacing at the onset. Additionally, thicker laminates experience quicker delamination growth. In summary, the $[0/90_{12}/0]$ laminate exhibits the most unfavorable behavior against delamination induced by matrix cracking.

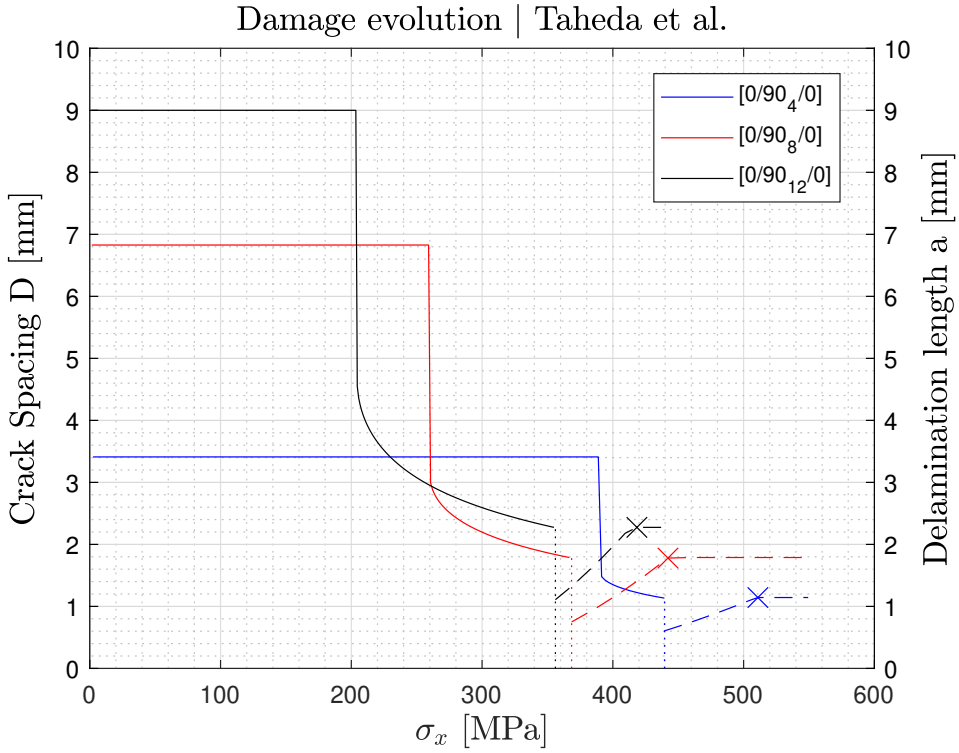

Figure 7.3: Damage evolution of $[0/90_4/0]$, $[0/90_8/0]$ and $[0/90_{12}/0]$ laminates under tension.

Not only can different laminates be compared using this representation, but also the influence of various properties on the general behavior of the same laminate can be easily assessed. Let's consider the previous $[0/90_4/0]$ laminate and vary its main properties. Figure 7.4 illustrates a variation of the longitudinal Young's modulus from -15% to +15%. As observed, the point of crack initiation remains the same since it depends solely on the thickness of the 90º plies, which remains constant in this case. However, the delamination onset load increases with an increasing value of E_1. The delamination growth also occurs at higher loads but follows the same trend. This behavior may be attributed to the fact that stiffer 0º plies, associated with higher E_1 values, bear a larger portion of the loads, leaving less load available for crack propagation and delamination growth.

In Figure 7.5, we vary the transverse Young's modulus E_2 within a range of ±15%. The point at which Kassapoglou & Socci's model "kicks-in" remains constant at the same crack spacing but it occurs at higher loads for decreasing E_2 values. Interestingly, the behavior is opposite to that observed for E_1. Increasing E_2 reduces the delamination onset load, which aligns with the closed-form equation 5.29 derived in section 5.4.1. This equation indicates that the onset load is inversely proportional to E_2 and directly proportional to the transverse in-situ strength Y_{is}^T. Moreover, it is noteworthy that E_2 significantly influences the delamination initial length. Lower E_2 values lead to higher initial lengths, but the range of loads for delamination growth becomes narrower compared to the influence of E_1. This suggests that higher E_2 values

result in improved crack and delamination behavior since these occur at higher loads. The explanation lies in the fact that a higher transverse Young's modulus makes the 90º ply under tension stiffer and these plies are critical sites for crack initiation.

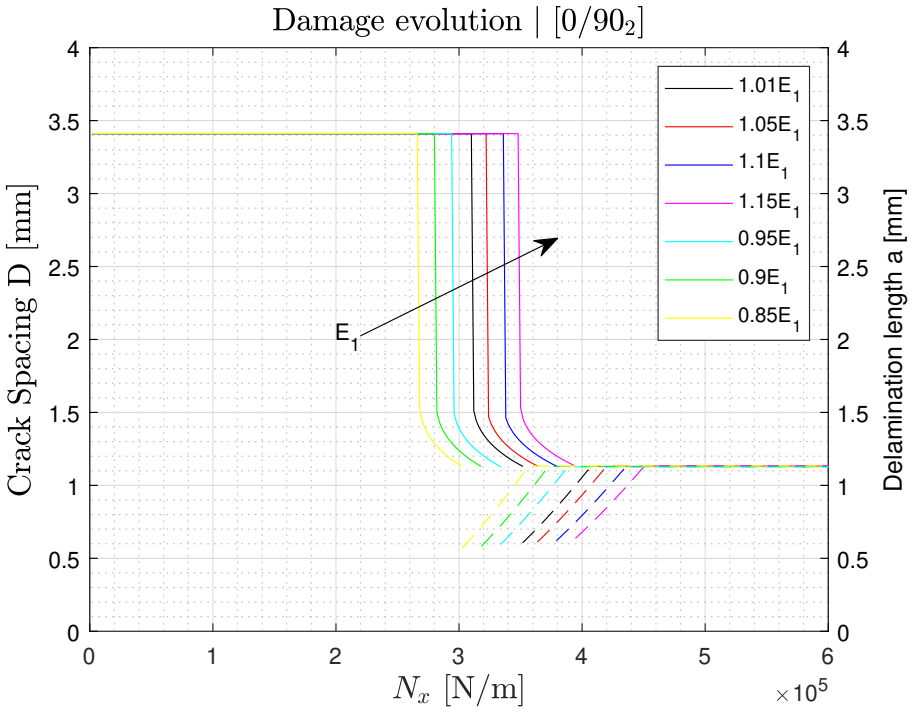

Figure 7.4: Influence of E_1 in a $[0/90_4/0]$ laminate under tension.

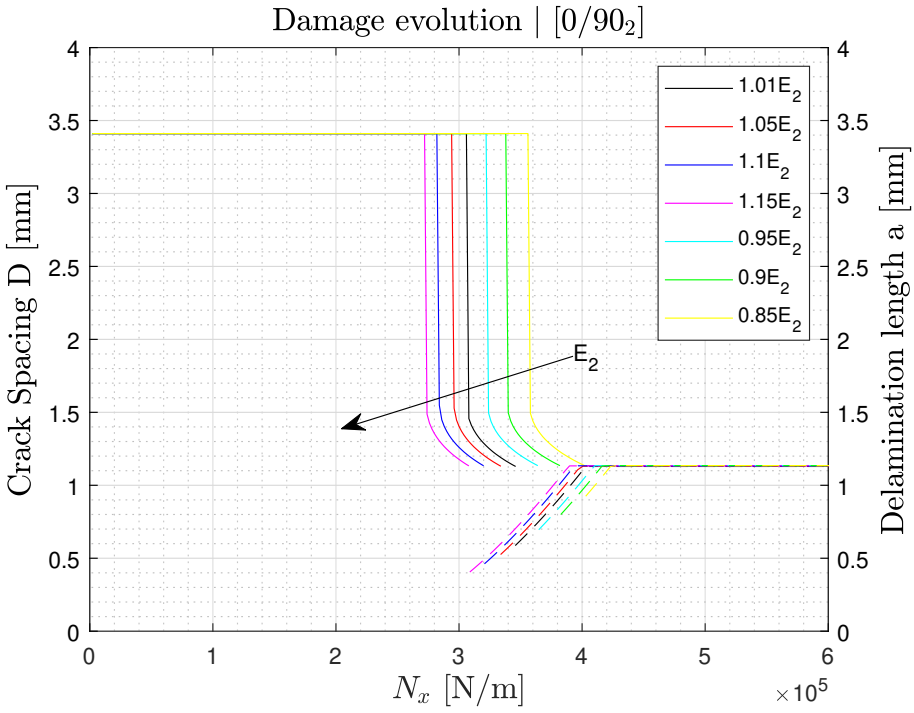

Figure 7.5: Influence of E_2 in a $[0/90_4/0]$ laminate under tension.

Lastly, the study also examines the effect of varying the transverse in-situ strength, Y_{is}^T. As depicted in Figure 7.6, it significantly influences crack formation and delamination onset, which is sensible considering it is the driving factor that determines when a new crack will appear (refer to section 4.2). Moreover, it plays a crucial role in the closed-form expression for determining the delamination onset load (see eq.5.29), where it is directly proportional to the onset load. Additionally, although not distinctly visible in the figure, lower values of Y_{is}^T result in shorter initial delamination lengths.

Notably, the delamination growth remains unaffected by the transverse in-situ strength, as evident from the dashed parts of the curves. The delamination growth, described by the SERR expression G^{cr+del}, does not consider Y_{is}^T since it solely accounts for the energy dissipated by increasing the delaminated area. Furthermore, Y_{is}^T is not explicitly defined in G_{IIR}, which governs the critical values for delamination growth. Hence, the delamination growth model doesn't directly incorporate the parameter Y_{is}^T, but the constants within G_{IIR} might have a dependence on it. Given that the constants accessible are those derived by Takeda & Ogihara for a particular material, the manner in which the material impacts these constants and consequently the model remains to be studied. Considering that delaminations predominantly arise at ply interfaces rather than being directly linked to ply strength, it could be argued that the influence of the material might not be profoundly critical. Nonetheless, it is likely that Y_{is}^T could exert a certain level of influence to some degree.

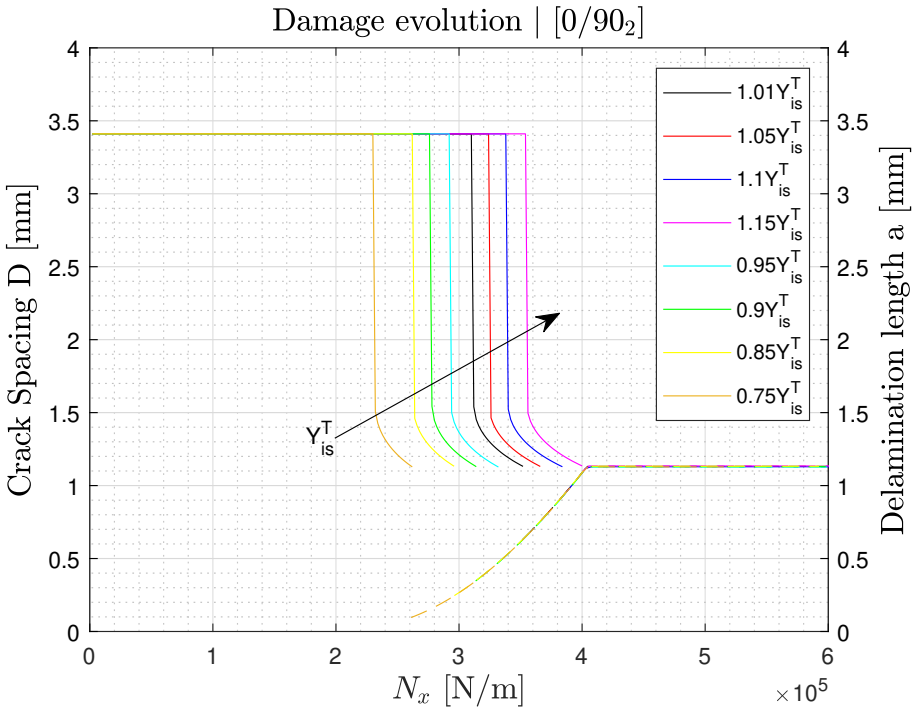

Figure 7.6: Influence of Y_{is}^T in a $[0/90_4/0]$ laminate under tension.

Previously, predictions were made for cross-plies under the assumption that the mode II interlaminar fracture toughness G_{IIR} accurately determines a critical SERR value since delamination grows parallel to the laminate longitudinal axis. Now, $[0/\theta_2]_s$ laminates are studied to draw conclusions about the applicability of the delamination growth model and more specifically, the use of G_{IIR}. The crack propagation and delamination onset models are not restricted by any layup (as long as it is symmetrical) and will work fine. However, as

mentioned in section 6.2.1, when the interface in which a laminate is growing is not driven by pure in-plane shear, the use of G_{IIR} may no longer be an accurate option (refer to Figure 6.4).

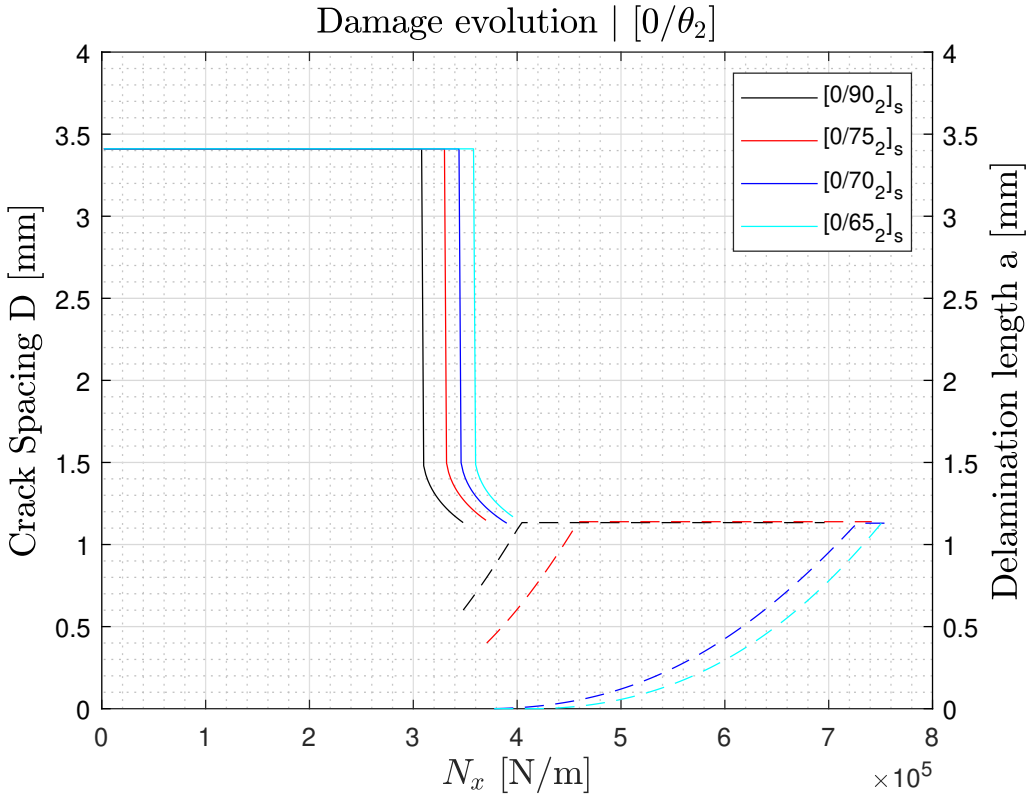

Figure 7.7: Damage evolution in $[0/\theta_2]_s$ laminates under tension.

Figure 7.7 illustrates $[0/\theta_2]_s$ laminates subjected to tension for $\theta = 90, 75, 70$ and 65. In these laminates, the central plies experience both local shear and transverse tension (except the 90º), leading to an expected mode II and mode III interaction in the delamination growth process. Observing the behavior, the $[0/75_2]_s$ laminate, which has relatively low local shear, behaves similarly to the cross-ply but with the onset of delamination occurring at a higher load as well as the delamination growth range. On the other hand, the $[0/70_2]_s$ and $[0/65_2]s$ laminates exhibit a sudden change in behavior, with the onset of delamination also happening at a higher load. These laminates have an extremely small initial delamination length, almost close to zero, which might not be an accurate value comparing it with the cross-ply values and considering that the D_{onset} is quite similar. Moreover, their delamination growth shows a highly non-linear pattern, requiring a broad range of loads for complete delamination growth. This behavior is attributed to the fact that the SERR for delamination growth G^{cr+del} at the onset is almost smaller than the mode II interlaminar fracture toughness (G_{IIR}) for all a values.

Let's examine Figure 7.8, which illustrates the approach used to predict delamination growth for the $[0/70_2]s$ laminate, and compare it with Figure 6.6, corresponding to the $[0/90_2]s$ laminate. At the onset, G^{cr+del} for the $[0/70_2]s$ laminate intersects very closely with $GIIR$ at $a = 0$. This indicates that the mode II interlaminar fracture toughness is almost higher than the actual SERR required for delamination growth, suggesting that delamination growth may not occur. Subsequent loading causes G^{cr+del} to intersect G_{IIR} over a very small range of a values, resulting in a non-linear delamination growth graph, as depicted in Figure 7.6. This

non-linearity explains the wide range of loading needed to achieve complete delamination growth ($a = D_{onset}$). These findings imply that the model predicts that delamination growth in the $[0/70_2]_s$ and $[0/65_2]s$ laminates is highly unlikely or that the G_{IIR} expression does not accurately capture the energy required for the delamination growth. Since these laminates exhibit a significant amount of shear, it is possible that a combined mode II + III expression for the interlaminar fracture toughness is necessary.

For $\theta < 65^{o}$, our model does not predict delamination growth, despite being able to obtain the delamination onset load using the model presented in section 5. This onset load seems accurate since the behaviour follows the ascending trend for lower θ values. These observations support the idea that the issue may lie in the value of G_{IIR} used and the proposed delamination growth model may only be suitable for laminates in which delamination is driven mainly by mode II.

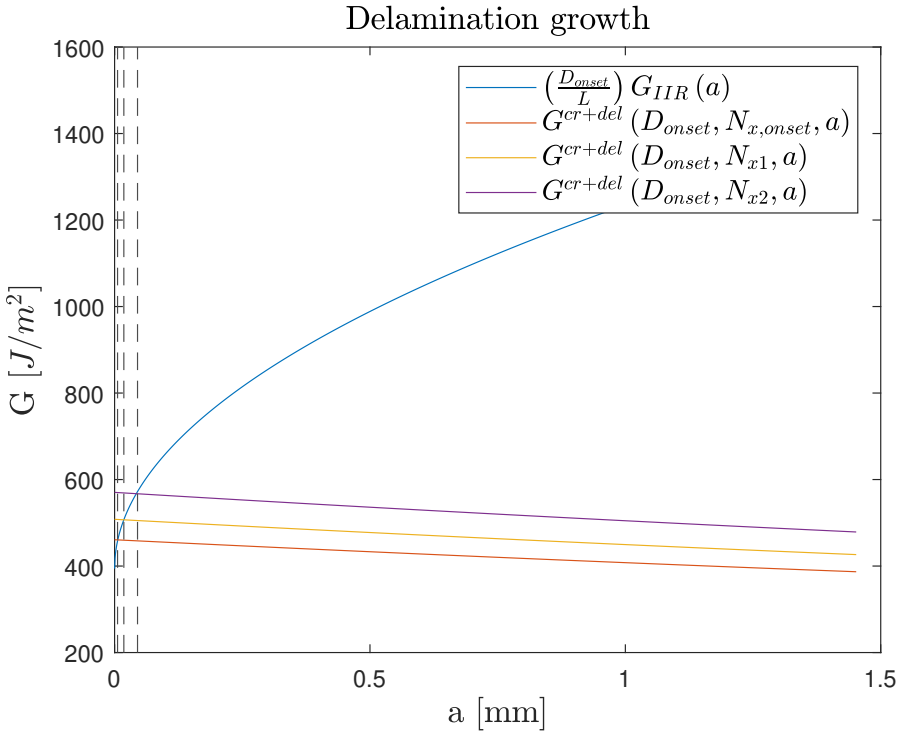

Figure 7.8: G^{cr+del} vs G_{IIR} in a $[0/70_2]_s$ laminate under tension.

This section has demonstrated the potential of the integrated models presented in this thesis, effectively representing the complete process of crack initiation, propagation, delamination onset induced by these cracks and the subsequent growth of these delaminations. The ability to rapidly and quantitatively compare different laminates and material properties allows for quick conclusions regarding their behavior against damage, making it particularly valuable during design phases.

Moreover, the accuracy of these models has been demonstrated, making them suitable for predicting delamination onset loads, crack spacings and delamination lengths with reasonable precision. Specially good correlation is obtained for cross-plies. This predictive capability further enhances their practical utility in engineering applications. Overall, the combined analytical models offer a comprehensive toolset for understanding and predicting the behavior of laminated composites under the influence of cracking and delamination, fostering more informed and efficient decisions.

8

Conclusions

The objective of this research was to develop an analytical model for studying the behavior of delaminations originating from matrix cracks. The model consist of three analytical components: a matrix crack propagation model, a delamination onset model and a delamination growth model. These components are built on a robust physical foundation and are well-suited for practical/realistic applications, such as design and damage assessment. This section includes a comprehensive discussion of the methodology employed, the results obtained, the validation and the applicability of the models.

All the models presented in this study are entirely analytical, providing inherent speed and efficiency. Their strong mathematical and physical foundations make them highly interpretable and easily generalizable or improvable. Moreover, they enable a comprehensive examination of various parameters and their sensitivity. The study derives closed-form expressions for the Strain Energy Release Rate (SERR) related to crack propagation (G_{cr}), delamination onset ($G_{cr+delonset}$) and delamination growth ($G_{cr+delgrowth}$) for any given symmetrical laminate. An exception is found in section 5.4.2 where an iteration is needed to obtain the solution of eq.5.31 (refer to Figure 5.20). However, this numerical solution is not computationally intensive. For modeling the damage of a cross-ply, two material properties that are not easily obtained are required: the transverse in-situ strength (Y_{Tis}) and a mode II interlaminar fracture toughness relation with respect to the delamination length ($G_{IIR} = f(a)$). In the case of a general symmetrical laminate, additional parameters, such as the shear in-situ strength (S_{is}) and the yield shear strain (γ_Y), are needed. These parameters can be reasonably approximated, and if precise experimental values are desired, they only need to be obtained once per material. Considering the model's versatility in analyzing any given symmetrical laminate, it proves to be a valuable tool for practical applications and can be highly useful in various scenarios.

Regarding the methodology of the proposed models (section 3): The underlying idea for all models is the use of the Strain Energy Release Rate (SERR) to assess different damage scenarios. The concept is relatively straightforward: derive SERR expressions associated with specific processes (crack propagation, delamination onset and delamination growth) and then compare these expressions to identify critical points, particularly in terms of the main variable, which, in this case, is the crack spacing. These critical values establish distinct regions where one process becomes more probable than the others. One of the notable advantages of this approach is that the critical values of each SERR expression are self-defined by utilizing the other derived SERR expressions. This eliminates the need for experimental determination of these critical

values. Additionally, this methodology allows for the easy incorporation of additional damage modes, enabling meaningful comparisons among different damage mechanisms. The SERR concept has a long-standing history in composite fracture mechanics and is strongly connected to the physics underlying the damage processes. As a result, this approach enhances the interpretability and provides a qualitative and quantitative understanding of the mechanisms at play.

Regarding the applicability and validation of the models (sections 4.5, 5.5 and 6.3): The matrix crack propagation model has undergone extensive validation using test data for a cross-ply laminate. However, further comparison and validation are needed for more complex and generic layups. The model shows great versatility and can be applied to any symmetrical laminate subjected to tension or tension + shear without any specific restrictions. Nevertheless, it is essential to assess how well the model predicts crack propagation in laminates where most plies present a significant likelihood of crack propagation, as most validation has been conducted for cross-ply laminates or layups containing 90^{o} plies. Similarly, the delamination onset model can technically be applied to any symmetrical laminate under tension or tension + shear, as long as only one interface is critical for the initiation of delamination (in each symmetric half). However, if in more than two interfaces delaminations are considered, some modifications must be made in the calculation of laminate stiffnesses (see eq. 5.7 - 5.18). On the other hand, the delamination growth model has only been validated for cross-ply laminates, and the use of mode II interlaminar fracture toughness may not be suitable for laminates where local shear is present in the plies. Nonetheless, the proposed model is simple and represents a step in the right direction, showing promise if further refinement is undertaken. Once a combined mode II and III fracture toughness model is employed, its applicability could be expanded to any symmetrical laminate.

Regarding the study of the parameters and interpretability of the expressions derived (sections 4.4, 5.3 and 5.6: The obtained closed-form expressions offer valuable insights into various trends. The behavior of G^{cr} primarily depends on the stacking sequence and the thickness of the critical plies, while G^{cr+del}_{onset} is highly sensitive to the ratio t_1/t_c (as shown in Figure 5.14). The delamination growth expression, G^{cr+del}, exhibits a linear behaviour within the typical usage range. Interestingly, all SERR expressions for the four proposed cases behave similarly concerning the parameters. Particular attention must be given to obtaining accurate in-situ strengths values (Y^T_{is} and S_{is}), as they significantly impact the crack propagation and delamination onset models. The analytical nature of the model facilitates a quick understanding of the physical relationships between parameters and their influence on predictions. This understanding can pave the way for future researchers to make modifications, improvements and expansions of the expressions and the model itself.

Finally, regarding the practical use of the models (section 5.7 and 7): Their efficiency and analytical nature enable rapid comparison of the laminate behavior. Design curves for the delamination onset can be generated, facilitating the quick exploration of numerous parameter combinations. This allows for the comparison of different materials and layups simultaneously, without the need for complex simulations. As the model has been validated, even with its inherent errors, it becomes a powerful tool in the early stages of the design process. Furthermore, by combining crack propagation, delamination onset and growth plots, a wealth of information about a specific laminate can be readily obtained within seconds. These plots serve practical purposes, such as damage assessment in structures. For instance, if a non-destructive test is performed on a laminate, and an average distance for a ply is determined, these plots can provide insights into whether the laminate is approaching a critical area or if it is in a

safe range. While some additional work would be necessary to fully implement the models, their extension to include fatigue loading would be highly beneficial for practical use. Overall, these analytical models have the potential to offer valuable insights and streamline various engineering processes.

Based on the conclusions reached in this chapter, recommendations for future work are given in Section 9 which are arranged in descending order of priority.

9

Recommendations for future work

The proposed recommendations are arranged in descending order, starting with the most impactful and useful feature and gradually progressing to the less directly impactful but still relevant features.

- **Modify the crack propagation and delamination onset model (section 4 and 5) to take into account cracks in every ply.** Currently, the model assumes cracks only in critical plies based on the FPF criteria. While this works perfectly in a cross-ply or laminates with 90º plies under tension because matrix cracks will hardly appear in plies other than the 90º, other complex laminates with many ply orientations could suffer completely different individual crack propagation behaviours. To address this limitation, consider introducing a crack spacing variable for each ply orientation. However, it is acknowledged that this modification will increase the complexity of calculating analytical expressions for G^{cr}, G^{cr+del}_{onset} and G^{cr+del} as the stiffnesses and cracked areas A_{cr} will now depend on $D_1, D_2, ..., D_i$ where i represents the number of ply orientations (see Figure 9.1). This could lead to highly intricate analytical differentiations. This improvement will prove very useful in laminates in which most of its plies are prone to cracking.

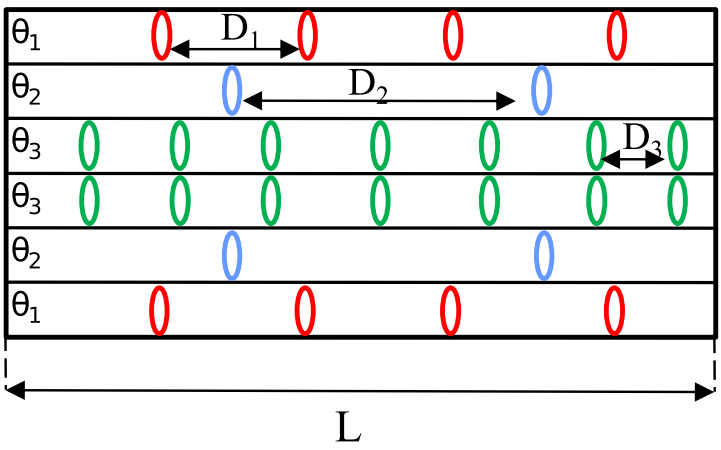

Figure 9.1: Symmetrical laminate with cracks in every ply.

- **Expand the model to take into account more complex delamination scenarios like multiple delaminations or different configurations emanating from the crack tips.** 4

delamination configurations are proposed but more complex scenarios could be devised and compared. Many delaminations occurring at the same time with different behaviours could be studied including again different delamination lengths variables depending on the interface.

- **Improve the delamination growth model proposed in section 6.2.1 using a mixed mode II+III interlaminar fracture toughness model.** The use of Mode II interlaminar fracture toughness restricts the model to situations where the delamination growth is close to an in-plane shear growth. Since the delamination onset model works for every symmetrical laminate, a delamination growth model that is as effective in every situation would be required.

- **Demonstrate that the crack spacing remains constant after the onset using the derived SERR expressions.** When considering a crack spacing D and introducing a delamination of length a, G^{cr+del} has to be always bigger than G^{cr} for that specific D in order to prove that no crack will appear after the onset D_{onset}. Mathematically, the following expressions must be satisfied:
$$\forall a, \forall D < D_{onset} : G^{cr+del}(a, D) > G^{cr}(D)$$

- **Include additional damage modes to the model to improve the predictions** (eg. free-edge delaminations, fiber fracture, fiber-matrix debonding...). It has been discussed briefly in section 6.3.1 how the SERR derived by O'Brien [13] for edge delamination can be combined with the proposed model to help to improve the predictions. Including a general method to predict free-edge delaminations, fiber fracture or other damage models can help to improve the correlation with reality and can make the plots derived in section 7 even more complete.

- **Devise a rigorous criterion to model the initial delamination length which is overestimated in the model.** While the overstimation of the initial length make the model conservative, a more precise method could be used to effectively capture the spontaneous process of the creation of the delaminations in the matrix crack tips.

- **Assume that the crack spacing varies during the delamination growth.** The assumption that the crack spacing is constant through the delamination growth is fair but an analysis of how the delamination behaves upon varying the crack distance at the same time as the delamination grows could give interesting information.

- **Validate the delamination onset model for laminates under combined loading**. No combined loading tests were found on the literature, nor FEM analysis. Either experimental data of FEM modelling would be required to validate the model for laminates under tension and shear.

- **Transition the model to fatigue loading.** SERR expressions are also used in fatigue loading to predict crack propagation and delamination growth so the derived expressions could be modified and maybe used for dynamic loading. These would require great effort as the dynamic effects in the composite laminates are complex and difficult to study analytically.

A

Material Properties

Table A.1: Material data used in the thesis.

	UT-E500/Epikote RIMR235		AS/3501-6		Fiberite 934/T300	
Property	Value	Source	Value	Source	Value	Source
E_1 [GPa]	41.4	[44]	139.9	[71]	128	[72]
E_2 [GPa]	13.1	[44]	11.1	[71]	7.2	[72]
G_{12} [GPa]	4.0	[44]	4.79	[71]	4	[72]
ν_{12}	0.30	[44]	0.27	[71]	0.3	[72]
t [mm]	0.34	[44]	0.132	[71]	0.125	[72]
γ_y	0.014*	[74]	0.0165	[75]	-	-
Y_{is}^t [MPa]	70.96*	[76]	60.03*	[77]	58.6	[78]
S_{is} [MPa]	-	-	140.31*	[77]	-	-
L [mm]	200 (140)	[44]	177.8	[71]	150	[72]

	Avimid K Polymer/IM6		Hercules 3501-6/AS4		T800H/3631	
Property	Value	Source	Value	Source	Value	Source
E_1 [GPa]	134	[72]	130	[72]	152.2	[7]
E_2 [GPa]	9.8	[72]	9.7	[72]	9.57	[7]
G_{12} [GPa]	5.5	[72]	5.0	[72]	5.0	[7]
ν_{12}	0.3	[72]	0.3	[72]	0.3	[7]
t [mm]	0.125	[72]	0.125	[72]	0.132	[7]
γ_y	-	-	-	-	-	-
Y_{is}^t [MPa]	92.82*	[72]	49.42*	[72]	65.09*	[79]
S_{is} [MPa]	-	-	-	-	-	-
L [mm]	150	[72]	150	[72]	30	[7]

	Hercules AS1/3501-6		Typical carbon/epoxy UD	
Property	Value	Source	Value	Source
E_1 [GPa]	130	[46]	128	[21]
E_2 [GPa]	10	[46]	7.2	[21]
G_{12} [GPa]	5	[46]	4	[21]
ν_{12}	0.3	[46]	0.3	[21]
t [mm]	0.169	[46]	0.14	[21]
γ_y	-	-	-	-
Y_{is}^t [MPa]	38.78*	[80]	58.6*	[78]
S_{is} [MPa]	120	[80]	-	-
L [mm]	200	[46]	150	[72]

* Value derived from data within given reference.

B

Reduced Shear Modulus Calculation

Socci & Kassapoglou [3] approximate the shear stress-strain curve as a bi-linear curve with initial slope G_{xy} and final slope k as shown in Figure B.1. For sufficient high loads, permanent shear strains γ_m are present on the ply as defined in point A in Fig. B.1. The permanent strain should be known in order to calculate the new slope of the line AB. The final slope k is obtained by ensuring that the areas under the bi-linear curve and the experimentally obtained stress-strain cuRve are the same.

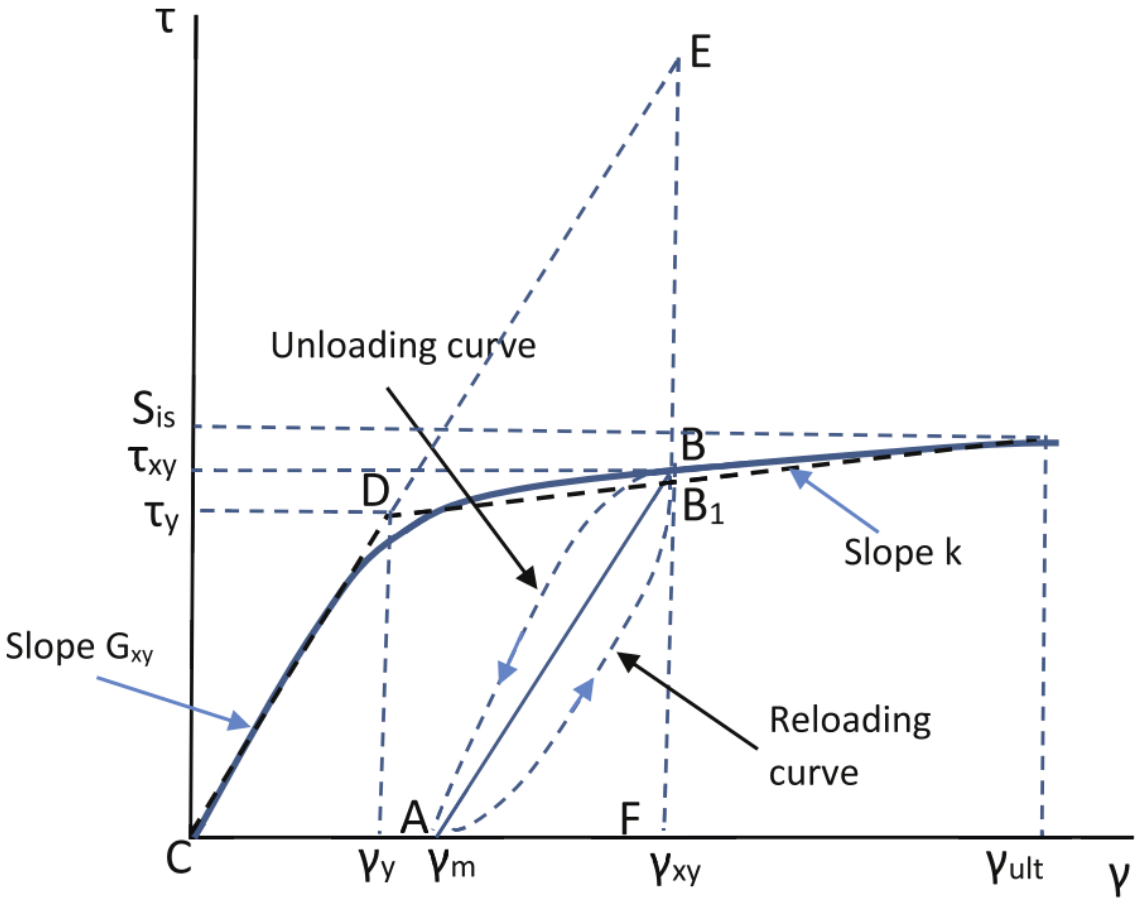

Figure B.1: Shear stress-strain curve approximated by a bi-linear curve. Obtained from [3]

Two quantities are now defined by the authors: the "unavailable" elastic energy which is not available due to the non-linearities of the curve and the "non-recoverable" strain energy because unloading from point B does not go to zero strain but to the permanent strain γ_m. For an applied strain γ_{xy} in a ply, the "unavailable" elastic energy is defined as the triangle DEB_1 in Fig. B.1. The "non-recoverable" strain energy is obtain as the are of the polygon CAB_1D. The permanent shear strain γ_m is obtained requiring that the ratio of the "unavailable" elastic energy to the total elastic energy (area CEF) is equal to the ratio of the "non-recoverable" energy to the total elastic-plastic energy (area CFB_1D) which gives:

$$\frac{DEB_1}{CEF} = \frac{CAB_1D}{CFB_1D} \quad \Rightarrow \quad \gamma_m = \frac{\left(G_{xy}\gamma_{xy} - \tau_{xy}\right)\left(\gamma_{xy} - \gamma_y\right)\left[\tau_{xy}\left(\gamma_{xy} - \gamma_y\right) + G_{xy}\gamma_{xy}\gamma_y\right]}{G_{xy}\gamma_{xy}^2\left(\tau_{xy} + G_{xy}\gamma_y\right)} \tag{B.1}$$

where γ_y is the yield shear strain, G_{xy} the shear modulus in the ply and τ_{xy} is the stress obtained from the bi-linear relation:

$$\tau_{xy} = G_{xy} + k(\gamma_{xy} - \gamma_y) \tag{B.2}$$

Then, the shear modulus due to the non-linearity is defined as follows:

$$G_{xy} = \frac{\tau_{xy}}{(\gamma_{xy} - \gamma_m)} \tag{B.3}$$

In addition of the non-linear behaviour, the shear stress in the ply will be reduced due to the presence of cracks if the shear applied to the ply is sufficiently high. The shear strain stress is obtained in [3] as:

$$\tau_{xy} = -\frac{8\nu_0 G_{xy}}{D}\sum \frac{sin\frac{n\pi}{2}}{n\pi\left(1 + e^{k_n D}\right)}\left(e^{k_n y} + e^{k_n D}e^{-k_n y}\right)cos\frac{n\pi z}{t_2} + \frac{2\nu_0}{D}G_{xy} \tag{B.4}$$

$\nu_0 = \gamma_a D/2$, $k_n = n\pi/t_2$, D is the distance between cracks, t_2 the thickness of the cracked ply, G_{xy} the shear modulus and z is the through thickness coordinate as shown in Fig.B.2.

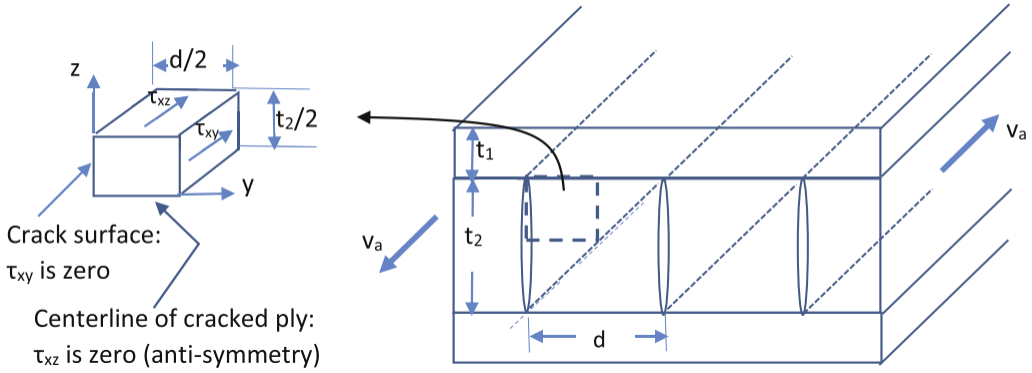

Figure B.2: Matrix cracks forming in a ply under pure shear. Obtained from [3]

In [3] can be demonstrated that if the shear stress is elastic for all z at the y location for interest, the average shear stress is defined as:

$$\tau_{xyav} = -\frac{16\nu_0}{D} G_{xy} \sum \frac{e^{k_n y} + e^{k_n D} e^{-k_n y}}{\left(1 + e^{k_n D}\right)(n\pi)^2} + \frac{2\nu_0}{D} G_{xy} \tag{B.5}$$

If the shear stress becomes non-linear for a portion $z_0 \leq z \leq t_2/2$, the average shear stress can be expressed by:

$$\tau_{xyav} = -\frac{16\nu_0}{D} G_{xy} \sum \frac{e^{k_n y} + e^{k_n D} e^{-k_n y}}{\left(1 + e^{k_n D}\right)(n\pi)^2} \left[k + \left(G_{xy} - k\right) sin\frac{n\pi}{2} sin\frac{n\pi z_0}{t_2}\right]$$
$$+\frac{2\nu_0}{D} G_{xy} \left[\frac{2z_0}{t_2} + \frac{k}{G_{xy}}\left(1 - \frac{2z_0}{t_2}\right)\right] + G_{xy}\gamma_y \left(1 - \frac{k}{G_{xy}}\right)\left(1 - \frac{2z_0}{t_2}\right) \tag{B.6}$$

z_0 is found as the value of z for which the right hand side of equation B.4 is equal to the "yield" shear stress $G_{xy}\gamma_y$. Evaluating eq. B.5 or eq. B.6 in y = D/2 right before cracking, the shear modulus in a cracked ply is finally defined as:

$$G_{xy,red} = \frac{\tau_{xyav}}{(\gamma_{xy} - \gamma_m)} \tag{B.7}$$

Substituing eq. B.5 & eq. B.1 in eq. B.7 and modifying the notation to make it uniform with the rest of the report, eq. **??** is obtained.

C

ABD matrix calculation

The constitutive equations of CLT [64] can be easily written in matrix form as:

$$\left[\begin{array}{c} N_x \\ N_y \\ N_{xy} \\ \hline M_x \\ M_y \\ M_{xy} \end{array}\right] = \left[\begin{array}{ccc|ccc} A_{11} & A_{12} & A_{16} & B_{11} & B_{12} & B_{16} \\ A_{12} & A_{22} & A_{26} & B_{12} & B_{22} & B_{26} \\ A_{16} & A_{26} & A_{66} & B_{16} & B_{26} & B_{66} \\ \hline B_{11} & B_{12} & B_{16} & D_{11} & D_{12} & D_{16} \\ B_{12} & B_{22} & B_{26} & D_{12} & D_{22} & D_{26} \\ B_{16} & B_{26} & B_{66} & D_{16} & D_{26} & D_{66} \end{array}\right] \left[\begin{array}{c} \varepsilon_x^0 \\ \varepsilon_y^0 \\ \gamma_{xy}^0 \\ \hline K_x \\ K_y \\ K_{xy} \end{array}\right] \tag{C.1}$$

Written in contracted form :

$$\begin{bmatrix} N \\ M \end{bmatrix} = \begin{bmatrix} A & B \\ B & D \end{bmatrix} = \begin{bmatrix} \varepsilon_x^0 \\ K \end{bmatrix} \tag{C.2}$$

By definition, the terms of the ABD matrix are expressed as:

$$A_{ij} = \sum_{k=1}^{n} \left[\bar{Q}_{ij}\right]_k (h_k - h_{k-1}) \tag{C.3}$$

$$B_{ij} = \frac{1}{2} \sum_{k=1}^{n} \left[\bar{Q}_{ij}\right]_k \left(h_k^2 - h_{k-1}^2\right) \tag{C.4}$$

$$D_{ij} = \frac{1}{3} \sum_{k=1}^{n} \left[\bar{Q}_{ij}\right]_k \left(h_k^3 - h_{k-1}^3\right) \tag{C.5}$$

$h_k - h_{k-1}$ is the thickness of of a k-ply and $\left[\bar{Q}_{ij}\right]_k$ is the stiffness matrix of a k-ply in global coordinates which are defined as follow:

$$\begin{aligned}
\bar{Q}_{11} &= U_1 + U_2\,cos(2\theta) + U_3\,cos(4\theta) \\
\bar{Q}_{22} &= U_1 - U_2\,cos(2\theta) + U_3\,cos(4\theta) \\
\bar{Q}_{12} &= U_4 - U_3\,cos(4\theta) \\
\bar{Q}_{66} &= U_5 - U_3\,cos(4\theta) \\
\bar{Q}_{16} &= \tfrac{1}{2}U_2\,sin(2\theta) + U_3\,sin(4\theta) \\
\bar{Q}_{26} &= \tfrac{1}{2}U_2\,sin(2\theta) - U_3\,sin(4\theta)
\end{aligned} \tag{C.6}$$

where

$$\begin{aligned}
U_1 &= \tfrac{3}{8}(Q_{11} + Q_{22}) + \tfrac{1}{4}Q_{12} + \tfrac{1}{2}Q_{66} \\
U_2 &= \tfrac{1}{2}(Q_{11} - Q_{22}) \\
U_3 &= \tfrac{1}{8}(Q_{11} + Q_{22}) - \tfrac{1}{4}Q_{12} - \tfrac{1}{2}Q_{66} \\
U_4 &= \tfrac{1}{8}(Q_{11} + Q_{22}) + \tfrac{3}{4}Q_{12} - \tfrac{1}{2}Q_{66} \\
U_5 &= \tfrac{1}{8}(Q_{11} + Q_{22}) - \tfrac{1}{4}Q_{12} + \tfrac{1}{2}Q_{66}
\end{aligned} \tag{C.7}$$

θ is the angle of the ply with respect to the global axis and Q_{ij} terms are defined as the reduced stiffnesses of the ply [64] and can be obtained using the material properties of the lamina (E_1, E_2, G_{12}, ν_{12} and ν_{21}) assuming that $\nu_{21} = (E_2/E_1)\nu_{12}$:

$$\begin{aligned}
Q_{11} &= \frac{E_1}{1 - \nu_{12}\nu_{21}} \\
Q_{22} &= \frac{E_2}{1 - \nu_{12}\nu_{21}} \\
Q_{12} &= \frac{\nu_{12}E_2}{1 - \nu_{12}\nu_{21}} \\
Q_{66} &= G_{12}
\end{aligned} \tag{C.8}$$

D

G^{cr} and G^{cr+del} 3D plots

A representation of the SERR expressions for crack propagation G^{cr} and delamination onset G^{cr+del}_{onset} are presented here with respect to their most 2 important parameters, the crack spacing D and the applied load σ_x. This 3D representations help to understand the trend of both function. Since it is assumed that it sufficiently explained during the report, this figures are presented here in the Appendix as an additional information.

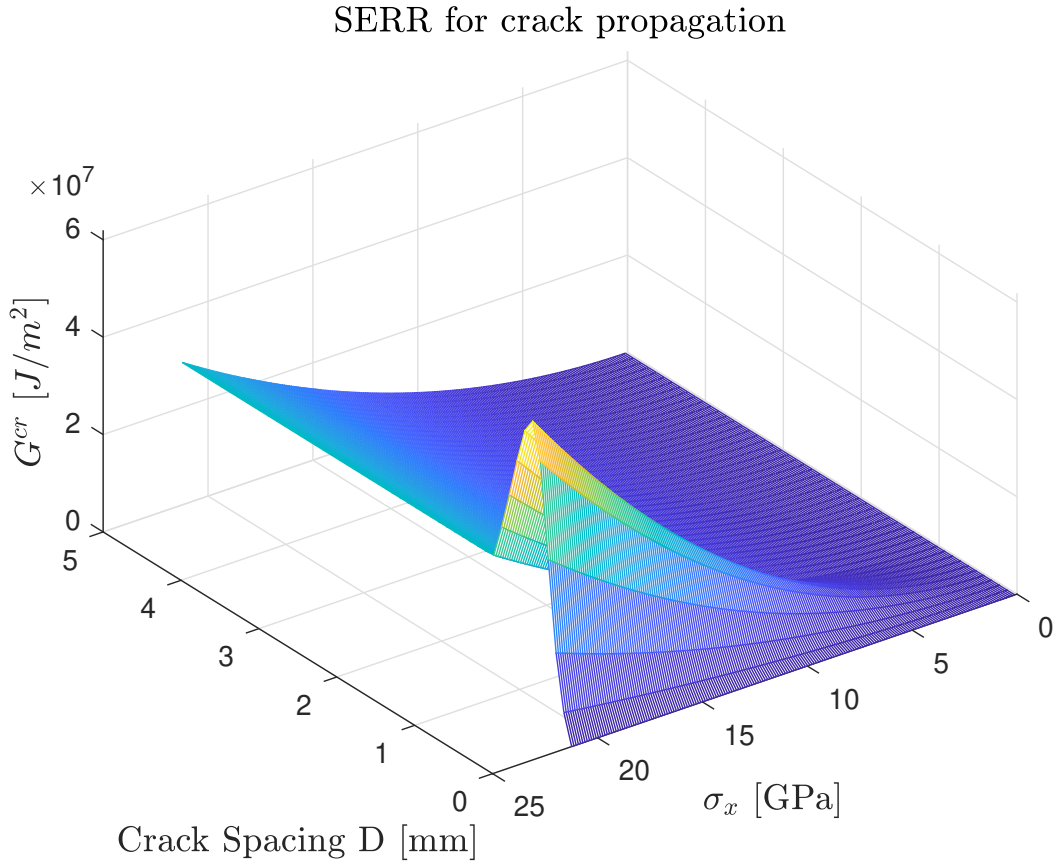

Figure D.1: Schematic of G^{cr} as a function of D and the applied stress σ_x for a generic symmetrical laminate.

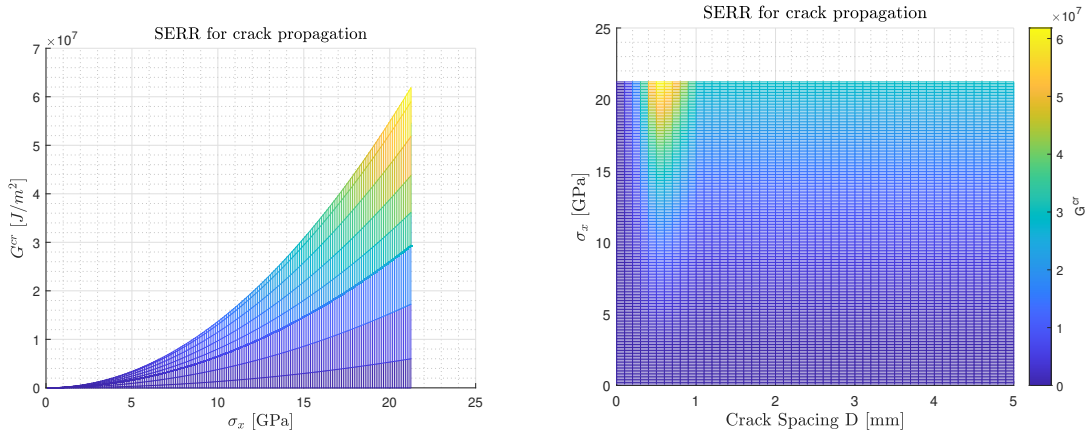

(a) G^{cr} vs σ_x **(b)** G^{cr} vs D

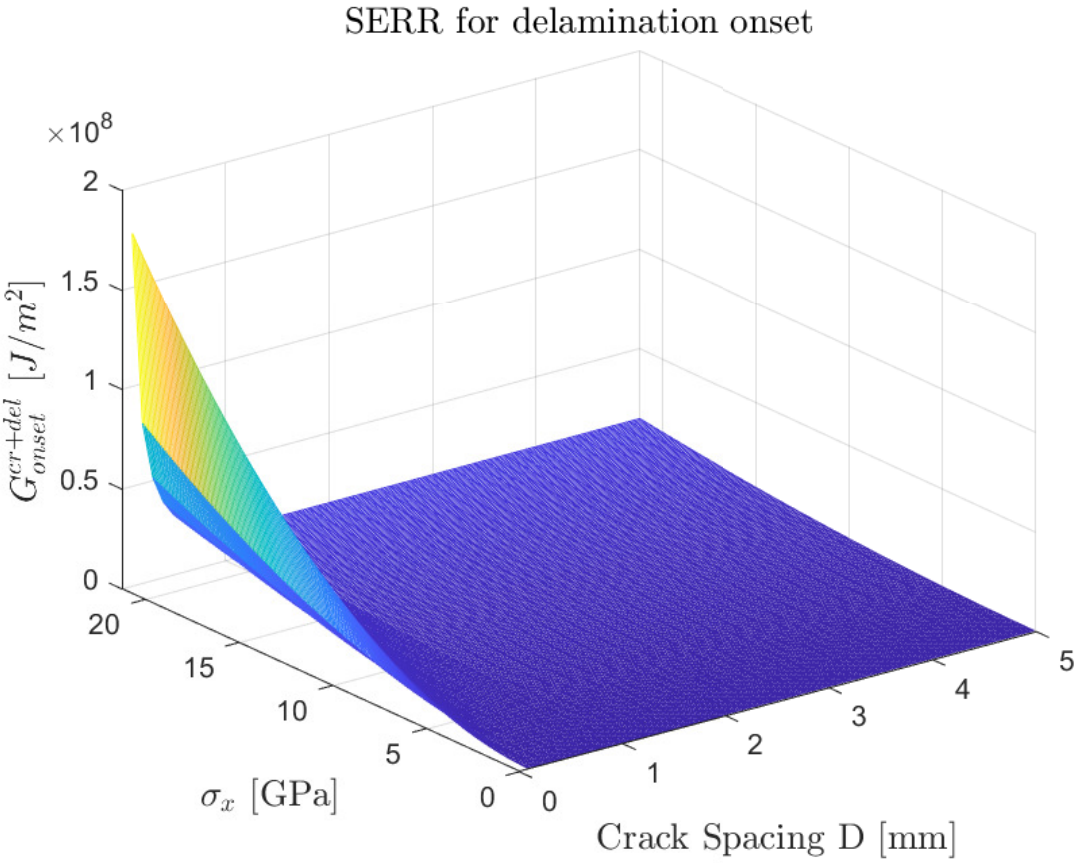

Figure D.3: Schematic of G^{cr+del}_{onset} as a function of D and the applied stress σ_x for a generic symmetrical laminate.

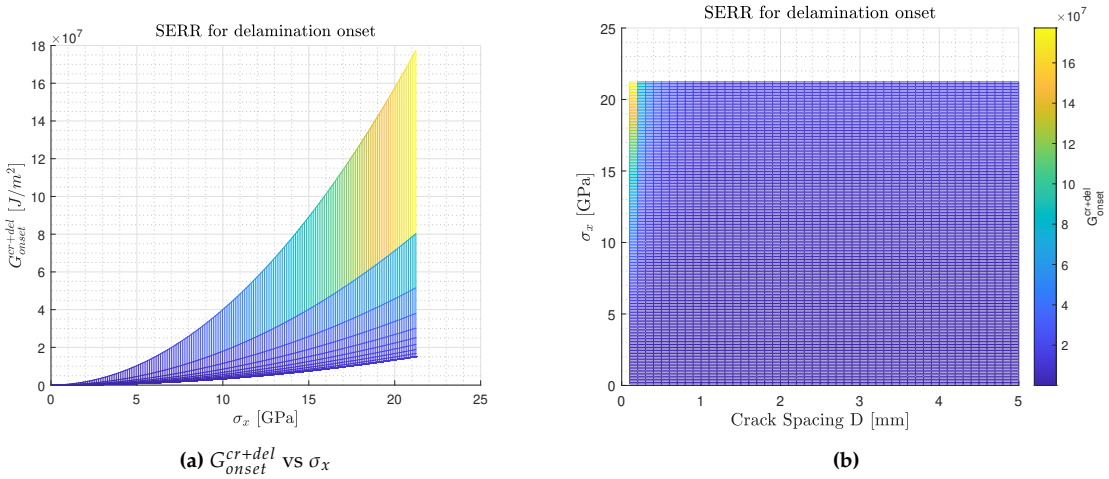

(a) G^{cr+del}_{onset} vs σ_x **(b)**

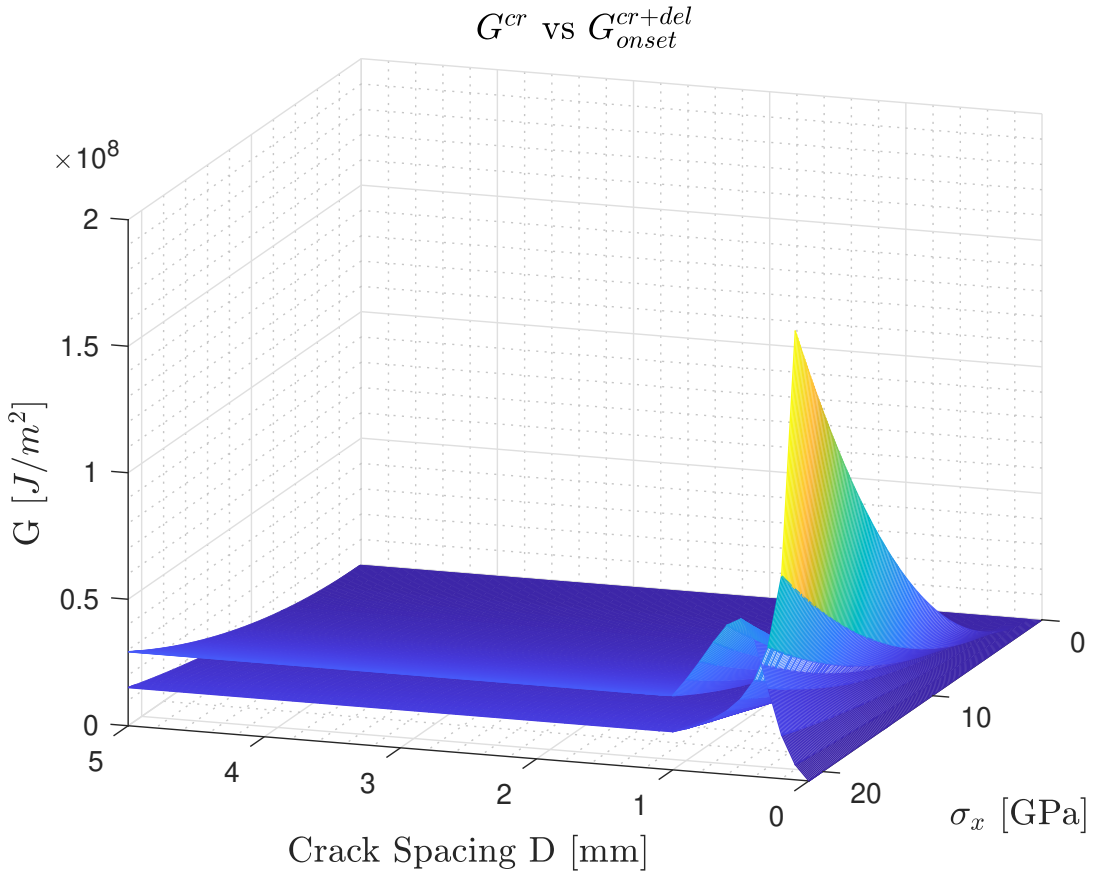

Figure D.5: Schematic of the intersection of G^{cr} and G^{cr+del}_{onset} as a function of D and the applied stress σ_x for a generic symmetrical laminate.

Bibliography

[1] M. Hajikazemi, L. N. McCartney, and W. Van Paepegem. "Matrix cracking initiation, propagation and laminate failure in multiple plies of general symmetric composite laminates". In: *Composites Part A: Applied Science and Manufacturing* 136 (Sept. 2020). ISSN: 1359835X. DOI: 10.1016/j.compositesa.2020.105963.

[2] N. Laws, G.J. Dvorak, and M. Hejazi. "Stiffness changes in unidirectional composites caused by crack systems". In: *Mechanics of Materials* 2.2 (1983), pp. 123–137. ISSN: 0167-6636. DOI: https://doi.org/10.1016/0167-6636(83)90032-7. URL: https://www.sciencedirect.com/science/article/pii/0167663683900327.

[3] C. A. Socci and C. Kassapoglou. "Prediction of matrix crack initiation and evolution and their effect on the stiffness of laminates with off-axis plies under in-plane loading". In: *Composites Science and Technology* 200 (Nov. 2020). ISSN: 02663538. DOI: 10.1016/j.compscitech.2020.108427.

[4] Chandra Veer Singh and Ramesh Talreja. "Evolution of ply cracks in multidirectional composite laminates". In: *International Journal of Solids and Structures* 47.10 (2010), pp. 1338–1349. ISSN: 0020-7683. DOI: https://doi.org/10.1016/j.ijsolstr.2010.01.016. URL: https://www.sciencedirect.com/science/article/pii/S0020768310000272.

[5] Nairn J. A. "Matrix microcracking in composites". In: *Polymer Matrix Composites edited by Talreja R. and Månson J.-A. E., Elsevier Science* (2000), pp. 403–432.

[6] M. Caslini, C. Zanotti, and T. K. O'Brien. "Study of Matrix Cracking and Delamination in Glass/Epoxy Laminates". In: *Journal of Composites Technology and Research* 9(4) (1987), pp. 121–130.

[7] N. Takeda and S. Ogihara. "Initiation and growth of delamination from the tips of transverse cracks in CFRP cross-ply laminates". In: *Composites Science and Technology* 52.3 (1994), pp. 309–318. ISSN: 0266-3538. DOI: https://doi.org/10.1016/0266-3538(94)90166-X.

[8] B. T. Rodini and J. R. Eisenmann. "An Analytical and Experimental Investigation of Edge Delamination in Composite Laminates". In: *Fibrous Composites in Structural Design* (1980), pp. 441–457. DOI: 10.1007/978-1-4684-1033-4_25.

[9] John A. Nairn. "On the use of shear-lag methods for analysis of stress transfer in unidirectional composites". In: *Mechanics of Materials* 26.2 (1997), pp. 63–80. ISSN: 0167-6636. DOI: https://doi.org/10.1016/S0167-6636(97)00023-9.

[10] Z. Hashin. "Analysis of cracked laminates: a variational approach". In: *Mechanics of Materials* 4.2 (1985), pp. 121–136. ISSN: 0167-6636. DOI: https://doi.org/10.1016/0167-6636(85)90011-0.

[11] Pedro Camanho et al. "A Micromechanics-Based Damage Model for the Strength Prediction of Composite Laminates". In: (Jan. 2006). DOI: 10.1007/1-4020-5370-3_223.

[12] C.T. Sun and Z.-H. Jin. "Modeling of composite fracture using cohesive zone and bridging models". In: *Composites Science and Technology* 66.10 (2006), pp. 1297–1302. ISSN: 0266-3538. DOI: https://doi.org/10.1016/j.compscitech.2005.10.013.

[13] T.K. O'Brien. "Characterization of delamination onset and growth in a composite laminate". In: *ASTM special technical publications* (1982), pp. 140–167.

[14] R. Talreja. "A synergistic damage mechanics approach to durability of composite material systems". In: *Progress in Durability Analysis of Composite Systems* (1996).

[15] R. Talreja. "A continuum mechanics characterization of damage in composite materials". In: *Proc. R. Soc. Lond.* (1985). DOI: http://doi.org/10.1098/rspa.1985.0055.

[16] J. Varna, R. Joffe, and R. Talreja. "A synergistic damage-mechanics analysis of transverse cracking $[/90_4]s$ laminates". In: *Composites Science and Technology* 61 (Apr. 2001), pp. 657–665. DOI: 10.1016/S0266-3538(01)00005-7.

[17] A. L. Highsmith and K. L. Reifsnider. "Stiffness-reduction mechanisms in composite laminates". In: *ASTM special technical publications* (1982), pp. 103–117.

[18] Maria Kashtalyan and Costas Soutis. "Analysis of local delaminations in composite laminates with angle-ply matrix cracks". English. In: *International Journal of Solids and Structures* 39.6 (Mar. 2002), pp. 1515–1537. ISSN: 0020-7683. DOI: 10.1016/S0020-7683(02)00007-0.

[19] Z Hashin. "Analysis of stiffness reduction of cracked cross-ply laminates". In: *Engineering Fracture Mechanics* 25.5 (1986), pp. 771–778. ISSN: 0013-7944. DOI: https://doi.org/10.1016/0013-7944(86)90040-8.

[20] S. S. T. Larijani and A. Farrokhabadi. "A variational approach for predicting initiation of matrix cracking and induced delamination in symmetric composite laminates under in-plane loading". In: *IEEE Journal of Selected Topics in Quantum Electronics* (Sept. 2018), pp. 855–868. ISSN: 21910359. DOI: 10.1515/secm-2016-0379.

[21] J. A. Nairn and S. Hu. "The initiation and growth of delaminations induced by matrix microcracks in laminated composites". In: *International Journal of Fracture* 57.1-24 (1992). ISSN: 1573-2673. DOI: 10.1007/BF00013005.

[22] A.S.D. Wang, M. Slomiana, and R.B. Bucinell. "Delamination Crack Growth in Composite Laminates". In: *Delamination and Debonding of Materials, ASTM STP 876* (1985), pp. 135–167.

[23] T. Okabe et al. "Experimental and numerical studies of initial cracking in CFRP cross-ply laminates". In: *Composites Part A: Applied Science and Manufacturing* 68 (2015), pp. 81–89. ISSN: 1359-835X. DOI: https://doi.org/10.1016/j.compositesa.2014.09.020.

[24] L.M.P. Durão, M.F.S.F. de Moura, and A.T. Marques. "Numerical prediction of delamination onset in carbon/epoxy composites drilling". In: *Engineering Fracture Mechanics* 75.9 (2008). Fracture of Composite Materials, pp. 2767–2778. ISSN: 0013-7944. DOI: https://doi.org/10.1016/j.engfracmech.2007.03.009.

[25] A. Riccio et al. "Numerical Investigation on Delamination Growth in Composite Panels Including Fibre-Bridging Effect". In: *Aerotecnica Missili Spazio* 97 (2018), pp. 34–39. DOI: 10.1007/BF03404763.

[26] Ali Delbariani-Nejad, Amin Farrokhabadi, and Mohammad Fotouhi. "Finite element reliability analysis of edge delamination onset due to interlaminar stresses in composite laminates". In: *Composite Structures* 288 (2022), p. 115410. ISSN: 0263-8223. DOI: https://doi.org/10.1016/j.compstruct.2022.115410.

[27] Andrea Ferrari, Sergio Fanelli, and Matteo Parlamento. "Finite Element Modelling of Delamination Onset in Polymeric Composite Material". In: *Advances in Fracture and Damage Mechanics XVIII*. Vol. 827. Key Engineering Materials. Trans Tech Publications Ltd, Feb. 2020, pp. 25–30. DOI: 10.4028/www.scientific.net/KEM.827.25.

[28] Jakub Rzeczkowski, Sylwester Samborski, and Marcelo de Moura. "Experimental investigation of delamination in composite continuous fiber-reinforced plastic laminates with elastic couplings". In: *Materials* 13 (22 Nov. 2020), pp. 1–17. ISSN: 19961944. DOI: 10.3390/ma13225146.

[29] Gordon Just, Ilja Koch, and Maik Gude. "Experimental Analysis of Matrix Cracking in Glass Fiber Reinforced Composite Off-Axis Plies under Static and Fatigue Loading". In: *Polymers* 14 (11 June 2022). ISSN: 20734360. DOI: 10.3390/polym14112160.

[30] Evanthia J. Pappa et al. "Experimental study on the interlaminar fracture properties of carbon fibre reinforced polymer composites with a single embedded toughened film". In: *Polymers* 13 (23 Dec. 2021). ISSN: 20734360. DOI: 10.3390/polym13234103.

[31] S. Gholizadeh. "A review of non-destructive testing methods of composite materials". In: *Procedia Structural Integrity* 1 (2016). XV Portugese Conference on Fracture, PCF 2016, 10-12 February 2016, Paco de Arcos, Portugal, pp. 50–57. ISSN: 2452-3216. DOI: https://doi.org/10.1016/j.prostr.2016.02.008.

[32] Xintao Huo et al. "Measurement of fracture parameters based upon digital image correlation and virtual crack closure techniques". In: *Composites Part B: Engineering* 224 (2021), p. 109157. ISSN: 1359-8368. DOI: https://doi.org/10.1016/j.compositesb.2021.109157.

[33] S.L. Ogin, P. Brøndsted, and J. Zangenberg. "1 - Composite materials: constituents, architecture, and generic damage". In: *Modeling Damage, Fatigue and Failure of Composite Materials*. Ed. by Ramesh Talreja and Janis Varna. Woodhead Publishing Series in Composites Science and Engineering. Woodhead Publishing, 2016, pp. 3–23. ISBN: 978-1-78242-286-0. DOI: https://doi.org/10.1016/B978-1-78242-286-0.00001-7.

[34] H. A. Luo and Y. Chen. "Matrix Cracking in Fiber-Reinforced Composite Materials". In: *Journal of Applied Mechanics* 58.3 (Sept. 1991), pp. 846–848. ISSN: 0021-8936. DOI: 10.1115/1.2897274.

[35] National Research Council. *Accelerated Aging of Materials and Structures: The Effects of Long-Term Elevated-Temperature Exposure: 4.Degradation Mechanisms*. Accessed: 2023-06-12. 1996. URL: https://nap.nationalacademies.org/read/9251/chapter/6#24.

[36] E. S. Folias. "On the Prediction of Failure at a Fiber/Matrix Interface in a Composite Subjected to a Transverse Tensile Load". In: *Journal of Composite Materials* 25.7 (1991), pp. 869–886. DOI: 10.1177/002199839102500706.

[37] Anbu Clemensis Johnson, Simon A. Hayes, and Frank R. Jones. "The role of matrix cracks and fibre/matrix debonding on the stress transfer between fibre and matrix in a single fibre fragmentation test". In: *Composites Part A: Applied Science and Manufacturing* 43.1 (2012), pp. 65–72. ISSN: 1359-835X. DOI: https://doi.org/10.1016/j.compositesa.2011.09.005.

[38] S.L. Ogin, P.A. Smith, and P.W.R. Beaumont. "Matrix cracking and stiffness reduction during the fatigue of a (0/90)s GFRP laminate". In: *Composites Science and Technology* 22.1 (1985), pp. 23–31. ISSN: 0266-3538. DOI: https://doi.org/10.1016/0266-3538(85)90088-0.

[39] Zuorong Chen and Wenyi Yan. "A shear-lag model with a cohesive fibre–matrix interface for analysis of fibre pull-out". In: *Mechanics of Materials* 91 (2015), pp. 119–135. ISSN: 0167-6636. DOI: https://doi.org/10.1016/j.mechmat.2015.07.007.

[40] M. Hajikazemi and M.H. Sadr. "A variational model for stress analysis in cracked laminates with arbitrary symmetric lay-up under general in-plane loading". In: *International Journal of Solids and Structures* 51.2 (2014), pp. 516–529. ISSN: 0020-7683. DOI: https://doi.org/10.1016/j.ijsolstr.2013.10.024. URL: https://www.sciencedirect.com/science/article/pii/S0020768313004137.

[41] John A. Nairn and Shoufeng Hu. "The formation and effect of outer-ply microcracks in cross-ply laminates: A variational approach". In: *Engineering Fracture Mechanics* 41.2 (1992), pp. 203–221. ISSN: 0013-7944. DOI: https://doi.org/10.1016/0013-7944(92)90181-D.

[42] W. Van Paepegem and J. Degrieck. "Modelling the nonlinear shear stress-strain response of glass fibre- reinforced composites. Part II: model development and finite element simulations". In: *Composites Science and Technology* 66 (2006), pp. 1455–1464.

[43] Singh C.V. and Talreja R. "Evolution of ply cracks in multidirectional composite laminates". In: *International Journal of Solids and Structures* 47.10 (2010), pp. 1338–49. ISSN: 0020-7683. URL: https://urn.kb.se/resolve?urn=urn:nbn:se:ltu:diva-10146.

[44] P. A. Carraro et al. "Delamination onset in symmetric cross-ply laminates under static loads: Theory, numerics and experiments". In: *Composite Structures* 176 (Sept. 2017), pp. 420–432. ISSN: 02638223. DOI: 10.1016/j.compstruct.2017.05.030.

[45] A. S. D. Wang et al. "Cumulative Damage Model for Advanced Composite Materials". In: *Technical Report, AFWAL-TR-84-4004, Air Force Wright Aeronautical Laboratories, Dayton, OH* (1984).

[46] J. C. Brewer and P. A. Lagace. "Quadratic Stress Criterion for Initiation of Delamination". In: *Journal of Composite Materials* 22.12 (1988), pp. 1141–1155. DOI: 10.1177/002199838802201205. URL: https://doi.org/10.1177/002199838802201205.

[47] A. S. D.. Wang. "Fracture Mechanics of Sublaminate Cracks in Composite Laminates". In: *Characterization, Analysis and Significance of Defects in Composite Materials, Conference Proceeding No. 355, NATO Advanced Group on Aeronautic Research and Development* (1983), pp. 15–1.

[48] F.W. Crossman et al. "Initiation and Growth of Transverse Cracks and Edge Delamination in Composite Laminates Part 2. Experimental Correlation". In: *Journal of Composite Materials* 14.1 (1980), pp. 88–108. DOI: 10.1177/002199838001400107.

[49] S.H. Lem and S. Li. "Energy release rates for transverse cracking and delaminations induced by transverse cracks in laminated composites". In: *Composites Part A: Applied Science and Manufacturing* 36 (11 Nov. 2005), pp. 1467–1476. ISSN: 1359835X. DOI: 10.1016/j.compositesa.2005.03.015.

[50] T.K. O'Brien and S. A. Salpekar. "Combined effect of matrix cracking and stress-free edge on delamination". In: 1991.

[51] J.C.J. Schellekens and R. De Borst. "Free edge delamination in carbon-epoxy laminates: a novel numerical/experimental approach". In: *Composite Structures* 28.4 (1994), pp. 357–373. ISSN: 0263-8223. DOI: https://doi.org/10.1016/0263-8223(94)90118-X.

[52] L. Lammerant and I. Verpoest. "The interaction between matrix cracks and delaminations during quasi-static impact of composites". In: *Composites Science and Technology* 51.4 (1994), pp. 505–516. ISSN: 0266-3538. DOI: https://doi.org/10.1016/0266-3538(94)90083-3. URL: https://www.sciencedirect.com/science/article/pii/0266353894900833.

[53] Hamed Pakdel and Bijan Mohammadi. "Characteristic damage state of symmetric laminates subject to uniaxial monotonic-fatigue loading". In: *Engineering Fracture Mechanics* 199 (Aug. 2018), pp. 86–100. ISSN: 00137944. DOI: 10.1016/j.engfracmech.2018.05.007.

[54] J.F. Shackelford et al. *Introducción a la ciencia de materiales para ingenieros*. Pearson Educación, 2005. ISBN: 9788420544519. URL: https://books.google.com.cu/books?id=mJd0AAAACAAJ.

[55] Soo-Jin Park and Min-Kang Seo. "Chapter 4 - Solid-Solid Interfaces". In: *Interface Science and Composites*. Ed. by Soo-Jin Park and Min-Kang Seo. Vol. 18. Interface Science and Technology. Elsevier, 2011, pp. 253–331. DOI: https://doi.org/10.1016/B978-0-12-375049-5.00004-9.

[56] Syafiqah Nur Azrie Bt Safri, M.T.H. Sultan, and Mohammad Jawaid. "7 - Damage analysis of glass fiber reinforced composites". In: *Durability and Life Prediction in Biocomposites, Fibre-Reinforced Composites and Hybrid Composites*. Ed. by Mohammad Jawaid, Mohamed Thariq, and Naheed Saba. Woodhead Publishing Series in Composites Science and Engineering. Woodhead Publishing, 2019, pp. 133–147. ISBN: 978-0-08-102290-0. DOI: https://doi.org/10.1016/B978-0-08-102290-0.00007-6.

[57] D.D.R. Cartié and P.E. Irving. "Effect of resin and fibre properties on impact and compression after impact performance of CFRP". In: *Composites Part A: Applied Science and Manufacturing* 33.4 (2002), pp. 483–493. ISSN: 1359-835X. DOI: https://doi.org/10.1016/S1359-835X(01)00141-5.

[58] Stephen R. Hallett et al. "Modelling the interaction between matrix cracks and delamination damage in scaled quasi-isotropic specimens". In: *Composites Science and Technology* 68 (1 Jan. 2008), pp. 80–89. ISSN: 02663538. DOI: 10.1016/j.compscitech.2007.05.038.

[59] Jong-Il Kim, Yong-Hak Huh, and Yong-Hwan Kim. "Static Residual Tensile Strength Response of GFRP Composite Laminates Subjected to Low-Velocity Impact". In: *Applied Sciences* 10.16 (2020). ISSN: 2076-3417. DOI: 10.3390/app10165480.

[60] L. Iannucci. "Dynamic delamination modelling using interface elements". In: *Computers Structures* 84.15 (2006), pp. 1029–1048. ISSN: 0045-7949. DOI: https://doi.org/10.1016/j.compstruc.2006.02.002. URL: https://www.sciencedirect.com/science/article/pii/S004579490600023X.

[61] Paul A. Lagace. "Nonlinear stress-strain behaviour of graphite/epoxy, in: Proceedings of 25th Structures, Structural Dynamics and Materials Conference, Palm Springs CA laminates." In: 1984, pp. 63–73. URL: https://www.scopus.com/record/display.uri?eid=2-s2.0-0021122634&origin=inward.

[62] W. Van Paepegem, I. De Baere, and J. Degrieck. "Modelling the nonlinear shear stress–strain response of glass fibre-reinforced composites. Part II: Model development and finite element simulations". In: *Composites Science and Technology* 66.10 (2006), pp. 1465–1478. ISSN: 0266-3538. DOI: https://doi.org/10.1016/j.compscitech.2005.04.018.

[63] Soo Jin Park and Min Kang Seo. *Solid-Solid Interfaces*. Vol. 18. 2011, pp. 253–331. DOI: 10.1016/B978-0-12-375049-5.00004-9.

[64] A T Nettles. *Basic Mechanics of Laminated Composite Plates (NASA. Marshall Space Flight Center)*. 1994.

[65] A.S.D. Wang. "Initiation and growth of transverse cracks and edge delamination in composite laminates. Part 1. An energy method". In: *Journal of Composite Materials* 14.1 (1980), pp. 71–87. URL: https://iccm-central.org/Proceedings/ICCM3proceedings/papers/ICCM3_V1_13.pdf.

[66] F.W. Crossman et al. "Initiation and Growth of Transverse Cracks and Edge Delamination in Composite Laminates Part 2. Experimental Correlation". In: *Journal of Composite Materials* 14.1 (1980), pp. 88–108. DOI: 10.1177/002199838001400107. URL: https://doi.org/10.1177/002199838001400107.

[67] Q. Sun et al. "In-situ effect in cross-ply laminates under various loading conditions analyzed with hybrid macro/micro-scale computational models". In: *Composite Structures* 261 (Apr. 2021). ISSN: 02638223. DOI: 10.1016/j.compstruct.2021.113592.

[68] Masood Nikbakht et al. "Delamination evaluation of composite laminates with different interface fiber orientations using acoustic emission features and micro visualization". In: *Composites Part B: Engineering* 113 (2017), pp. 185–196. ISSN: 1359-8368. DOI: https://doi.org/10.1016/j.compositesb.2016.11.047.

[69] Chingshen Li, Fernand Ellyin, and Alan Wharmby. "On matrix crack saturation in composite laminates". In: *Composites Part B: Engineering* 34.5 (2003), pp. 473–480. ISSN: 1359-8368. DOI: https://doi.org/10.1016/S1359-8368(03)00020-9.

[70] S. Lacaze and L. Anquez. "Modelling of transverse crack growth and saturation in cross-ply laminates". In: *Journal of Materials Science* 27.22 (1992), pp. 5982–5988. DOI: 10.1007/BF01133740.

[71] P.C. Chou, A.S.D. Wang, and H. Miller. "Cumulative DamageModel for Advanced Composite Materials, Phase I, Final Report." In: *AFWAL-TR-82-4083* (1982). URL: https://apps.dtic.mil/sti/pdfs/ADA122859.pdf.

[72] Siulie Liu and John A. Nairn. "The Formation and Propagation of Matrix Microcracks in Cross-Ply Laminates during Static Loading". In: *Journal of Reinforced Plastics and Composites* 11.2 (1992), pp. 158–178. DOI: 10.1177/073168449201100204. URL: https://doi.org/10.1177/073168449201100204.

[73] "ASTM D 7905/D7905M-14, ASTM Int. Standard Test Method for Determination of the Mode II Interlaminar Fracture Toughness of Unidirectional Fiber-Reinforced Polymer Matrix Composites". In: *ASTM International* (2014). DOI: 10.1520/D7905_D7905M-19E01.

[74] P.D. Soden, M.J. Hinton, and A.S. Kaddour. "Lamina properties, lay-up configurations and loading conditions for a range of fibre-reinforced composite laminates". In: *Composites Science and Technology* 58.7 (1998), pp. 1011–1022. ISSN: 0266-3538. DOI: https://doi.org/10.1016/S0266-3538(98)00078-5. URL: https://www.sciencedirect.com/science/article/pii/S0266353898000785.

[75] Antonio Argüelles et al. "Influence of the Matrix Type on the Mode I Fracture of Carbon-Epoxy Composites Under Dynamic Delamination". In: *Experimental Mechanics* 51 (Mar. 2011), pp. 293–301. DOI: 10.1007/s11340-010-9364-0.

[76] Janis Varna, Roberts Joffe, and Ramesh Talreja. "A synergistic damage-mechanics analysis of transverse cracking [±/904]s laminates". In: *Composites Science and Technology* 61 (Apr. 2001), pp. 657–665. DOI: 10.1016/S0266-3538(01)00005-7.

[77] AS Kaddour et al. "Mechanical properties and details of composite laminates for the test cases used in the third world-wide failure exercise". In: *Journal of Composite Materials* 47.20-21 (2013), pp. 2427–2442. DOI: 10.1177/0021998313499477. URL: https://doi.org/10.1177/0021998313499477.

[78] Scott R. Finn, Ye-Fei He, and George S. Springer. "Delaminations in composite plates under transverse impact loads — Experimental results". In: *Composite Structures* 23.3 (1993), pp. 191–204. ISSN: 0263-8223. DOI: https://doi.org/10.1016/0263-8223(93)90222-C.

[79] Atsushi Hosoi and Hiroyuki Kawada. "Fatigue Life Prediction for Transverse Crack Initiation of CFRP Cross-Ply and Quasi-Isotropic Laminates". In: *Materials* 11 (2018). URL: https://api.semanticscholar.org/CorpusID:51619579.

[80] Altair Engineering Inc. *ESAComp - Software for Analysis and Design of Composites*. Available at: http://www.esacomp.com. 2020.0.0.22. 2020.